Study on A Thermally Driven Refrigerator Based on an Organic Rankine Cycle and Vapor Compression Refrigeration Combined by Single Rotor Expander-Compressor

Saif Fraih K Alshammari

In partial fulfilment of the requirements for the degree of Doctor of Philosophy at the University of Glasgow

Systems, Power, and Energy Research Division

James Watt School of Engineering

University of Glasgow

November 2023

ABSTRACT

Environmental degradation is still a major global concern as a result of the widespread usage of high-grade energy derived from fossil fuels, which emit greenhouse gases in abundant. Countries and companies all over the world are dealing with these issues, looking for sustainable and environmentally beneficial solutions. One such promising path is using the organic Rankine cycle (ORC) to capture heat, particularly from low temperature sources. The ORC's ability to convert otherwise wasted energy into useable power places it at the forefront of strategies aimed at reducing emissions and combating environmental impact. Given this context, this study goes thoroughly into the novel single rotor expander-compressor device's innovative potential. This device, which is intended for use in both a VCR cycle and an ORC, is positioned as a transformative tool in energy optimization and sustainable refrigeration. A detailed and comprehensive numerical model of the ORC-VCR was constructed to accurately describe and assess the performance of this integrated system. This model serves as a predictive tool for practical use cases to ensure its accuracy and reliability. The study rigorously evaluated the thermal efficiency of this integrated cycle. Thorough evaluations were conducted, taking into account the varying temperatures at which evaporation occurs in both the ORC (62.75 °C – 89.7 °C) and VCR (-20 °C – 5 °C) systems, the range of temperatures at which condensation occurs in the ORC system (20 °C – 45 °C), and the rotor speed (500 – 3000 rpm), all while keeping the heat source temperature constant (95 °C). These characteristics played a crucial role in understanding the operating limits and effectiveness of the combined system. The maximum cooling performance achieved was 5.38 kW, with a heat to cooling efficiency of 56%, attained at an ORC evaporation temperature of 62.75°C and a VCR temperature of -5°C, alongside an ORC condensation temperature of 20.5°C. it was observed that cooling performance consistently improved

with increasing rotor speeds, whereas rotor speed changes did not affect the heat-to-cooling efficiency. Other than energy analysis of the system, exergy analysis was conducted for the same system. By analyzing the exergy destruction contributions of each component within the ORC-VCR system, it was found that the ORC evaporator had the most substantial impact on total exergy destruction. However, the VCR evaporator's contribution could significantly increase if the evaporation temperature in the VCR were further reduced. The highest overall exergy efficiency recorded was 63%, with ORC and VCR evaporation temperatures set at 62.75 °C and -5 °C, respectively, and an ORC condensation temperature of 20.5 °C. Notably, overall exergy efficiency remained unaffected by variations in rotor speed.

In addition, this study explores the field of refrigerants, assessing other prospective refrigerants such as R245fa, R123, R134a, R1234ze(E), R1234yf, and Butane. Their performance is evaluated based on important indications, namely the heat-to-cool ratio efficiency, exergy efficiency, and the overall system efficiency. After this in-depth investigation, an examination of the VCR-ORC integration's potential influence on the environment was carried out, with a particular focus on aspects including consumption of fuel and CO2 emissions. In its essence, this research offers a perspective on the environmentally responsible integration of VCR and ORC systems. By combining these cycles, not only demonstrating the potential for improving energy efficiency, but also propose ways to address the urgent problem of emissions of greenhouse gases.

ACKNOWLEDGEMENTS

In the name of Allah, the Most Merciful, the Most Compassionate, I begin by expressing my profound gratitude for the wisdom, strength, and peace granted to me, which were instrumental in the completion of my doctoral journey.

I extend my deepest appreciation to my esteemed supervisor, Professor Zhibin Yu, for his unwavering support, guidance, and patience. His expertise and enthusiasm have been a great encouragement throughout my research.

Special thanks to Dr. Sambhaji Kadam, who has worked as my co-supervisor. His support and guidance throughout this journey were great motivations for me. Also, special thanks to Dr. Zahra Ouderji for her support, guidance, and motivations during my Ph.D.

A special note of thanks goes to the Saudi government, the Ministry of Education, and Jouf University for their invaluable scholarship and support, which have been pillars of my academic pursuit.

Special thanks to my friend Dr. Skriptyan Syuhri for his support and motivation during our study at James Watt school of engineering.

To my family, especially my mother, whose endless prayers and encouragement have been my stronghold; the blessed memory of my grandfather, who continues to inspire me beyond words; my loving wife, whose support and sacrifices were indispensable; and my children, Sahab, Nada, and Khalid, who provided me with the joy and inspiration to persevere—I owe an immeasurable debt of gratitude.

I also wish to extend my sincere thanks to my colleagues in Professor Zhibin Yu's group, and my friends in Glasgow that has been part of my life during this significant phase. Your support has not gone unnoticed.

DECLARATION

I declare that, unless explicitly stated to be the contribution of others, that this thesis is entirely my own work and has not been submitted for any other degree, at the University of Glasgow or elsewhere.

Saif Alshammari

November 2023

PREFACE

- Part of this thesis has been published in the following journal paper:

Alshammari, Saif, Sambhaji T. Kadam, and Zhibin Yu. "Assessment of single rotor expander-compressor device in combined organic Rankine cycle (ORC) and vapor compression refrigeration cycle (VCR)." *Energy* 282 (2023): 128763.

- During PhD I have participated in building combined organic Rankine cycle and vapor compression refrigeration prototype, running the system, investigation, and data collection:

Liang, Youcai, Andrew Mckeown, Zhibin Yu, and **Saif Fraih K. Alshammari**. "Experimental study on a heat driven refrigeration system based on combined organic Rankine and vapour compression cycles." *Energy Conversion and Management* 234 (2021): 113953.

- Conferences:

1- **Saif Alshammari**, Sambhaji T. Kadam, Zhibin Yu. " Potential of thermally driven refrigerator using single rotor expander-compressor device. " 14th International Green Energy Conference, 4-8 July 2022, Virtual.

2- **Saif Alshammari**, Sambhaji T. Kadam, Zahra H. Ouderji, Zhibin Yu. " Exergy analysis of organic Rankine cycle and vapor compression refrigeration combined by single rotor expander compressor (compander). " 15th International Green Energy Conference, 10-13 July 2023, Glasgow.

- Award:

IGEC2022 Best Student Paper Award Honourable Mentions

IGEC2022-144 *POTENTIAL OF THERMALLY DRIVEN REFRIGERATOR USING SINGLE ROTOR EXPANDER-COMPRESSOR DEVICE*.

- **Saif Alshammari**, Sambhaji T. Kadam, Zhibin Yu; James Watt School of Engineering, University of Glasgow.

Table of Contents

List of Figures

List of Tables

Nomenclature

compr	Compressor.
Cond	Condensation.
COP	Coefficient of performance.
COPs	Overall coefficient of performance.
CPR	Compression pressure ratio.
CWS	Cooling Water Stream.
E	Exergy destruction, kW.
E	Expander.
EPR	Expansion pressure ratio.
Eva	Evaporation.
f	Fuel.
H	Higher.
H-C	Heat to cooling.
HeatX	Heat Exchanger.
h	Enthalpy, kJ/kg.
L	Lower.
LHV	Lower heating value.
$\dot{m}$	Mass flow rate, kg/s.
o	Dead state.
ORC	Organic Rankine Cycle.
P	Pressure, bar.
PL	Partial load.
Prime	Thermal energy required, kW.
$\dot{Q}$	Rate of heat, kW.

s	Specific entropy, $kJ/kg^{-1}K^{-1}$.
sub	Subcooled.
sup	Superheated.
T	Temperature, ℃.
V	Displacement volume, cm^3/rev.
VCR	Vapor compression refrigeration
$\dot{W}$	Power, kW.

Greek Letters

ρ	Density, kg/m^3
η	Thermal efficiency.
ω	shaft speed, rpm.

Chapter 1: Introduction

1.1 Background

The rising use of fossil fuels and the resulting release of greenhouse gases present a global concern that is both alarming and threatening, as it contributes to the escalating impact of global warming [1]. The estimated crude oil consumption was 86.4 million barrel per day in 2010, and is reached to 97.3 million barrels/day in 2022 [2]. This enormous usage of the fossil fuel combustion detrimentally adds to the overall emissions of greenhouse gases worldwide by around 65%. Coal, oil, and natural gas are accountable for 45%, 35%, and 20% of these emissions on a global scale, respectively [3]. This increased use of fossil fuels leads to a various environmental and economic challenges, including acid rain, the diminishing ozone layer, the dwindling of natural resources, and the increase in global temperatures [4].

A significant related problem is the ongoing rise in average surface air temperature, which has seen a sharp rise of over 0.5°C since the 1970s [5]. This trend has led to a higher demand for cooling systems like refrigeration and air conditioning, which currently use 20% of the world's fossil-fuel-powered electricity. It is expected that the consumption of these systems will almost double, from 3900 terawatt-hours (TWh) in 2018 to an estimated 7500 TWh by the year 2050 [6, 7]. Additionally, leakage of refrigerants into the atmosphere exacerbates the problem of global warming. The intricate relationship between fossil fuel consumption, greenhouse gas emissions, and refrigeration and air conditioning systems present a potential environmental threat. Recognising this, the Paris Agreement came into effect in November 2016, with the goal of keeping global warming below 2°C while promoting sustainable development [8]. Around 17% of the electricity utilised globally is consumed by cooling technology, particularly in the residential and

industrial sectors [9]. As a result, researchers are drawn to low-temperature heat sources like waste heat, solar, geothermal, and biomass, which are typically unused but have the potential to enhance both social and environmental sustainability.

1.2 Motivation

Waste heat at low temperature is available in abundant in various industrial sectors, however its direct conversion to cooling is challenge and needs appropriate and reliable technology like ORC. Conventionally, ORC system is indirectly connected to VCR system in which ORC system used to generate electricity which can be used to drive the compressor of VCR which poses challenges such as:

- Combined system losses are high due to multiple conversion of waste heat to compressor power and overall system become bulky.
- Combined system become complex due to presence of additional component like electric generator and coupling arrangements which makes system bulky. Thus, the cooling to weight ratio is low.
- Requires frequent maintenance due to multiple moving parts such as separate expander, couplings, generator, compressor which increases maintenance cost.

Alternatively, the ORC can be directly connected to drive the compressor of the vapor compression refrigeration (VCR) system. In direct coupling, there are two approaches: one involves connecting the expander shaft and the compressor shaft through a transmission unit, while the other entails mounting both the expander and compressor on a shared shaft.

These two arrangements have their own drawbacks as:

- Use of the transmission unit involve gear box arrangement like belt and drive or gear box, which could lead to losses in transmission, difficulties in maintaining system balance, and increased system complexity and costs.

- In a common shaft expander-compressor arrangement, the compressor and expander are enclosed in separate casing and hence expansion and compression process cannot be improved which eventually affect the thermal efficiency of the combined ORC-VCR system.

Overall, in both indirect and direct coupling of ORC system with VCR system subject to system complexity, loss of energy, low cooling to weight ratio, high maintenance, and capital cost. These problems can compromise the reliability of the ORC system. However, this situation offers a distinctive opportunity to enhance the compression and expansion processes by acquiring single rotor expander-compressor device to enhance the thermal efficiency of the ORC-VCR system by minimizing thermal losses.

1.3 Novelty of the study

This thesis explores the integration of vapor compression refrigeration and organic Rankine cycle systems, employing a novel single rotor expander-compressor for improved energy efficiency and reduced environmental impact. Through meticulous numerical modelling, validated by experimental data, it examines the influence of operational parameters on the combined system's performance. The study reveals that the system's thermal performance is significantly affected by the ORC's evaporator and condenser temperatures, alongside the rotor speed, impacting the cooling capacity and efficiency optimally.

Key findings highlight that optimal cooling performance is achieved with specific temperature settings, demonstrating the system's potential in enhancing energy utilization and minimizing greenhouse gas emissions. Additionally, the analysis of various refrigerants points to R123 and R1234yf as superior choices due to their efficiency and lower environmental footprint. The integration of ORC-VCR, along with strategic

refrigerant selection, offers a promising avenue for sustainable energy solutions, addressing pressing environmental concerns.

In essence, this research provides critical insights into ORC-VCR systems' efficiency and environmental benefits, laying the groundwork for further advancements in sustainable cooling and heating technologies.

1.4 Thesis outline

This thesis is organised in 7 chapters, Chapter 1 provides brief introduction to the research problem.

Chapter 2 presents detailed literature associated with the integration of ORC and VCR system. First, low temperature waste heat sources, use of waste heat, and available cooling technology have been presented. In addition, different heat driven refrigeration technologies have been discussed followed by detailed literature pertinent to ORC. This covers various aspect of VCR, ORC, and integrated ORC-VCR such as energy performance (first low analysis), exergy analysis (second low assessment). The conclusions emerging from the literature review and the objectives of the present work have been reported at the end of this chapter. This literature review serves as a valuable resource for comprehending the thermodynamic principles and concepts underpinning each of these technologies, their design methodologies and optimization strategies, and as a means to validate the ongoing research.

Chapter 3 deals with basic principles of combined ORC and VCR system. This demonstrates the principle of thermodynamics (first and second law of thermodynamics) and associated mathematical equations. These incudes model development using simulation tool, i.e., Aspen Plus modelling, mathematical equations for performance indicators such as coefficient of performance, heating to cooling efficiency, exergy

destruction and efficiency, and environmental impact. Moreover, this chapter addresses the validation of the single rotor expander-compressor device as well as combined ORC-VCR cycle with experimental data from previously published literature.

In chapter 4 the comprehensive energy analysis is reported consisting of studying the effect of ORC and VCR evaporation temperatures, the ORC condensation temperature, speed of the new expander-compressor device, degree of subcooling, degree of superheating on the ORC-VCR combined system. The energy performance indicators considered are heat-to-cooling ratio, thermal efficiency of ORC, EPR, COP of VCR, CPR.

Chapter 5 is devoted to a comprehensive evaluation of the exergy destruction associated with ORC-VCR system using single rotor expander-compressor. The effects of different parameters such as evaporation temperature of ORC and VCR, condensation temperature of ORC and speed at constant temperature heat source (water) on the overall exergy efficiency of the whole system are presented.

In Chapter 6 chapter, six working fluids have been chosen as potential candidates for an ORC-VCR integrated system, and they have been compared to one another in terms of their impact on energy performance, exergy destruction and efficiency and environment. After then, the technical characteristics of the working fluids are discussed. In this chapter, the same working fluid was used throughout both cycles of the ORC-VCR.

Finally, the overall conclusions of the present work and the recommendations for future work have been discussed in chapter 7.

Chapter 2: Literature Review

2.1 Introduction

This chapter describe the available low temperature waste heat sources, use of waste heat, and the available refrigeration technology. Moreover, refrigeration technologies that are driven thermally and their comparison with the conventional vapor compression refrigeration cycle have been discussed. Furthermore, the power cycles that can be a prime mover for the conventional vapor compression refrigeration cycle were outlined. Special attention has been paid to the organic Rankine cycle and described and discussed in detail including its advantages over other power cycles. Moreover, relevant literature to the combined organic Rankine cycle and vapor compression refrigeration cycle and available coupling methods to coupled them together have been presented. In addition, the single rotor expander-compressor (compander) was presented and its suitability to be a new method to combined organic Rankine cycle and vapor compression refrigeration cycle was discussed. Finally, the conclusions drawn from the reviewed literature and the objectives of the present study have been presented.

2.2 Low temperature waste heat sources

There are several energy resources from where heat can be recovered. These sources are classified based on temperature at which heat is available as presented in table 2-1. The focus of presented study is on ultra-low temperature (<120 °C) and low temperature (120 to 230 °C). This range generally available in internal combustion engine and waste heat at low temperature from the industrial process are attractive heat sources as they can easily be accessible for conversion even at low scale [10].

Table 2-1: Categories of waste heat based on the temperature range [10, 11].

Categories of waste heat	Ranges of temperature
Ultra- high temperature	>870 °C
High temperature	650-870 °C
Medium temperature	230-650 °C
Low temperature	120-230 °C
Ultra-low temperature	<120 °C

2.2.1 Internal combustion waste heat

In accordance with the principles of the second law of thermodynamics, it is important to recognize that not all the thermal energy generated during the combustion process can be effectively converted into useful mechanical work. It is estimated that approximately 55% of the energy contained within fossil fuels is lost as waste within the internal combustion engine. Among these losses, approximately 30-40% are attributed to energy dissipation in the form of exhaust gases, with an additional 15% being lost through heat dissipation in the engine's cooling system. The coolant fluid in the engine jacket has been observed to have temperatures ranging from 80-90°C [12].

2.2.2 Industrial waste heat

Waste heat is the thermal energy generated as a byproduct when a machine or any energy-consuming process performs its intended work. This release of waste heat is an inherent consequence of the principles of thermodynamics. It's important to note that waste heat possesses diminished usefulness compared to the initial energy source. Table 2-2 presents few industrial processes where heat is available in huge quantity but relatively at low temperature, especially close to ~ 230 °C [10].

Table 2-2: Industrial processes with low temperature waste heat [10, 13, 14].

Industrial Sector	Low-Grade Waste Heat Source	Temperature (°C)
Petrochemical	Stack gas from crude distillation	156
	Stack gas from vacuum distillation	216
	Exhaust from ethylene furnace	149

Iron/steel making	Waste gas from coke oven	200
	Blast furnace gas	450
	Exhaust gases from Cowper regenerators	250
	Exhaust gases from electric arc furnaces	204
Aluminium	Exhaust from aluminium casting with a stack melter	121
Food and drink	Extracted air from cooking with fryers or ovens	150–200
	Exhaust from drying with spray/rotary dryers	110–160
	Water vapor from evaporation and distillation	100
Textile	Dyed wastewater from drying	90–94
	Stenter exhaust for fabric drying and finishing	180
	Wastewater rejected from heat exchangers	58–66
Paper	Waste steam from slag flushing in furnace	95–100
	Wastewater from slag flushing in furnace	65–85
	Cooling water from furnace wall cooling	35–45
Cement	Exhaust from cement kilns using 5- or 6-stage preheaters	204–300
	Hot air discharged from clinker coolers	100
Chemical and Pharmaceutical	Distillation processes	100–300

2.3 Use of waste heat

There are several applications where low-grade waste heat can be used as a heat source in heating, cooling and power generation as presented in table 2-3. This thesis focuses on utilization of the low-grade heat for cooling application. Low-grade thermal energy can be harnessed for cooling purposes by incorporating it into an absorption refrigeration system, and it can also be used in an Organic Rankine Cycle (ORC) for both cooling and power generation applications [15, 16]. The adsorption refrigeration system is generally appropriate for large-scale use because of its considerable size, operational intricacy, and relatively low thermal efficiency. On the other hand, the Organic Rankine Cycle (ORC) is a developed technology that exhibits considerable promise in transforming low-temperature heat sources into useful energy, rendering it appropriate for smaller-scale applications [17-19].

Table 2-3: Integrated and developed WHR technologies based on temperature range[11, 13, 20-22].

Category	Integrated Technologies	
	<120 °C	**120–250 °C**
Waste heat to heat	Heat pumps	Heat pumps
	Absorption HP	
Waste heat to cold	Absorption chiller	-
Waste heat to power	ORC	ORC
	Thermoelectric	Kalina cycle
		Thermoelectric
Heat Exchange	Shell, tube and plate heat exchangers	Shell, tube and plate heat exchangers
	Air preheaters	Heat pipe exchanger
	Direct contact water heaters	Metallic heat wheel
	Non-metallic heat exchangers	Convection recuperator

The organic Rankine cycle (ORC) represents a specific thermodynamic cycle, distinct from the conventional Rankine cycle. It derives its name from its utilization of an organic fluid with a relatively high molecular mass, in contrast to water, and possessing a lower vaporization temperature. This unique fluid characteristic enables the ORC to harness heat from lower-temperature sources, including biomass combustion, industrial waste heat, geothermal energy, and solar ponds. The ORC efficiently transforms low-temperature heat into productive work, which can subsequently be used to drive the compressor [23].

2.4 Available refrigeration technologies

There are several refrigeration technologies available, some of them are commercially available in the market and few of them are under research and development [24]. This includes refrigeration systems based on vapor compression technologies and non-vapor compression technologies. The classifications of non-vapor compression technologies are presented in figure 2-1.

Some of these technologies are thermally driven which includes Evaporative Liquid Desiccant, Ground-Coupled Solid Desiccant, Stand-Alone Liquid Desiccant, Stand-Alone Solid Desiccant, Absorption, Adsorption, and Ejector. The major drawback associated with these technologies their lower performance compared to the well-established conventional vapor compression refrigeration technology. Moreover, there is an ambiguity on cost, efficiency, reliability, maintenance requirements, occupant comfort, and safety associated with this thermally driven refrigeration technology.

Meanwhile, vapor compression systems, which utilize electrically driven compressors, have gained popularity and become the dominant technology in heating, ventilation, and air conditioning (HVAC) due to their scalability, reliability, use of non-toxic and non-flammable refrigerants, reliance on electricity, and their relatively compact size[24]. In VCR system, the refrigerant systematically undergoes phase changes to achieve desired cooling effect at the expense of high-grade electricity to drive the compressor. Alternatively, the compressor of the VCR can be drive by connecting it to ORC cycle which recover the heat from waste heat sources and covert it to work required to drive the compressor.

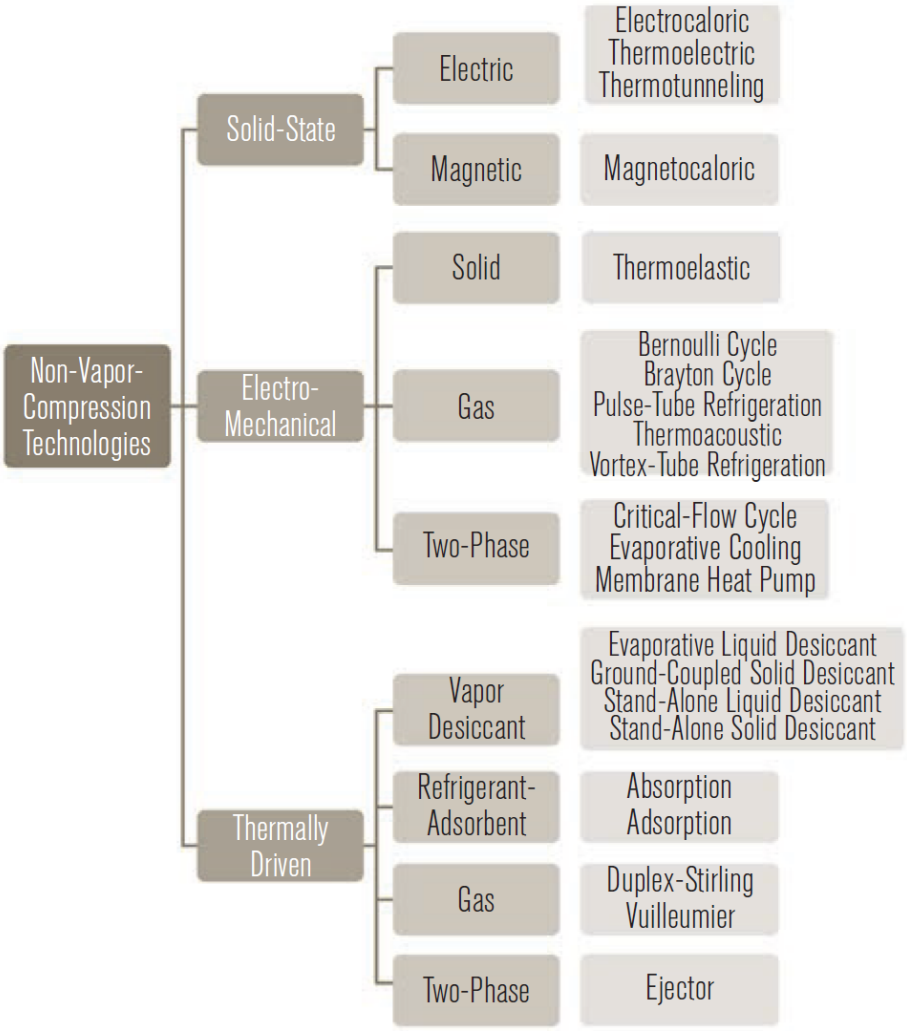

Figure 2-1: Non-vapor compression refrigeration technologies [24].

2.5 Thermally driven refrigeration technologies

This section described the thermally driven refrigeration technologies that have the ability to convert heat to cooling directly from low temperature heat sources. These technologies include absorption refrigeration, adsorption refrigeration, and desiccant refrigeration. Their working principle, challenges, and achieved performance are discussed. However, there are some refrigeration technologies used to convert heat to cooling but that required power cycle to convert the heat to mechanical power then supplied to the refrigeration cycle such combined ORC-VCR.

2.5.1 Absorption Refrigeration

The absorption refrigeration cycle is consisting of processes that can produce cooling effects by using mixture of two or more working fluids with the help of some addition of heat. Basically, it is systematic arrangement of several heat exchangers to achieve desired cooling effect. In absorption refrigeration the primary working fluid is refrigerant, and the secondary working fluid is the absorbent. The absorbent is used to circulate and absorb the refrigerant. Figure 2-2 shows the basic working principle of the absorption refrigeration cycle. This cycle consists of an evaporator, expansion valve and condenser very similar to the compression vapor cycle. However, in the absorption cycle the thermal compressor replaced the conventional mechanical and electrical compressor. The cycle starts with a thermal compression in the absorber where the liquid mixture of the refrigerant and the absorbent has high concentration of the absorbent. The refrigerant in vapor phase leaves the evaporator to be absorbed by this mixture to increase the concentration of the liquid refrigerant before it being pumped to the high-pressure side. The absorber needs to perform heat rejection to a lower temperature sink because during the absorption process heat is released. After the mixture with high concentration of the refrigerant pumped to the high-pressure side, it inters the generator where heat addition process is performed. In this process, the refrigerant being vaporised moved to the condenser, while the rest of the mixture with high concentration of the absorbent is expanded in the throttling valve to be sent back to the low-pressure side to enable the cycle to repeat. Absorption refrigeration cycle equipped with two generators, known as double effect units, demonstrate superior efficiency when compared to single-effect counterparts. However, as the number of effects increases to three or more, the gains in performance become progressively less significant [25-27].

Choosing an appropriate pair of refrigerant and absorbent is an important key point to complete the absorption process successfully [28]. The pair of working fluid is selected in such a way that absorbent has great affinity towards refrigerant. Ammonia-water and lithium bromide-water are the most commonly used pairs in absorption refrigeration cycles. For low temperature application below 0℃, ammonia (refrigerant) and water (absorbent) pair are used [29]. In the other hand, lithium bromide (absorbent) and water (refrigerant) are used for cooling application over 4℃ [30].

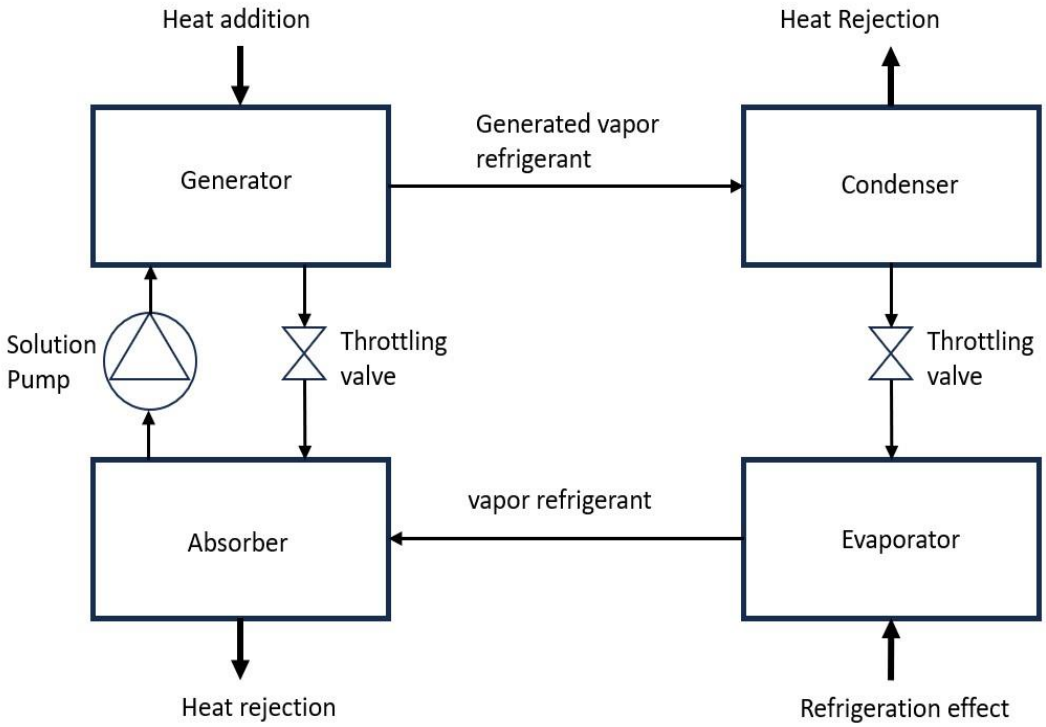

Figure 2-2: Schematic diagram of the absorption refrigeration cycle.

Although, there are many working fluids have been studied in absorption refrigeration such as R22 and R21 and have been suggested due to their high solubility in many organic solvents. Dimethly Ether of Tetracthylene Glycol (DMETEG) and Dimethyl Formamide (DMF) are examples of the solvents that have stood out. However, Ammonia-water and lithium bromide-water reported to be the most successful working fluids for absorption refrigeration [30-32].

Water-ammonia has been used mostly for heating and cooling application. Water and ammonia have more stability for wide range of operation temperature and pressure. The high latent heat of vaporization gives the ammonia the priority to perform an efficient performance of the system. As the freezing point of ammonia is -77℃, it has the ability to work in low temperature purposes [33]. Due to the volatility of the water and ammonia, the cycle should include one more component which is the rectifier. The purpose of this component is to separate water from ammonia, as water tends to evaporate along with ammonia in the process because of low difference in their boiling point. Without a rectifier, water would accumulate within the evaporator, thereby causing a detriment to the overall system performance [25]. There are additional drawbacks, including its elevated pressure requirements, toxicity, and corrosive impact on copper and copper alloys [34].

Absorption refrigeration achieved coefficient of performance (COP)

A triple-effect ammonia-water cycle achieved a COP of 1.9 with a generator temperature of 227°C, condenser temperature of 30°C, and evaporator temperature of 10°C [35]. A double-effect parallel flow ammonia-water cycle reached a COP of 1.5 with a high generator temperature of 192°C, condenser/absorber temperatures of 42°C, and evaporator temperature of 10°C [36]. A single-effect ammonia-sodium thiocyanate cycle achieved a COP of 1.0 with generator, condenser, absorber temperatures of 120°C, 40°C, 40°C ,respectively and an evaporator temperature of 10°C [37]. A single-effect ammoina-water-TiO2 nanofluid cycle attained a COP of 1.0 with a generator temperature of 120°C, condenser/absorber temperature of 40°C, and evaporator temperature of 2°C [38]. A hybrid absorption-compression cycle reached a COP of 1.8 with a generator temperature of 120°C, condenser/absorber temperatures of 30°C, and evaporator temperature of -10°C [28]. In general, the maximum COPs are attained with relatively high generator

temperatures (120°C or above), low condenser and absorber temperatures (30-40°C), and low evaporator temperatures (0-10°C). Multi-effect and hybrid cycles require the highest generator temperatures to achieve their peak COP performance [28].

Absorption refrigeration limitations:

Absorption refrigeration systems employing binary working pairs have gained significant attention recently, with extensive research focusing on their exceptional attributes, including their superior thermal conversion efficiency, robust operating stability, and reliability [39]. However, absorption refrigeration systems still hold a relatively smaller market share compared to the conventional vapor compression refrigeration systems commonly found in traditional refrigeration applications. This disparity can be attributed to the constraints posed by their limited choice of binary working fluids and the comparatively lower overall system performance in comparison to vapor compression refrigeration [40].

2.5.2 Adsorption Refrigeration

Sorption refrigeration technologies involve both absorption and adsorption refrigeration systems, both recognised and studied within this field. These systems are characterised by their reliance on heat as the primary driving force for generating the required refrigeration effect, which distinguishes them from traditional mechanical vapor-compression units, earning them the title of compressor-free systems.

It's important to note that adsorption refrigeration systems can be powered by low-grade heat sources, with a minimum temperature requirement of 50°C to start the refrigeration cycle [41]. In contrast, absorption refrigeration systems require a substantially higher minimum temperature of 90°C for the successful start and operation of the refrigeration process [25].

Absorption refrigeration systems are distinguished by their cyclical nature, which allows for continuous operation. In contrast, basic adsorption refrigeration systems operate in a batch-type process. To address this operational disparity, an advanced approach involves the utilization of multiple adsorbent beds, enabling a nearly continuous operation. It's important to note that adsorption refrigeration systems employ solid adsorbents, while absorption refrigeration systems use liquid absorbents [25].

Figure 2-3 shows the basic working principle of the adsorption refrigeration cycle. In order to produce refrigeration effect, a pair of solid-refrigerant known as (adsorbent-adsorbate) is utilised by the adsorption refrigeration cycle.

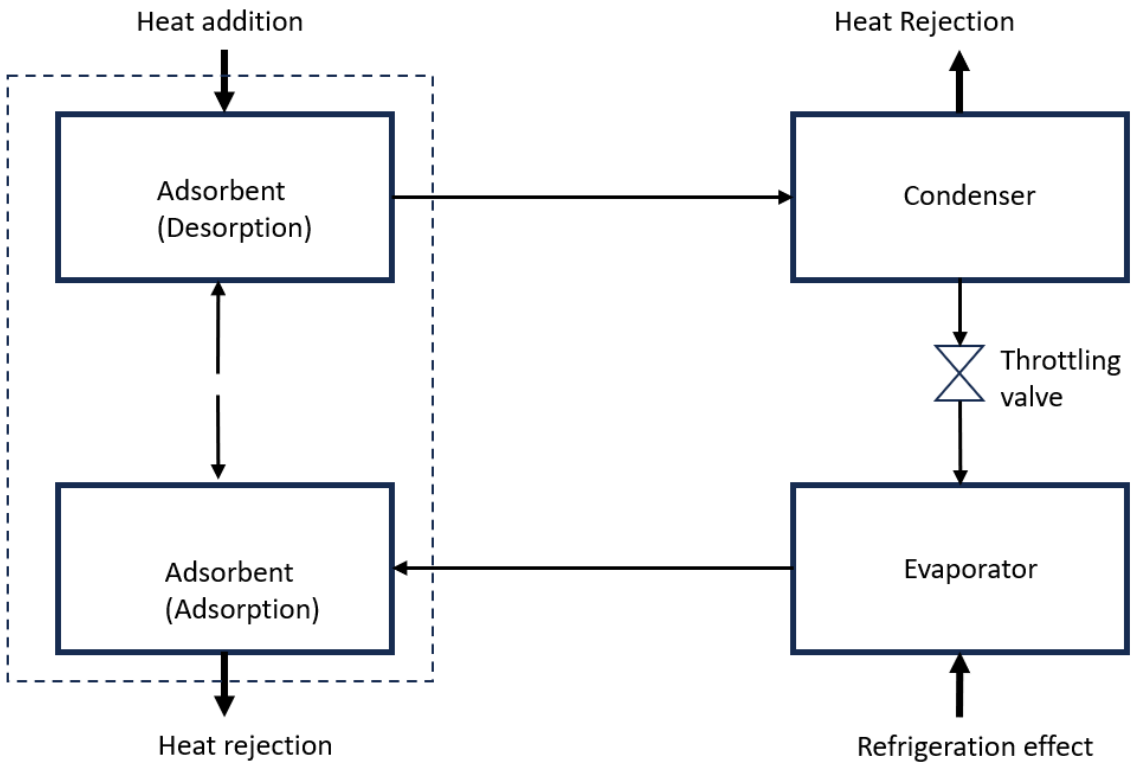

Figure 2-3: Schematic diagram of the adsorption refrigeration cycle

The cycle starts by adding heat from external source to the solid adsorbent that saturated with the refrigerant from the previous run. This heat addition allows the solid adsorbent to desorb the refrigerant in vapor phase. Once the condenser pressure is reached, the refrigerant will flow to the condenser to reject heat which will change the refrigerant

phase to liquid. The liquid refrigerant will be expanded through the expansion valve to reach the desired evaporation pressure corresponding to desired evaporating temperature. The liquid refrigerant will enter the evaporator and absorb heat from the refrigerated zone in order to get refrigeration effect. The vapor refrigerant flows to the second bed where it being adsorbed. In a cyclical way, the desorbing and adsorbing beds interchange roles to achieve system regeneration. Within the multibed adsorption arrangement, a notable advantage arises from the capacity for effective heat and mass recovery between the beds. This feature plays a pivotal role in significantly elevating the overall performance of the system [42].

The foundation of an adsorption refrigeration system relies significantly on the attributes of its working pairs. To align with the fundamental principles and operational characteristics of such systems, the adsorbent material should possess certain critical characteristics. These include a substantial adsorption capacity, a notable sensitivity of adsorption capacity to temperature fluctuations, a relatively flat desorption isotherm, and a high degree of compatibility with the chosen refrigerant [42].

Conversely, when considering the refrigerant component, the criteria are quite analogous to those employed in vapor compression refrigeration systems. This encompasses requirements such as a high latent heat per unit volume, an appropriate freezing point and saturation vapor pressure, non-toxicity, non-flammability, resistance to corrosion, and robust thermal stability, among others. However, it's important to acknowledge that, in practice, finding working pairs that fully and seamlessly meet all these stringent requirements can prove to be a challenging endeavour [43].

There are some working pairs are commonly used in adsorption cycle such as silica gel-water [44, 45], zeolite-water[46], zeolite-ammonia[47], activated carbon-ammonia[47], and activated carbon-methanol[48].

Adsorption refrigeration achieved coefficient of performance (COP)

A study was conducted to investigate the performance of the adsorption refrigeration cycle the utilised activated carbon-ammonia working pair. The study compared three different configurations; one bed single stage, two bed double stage, and three bed triple stage. The heat source temperature was varied from 50°C to 100°C while the condenser temperature was in range of 20-40°C. The results showed the evaporation temperature can be in the range of -25 to 15°C while the maximum COP was 0.55 [49]. Silica gel-water pair was also investigated in another study when the heat source temperature was 85°C and the condenser temperature 30°C, the evaporation temperature was 7°C and the reported COP is 0.25 [50]. An adsorption refrigeration system was analysed to produce both cold water and cold air. The heat source temperature was varied from 50°C to 80°C while the coolant temperature was 25°C. The maximum COP reached was 0.238 under heat source temperature of 60°C [51]. Moreover, a study conducted to utilise the waste heat from a truck coolant loop when the coolant temperature was 90°C. Zeolite-water working pair was used in the examined adsorption refrigeration system. The results showed that the maximum COP was 0.6 while the evaporation temperature was 10°C [52].

Adsorption refrigeration limitations:

The adsorption refrigeration system has the ability to produce refrigeration and cooling effects together with low grade heat source with lower temperature. However, the adsorption refrigeration system considered as a bulky and heavy construction. Moreover, it is costly to build, and the batch operation way is still a challenge. In addition, the adsorption COP is very low comparing it to the vapor compression system that popular in refrigeration and air conditioning systems [53].

2.5.3 Desiccant cooling system

Desiccant cooling is a technology that has the ability to utilise the low temperature heat source in order to produce cooling effect. It can be driven with heat source temperature starting from 60°C to 95°C [9]. As shown in Figure 2-4, desiccant cooling involves the dehumidification of incoming air by its passage through a desiccant material, subsequently achieving the desired indoor temperature by drying the air. In order to maintain the system's continuous operation, the moisture adsorbed or absorbed by the desiccant material must undergo a regeneration process. This regeneration process is essential to prepare the desiccant material for effective moisture adsorption in the subsequent cycle. The regeneration process is accomplished by elevating the temperature of the desiccant material to a level specific to the nature of the desiccant in use. In desiccant cooling the water is employed as the refrigerant. Desiccant systems have the versatility to employ either solid or liquid desiccants. Solid desiccants frequently chosen for these applications encompass activated silica gel, titanium silicates, alumina, natural and synthetic zeolite, molecular sieves, among others. Conversely, liquid desiccants encompass substances such as lithium chloride, lithium bromide, tri-ethylene glycol, calcium chloride, and potassium formate [54-56].

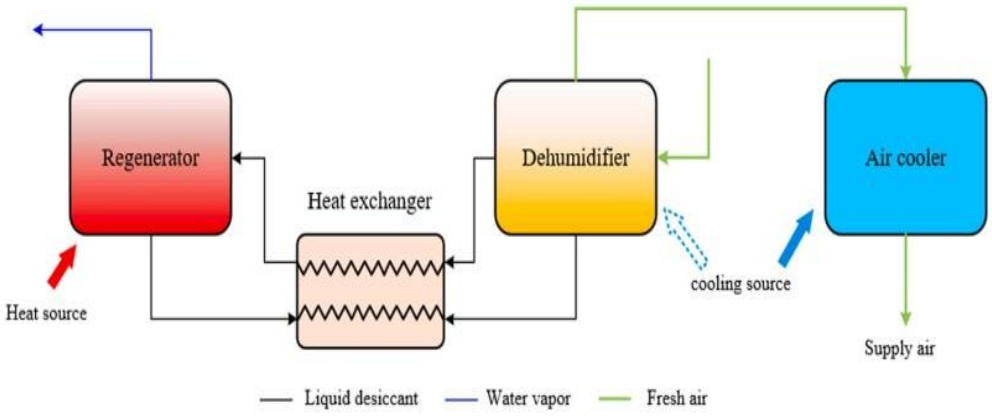

Figure 2-4: Schematic diagram of liquid desiccant system [57].

Desiccant cooling system performance achieved.

The performance of a two stages desiccant cooling system integrated with evacuated glass tube solar air collectors was assessed in a hot and humid climate in China [58]. The findings indicated that the COP of the system could achieve value of 1, while the supplied air temperature remained at approximately 18°C with a humidity level of 60%. Notably, the two stages desiccant cooling System required a significantly lower regeneration temperature compared to the two stages desiccant cooling System. Another study investigated the feasibility of two-stage solar desiccant cooling systems as alternative, energy-efficient solutions for buildings in Malaysia. The study results showed that the solar desiccant cooling system, operating in both ventilation and recirculation modes can improved the room conditions with temperature and relative humidity levels close to 25.5°C and 61%-66%, respectively. In addition, the solar hybrid desiccant cooling system COP could reach a value of 0.84 [59].

Desiccant cooling system limitations

Desiccant cooling systems are considered to be high costly to build. Moreover, the materials used in desiccant cooling system are corrosive that can led to damage in the system component and required more maintenance. The presence of liquid desiccants entrained within the supply air stream has the potential to result in substantial health hazards for building occupants. Significant-sized pumps are necessary to manage substantial quantities of liquid desiccants which will consume more power [56, 60].

In addition, there is another thermally driven refrigeration system called ejector refrigeration described here briefly, and it is considered as a thermomechanical system. Ejector refrigeration systems offer the potential to harness low-grade energy sources to achieve cooling effect. However, this system has faced challenges, primarily stemming from their notably low COP and sensitivity to environmental conditions. Their inflexible operational requirements mean they struggle to provide the desired cooling temperatures

under standard ambient conditions without demanding excessively high driving temperatures, resulting in reduced overall efficiency [61-65]. Due to these limitations, ejector refrigeration systems were excluded from comparisons with other thermally driven cooling technologies.

Overall, thermally driven refrigeration systems are struggling with lower coefficient of performance and complex in nature. Moreover, the batch wise operation of thermally driven adsorption system is another challenge. Alternatively in the field of refrigeration technologies, mechanical vapor compression refrigeration, characterized by the utilization of a compressor and a volatile working fluid within a closed-loop system, stands out for its exceptional COP when applied in real-world scenarios. This COP superiority places it ahead of existing refrigeration technologies. Mechanical vapor compression refrigeration enjoys widespread adoption across various industrial sectors, such as automotive, commercial, and household applications. Its extensive use highlights its reputation as an efficient and versatile cooling solution for meeting diverse needs within these sectors [66].

2.6 Vapor compression refrigeration

In real-world applications, vapor-compression refrigeration systems hold the position as the most prevalent and widely adopted refrigeration systems [67, 68]. The vapor compression refrigeration systems involve the working fluid (refrigerant) undergoing phase changes as a fundamental part of its operation. As shown in Figure 2-5, the vapor compression refrigeration delivers the refrigeration effect in the process where the refrigerant absorbs the heat from refrigerated or cooled zone through the evaporator. In this process, the refrigerant will change phase to saturated vapor or superheated vapor. Then, the refrigerant undergoes a compression process in the compressor, in which its pressure increased to the condensation pressure. It will pass through the condenser, in

which the refrigerant will perform heat rejection and the change the phase from vapor to saturated or subcooled liquid. The liquid refrigerant flows through the expansion valve, in which its pressure will decrease to the evaporation pressure and the phase changes to partially vapor. The refrigerant will flow back to the evaporator and the cycle is repeated.

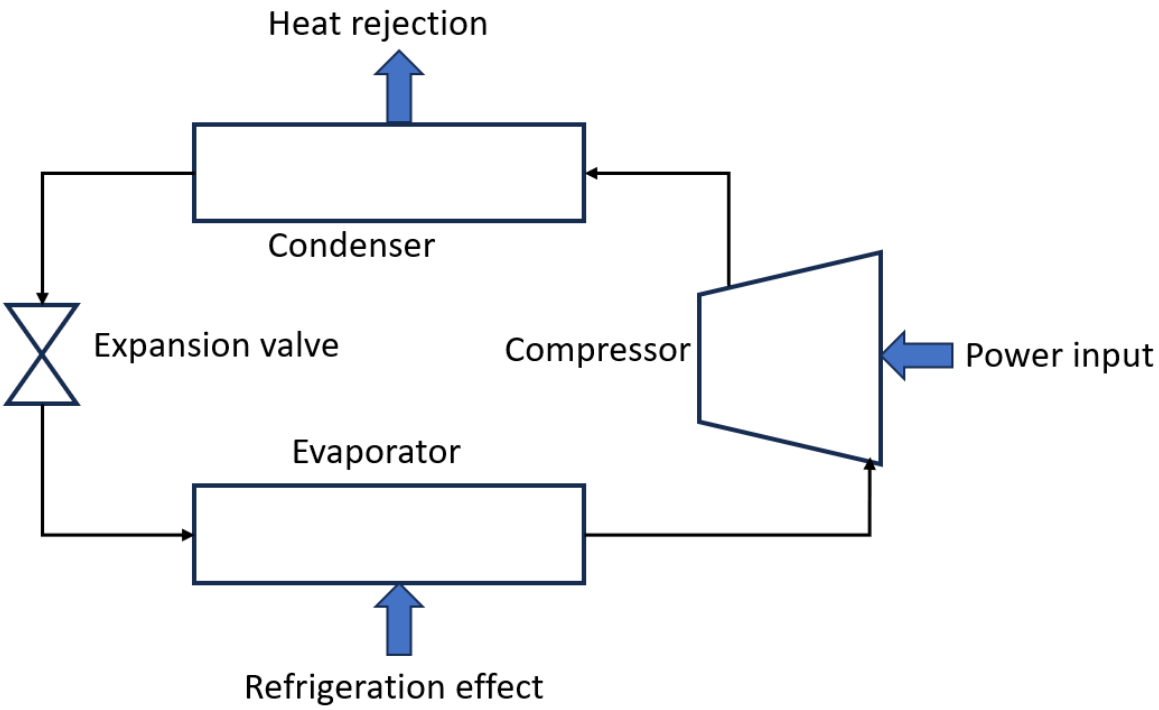

Figure 2-5: Schematic diagram of vapor compression refrigeration cycle.

Mainly in the vapor compression refrigeration systems the compressor is driven by electric motor supplied by the grid electricity in buildings and industries. However, there are another prime mover such as steam turbines, internal combustion engines, and Organic Rankine cycle which can be used to drive the vapor compression refrigeration system.

2.6.1 Vapor compression refrigeration prime movers

Steam turbine

The steam turbine, known as the Rankine cycle, stands as one of the time-honoured and well-established heat engines. In this cycle, water takes on the role of the working fluid

and undergoes a process of boiling and superheating, typically driven by a high energy heat source such as fossil fuels or nuclear reactions. Subsequently, this high-energy fluid is directed through the turbine, where it can experience expansion in either a single or multiple stages to produce mechanical power. The turbine's shaft is intimately linked with an electrical generator, facilitating the conversion of this mechanical energy into electrical power. However, in case of the steam turbine coupled to vapor compression refrigeration, the mechanical power produced by the turbine shaft is directly connected to the compressor. Simultaneously, the high-temperature, low-pressure water vapor is subjected to condensation process within the condenser [69].

Presently, in some commercial chillers in which steam turbine used as prime mover to drive vapor compressor cycle exclusively employ R134a as the refrigerant [70]. These systems are most effective when supplied with superheated steam, ranging from 95 kPa to 1,150 kPa, with temperatures reaching up to 315°C [71]. The development of thermal performance in steam turbine refrigeration systems is closely linked to the increase of steam pressure and superheating.

Steam, as a working fluid, exhibits a relatively low density, resulting in substantial volumetric flow rates, and a low molecular weight, yielding significant energy release during expansion [72]. Consequently, multiple stages and large diameter blades are required in steam turbine to have speed match with the compressor to increase the system efficiency [73].

In contrast to other thermally driven refrigeration technologies explored in this chapter, vapor compression refrigeration driven by steam turbine does not have the ability to utilis the heat from the waste heat sources directly. Instead, waste heat steam generator or steam boiler must be equipped in order to convert water to steam [21]. Due to the high difference in the water density between liquid phase and gas phase, large size boiler or

steam generator is required in order to efficiently produce the steam [73]. In addition, similar to multi-effect absorption chillers, steam generation technologies require waste heat sources at temperatures exceeding the range commonly associated with low temperature waste heat sources.

Internal Combustion Engines ICE

Using internal combustion engines as a prime mover for the vapor compression refrigeration is mostly common in the refrigerated trucks [74]. The compressor within a refrigeration system is typically powered by the engine, increasing the engine load that significantly leads to an increase in fuel consumption and the emission of higher quantities of exhaust gasses [75]. It is noteworthy that refrigeration systems employed in refrigerated trucks operate under significantly more challenging environmental conditions when compared to stationary systems. As a result, these mobile refrigeration units tend to exhibit a diminished coefficient of performance (COP). The COP, denoting the ratio of refrigerating capacity to power consumption, exhibits variability in response to fluctuating conditions. For example, the VCR COP spans a range from approximately 0.5 when working to maintain a space temperature of -20°C, to approximately 1.5 to 1.75 when it works to maintain a space temperature of 3°C, all while the surrounding environmental temperature remains at 30°C [76, 77].

2.7 Organic Rankine Cycle

Organic Rankine Cycle is one of thermodynamic cycles that convert heat into work. ORC works on the same principle of Rankine Cycle. However, the major difference between conventional Rankine cycle and Organic Rankine cycle that the former uses water while the latter uses organic fluids such as refrigerants instead of water. Figure 2-6 presented

the ORC configuration that consists of condenser, pump, evaporator, and expansion device. Firstly, the working fluid is pressurised by the pump at constant entropy and pumped to the evaporator (process 1-2). Next, the working fluid is boiled and vaporised in the evaporator at constant pressure (Process 2-3). Then, the working fluid is expanding in an expansion device at constant isentropic and the mechanical power produced is used to drive the refrigeration compressor (Process 3-4). Finally, the working fluid is condensing at constant pressure in the condenser and changed to liquid phase (Process 4-5), and the cycle is repeated. For the VCR side, the compressor increases the vapor refrigerant pressure, the high-pressure refrigerant enters the condenser and fully condensed to liquid followed by a throttling process. The refrigerant leaves the throttle valve to the evaporator where the cooling effect in produced. Finally, the refrigerant leaves the evaporator to the compressor to repeat the cycle.

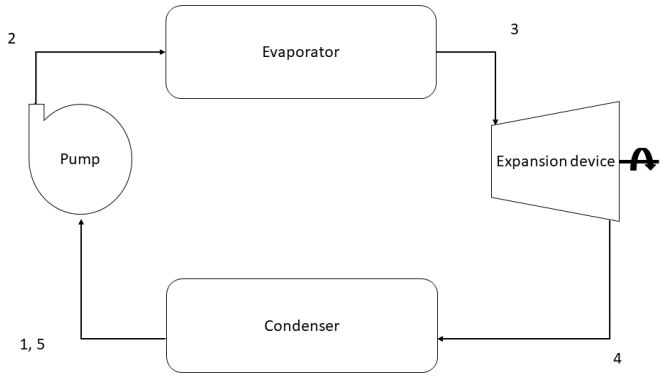

Figure 2-6: Schematic represent the typical Organic Rankine Cycle

The most characteristic of the fluids used in ORC that their boiling point is relatively low. Furthermore, that's lead to a low latent heat of vaporization. The low boiling point fluids have the advantage to exploit the low-grade heat energy better than the water [78].

Larjola [79] concluded that low to medium grade heat sources can be used as a source of useful power and the foremost viable cycle to do that is the ORC. The Organic Rankine

Cycle is used to utilise the low-grade temperature heat source. Due to the low heat source temperature the ORC has a lower Carnot efficiency than the cycles using higher heat source temperature. Dai, et al. [80] implemented an optimisation of an ORC to exploit thermal energy from 145°C heat source and the cycle efficiency reach to 12%. Liu, et al. [81] presented an off-design numerical investigation of an Organic Rankine cycle system to work as waste heat recovery, the highest efficiency achieved was 6.47% when the temperature of the heat source was 200°C. Shao, et al. [82] achieved experimentally an efficiency of 5.5% while the heat source temperature was 140 °C. Miao, et al. [83] built an ORC rig and the working fluid was R123 and the temperature of the heat source was 150°C, the cycle efficiency achieved was 6.1%. Park, et al. [84] conducted a review on the experimental results of ORC, the authors show that the maximum efficiency has been achieved experimentally was around 12%.

The literature mentioned above indicate that the ORC efficiency appears to be relatively low. Also, the experimental results indicate lower efficiency than the thermotical investigation results. As a reason of the low efficiency of the ORC utilising low grade temperature heat source, any improvements in the efficiency can have a significant consequence on the viability of the system.

2.7.1 Working Fluid in Organic Rankine Cycle

The selection of the working fluid plays a significant role in the ORC efficiency and associated impact on the environment. The working fluids employ in the ORC system should have low global warming potential (GWP) and low ozone depletion potential (ODP) [85]. As reported by Lee, et al. [86], the working fluid's boiling point, critical pressure and molecular weight have an observable effect on the thermal efficiency of ORC. Mostly, the organic fluids used are hydrocarbons and refrigerants. Organic fluids

have exceptional benefits more than water because they can change phase by low heat source temperatures. That gives Organic Rankine cycle the ability to convert low to medium grade heat source to useful work. [87].

In contrast to traditional Rankine cycles, Organic Rankine cycle will require a relatively small components size because the organic fluid have high density. When the density goes high the volumetric flow ratios will go low and, afterward, the system components size will be relatively smaller. In situations where the heat source temperature is very high, its useful to use water without taking in account the thermal decomposition because of the water thermal stability [88]. By contrast, in situations where the heat source temperature is low, its useful to use organic fluids because they have a low boiling point. The characteristic of low boiling point allows to change phase at low temperature.

The selection of working fluid is depending on the application and the cycle conditions. As can be seen in Figure 2-7, working fluids are categorised into three types: dry, isentropic, and wet. This classification is based on the shape of the saturation line on T-s diagram [89]. Isentropic and dry fluids have huge benefits for expansion machines because they still superheated at the expander outlet and avoid the working fluid condensation which cause damages to the internal parts of expander during the expansion [90]. Also, isentropic and dry working fluids don't require a superheating before the expansion process, that will lead to a smaller evaporator [91]. However, if the fluid is too dry, the vapour will leave the expander after the expansion process with extensive overheat, which is a wasted energy and will increase the cooling load in the condenser [92]. If the expansion ratio is relatively high wet fluids have the issue that the condensation occur during the expansion process which will lead to damages inside the expander and consequently the isentropic efficiency of the expander will decrease [93]. Thus, the wet working fluids must be superheated before entering the expander to avoid

condensation during the expansion process. Therefore, it is not recommended to use wet fluid in the ORC [94].

Working fluid with low liquid specific heat, high density, and high latent heat are desirable, fluids with high density and latent heat utilise more thermal energy during the evaporation process and that will decrease the heat exchanger size and the working fluid flow rate, and power consumed by the pump [95]. On the contrary, yamamoto, et al. [96] recommended that best working condition can be achieved when the working fluid is a saturated vapor in the beginning of the expansion process, that can happen with the low latent heat working fluid. Chen, et al. [78] proposed a theoretical analysis of the enthalpy change during the expansion process, the results show that the high latent heat working fluids can produce high output power. Additionally, working fluids that have high density require a relatively smaller system component. Above discussion implies that the working fluids with high density and latent heat and low liquid specific heat are correlated to a high output power.

Hung [94] examined and compared the efficiency of ORC using different dry fluids. benzene, toluene, p-xylene, R113 and R123. The results show that benzene has the lowest efficiency, while p-xylene presented the highest efficiency. R123 and R113 presented higher performances than the other two in terms of recovering low-temperature waste heat. Zhang, et al. [97] demonstrate that R218, R125 and R41 achieve the maximum amount of energy in case of waste heat recovery. R600a, R600, R245fa, R123 and R245ca produce the maximum values of thermal and exergy efficiency. In case of heat transfer area, R152a, R134a, R600 and R143a need the smallest evaporator and condenser. Dai, et al. [80] reported that the maximum heat transfer was achieved by using R236ea, when the heat source temperature was 145 °C. But the system reach the maximum first law efficiency by utilising R113. There is no single fluid can be selected as the better working

fluid, because the selection criteria depend several considerations such as the heat source characteristics and the cycle conditions.

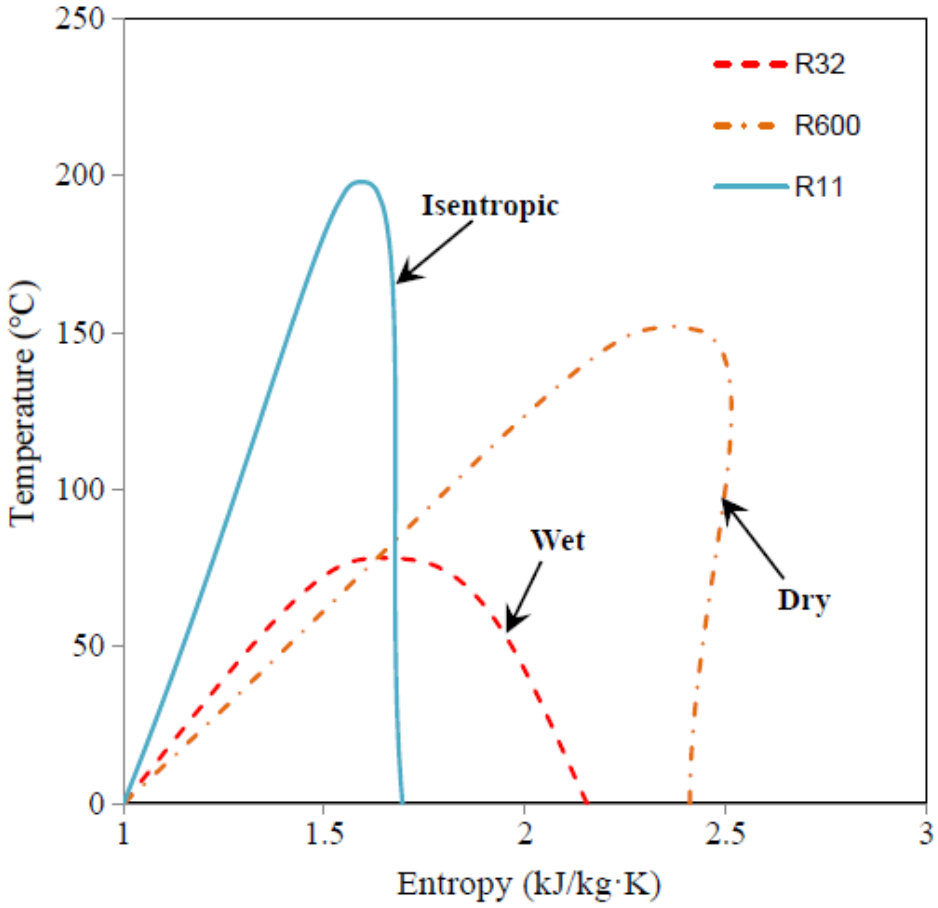

Figure 2-7: Categories of working fluids [89].

2.7.2 Expansion machines in Organic Rankine Cycle

In organic Rankine cycle, the expansion process occurs in the expander machine has an important effect on the cycle efficiency and the produced power. There are two categories of expansion machines used in ORC. Firstly, the velocity category such as the radial and axial turbines. Secondly, the positive displacement expanders such as scroll expander, screw expander, rotary vane expander, and piston expander [98, 99]. For low speed and power applications, positive displacement expanders are used more than turbines [100]. Positive displacement expanders have a defined volume change between their input and output, resulting from the geometric limitations of the device.

In contrast, turbomachines, which commonly include radial or axial flow turbines, generate shaft work through rotational force, derived from a pressure difference across their blades. Turbines are designed with a gap between the blades and the casing to allow rotation. One of the drawbacks of turbines is the leakage occurs at these blades tips which led to inefficient expansion. As the size of the turbines decreases, the power loss from this leakage increases which represent significant decrease in the output power [101]. This makes positive displacement expanders more suitable for smaller ORC systems due to factors like higher pressure ratios, slower rotational speeds, and lesser flow rates compared to turbomachines [102]. Another advantage of positive displacement devices is their resilience against liquid droplet formation during expansion, a process that can severely damage turbine blades by causing erosion [98]. This necessitates keeping the working fluid in a superheated state when working with turbines. In terms of power output, scroll and vane machines typically function within the 1-10 kW, screw expander works between 15-200 kW, reciprocating pistons fall in the 20-100 kW, and turbines operate starting from hundreds of kW and can reach into the Mega Watt range [23].

2.8 Combined ORC-VCR

The concept of combining ORC with VCR is accomplished by connecting the ORC expander with the VCR compressor through a mechanical coupling such as gears, belts, or shafts as shown in Figure 2-8. The most feature of ORC-VCR is the ability to produce electricity when cooling or heating is not needed.

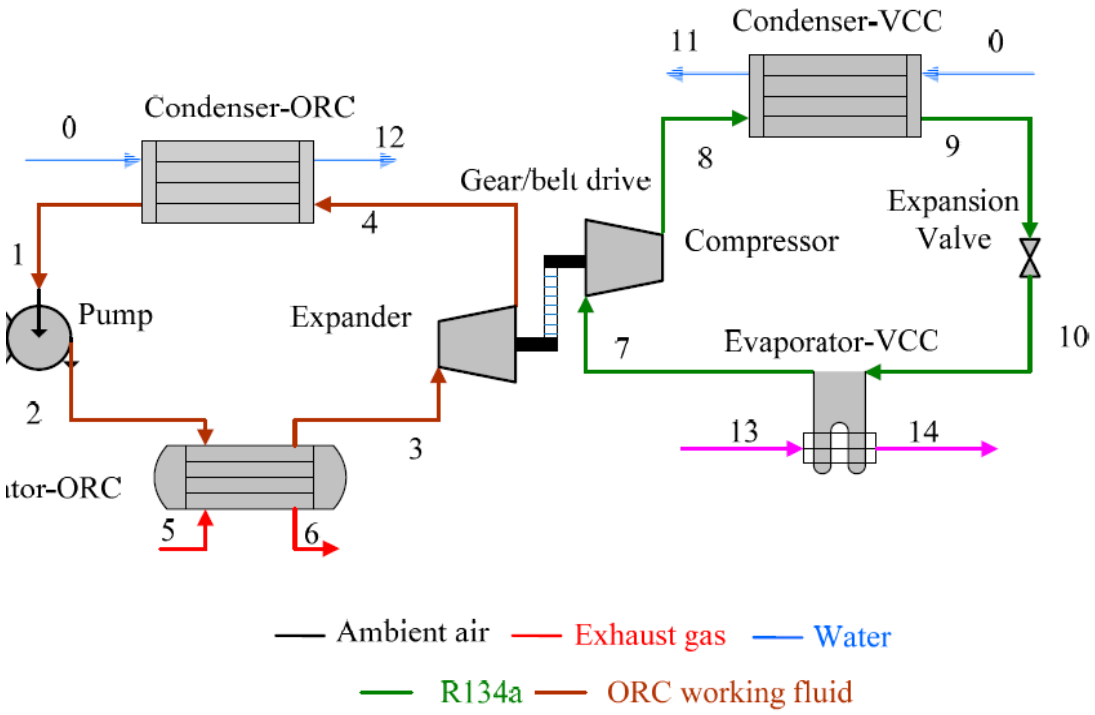

Figure 2-8: Schematic diagram of combined ORC-VCR [103]

Prigmore and Barber [104] developed and demonstrated a 1-kW solar-powered ORC system to electrify and/or drive a 3-ton air condition unit. An ORC uses R113, while an air conditioner works with R12 and a solar collector providing hot water at 102 °C. They found that considering 30% solar collector efficiency, the coefficient of performance and system thermal ratio of the combined Rankine/air conditioning system are 0.71 and 0.21, respectively. Lior [105] studied a solar powered combined ORC-VCR cycle for cooling and heating applications. They revealed that the system can save up to 60% of energy compared to an electrically powered system with the same heating and cooling requirements. Wang et al. [106] observed that the overall COP of an integrated ORC-VCR

cycle can reach 0.66 under extreme conditions where the outdoor temperature at 48.9 °C . Chahartagi et al. [107] carried energy and exergy analysis of combined cooling, heating and power generation system and observed that the overall increase in energy efficiency of the entire system is 57%. Aphornratana and Sriveerakul [108] evaluated the performance of a vapor compression refrigeration cycle operated by a heat-driven ORC, in which both cycles share the same condenser and use the same working fluid (R134a and R22). The results show that the overall COP can reach up to 0.6 when both cycles are operated with R22. They further suggested that the ratio of the expander piston area to the compressor piston area strongly influences the overall COP of the system. Mahmoudan, et al. [109] presented a combined ORC-VCR connected to steam Rankine turbine and a gas turbine to increase the efficiency of the cogeneration system. The results showed that the system could produce 303.8 kW of cooling effect. Similarly, Liang [110] experimentally studied the combined ORC-VCR to generate the refrigerating effect using low-grade temperature heat source using R245fa and R134a, respectively. The two cycles were coupled using a belt transmission unit and the heat source temperature was 95 °C. The results show that the system can produce 1.8 kW of refrigeration effects at – 4 °C while the overall performance can reach 0.18.

Fewer literature is available pertinent to experimental assessment of single rotor expander-compressor in ORC-VCR applications [103]. Wang et al. [111] experimentally demonstrated a new configuration of an ORC-VCR system using a scroll type of expander to drive a scroll type of compressor and an efficient microchannel heat exchanger. They concluded that the use of scroll expander and compressor facilitates high performance with reduced size and weight of system. Garland et al. [112] developed a prototype of ORC-VCR using magnetic coupling centrifugal turbine and compressor. The system operates using low-grade waste heat source at 106 °C and produces 250 kW of cooling.

Similarly, Grauberger et al. [113] experimentally demonstrated the performance of an ORC-VCR system (264 kW) using a direct coupled centrifugal turbine and compressor. The above lietrature represents the potential of the organic Rankine cycle in operating a vapor compression refrigeration system by direct coupling to drive compressor. In direct coupling either the expander shaft and the compressor shaft are connected through the transmission unit or both the expander and compressor are mounted on a common shaft. The latter arrangement may be more effective as the former may lead to transmission losses, balancing problems and additional system complexicity and cost. These issues can undermine the reliability of ORC. Liang [103] observed that the ORC-VCR system with a belt transmission unit has better performance and higher reliability than the common shaft arrangement. However, this discrepancy can be attributed to the consideration of the different working fluid in ORC under belt transmission (R245ca) and common shaft (R1233zd), which have different evaporation pressure.

2.9 Single rotor expander-compressor (compander)

The new single rotor expander-compressor device is a positive displacement device consisting of four chambers mounted on a common spherical rotor and enclosed in a single casing. Figure 2-9 shows the internal arrangement of the new device, which consists of two symmetrical halves (side A and side B) that act as expander and compressor and vice versa. Each half consists of a pair of double acting chambers as suction chamber and discharge chamber, i.e., suction port A, discharge port A, suction port B, and discharge port B. The displacement of side A is 15.7 cm^3 and that of side B is 23 cm^3. The chamber on each side rotates with the rotor and are designed in such a way that the rotation of the rotor properly opens and closes the inlet port and outlet port on both sides, enabling precise valveless operation of the device.

During 180° rotation, the two chambers on opposite sides (i.e., suction port A and suction port B) allow suction of the working fluid while the respective partner chambers compress and displace the working fluid through the discharge port (i.e., discharge port A and discharge port B). Fluid sealing is achieved very closely and thus the fluid from side A perfectly sealed from side B and vice versa and in the suction and discharge chambers of the same side. Detailed information about the device is available in refs. [114-116].

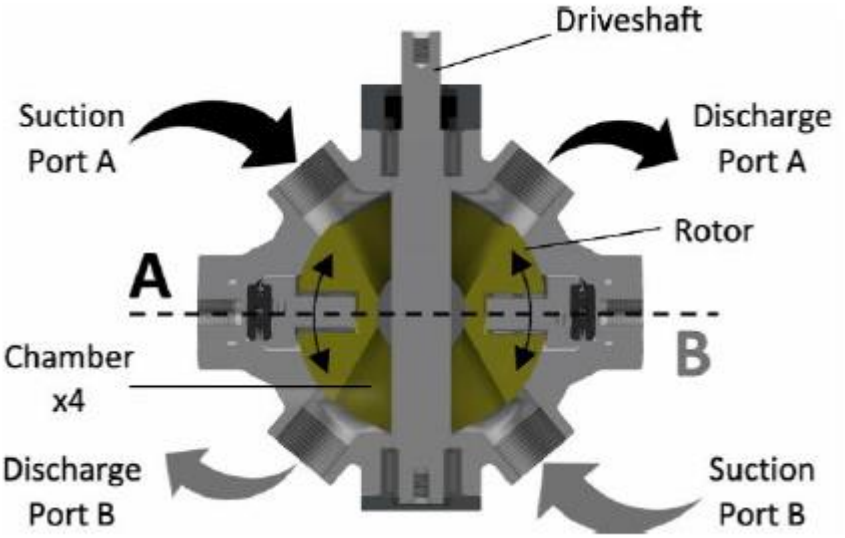

Figure 2-9: The novel single rotor expander-compressor (compander) [117]

2.10 Justification of Current work

Conventionally, in a common shaft expander-compressor arrangement, the compressor and expander are enclosed in separate casing. This presents a unique opportunity to improve the compression and expansion process to further improve thermal efficiency of the ORC-VCR system by reducing thermal losses. Thermally, the expansion process prefers to be heated, while a compression process prefers to be cooled [118, 119]. In a conventional vapor compression system, the heat of compression is transferred to the refrigerant raising the discharge temperature. This leads to an increase in specific volume at discharge and the compressor consumes more power due to isentropic compression. In

contrast, the expansion in the conventional expander of ORC should be heated facilitating more power generation.

Changes in one component of the system can significantly affect the thermal performance of the entire system. Therefore, common shaft expander-compressor technology enclosed in a single casing should be exploited to further improve the expansion and compression processes of the ORC-VCR system. Recently, Jiang et al. [120] experimentally investigated a single rotor volute type expander-compressor enclosed in a single casing and concluded that the system can achieve good efficiency and stability. In this context, the current work addresses the potential of a new single rotor expander-compressor in which one side acts as expander while the other acts as a compressor enclosed in a single casing used in ORC-VCR applications. In the new expander-compressor device, the heat of compression from the compressor side can be used on the expansion side, resulting in improved efficiency of both expansion and compression processes. Hence, the ORC-VCR system enhanced by incorporating the compander can be more efficient because the heat conduction within the device will benefit both expansion and compression processes than conventional ORC-VCR system with separate compressor and expander though mounted on the same shaft.

Additionally, this new device eliminates the need for a generator to convert mechanical power to electricity and an electrical motor to convert electricity to mechanical power, thereby reducing energy conversion losses and thus increasing energy efficiency. Overall, the new device can offer improved compression and expansion processes, enhanced system efficiency, overall compactness and ultimately systems cost-effectiveness. However, the use of similar device for ORC-VCR systems with conventional refrigerants has not been explored. A new single rotor expander-compressor in air cycle for cooling application has been studied by Fenton, et al. [114] and Subert, et al. [116]. They

concluded that the device has the potential to overcome the performance limitations of conventional air cycles. Furthermore, Zhang et al. [115] reported based on experimental results that isentropic efficiency of the same device can reach 80%.

The aim of this thesis is to numerically investigate the potential of a new device in an integrated ORC-VCR from the perspective of first and second law efficiency. In this study, steady-state modelling was strategically employed to deeply understand the ORC-VCR system's performance, with a special focus on the integration of a compander. Given the compander's innovative nature and the scarcity of studies on this device, establishing a foundational analysis through steady-state modelling was essential. This approach allowed for an in-depth examination of the system's thermodynamic properties and operational efficiency in a simplified and controlled settings, providing a benchmark for identifying potential improvements and design optimizations. This approach provides essential insights into system performance under ideal conditions, paving the way for future dynamic modelling to address real-world system and practical applications. A numerical model of the ORC-VCR cycle has been developed using ASPEN Plus and both the new single rotor expander-compressor device and the ORC-VCR system have been validated by comparing with previously published experimental data. The thermal performance of the ORC-VCR system with the new device is investigated under various system parameters such as expander inlet pressure, shaft speed, ORC evaporation and condensation temperatures. Parametric analysis provides a better understanding of the system parameters on the ultimate thermal performance of the entire ORC-VCR system. Heat-to-cooling efficiency is used as an energy indicator and overall exergy efficiency is used as an exergy indicator.

Chapter 3: Basic principles, Numerical modelling, and validation

3.1 Introduction

In this chapter, the thermodynamics of the ORC and the VCR are discussed and described. The proposed ORC-VCR system is presented, assumptions made while developing models are presented. The combined ORC-VCR system is developed using Aspen Plus simulation tool and the validation of the ORC-VCR model with experimental results published in the literature as well as the validation of the single rotor expander compressor is presented.

3.2 Combined ORC-VCR System

Figure 3-1 shows a schematic diagram of the ORC and VCR interconnected by a new single rotor expander-compressor device. One side of the device acts as an expander in the ORC, while the other side is the compressor of the VCR. ORC consists of pump (PUMP), evaporator (EVAORC), expander (EXPANDER) and condenser (CONDORC). The liquid phase working fluid is pumped into the evaporator of the ORC, where it is boiled until completely vaporized and then passes through the expander imparting work and finally enters the condenser of the ORC to liquify.

VCR cycle consists of evaporator (EVAVCR), compressor (COMPRESO), condenser (CONDVCR), and expansion valve (EXPV). The vapor phase working fluid is compressed by the compressor which receives power from the expander of the ORC and condenses in the condenser, then expands to lower its temperature and finally evaporates completely in the evaporator. The work produced by the expander of ORC is fed directly to the compressor of VCR as they share the same shaft.

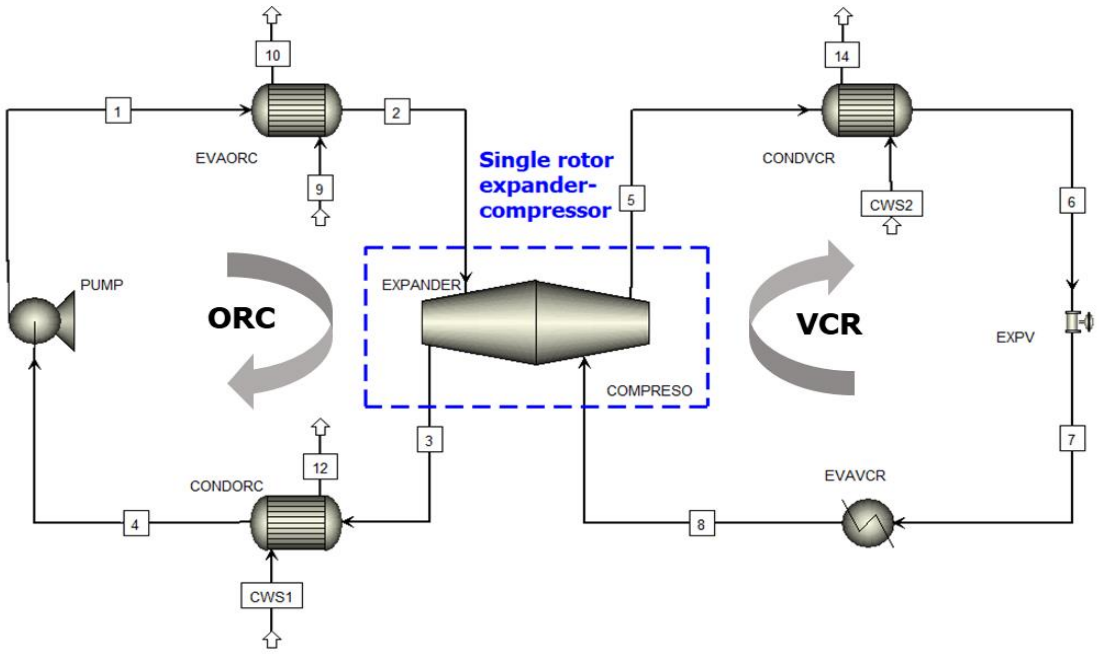

Figure 3-1: Schematic diagram of the ORC-VCR system

Figure 3-2 presents corresponding pressure-enthalpy diagram of the combined ORC-VCR system.

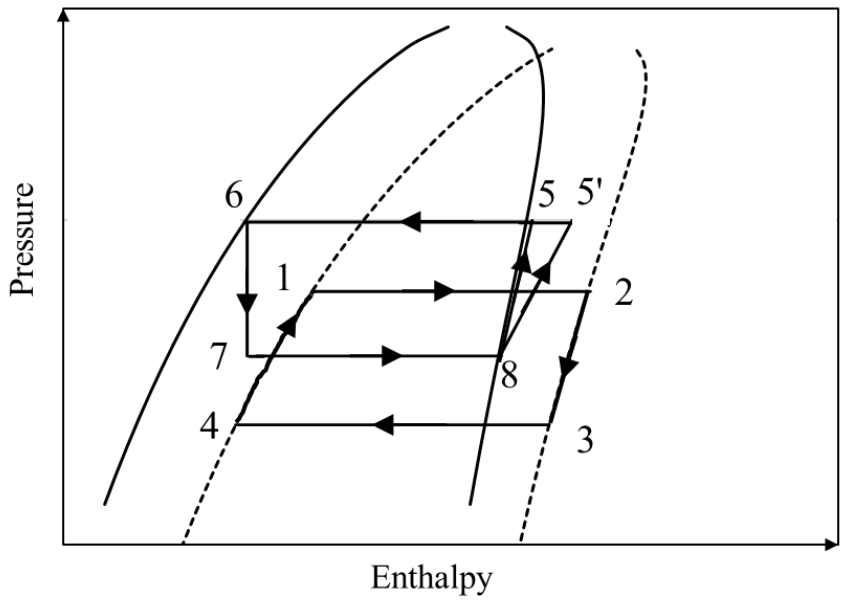

Figure 3-2: Pressure-enthalpy diagram of current ORC-VCR system. Cycle 4-1-2-3 is ORC cycle and cycle 8-5-6-7 is VCR cycle.

Two separate envelopes of pressure-enthalpy are presented since in the current paper two different working fluids are used. The work generated by process 2-3 of ORC is supplied to drive the compressor (process 8-5') of VCR.

3.3 Energy modeling

3.3.1 ORC Energy model

The mass flow rates for ORC is obtained by Eq. 3.1 Using the chamber volume of the expander (V_E) in the device, with assuming 100% volumetric efficiency [115], the following equations apply:

$$\dot{m}_{ORC} = \rho_2 N V_E \omega / 60 \quad (3.1)$$

Where N is equal to 2 as one complete cycle is of 180 degrees and ω is the shaft speed in rpm.

Evaporator (ORC_EVA):

The initial stage of the Organic Rankine Cycle (ORC) involves the process of heat addition. During this stage, the organic working fluid within the system absorbs heat from an external heat source. The latent heat absorbed by the working fluid in the evaporator (1-2) as shown in Figure 3-2 is equal to the specific enthalpy difference of the inlet and outlet of the evaporator multiplied by the ORC working fluid mass flow rate as shown in Eq. 3.2

$$\dot{Q}_{ORC-EVA} = \dot{m}_{ORC} \times (h_2 - h_1) \quad (3.2)$$

Expander (ORC Expander):

In this stage, the organic fluid, which has been heated, is directed through an expander. As it passes through the expander, the fluid expands and exerts force on the expander blades, thereby transforming a portion of its internal energy into mechanical work. The output power of the expander (2-3) as shown in Figure 3-2 is equal to the specific enthalpy

difference across the expander multiplied by the ORC working fluid mass flow rate as shown in Eq. 3.3

$$\dot{W}_{ORC-Expander} = \dot{m}_{ORC} \times (h_2 - h_3) = \eta_{expander} (\dot{m}_{ORC} \times (h_2 - h_{3s})) \quad (3.3)$$

Condenser (ORC_COND):

The energy output, specifically the heat rejection, occurs when the organic fluid, having undergone the expansion process, transitions to a state of lower energy. Subsequently, it is directed towards the condenser, where it releases thermal energy to a cooling medium, such as air or water. The heat rejection process facilitates the release of heat from the working fluid to the surrounding environment, thereby decreasing its internal energy to its original state. The latent heat rejected by the working fluid in the condenser (3-4) as shown in Figure 3-2 is equal to the difference of the specific enthalpy across the condenser multiplied by the ORC working fluid mass flow rate as shown in Eq. 3.4

$$\dot{Q}_{ORC-COND} = \dot{m}_{ORC} \times (h_3 - h_4) \quad (3.4)$$

Pump (ORC Pump):

Finally, the organic fluid is pumped back to the heat source to repeat the cycle again. In ORC, the pump is used to pressurize the liquid working fluid and pump it from the condenser to the evaporator (4-1) as shown in Figure 3-2 The specific enthalpy difference across the pump multiplied by the working mass flow rate is equal to the power consumed by the pump as shown in Eq.3.5

$$\dot{W}_{ORC-pump} = \frac{\dot{m}_{ORC} (h_1 - h_4)}{\eta_{Pump}} \quad (3.5)$$

The efficiency of the first law of thermodynamics for an Organic Rankine Cycle (ORC) can be defined as the ratio of the net work output generated by the cycle and the total heat input supplied to the cycle. In a mathematical context, it can be represented as in Eq.3.6

$$\eta_{th,ORC} = \frac{\dot{W}_{ORC-Expander} - \dot{W}_{ORC-pump}}{\dot{Q}_{ORC-EVA}} \quad (3.6)$$

3.3.2 VCR Energy model

The mass flow rates for VCR are obtained by Eq.3.7. Using the chamber volume of the compressor (V_C) in the device, the following equations apply [115]:

$$\dot{m}_{VCR} = \rho_8 N V_C \omega / 60 \quad (3.7)$$

Where N is equal to 2 as one complete cycle is of 180 degrees and ω is the shaft speed in rpm.

Evaporator (VCR EVA)

The VCR system functions by absorbing heat from the surrounding environment or the refrigerated compartment that requires cooling. The process of heat absorption takes place under conditions of low temperature and pressure, commonly observed at the evaporator coil. The latent heat absorbed by the working fluid in the evaporator (7-8) as shown in Figure 3-2 is equal to the specific enthalpy difference of the inlet and outlet of the evaporator multiplied by the VCR working fluid mass flow rate as shown in Eq. 3.8

$$\dot{Q}_{VCR-EVA} = \dot{m}_{VCR} \times (h_8 - h_7) \quad (3.8)$$

Compressor (VCR Compressor):

The process of energy conversion, specifically in the context of work, involves the transformation of absorbed heat, resulting in a phase transition of the refrigerant from a low-pressure vapour state to a high-pressure vapour or gas state. The procedure is facilitated through the utilisation of a compressor, which serves to compress the refrigerant, thereby increasing both its temperature and pressure. The input power to the compression process is presented by process (8-5') as shown in Figure 3-2 and is equal to the specific enthalpy difference across the compressor multiplied by the VCR working fluid mass flow rate. η_{comp} is the isentropic efficiency of the compressor as shown in Eq.

3.9 It is assumed the input power to the compressor equal to the output power of expander as shown in Eq.3.10 :

$$\dot{W}_{VCR-compressor} = \frac{\dot{m}_{VCR}(h_{5'} - h_8)}{\eta_{comp}} \quad (3.9)$$

$$\dot{W}_{VCR-compressor} = \dot{W}_{ORC-Expander} \quad (3.10)$$

Condenser (VCR COND):

The refrigerant, which is at a high pressure and temperature, proceeds to the condenser coil where it dissipates heat to the surrounding environment, typically air or water. The heat rejection process takes place at elevated levels of temperature and pressure. The latent heat rejected by the working fluid in the condenser (5'-6) as shown in Figure 3-2 is equal to the difference of the specific enthalpy across the condenser multiplied by the VCR working fluid mass flow rate as shown in Eq. 3.11

$$\dot{Q}_{VCR-COND} = \dot{m}_{VCR} \times (h_{5'} - h_6) \quad (3.11)$$

Expansion valve (VCR EXPV):

After the heat rejection process, the refrigerant becomes a high-pressure liquid and is expanded through an expansion valve or an expansion device. This causes its temperature and pressure to drop, preparing it to repeat the cycle by entering the evaporator coil again. The purpose of the expansion valve is to reduce the working fluid pressure from the condensation pressure (high pressure side) to the evaporation pressure (low pressure side). The specific enthalpy difference across the expansion valve is assume to zero which mean the expansion process is isenthalpic as shown in Eq.3.12:

$$h_6 = h_7 \quad (3.12)$$

The first law of thermodynamics efficiency for a vapor compression refrigeration cycle is the ratio of the cooling effect produced (the amount of heat removed from the refrigerated space) to the energy input required to drive the compressor, it is known as the

coefficient of performance (COP). Mathematically, it can be expressed as shown in Eq.3.13

$$\mathrm{COP} = \frac{\dot{Q}_{\mathrm{VCR-EVA}}}{\dot{W}_{\mathrm{VCR-compressor}}} \tag{3.13}$$

3.4 Exergy modelling

Exergy equations are provided below, which are derived from the models presented in Refs. [121-124]. Eq.3.14 the exergy balance.

$$\dot{E}_d = \sum \dot{m}_{in}\, e_{in} - \sum \dot{m}_{out}\, e_{out} - \dot{W} + \sum \dot{Q}_j \left(1 - \frac{T_0}{T_j}\right) \tag{3.14}$$

Where:

$\dot{E}_d$: the destroyed exergy rate in kW.

e_{in} : the input specific exergy in kJ/kg.

e_{out} : the output specific exergy in kJ/kg.

$\dot{m}_{in}$: the inlet mass flow rate in kg/s.

$\dot{m}_{out}$: the outlet mass flow rate in kg/s.

$\dot{W}$: the system output power in kW.

$\dot{Q}_j$: the heat transfer rate to the system in kW.

T_0 : the ambient temperature in K.

T_j : the component temperature in K.

There are four components that make up the specific exergy: kinetic, chemical, potential, and physical. Exergies, both potential and kinetic, are negligible. Because no chemical components leave the system and enter the environment, the chemical exergy term is disregarded [121]. Therefore, only the physical exergy is considered here. One can write down the formula for the exergy at any point j, $e_{f,j}$, can be defined as Eq.3.15:

$$e_{f,j} = h_j - h_0 - [T_0 * (s_j - s_0)] \quad (3.15)$$

Where:

h_j : the specific enthalpy at point j in kJ/kg.

h_0 : the specific enthalpy for the same point if point j was at the dead state.

s_j: the specific entropy at pint j in kJ/kg.

s_0: the specific entropy for the same point if point j was at the dead state.

T_0: the temperature at the dead state in K.

3.4.1 ORC Exergy Model

Evaporator (ORC_EVA):

The exergy destruction across the ORC evaporator is shown in Eq. 3.16:

$$\dot{E}_{d,ORC-EVA} = \dot{m}_{ORC} \times T_0 \times \left[s_{out} - s_{in} - \left(\frac{q_{ORC-EVA}}{T_{ORC-EVA}}\right)\right] \quad (3.16)$$

Where $\dot{m}_{ORC}$ is the ORC working fluid mass flow rate in kg/s. s_{out} and s_{in} are the specific entropy in kJ/kg at the ORC evaporator outlet and inlet, respectively. $q_{ORC-EVA}$ is the specific heat transferred to the working fluid in the evaporator in kJ/kg. $T_{ORC-EVA}$ is the working fluid temperature at the evaporator in K.

Expander (ORC Expander):

The exergy destruction across the expander is shown in Eq. 3.17:

$$\dot{E}_{d,ORC-Expander} = \dot{m}_{ORC} \times T_0 \times (s_{in} - s_{out}) \quad (3.17)$$

Where s_{in} and s_{out} are the specific entropy in kJ/kg at the expander inlet and outlet, respectively.

Condenser (ORC_COND):

The exergy destruction across the ORC condenser is shown in Eq.3.18:

$$\dot{E}_{d,ORC-COND} = \dot{m}_{ORC} \times T_0 \times \left[\left(\frac{q_{ORC-COND}}{T_{COND}}\right) - (s_{in} - s_{out})\right] \quad (3.18)$$

Where $q_{ORC-COND}$ the specific heat transferred from the working fluid in the ORC condenser in kJ/kg. T_{COND} is the condenser temperature in K. s_{in} and s_{out} are the specific entropy in kJ/kg at the condenser inlet and outlet, respectively.

Pump (ORC Pump):

The exergy destruction across the pump is shown in Eq.3.19:

$$\dot{E}_{d,ORC-pump} = \dot{m}_{ORC} \times T_0 \times (s_{out} - s_{in}) \quad (3.19)$$

Where s_{out} and s_{in} are the specific entropy in kJ/kg at ORC pump outlet and inlet, respectively.

3.4.2 VCR Exergy Model

Evaporator (VCR_EVA)

The exergy destruction across the VCR evaporator is shown in Eq.3.20:

$$\dot{E}_{d,VCR-EVA} = \dot{m}_{VCR} \times T_0 \times \left[s_{in} - s_{out} - \left(\frac{q_{VCR-EVA}}{T_{VCR-EVA}}\right)\right] \quad (3.20)$$

Where $\dot{m}_{VCR}$ is the VCR working fluid mass flow rate in kg/s. s_{in} and s_{out} are the specific entropy in kJ/kg at the VCR inlet and outlet, respectively. $q_{VCR-EVA}$ is the specific heat transferred in kJ/kg to the working fluid in the VCR evaporator. $T_{VCR-EVA}$ is the VCR evaporator temperature in K.

Compressor (VCR Compressor):

and the exergy destruction across the VCR compressor is shown in Eq.3.21:

$$\dot{E}_{d,VCR-compressor} = \dot{m}_{VCR} \times T_0 \times (s_{out} - s_{in}) \quad (3.21)$$

Where s_{out} and s_{in} are the specific entropy in kJ/kg at the compressor outlet and inlet, respectively.

Condenser (VCR_COND):

The exergy destruction across the VCR condenser is shown in Eq.3.22:

$$\dot{E}_{d,VCR-COND} = \dot{m}_{VCR} \times T_0 \times \left[\left(\frac{q_{VCR-COND}}{T_{COND}}\right) - (s_{in} - s_{out})\right] \quad (3.22)$$

Where $q_{VCR-COND}$ is the specific heat transferred from the working fluid in the condenser in kJ/kg. T_{COND} is the VCR condenser temperature in K. s_{in} and s_{out} are the specific entropy in kJ/kg at the VCR condenser inlet and outlet, respectively.

Expansion valve (VLV-100):

The exergy destruction across the VCR expansion valve is shown in Eq.3.23:

$$\dot{E}_{d,exp} = \dot{m}_{VCR} * T_0 * (s_{out} - s_{in}) \quad (3.23)$$

Where s_{out} and s_{in} are the specific entropy in kJ/kg at the expansion valve inlet and outlet, respectively.

3.5 Performance indicators for the combined ORC-VCR

In order to evaluate the combined ORC-VCR, the following indicators have been taken in account. Firstly, the overall performance COPs is referring to thermal efficiency of ORC multiplied by the COP of VCR as showing in Eq.3.24. Secondly, the heat to cooling efficiency which refers to ratio of the heat energy being utilised by the ORC to the cooling effects being produced by the VCR as shown in Eq.3.25.

Overall exergy efficiency is another indicator has been to chosen to evaluate the combined cycle from exergy point of view as shown in Eq.3.26 [124]. The exergy destruction occurred within the system is considered and the effect of the outside variable such as cooling water and source temperature are neglected to check feasibility of the device [124].

EPR is the expansion pressure ratio which is the ratio of working fluid pressure at the expander inlet P_{in-exp} to the working fluid pressure at the expander outlet $P_{out-exp}$ as shown in Eq.3.29. CPR is the compression pressure ratio which is the ratio of the working fluid pressure at the compressor outlet $P_{out-comp}$ to the working fluid pressure at the

compressor inlet $P_{in-comp}$ as shown in Eq.3.30. Both EPR and CPR, are used to evaluate the effect expander pressure ratio and the compressor pressure ratio on the performance of the combined cycles.

$$COPs = \eta_{th,ORC} \times COP \tag{3.24}$$

$$\eta_{H-C} = \frac{Q_{eva,VCR}}{Q_{eva,ORC}} \tag{3.25}$$

$$\eta_{oval-ex} = \frac{\dot{E}_{cooling}}{\dot{E}_{in}} \tag{3.26}$$

$$\dot{E}_{cooling} = \dot{E}_{out} - \dot{E}_{in} \tag{3.27}$$

$$\dot{E}_{in} = (\dot{E}_{out} - \dot{E}_{in}) + \dot{W}_{ORC-pump} \tag{3.28}$$

$$EPR = \frac{P_{in-exp}}{P_{out-exp}}\bigg|_{ORC} \tag{3.29}$$

$$CPR = \frac{P_{out-comp}}{P_{in-comp}}\bigg|_{VCR} \tag{3.30}$$

Where $\dot{E}_{cooling}$ is exergy destruction across the evaporator of the VCR system and $\dot{E}_{in}$ is the total exergy destruction across the evaporator of the ORC and the pump input power.

3.6 Environmental analysis

The refrigeration and air conditioning sector holds considerable importance in current society as it fulfils crucial functions of cooling and heating services. Nevertheless, the environmental ramifications of these systems, including their role in the release of greenhouse gases, have generated apprehension. The objective of this section is to conduct an assessment of combined ORC and VCR from environment perspective. This evaluation will also take into account the utilization of different refrigerants within these technologies. Furthermore, the technical requirements of gas engines employed. The

methodology and the equations used to assess the environmental impact of a gas engine, focusing on factors like fuel consumption and CO2 emissions are discussed [125].

$$\mathrm{Q_{Prime}} = \dot{\mathrm{m}}_{\mathrm{ORC}}(\mathrm{h_{out}} - \mathrm{h_{in}}) \tag{3.31}$$

The value of Q_{Prime} is the quantity of thermal energy required by the ORC system that should be recovered from the gas engine. The computation is dependent on two crucial variables: $\dot{m}_{ORC}$, which denotes the ORC mass flow rate, and the difference in enthalpy between outlet h_{out} and inlet h_{in} points in the ORC evaporator.

To determine how much fuel must flow through the gas engine to generate the desired amount of thermal energy ($\dot{Q}_{Prime}$), the function $m_{f,PL}$ is used. This equation uses an exponential function to modify the fuel's Lower Heating Value for the current partial load as shown in Eq.3.32:

$$\dot{\mathrm{m}}_{\mathrm{f,PL}} = \frac{\dot{\mathrm{Q}}_{\mathrm{Prime}}}{\mathrm{LHV}((5.1396\,\exp^{-0.02619\,\mathrm{PL}}) + (11.346\,\exp^{0.001194\,\mathrm{PL}}))} \tag{3.32}$$

The term PL is commonly employed in reference to partial load, which refers the load percentage applied on the gas engine. Partial load refers to the condition in which an engine is not functioning at its maximum or full load capacity, but rather at a fraction or percentage of its maximum capacity. Within the present work, the value was assumed to be at 30%, denoting that the engine works at 30% of its designated power capacity [75]. LHV refers to the Lower Heating Value, a parameter that characterizes the energy content of the fuel employed. In the present context, the fuel is natural gas. The Lower Heating Value is a measure that quantifies the energy released during the complete combustion of a given mass of natural gas. The LHV commonly assigned to natural gas is typically 45,000 units, a number commonly observed for this particular fuel.

The annual fuel consumption is measured in kilos and is represented by the $m_{Fuel-year}$ variable. This can be accomplished by solving Eq.3.33:

$$\dot{m}_{\mathrm{Fuel-year}} = m_{f,PL}(3600 \times 24 \times 6000) \quad (3.33)$$

where 6000 stands for the total number of hours that the system is in operation throughout the course of a year [125].

The yearly CO_2 emissions in terms of environmental impact in kilograms as shown in Eq.3.34:

$$\dot{m}_{\mathrm{CO2-year}} = \dot{m}_{\mathrm{Fuel-year}}(\mathrm{Rate}_{CO_2\ \mathrm{generation}}) \quad (3.34)$$

$Rate_{CO_2\ generation}$ refers to the rate at which CO_2 is produced per unit of fuel consumed that is subject to the particular fuel type and the prevailing circumstances of combustion. This rate is assumed as 3.05 kilos of CO_2 generated per kilogram of fuel burned.

This methodology explains the step-by-step process used to assess the environmental impact of the gas engine's fuel consumption and CO_2 emissions. It takes into account factors like the engine's load, fuel properties, and the CO_2 system's heat generation to provide insights into the annual carbon emissions associated with the gas engine [126].

3.7 Model development of combined ORC-VCR

The model of ORC-VCR is developed in ASPEN PLUS® process simulator (V12.1) [127] as presented in Figure 3-1. ASPEN plus is a chemical process simulator embedded with a rich data bank of fluids used in different process which allows building a process model and carryout complex calculations [128]. This unique feature makes it suitable for qualitative and quantitative investigation of several industrial applications, including (but not limited to) air separation units [129], combustion processes [130], biomass gasification [131], hydrogen production [132], gas to liquid process [133], to name but a few. Moreover, it has been widely accepted in the refrigeration sector to analyse different refrigeration cycles as well as their integration with each other such as vapor absorption refrigeration system [134, 135], adsorption refrigeration cycle [136], vapor compression

refrigeration system [137], integration of vapor compression-absorption refrigeration [138] and also adopted in assessing an organic Rankine cycle [139]. These literatures suggest the suitability of ASPEN plus in assessing refrigeration cycles and hence this platform is explored in the current model development of combined organic Rankine cycle coupled with vapor compression system and its analysis.

Two separate refrigerants have been used as working fluid in ORC and VCR system. R245fa is used as the working fluid for ORC while R134a is the working fluid for VCR and water is the heating and cooling mediums. R245fa is chosen in ORC system as a working fluid due to its desired thermodynamic properties, low flammability and toxicity, and compatibility with components material. In the VCR subsystem, R134a is chosen as the refrigerant because of its current popularity in refrigeration system and mobile air-conditioning applications. Table 3-1 presents the general properties indices of both refrigerants under consideration.

Table 3-1: Refrigerants with environmental, health and safety properties

Refrigerants	Atmospheric lifetime (years)	ODP*	GWP*	ASHRAE safety group*	ASHRAE Flammability*
R245fa	7.7	0	858	B1	No
R134a	14	0	1430	A1	No

* ASHRAE Handbook, Fundamentals (SI Edition), 2017, Chapter 29, Atlanta.

Thermodynamic and transport properties such as temperature, pressure, density, enthalpy, entropy, viscosity are derived using the inbuilt REFPROP model as it is suitable for the fluids under consideration (i.e., R245fa, R134a and water). This is because the reference fluid properties model (REFPROP which developed by National Institute of Standards and Technology (NIST)) is the most accurate model available currently for the pure and mixture refrigerants as it offers precise and dependable data derived from experimental

measurements [140]. In this model, the thermodynamics properties of pure fluid are obtained using three models namely equations of state explicit in Helmholtz energy, the modified Benedict-Webb-Rubin equation of state, and an extended corresponding states (ECS) model. Thus, this model is suitable for the pure working fluids considered in the current analysis which are R245fa, R134a and water.

All heat exchangers, except evaporator of the VCR, are considered counter-flow configurations and are modelled using HeatX model. The HeatX model is suitable for detailed zone analysis with heat transfer coefficient and pressure drop estimation for single-phase and two-phase flow. The detailed analysis of heat exchangers has not been conducted as it is not main focus of current study. However, this model is adopted in current study as is also suitable to perform only heat and material balance calculations [128]. For evaporator of VCR, heater block is used which can determines the thermal and phase conditions of a mixture. A list of all the operational units presented in Table 3-2 and corresponding ASPEN Plus models adopted from its library are presented in Table 3-2. Following are the assumptions considered in the current study.

- Pressure loss occur in the components and piping across both ORC and VCR systems are negligible.
- Heat losses to or from the surrounding are neglected.
- Pump efficiency is assumed to be 75%, and isentropic efficiency of expander and compressor is assumed to be 80% [115], respectively.
- A minimum temperature approach for all heat exchangers is considered as 5 °C.
- Cooling water for both system is supplied at a temperature of 15 °C.

Table 3-2 provides explicit information about the input requirements under consideration and their ranges for each component of the ORC-VCR unit presented in Table 3-2.

Table 3-2: Details of system components adopted from ASPEN Plus library.

Sr. No	Components	Abbreviation	ASPEN Plus model	Inputs
ORC				
1	Pump	PUMP	Pump	• Outlet pressure (5 bar – 10 bar). • Pump efficiency, 75% [141].
2	Evaporator	EVAORC	HeatX	• Heating water temperature = 95 °C and mass flow rate = 1 kg/s [110, 142]. • Working fluid at the evaporator outlet is saturated vapour (x_{EVAORC} = 1). • Minimum temperature approach (5 °C) [143].
3	Expander	EXPANDER	Turbine	• Isentropic efficiency, 80% [115]. • Displacement volume (15.7 cm^3). • Discharge pressure (condensation pressure) (1.227 bar – 2.945 bar).
4	Condenser	CONDORC	HeatX	• Cooling water temperature (15 °C) and mass flow rate (1 kg/s). • Working fluid at the outlet of the condenser is saturated liquid ($x_{CONDORC}$ = 0). • Minimum temperature approach (5 °C)

VCR

1	Compressor	COMPRESO	Compr	• Expander output is fed to compressor as input ($\dot{W}_{EXPANDER} = \dot{W}_{COMPRESO}$). • Displacement volume (23 cm^3). • Isentropic efficiency, 80% [115].
2	Condenser	CONDVCR	HeatX	• Cooling water temperature (15 °C-40 °C) and mass flow rate (1 kg/s). • Working fluid at the outlet of the condenser is saturated liquid ($x_{CONDVCR} = 0$). • Minimum temperature approach (5 °C).
3	Expansion valve	EXPV	Valve	• VCR evaporation pressure (1.327 bar – 3.496 bar).
4	Evaporator	EVAVCR	Heater	• Working fluid at the evaporator outlet is saturated vapour ($x_{EVAVCR} = 1$). • Minimum temperature approach (5 °C).

3.8 Model validation

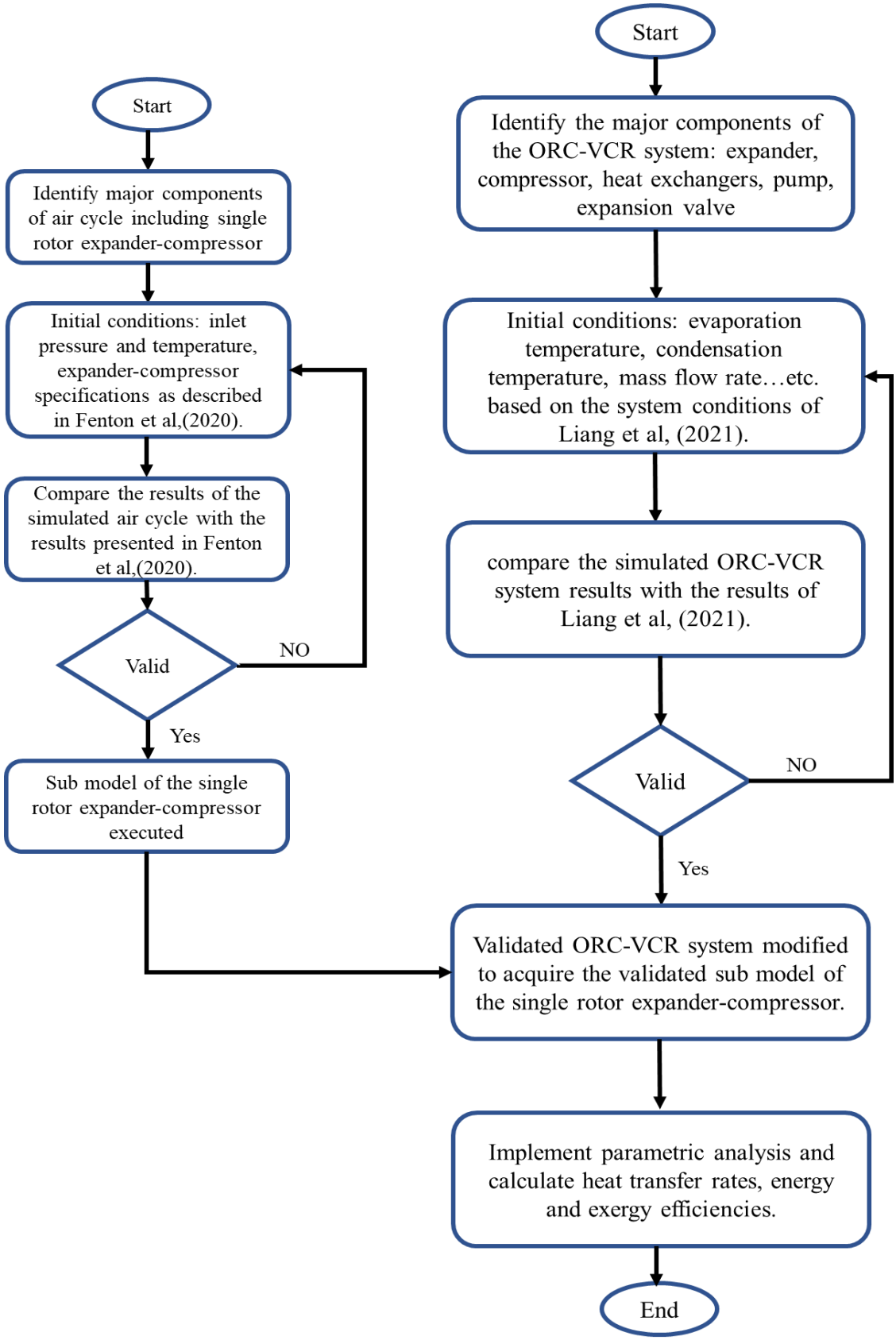

Figure 3-3: Flowchart of procedure followed in ORC-VCR simulation and validation.

The validation is conducted in two steps, first is the validation of the single rotor expander-compressor device and second is the validation of complete ORC-VCR system with experimental data. The validation procedure is presented in Figure 3-3.

3.8.1 Validation of single rotor expander-compressor

In order to ensure the accuracy of the numerical simulation, first step followed here is the validation of a single rotor expander-compressor system presented in Figure 3-4.

This model is developed in ASPEN plus and compared with a reference system for validation [114]. They used air as the working fluid to enter the expander at 25 °C and 1 bar and expands to 0.6 bar, and the corresponding temperature is -8 °C. The speed varies between 500 rpm to 3000 rpm while keeping inlet and outlet conditions the same.

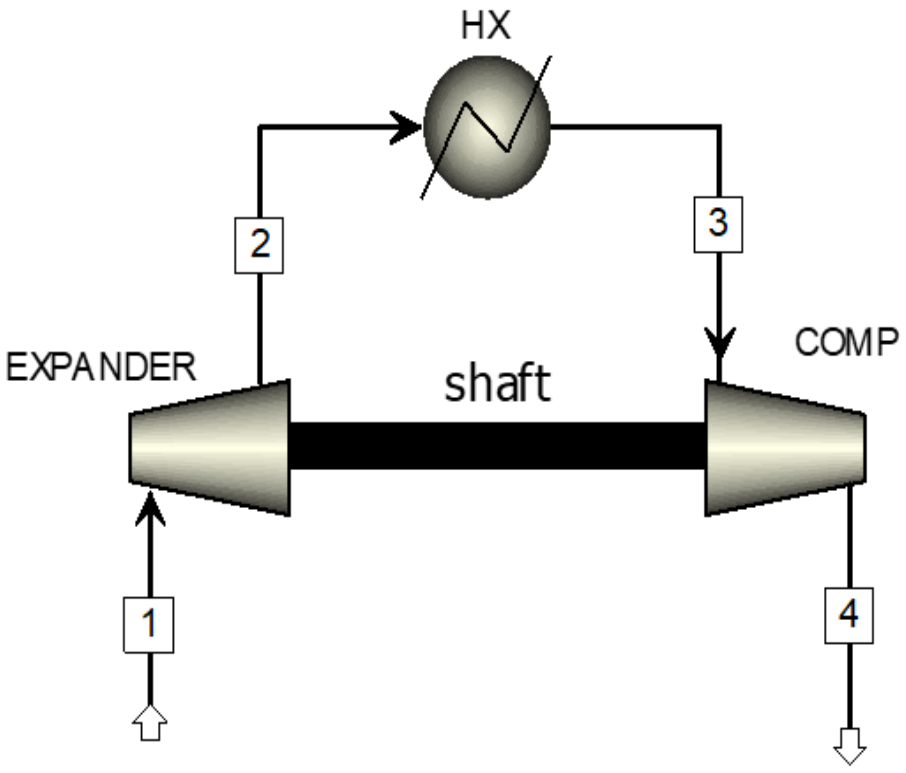

Figure 3-4: system configuration of validation of a new single rotor expander-compressor device with experimental data of Fenton, et al. [114].

The resulting mass flow rate of the received air is compared with data of reference data [114] and presented with respect to shaft speed in Figure 3-5. The results show a particularly good correlation between the reference model results and the presented simulation results with a maximum deviation of less than 1%.

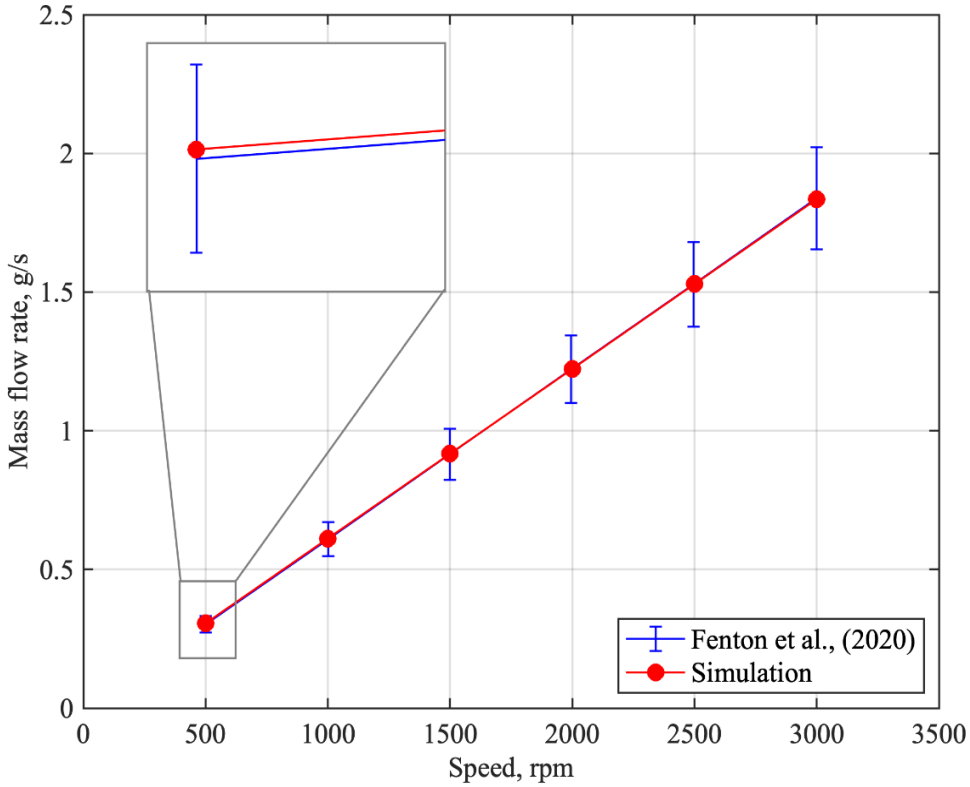

Figure 3-5: Comparison of mass flow rate of validation of a new single rotor expander-compressor device with experimental data of Fenton, et al. [44].

3.8.2 Validation of ORC-VCR system

After validating the new device, the numerical model of the complete ORC-VCR is developed and validated against the experimental results of Liang et al. [110]. They used two separate devices connected by a belt drive mechanism which has a speed ratio of 1.71 to transmit the mechanical power from the ORC system to the VCR as shown in Figure 3-6.

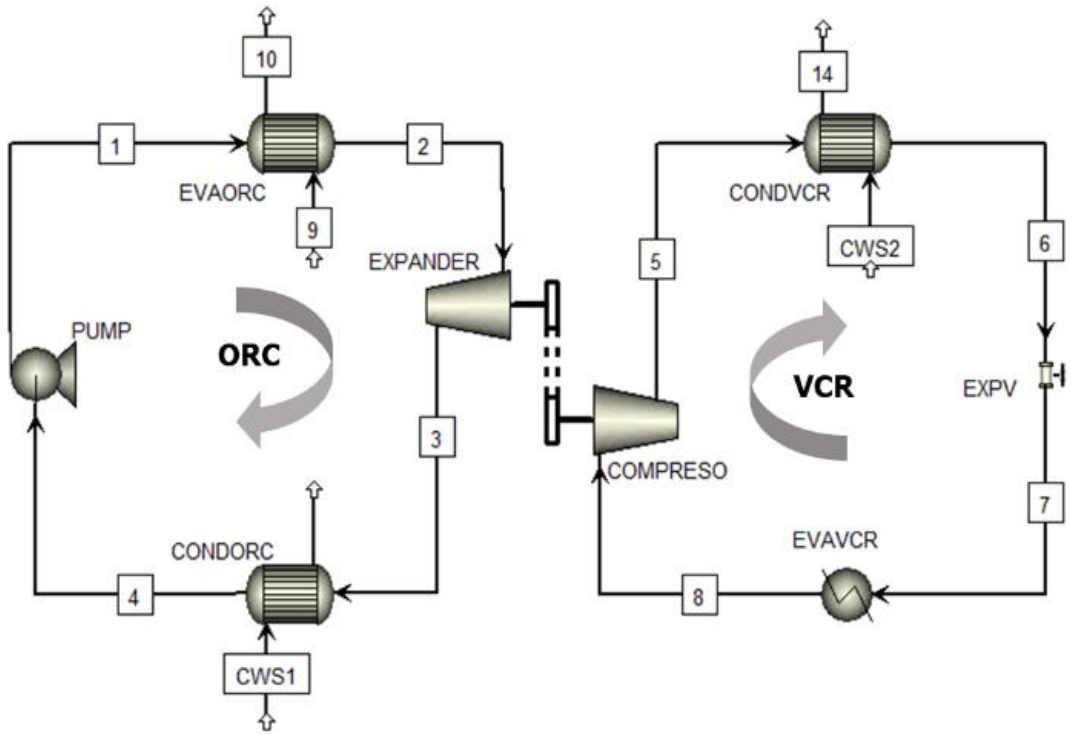

Figure 3-6: System configuration Liang, et al. [110].

In their study, the amount of work produced by the expander is not same as that of the work supplied to the compressor due to losses in the belt drive. This transmission losses are accounted by relating expander work and compressor work in the model. An empirical equation is developed using their experimental data to account for the transmission losses data which represents the relationship between power output of expander and mass flow rate, as presented by Eq.35:

$$\dot{W}_{comp} = -0.7964 \times (\dot{W}_{exp}{}^{2}) + 1.2306 \times (\dot{W}_{exp}) - 0.2241 \qquad (3.35)$$

Where, $\dot{W}_{comp}$ is the compressor input work in kW, and $\dot{W}_{exp}$ is the expander output power in kW.

Figure 3-7 presents a comparison between the present numerical model of the ORC-VCR system and the experimental results under different ORC mass flow rates. It is observed that the numerical simulation results show good agreement with the experimental data with a maximum deviation of about 5.6%. The small deviation between current model and experimental data can be attributed to the heat losses f rom the system during the

experiments, instrumentation error during the measurement. In current analysis, the model presented in Figure 3-7 is modified by assuming that the work developed by the expander is fed completely to the compressor of the VCR.

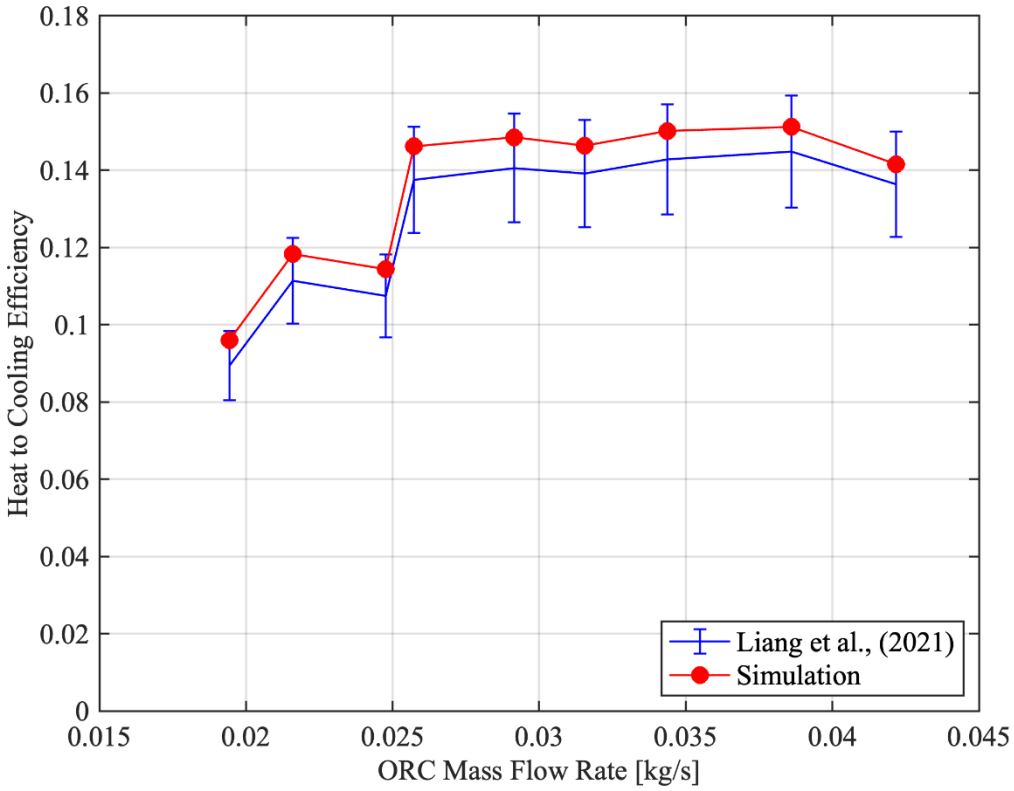

Figure 3-7: Comparison of current ORC-VCR model with experiment results in terms of ORC mass flow rate and heat to cooling efficiency.

In current work, the model presented in Figure 3-6 is modified by assuming that the work developed by the expander is fed completely to the compressor of the VCR which similar to Figure 3-1.

An influence of the several operating parameters such as evaporation temperature of ORC (62.75 °C – 89.7 °C) and VCR (-20 °C – 5 °C), condensation temperature of ORC (20 °C – 45 °C) and speed (500 – 3000 rpm) at constant heat source (water) temperature of 95 °C on performance of VCR system have been investigated from energy, exergy and environment point of views. The performance indicator used to represent energy, exergy and environment are overall COP and heat to cooling efficiency, exergy destruction and

exergy efficiency, and CO2 emissions, respectively. Moreover, the thermal performance behaviour of different prospective refrigerants such as R245fa, R123, R134a, R1234ze(E), R1234yf, and Butane used in ORC and VCR is analysed in terms of energy, exergy, and environmental perspectives.

3.9 Summary

In this chapter, the energy and exergy models of the ORC, and the VCR were discussed. the mathematical equations related to the mass flow rate of the two side of the single rotor expander-compressor were presented. The environmental analysis methods and assumptions were discussed. The proposed ORC-VCR system was presented, assumptions made while developing models are presented. The combined ORC-VCR system is developed using Aspen Plus simulation tool and the validation of the ORC-VCR model with experimental results published in the literature as well as the validation of the single rotor expander compressor is presented. In addition, the parameters of the current study were presented.

Chapter 4: Energy Assessment of ORC-VCR Combined cycle coupled by Single Rotor Expander-Compressor

4.1 Introduction

This chapter presented the comprehensive energy analysis consist of studying the effect of ORC and VCR evaporation temperatures as well as the ORC condensation temperature on the ORC-VCR combined system. The effects of these parameters are presented in this chapter.

4.2 Assessing the optimal side of the expander.

The two refrigerants used in current study are pressure sensitive, hence it is crucial to select the side of the single rotor expander compressor device appropriately suitable in ORC and VCR system for given pair of the refrigerants. As the two sides of the device have varying volumes of displacement, a study has been conducted to determine the most suitable side for both the expansion and compression processes within the ORC and VCR subsystems for a specific pair of refrigerants. To achieve this, expansion, and compression of the R245fa and R134a have been carried out alternatively in small chamber and big chamber, respectively. Figure 4 displays how the inlet pressure at the ORC expander influences the discharge pressure of the VCR compressor at various ORC condensation temperatures, with a shaft speed set at 1000 rpm and the expander's displacement volume at 15.7 cm^3 (representing the smaller side). Similarly, Figure 4 shows the impact of the ORC expander inlet pressure on the discharge pressure of the VCR compressor for differing ORC condensation temperatures and a shaft speed of 1000 rpm, but with the

expander's displacement volume at 23 cm³ (indicating the larger side). This implies that when the expansion process occurs on the small side, the corresponding compression process takes place on the large side, and vice versa. In both Figure 4 and Figure 4 the critical pressure line corresponds to the critical pressure of the refrigerant used in the VCR subsystem, which is R134a.

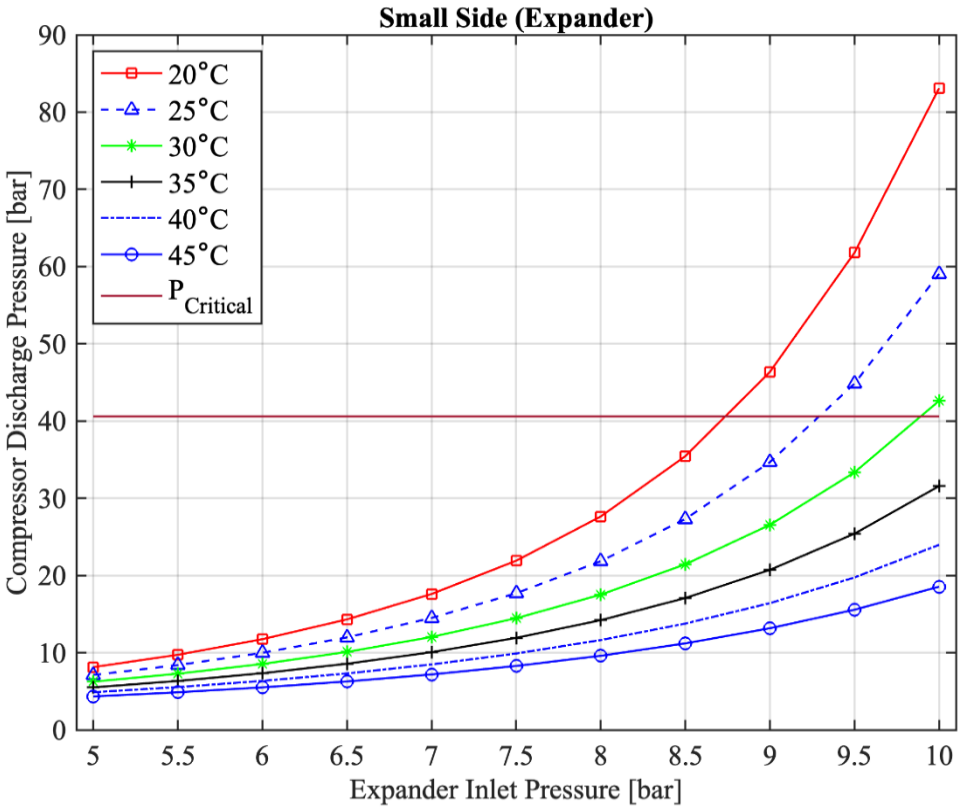

Figure 4-1: Expander inlet pressure against compressor discharge pressure: expander is the small side of the device.

In both cases, it's observed that a rise in the inlet pressure of the expander leads to a significant increase in the compressor's discharge pressure. An increase in the expander's inlet pressure enhances the power output of the expander, which in turn is supplied to the VCR compressor. Given that the volume flow rate and the evaporation temperature of the VCR system, $T_{eva,VCR}$ = 0 °C, are held constant, the mass flow rate does not change. Therefore, the only variable that can increase when the expander's inlet pressure rises is the discharge pressure of the compressor.

It has been noted that the increase in the compressor's discharge pressure is more pronounced when the inlet pressure to the expander rises, particularly when the expansion takes place on the big side compared to the small side. For example, when the expansion process occurs on the small side with a condensation temperature of 35°C, the discharge pressure reaches approximately 14.2 bar at an expander inlet pressure of 8 bar, as depicted in Figure 4.

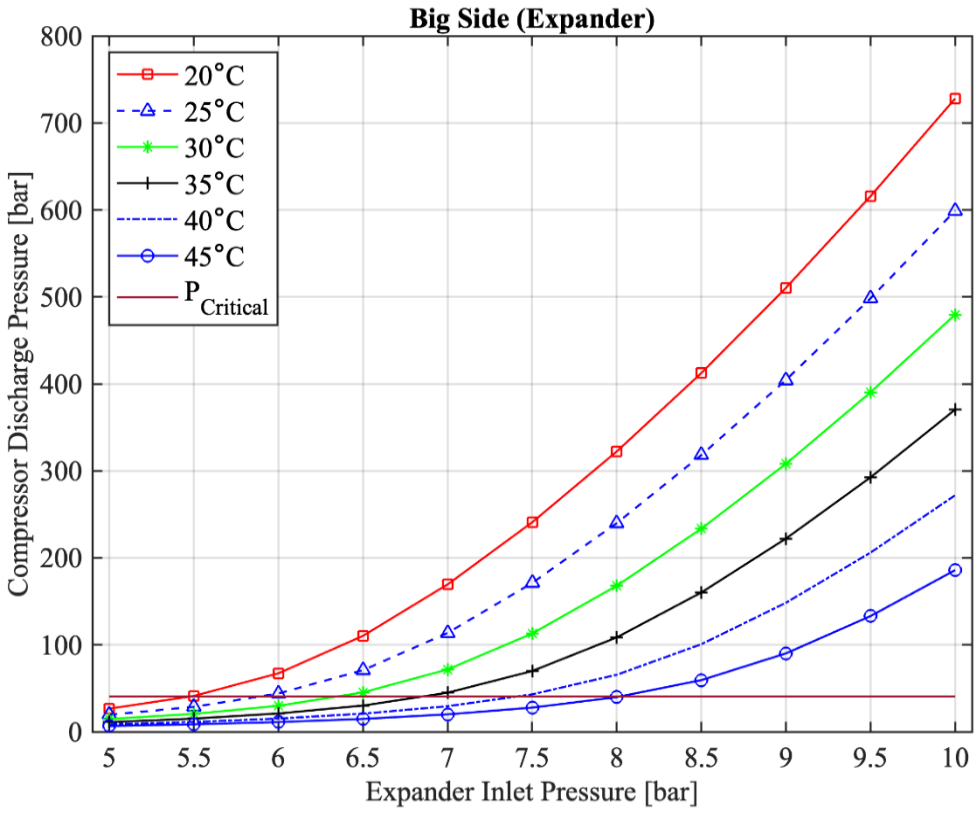

Figure 4-2: Expander inlet pressure against compressor discharge pressure: expander is the big side of the device.

Conversely, when the same conditions are applied to the larger side for the expansion process, the discharge pressure soars to 108 bar—surpassing the critical point of 40.59 bar for R134a—which is roughly six times higher than that of the small side. This is illustrated in Figure 4.

Furthermore, it's notable that raising the ORC condensation temperature results in a decrease in the compressor's discharge pressure. This reduction is attributed to a decrease

in the power generated by the expander, which is then supplied to the compressor. In the scenario involving the small side, with a constant expander inlet pressure of 8 bar, the compressor discharge pressure decreases from 27.6 bar to 9.6 bar as the ORC condensation temperature $T_{cond,ORC}$ increases from 20°C to 45°C, respectively. The decrease in discharge pressure is even more pronounced when the expansion takes place on the larger side. Figure 4, clearly illustrates that when the larger side operates as an expander, the increase in discharge pressure is steep, and in many operating conditions, it surpasses the critical pressure of the VCR refrigerant. Given this observation, in this study, the smaller side of the device is utilized as an expander, while the larger side functions as a compressor.

4.3 Comparison of expander output power

Figure 4-3 and Figure 4-4 show a comparison of the expander output power when the expansion process occurs in the small side and the big side of the single rotor expander-compressor, respectively. The output power was studied under different expander inlet pressure and different ORC condensation temperatures. As shown in Figure 4-4, the expander output power increases with the increase of the inlet pressure and that associated with the increase of the enthalpy at the expander inlet. Thus, the expander will produce more power. The variation of the ORC condensation temperature shows that the output power decreases with the increase of the condensation temperature and that due to the decrease of the enthalpy difference across the expander. In Figure 4-4, at specific ORC condensation temperature at 30 °C, increasing the expander inlet pressure from 7 bar to 10 bar, increase the output power by 87%.

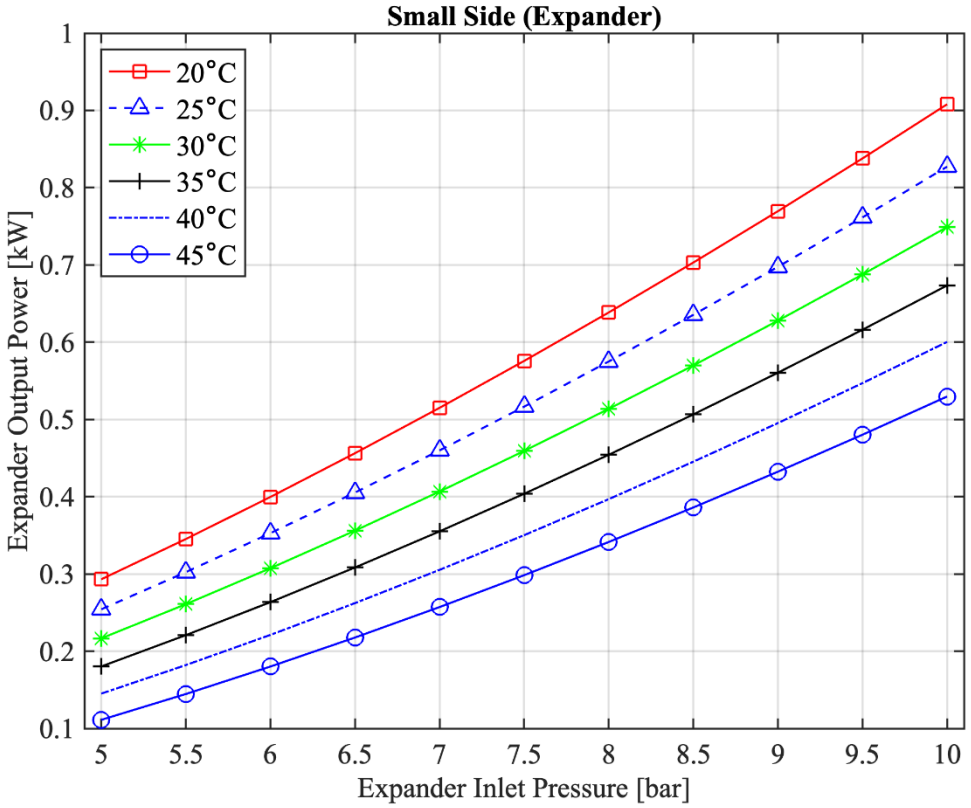

Figure 4-3: Expander output power with variation of inlet pressure and condensation temperature: small side.

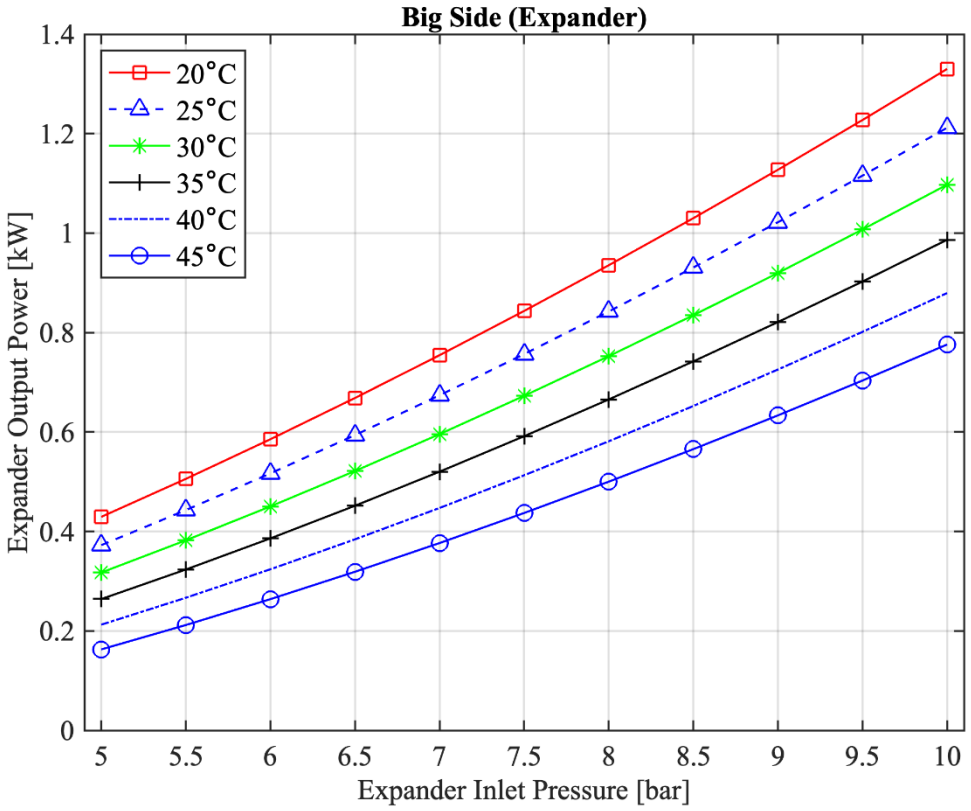

Figure 4-4: Expander output power with variation of inlet pressure and condensation temperatures: big side.

However, decreasing the ORC condensation temperature from 45 °C to 20 °C at specific inlet pressure 8 bar, increases the output power by 88%. Styding the expansion process in different sides of the single rotor expander-compressor shows that when the expansion process occurs in the small side produces lower power than when it occurs in the big side. This reduction in the output power is related to the different displacement of the two sides. At specific inlet pressure 8 bar and ORC condensation temperature 30 °C, the big side produced 44% output power higher than the small side. However, producing more power is not always wanted because the expander output power will be supplied completely to the VCR compression process and supplying more power will lead to increase the compressor discharge pressure to the critical pressure as described in Section 4.2.

4.4 Comparison of pump input power

Figure 4-5 and Figure 4-6 show a comparison of the pump input power when the expansion process occurs in the small side and the big side of the single rotor expander-compressor, respectively.

The pump input power studied under different expander inlet pressure and ORC condensation temperature. Increasing the inlet pressure of the expander is the responsibility of the pump. Thus, any increase in the expander inlet pressure requires more power input to the pump. In other hand, increasing the ORC condensation temperature leads to increase the condensation pressure which in turn reduces the pressure difference across the pump. Thus, the input power to the pump will be reduced. As shown in Figure 4-6, when the expander in the small side at a specific ORC condensation temperature 30 °C, increasing the expander inlet pressure from 7 bar to 10 bar increase the pump input power by 67%.

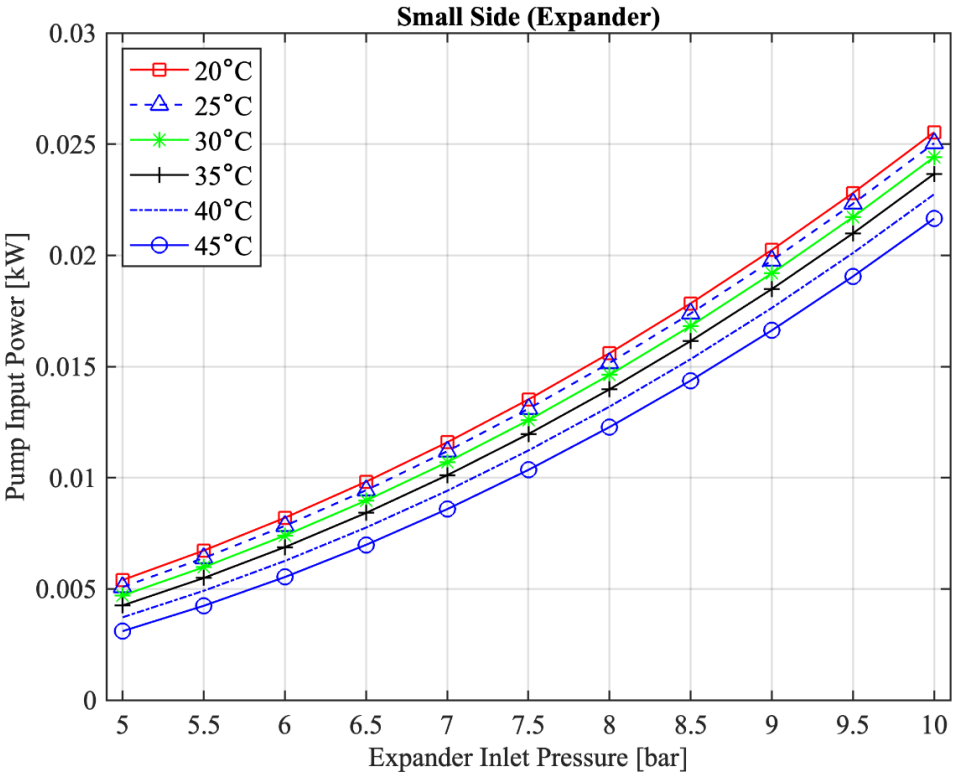

Figure 4-5: Pump input power with variation of expander inlet pressure and condensation temperature: when the expander in small side.

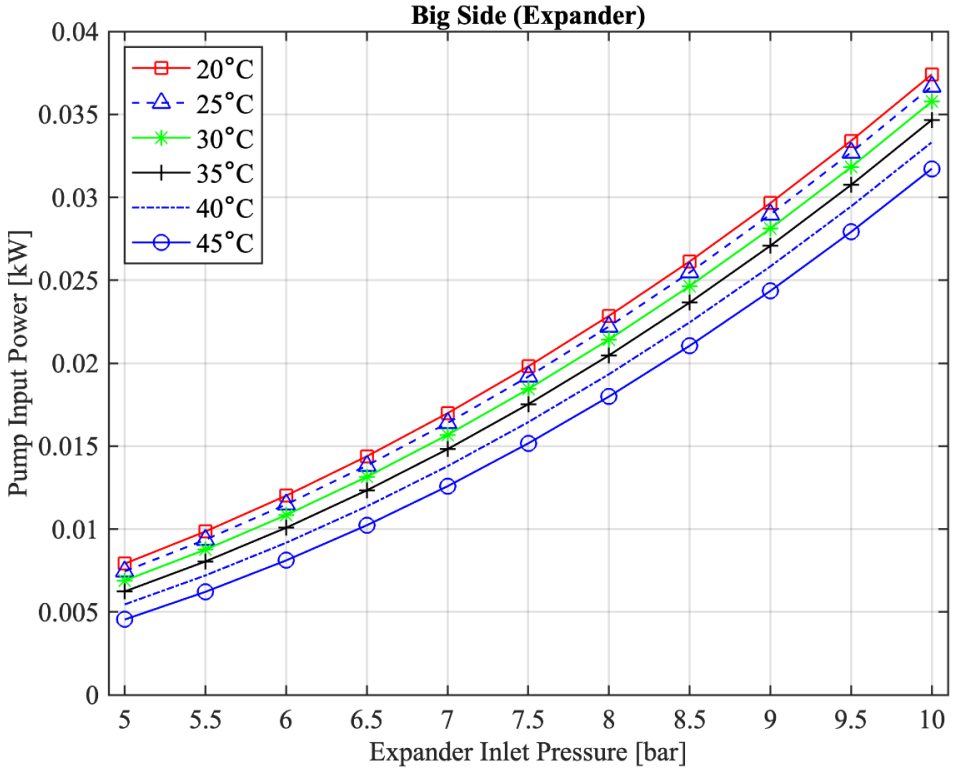

Figure 4-6: Pump input power with variation of expander inlet pressure and condensation temperature: when the expander in big side.

However, increasing the ORC condensation temperature from 20 °C to 45 °C at specific inlet pressure 8 bar, decreases the pump input power by 21%. Comparing the pump input power in the two cases where the expander in the small side and big side of the single rotor expander, shows that in the case of the expander in the big side consumes more input power to the pump. That can be explained by the increase in the volume flow rate of the working fluid throughout the cycle and that associated to the different in the two sides displacement. At specific inlet pressure 8 bar and ORC condensation temperature 30 °C, the pump consumes power in the case of the expander in the big side higher than when the expander in the small side by 46%

4.5 ORC Thermal efficiency and EPR with variation of ORC evaporation temperature

Figure 4-7 shows the thermal efficiency of the ORC and the expander pressure ratio (EPR) with the variation of the ORC evaporation temperature.

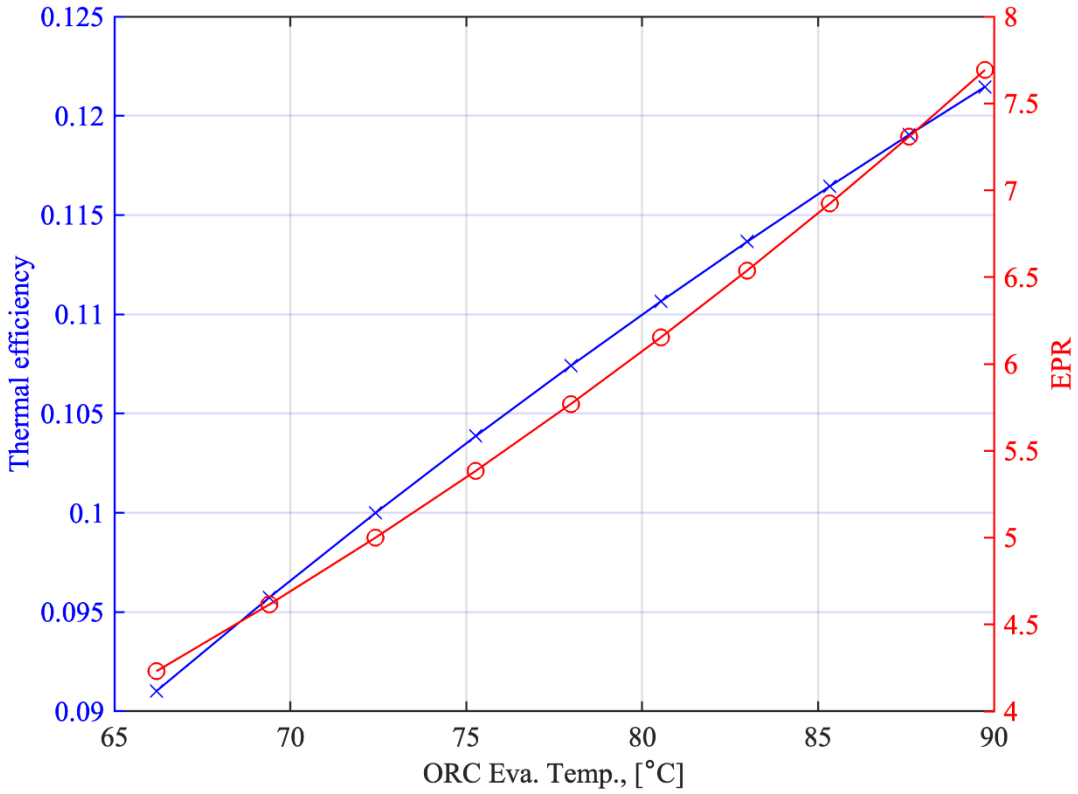

Figure 4-7: ORC evaporation Temperature against ORC thermal efficiency and EPR

This can be attributed to the increase in the enthalpy difference across the expander. This increase in the enthalpy results into an increase the output power. The maximum thermal efficiency was 0.122 observed when the evaporation temperature 90 ºC. Similarly, the expander pressure ratio was increasing with the ORC evaporation temperature because increment in evaporation temperature associated with increasing in the evaporation pressure. Thus, the pressure difference across the expander will increase rationally.

4.6 VCR COP and CPR with variation of ORC evaporation temperature

Figure 4-8 illustrate the relationship between the COP of the VCR and the compressor pressure ratio (CPR) with respective evaporation temperature of the ORC.

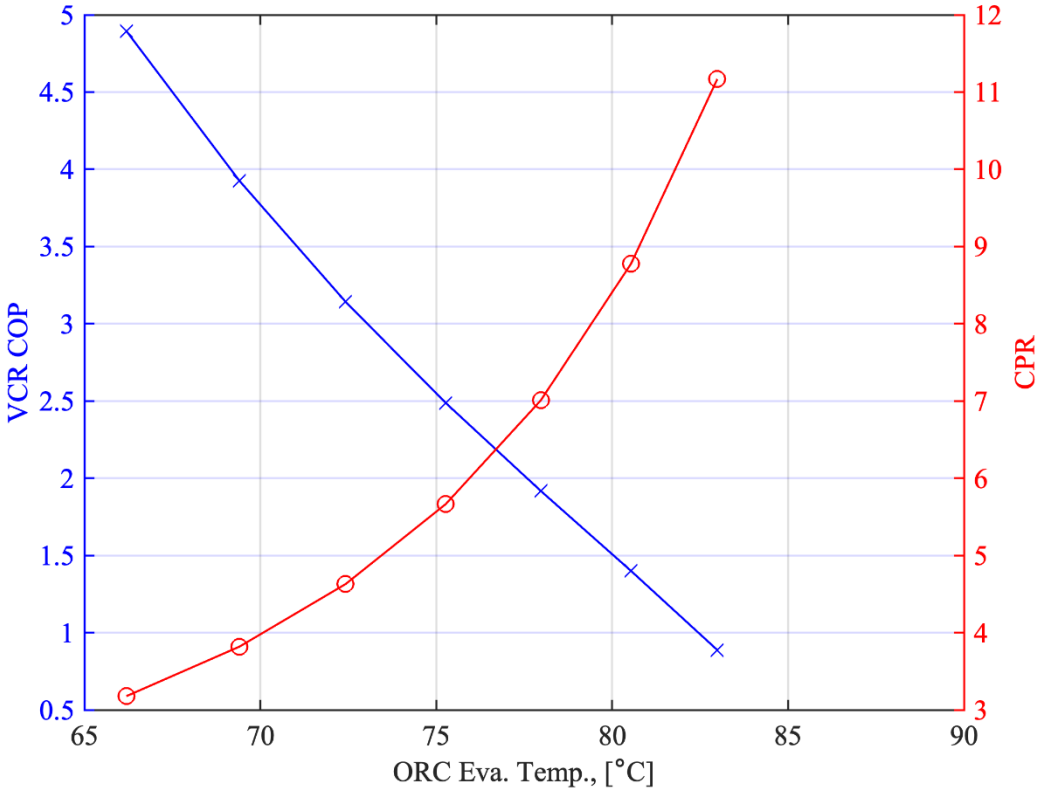

Figure 4-8: ORC evaporation Temperature against VCR COP and CPR

Here, CPR is defined as the pressure ratio between before compressor and after compressor. Increasing ORC evaporation temperature will lead to an increase in the compressor pressure ratio. This can lead to an increase in the input power to the VCR compressor, that results in raising the compressor output discharge pressure since the VCR evaporation pressure and the working fluid volume flow rate are constant. Increasing the ORC evaporation temperature will decrease the VCR COP due to the increase in the input power to the compressor while the evaporation pressure of the VCR stays constant.

4.7 Overall COPs and CPR with variation of ORC evaporation temperature

Figure 4-9 presents the overall COP of the combined cycles and the expansion pressure ratio with the ORC evaporation temperature.

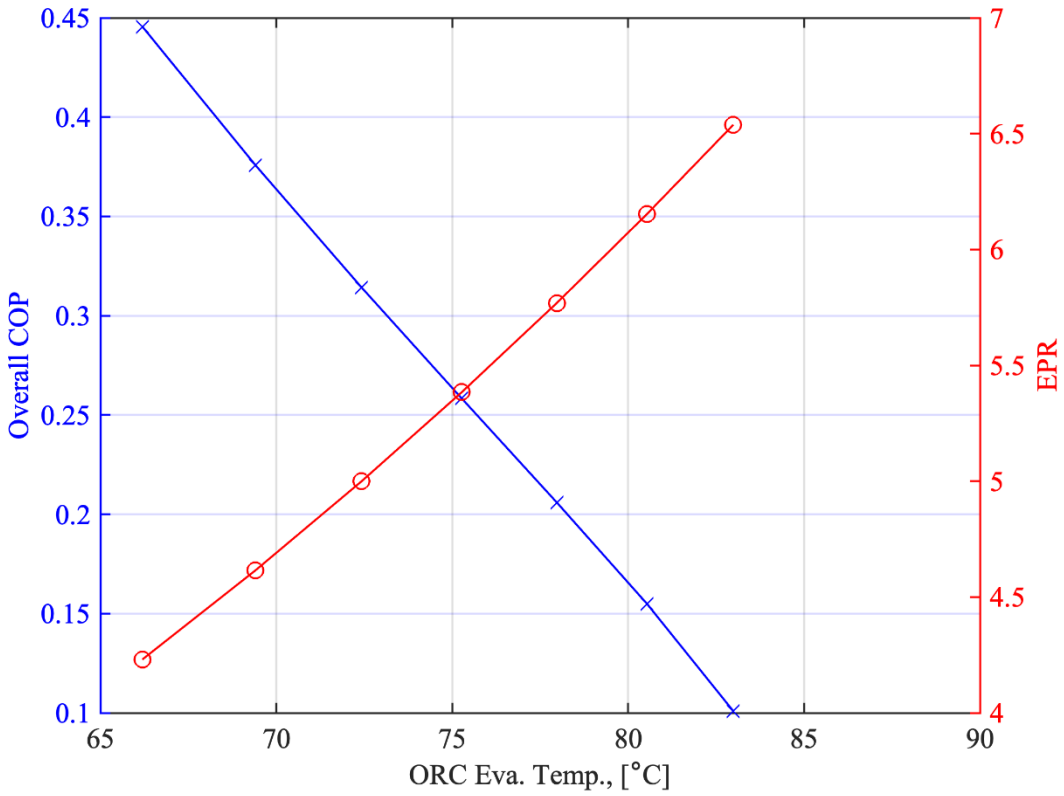

Figure 4-9: ORC evaporation temperature and EPR against overall COP

The overall COP decreases with the increase of the ORC evaporation temperature and it also decreases with the increase of the expansion pressure ratio. Since the increase of the ORC evaporation temperature and the expansion pressure ratio will increase the power supplied to the VCR subsystem, the heat rejected from the VCR condenser will be increased because the VCR evaporator has a constant evaporation pressure in turn, the COP of the VCR will decrease.

4.8 Effect of ORC evaporation and shaft speeds

4.8.1 Effects on $Q_{eva,ORC}$ and $Q_{eva,VCR}$

Figure 4-10 and Figure 4-11 display the heat rates in the evaporators of both the ORC, $Q_{eva,ORC}$, and VCR, $Q_{eva,VCR}$, systems, showing how they change with varying evaporation temperatures while the rotational speed of the single-rotor expander-

compressor ranges from 500 to 3000 revolutions per minute (rpm). For any fixed speed, the heat rate in the ORC's evaporator, $Q_{eva,ORC}$, rises in conjunction with an increase in the ORC's evaporation temperature, $T_{eva,ORC}$. This rise is due to an enhanced refrigerant mass flow rate within the ORC, a result of the increased refrigerant density at the evaporator's exit as vapor compressibility goes up with higher evaporation temperatures. Concurrently, while the evaporation pressure escalates, the latent heat associated with evaporation diminishes. Nonetheless, the influence of a rising mass flow rate overshadows the reduction in latent heat, which in turn leads to an upsurge in the heat rate of the ORC's evaporator, $Q_{eva,ORC}$. Notably, the heat rate of the ORC, $Q_{eva,ORC}$, is unaffected by the evaporation temperature in the VCR system. At a constant rotational speed of 500 rpm and regardless of the VCR's evaporation temperature, $T_{eva,VCR}$, , the ORC's heat rate, $Q_{eva,ORC}$, increases from 1.6 kW to 3.56 kW, marking a 122% increase, as the ORC evaporation temperature, $T_{eva,ORC}$, rises from 62.5 °C to 89.7 °C. Similarly, at a speed of 3000 rpm, the heat rate in the ORC, $Q_{eva,ORC}$, elevates from 9.6 kW to 21.2 kW within the same range of ORC evaporation temperatures. An increase in the mass flow rate consequently raises the power necessitated by the compressor, owing to an increase in the power output of the expander.

As the ORC evaporation temperature, $T_{eva,ORC}$, increased from 62.5°C to 89.7°C at a speed of 500 rpm, the work produced by the expander changed from 0.14 kW to 0.44 kW. At a higher speed of 3000 rpm, the expander work is 0.84 kW when $T_{eva,ORC}$ is 62.5°C, and it increases to 2.65 kW when $T_{eva,ORC}$ is 89.7°C.

.

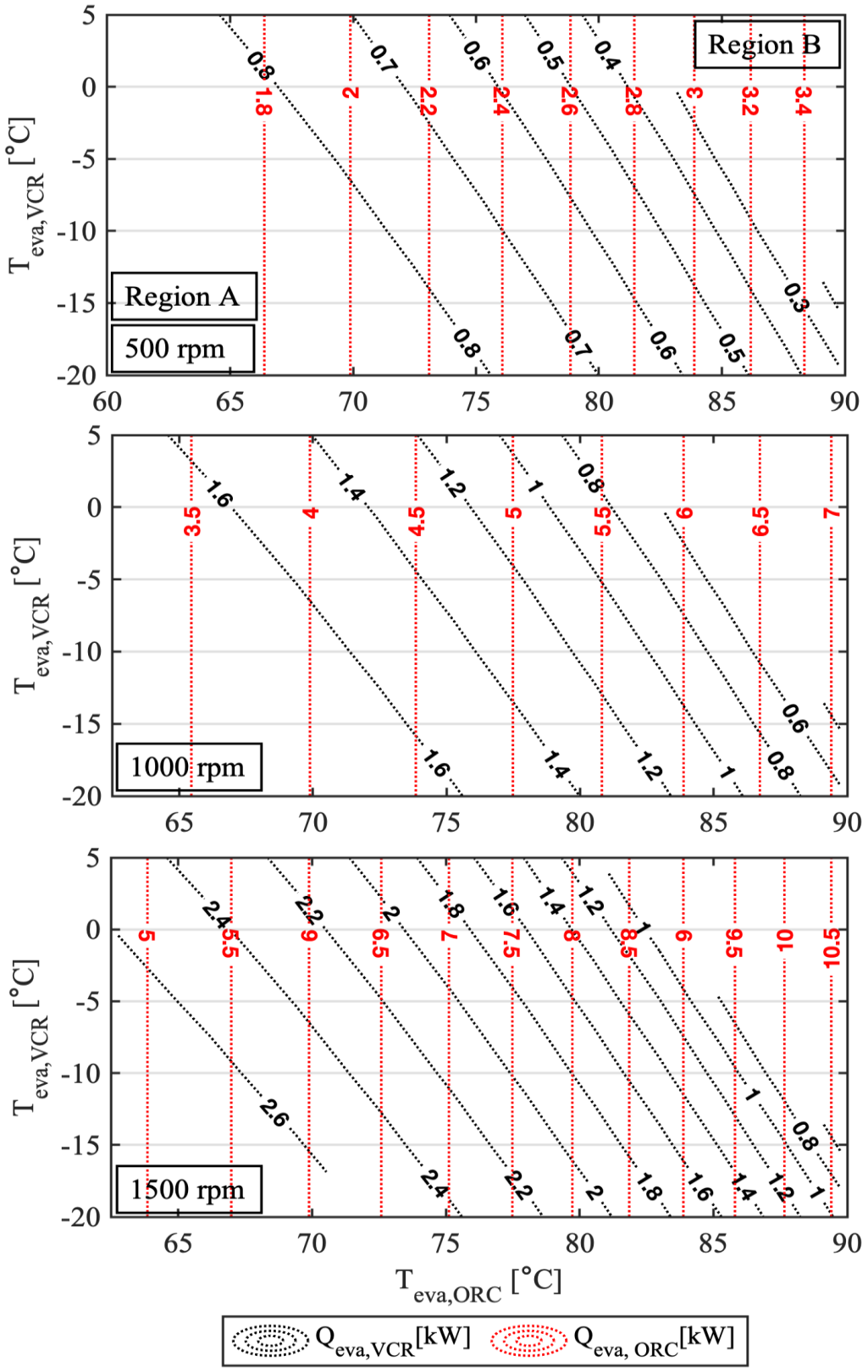

Figure 4-10: Variation of $Q_{eva,ORC}$ and $Q_{eva,VCR}$ under the influence of evaporation temperatures of ORC and VCR for different speeds and $T_{cond,ORC}$ = 20.5 °C. (500rpm, 1000 rpm, and 1500 rpm).

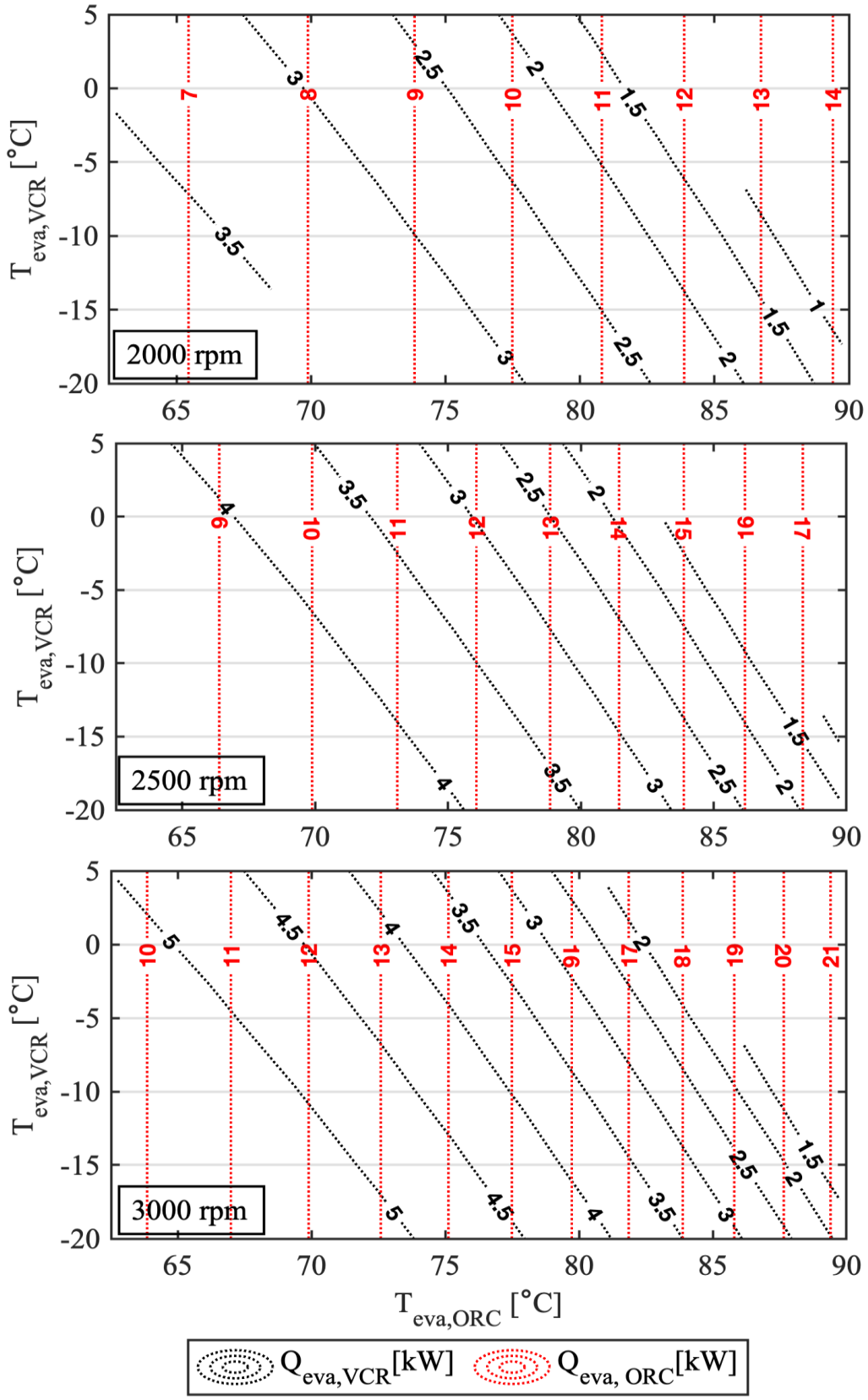

Figure 4-11: Variation of $Q_{eva,ORC}$ and $Q_{eva,VCR}$ under the influence of evaporation temperatures of ORC and VCR for different speeds and $T_{cond,ORC}$ = 20.5 °C. (2000 rpm, 2500 rpm, and 3000 rpm).

Increasing the work input to the compressor results in a higher outlet condensation pressure, as explained in section 4.2. When the VCR condensation pressure rises, there is also an increase in vapor quality following the expansion process. Consequently, in the VCR evaporator, a less amount of liquid refrigerant is involved in the heat absorption process. This leads to a reduction in $Q_{eva,VCR}$ at any given $T_{eva,VCR}$ as the ORC's evaporation temperature increases, with the VCR's mass flow rate remaining constant. For example, at 500 rpm and $T_{eva,VCR}$ = -20 °C, the maximum $Q_{eva,VCR}$ is 0.8 kW when $T_{eva,ORC}$ is 75 °C, whereas the minimum is 0.3 kW at 89.7 °C. At the same rotational speed, the highest cooling effect in the VCR evaporator, $Q_{eva,VCR}$, at a VCR evaporation temperature of 5°C, reaches 0.82 kW with the ORC evaporation temperature set to 62.75°C, and drops to a minimum of 0.34 kW at an ORC temperature of 80.5°C. Similarly, at a higher speed of 3000 rpm and a VCR evaporation temperature of -20°C, $Q_{eva,VCR}$ peaks at 5.15 kW for an ORC temperature of 72.4°C, and falls to its lowest at 1.19 kW for an ORC temperature of 89.7°C. When the VCR evaporation temperature is at 5°C and the rotor speed is at 3000 rpm, the maximum $Q_{eva,VCR}$ noted is 4.97 kW for an ORC temperature of 62.75°C, declining to 2.05 kW at an ORC temperature of 80.5°C. Nonetheless, the absolute maximum cooling effect achieved for the VCR, $Q_{eva,VCR}$, within the examined operating range is 5.38 kW, occurring at a rotor speed of 3000 rpm, with the ORC and VCR evaporation temperatures set at 62.75°C and -5°C, respectively.

The speed of the rotor is a critical factor in determining performance and $Q_{eva,ORC}$ in a linear manner with speed because of the greater volume displaced by both the expander and compressor sides of the device. When comparing to a baseline speed of 500 rpm, the average increments in $Q_{eva,ORC}$ and $Q_{eva,VCR}$ at speeds of 1000 rpm, 1500 rpm, 2000 rpm, 2500 rpm, and 3000 rpm are observed to be 200%, 300%, 400%, and 500% respectively.

4.8.2 Effects on Heat to Cooling Efficiency η_{H-C}

Figure 4-12 and Figure 4-13 show the variation of the ORC and VCR evaporation temperatures as well as the shaft speed of the single rotor expander-compressor and the system efficiency to convert heat to cooling. The heating to cooling efficiency is the ratio of the amount of cooling effects $Q_{eva,VCR}$ the VCR produced to the amount of heat being absorbed by the working fluid of the ORC $Q_{eva,ORC}$.

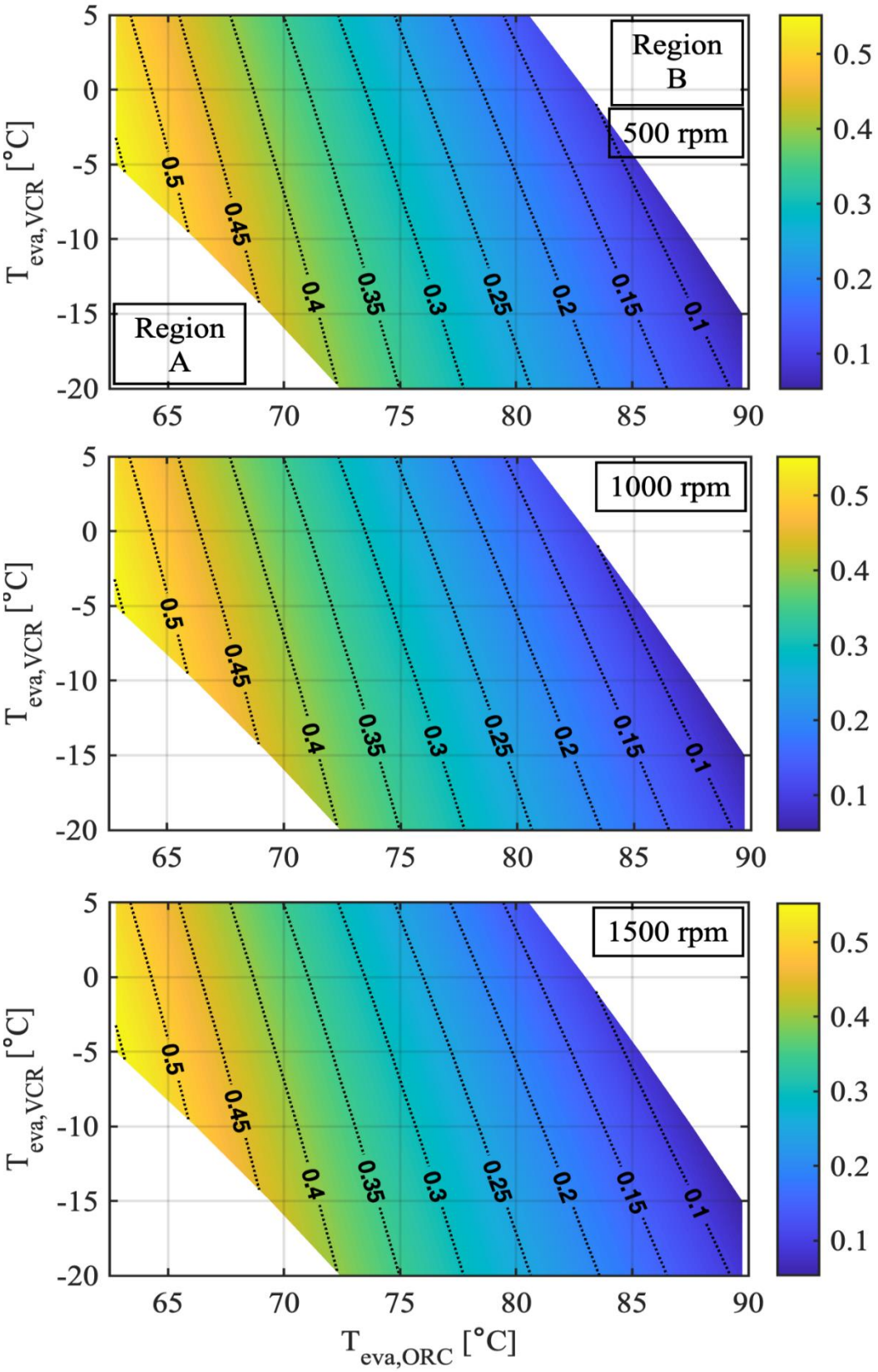

Figure 4-12: Variation of η_{H-C} under the influence of evaporation temperatures of ORC and VCR for different speeds and $T_{cond,ORC}$ = 20.5 °C. (500rpm, 1000 rpm, and 1500 rpm).

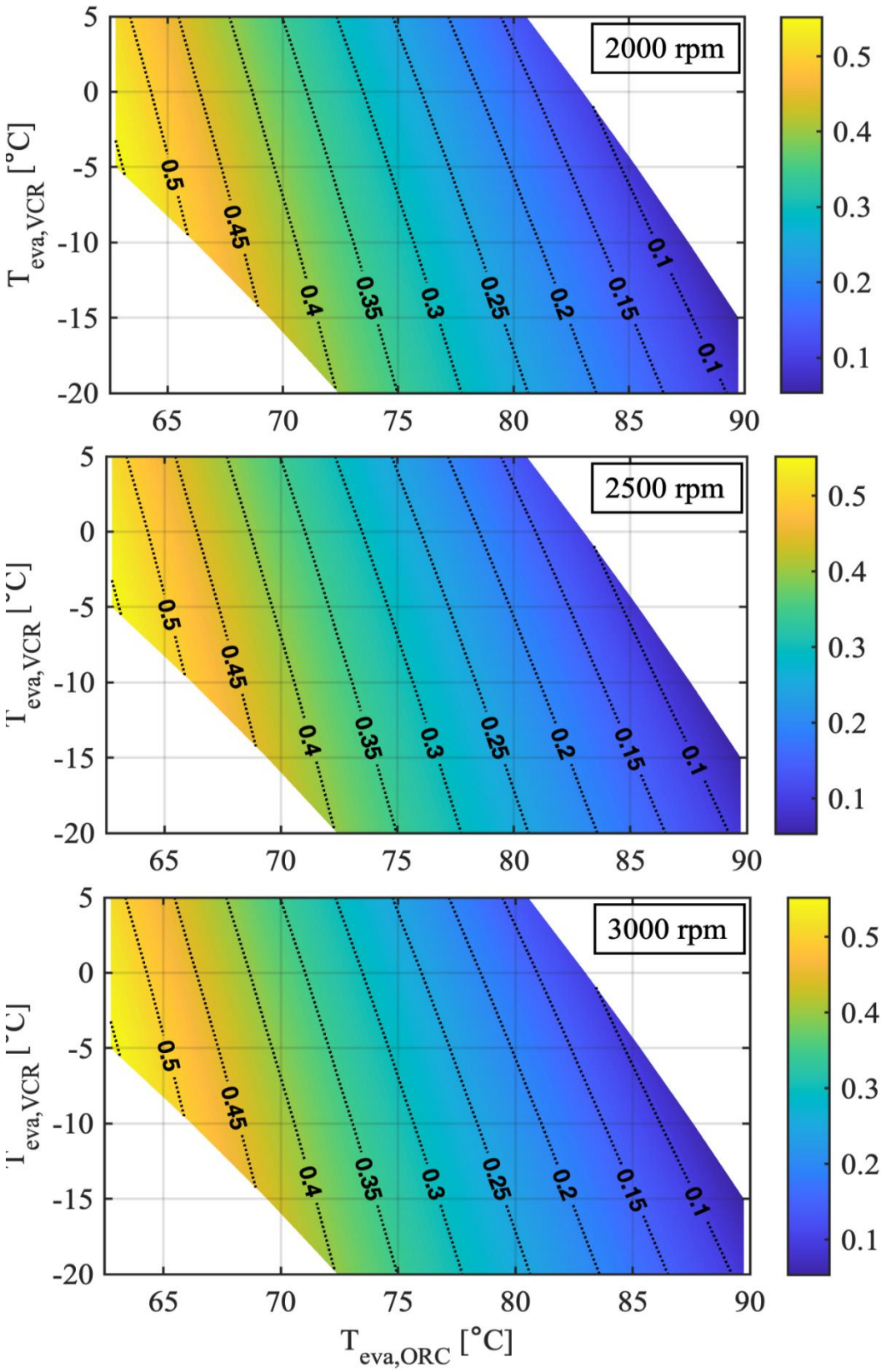

Figure 4-13: Variation of η_{H-C} under the influence of evaporation temperatures of ORC and VCR for different speeds and $T_{cond,ORC}$ = 20.5 °C. (2000 rpm, 2500 rpm, and 3000 rpm).

As seen in Figure 4-12 and Figure 4-13 the heat-to-cooling efficiency for all shaft speeds under consideration shows a decreasing trend with the increase in $T_{eva,ORC}$ which is attributed to the decreasing trend of $Q_{eva,VCR}$. It can be seen that, at 500 rpm and $T_{eva,VCR}$ = -20 °C, η_{H-C} varies between 40 % to 9 % when $T_{eva,ORC}$ increases from 72.4 °C to 89.7 °C. On the other hand, at $T_{eva,VCR}$ = 5 °C, η_{H-C} corresponds to $T_{eva,ORC}$ = 62.7 °C is 51 % and that to $T_{eva,ORC}$ = 80.5 °C is 6 %. It is found that the overall highest η_{H-C} of 56% is obtained at $T_{eva,ORC}$ = 62.75 °C and $T_{eva,VCR}$ = -5 °C. Furthermore, the rotor speed does not influence the heat-to-cooling efficiency showing the same magnitude for all speeds under consideration.

In Figure 4-10 and Figure 4-13, there are two blank regions as indicated by (Region A) and (Region B). For region A, at lower $T_{eva,ORC}$, the expander produces less power, which can be enough to run the compressor at high $T_{eva,VCR}$, but at $T_{eva,VCR}$, the difference between the compressor discharge stream temperature and the ambient temperature reaches the minimum temperature approach, which was set to 5 °C in the condenser of the VCR, as mentioned in Table 3-2. Thus, the complete condensation is not achieved in the condenser leading to two-phase entry of the refrigerant at the entry of the expansion device.

Under this circumstance, model do not converge and fail to generate reliable results. For Region B, when the output power of the expander started increasing, the compressor discharge pressure increased to the point where the compressor discharge pressure reached the critical pressure (for R134a, 40.593 bar). Thus, the condensation process was not completed. Consequently, the model does not converge and not able to produce cooling effects under these conditions.

4.9 Effect of ORC condensation temperature

4.9.1 Effects on $Q_{eva,ORC}$ and $Q_{eva,VCR}$

Figure 4-14 and Figure 4-15 show the effects of condensation temperature of ORC $T_{cond,ORC}$ on the $Q_{eva,ORC}$ and the $Q_{eva,VCR}$. Increasing $T_{cond,ORC}$ resulted in a slight decrease in $Q_{eva,ORC}$ and that can be attributed to increase in enthalpy at the evaporator inlet of ORC due to the increase in liquid refrigerant temperature at the evaporator inlet. Therefore, the enthalpy difference across the evaporator of ORC decreases because the enthalpy at its outlet is constant. $Q_{eva,ORC}$ decreases from 2.75 kW to 2.36 kW for 500 rpm when $T_{cond,ORC}$ increases from 20 °C to 45 °C. At 3000 rpm, $Q_{eva,ORC}$ is 16.51 kW at $T_{cond,ORC}$ = 20 °C and drops to 14.17 kW at $T_{cond,ORC}$ = 45 °C. Furthermore, increasing $T_{cond,ORC}$ increases the outlet pressure of the expander which reduces the power generated by the expander of ORC. This reduces the input power to the compressor of VCR subsystem reduces. At 500 rpm, the expander work is 0.32 kW at $T_{cond,ORC}$ = 20 °C and drop to 0.17 kW at $T_{cond,ORC}$ = 45 °C. When $T_{cond,ORC}$ increases from 20 °C to 45 °C, the expander work decreases from 1.92 kW to 1.02 kW for 3000 rpm.

The outlet pressure of the compressor (condensation pressure of VCR) decreases as the work supplied to compressor decreases. This results in a decrease in vapor quality after expansion which makes more liquid refrigerant available for the heat absorption process in the evaporator of VCR at the same evaporation pressure. Consequently, $Q_{eva,VCR}$ increases as the condensation temperature of the ORC increases, as presented in Figure 14. For 500 rpm, at $T_{eva,VCR}$ = -20 °C the maximum $Q_{eva,VCR}$ is 0.79 kW when $T_{cond,ORC}$ is 30 °C and the minimum is 0.66 kW at 20 °C. For the same speed, the maximum $Q_{eva,VCR}$ at $T_{eva,VCR}$ = 5 °C is 0.69 kW when $T_{cond,ORC}$ is 40 °C and the minimum is 0.62 kW when $T_{cond,ORC}$ is 35 °C.

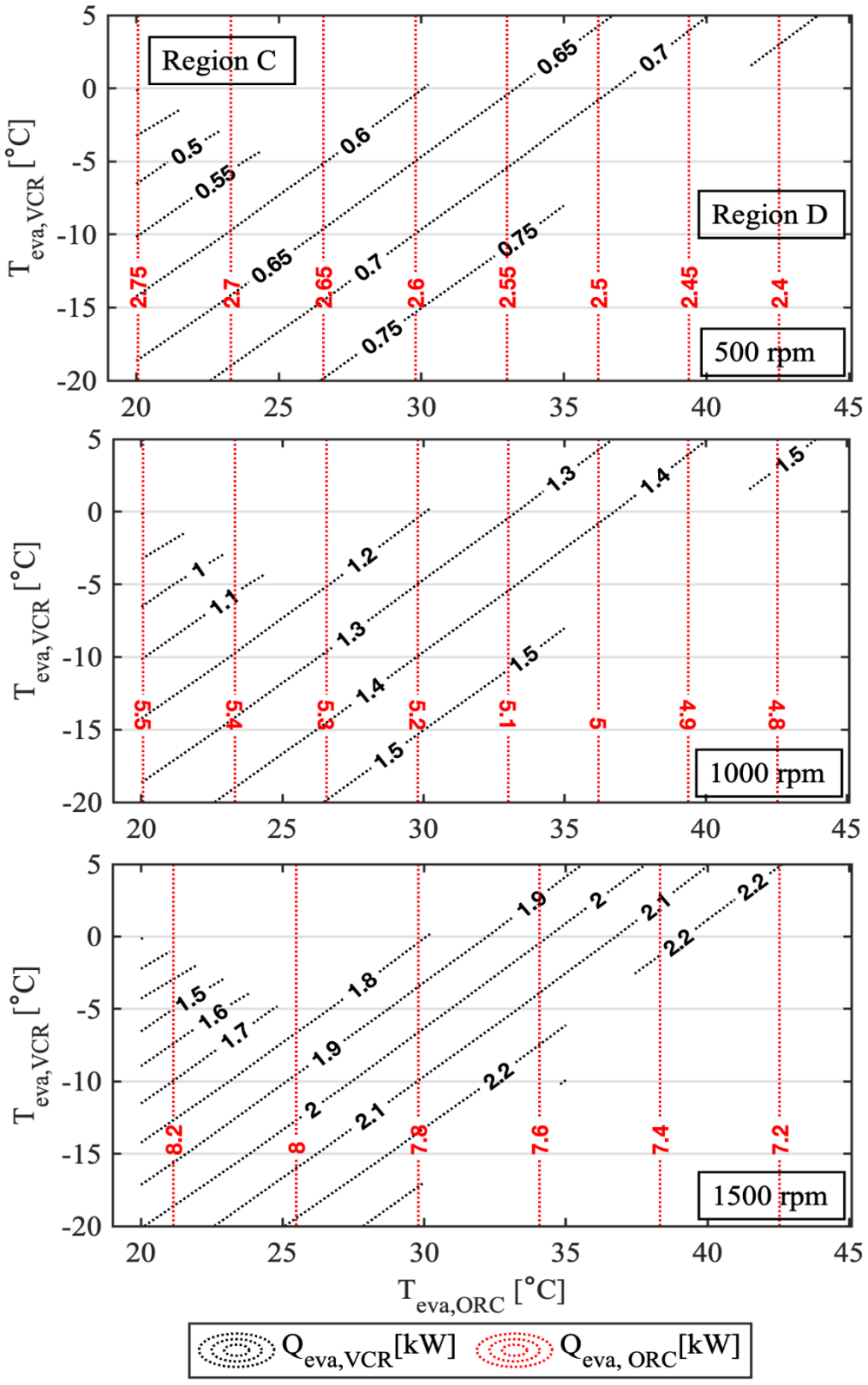

Figure 4-14: Variation of $Q_{eva,ORC}$ and $Q_{eva,VCR}$ under the influence of condensation temperatures of ORC and VCR for different speeds and evaporation temperature of ORC is 80.53 °C. (500rpm, 1000 rpm, and 1500 rpm).

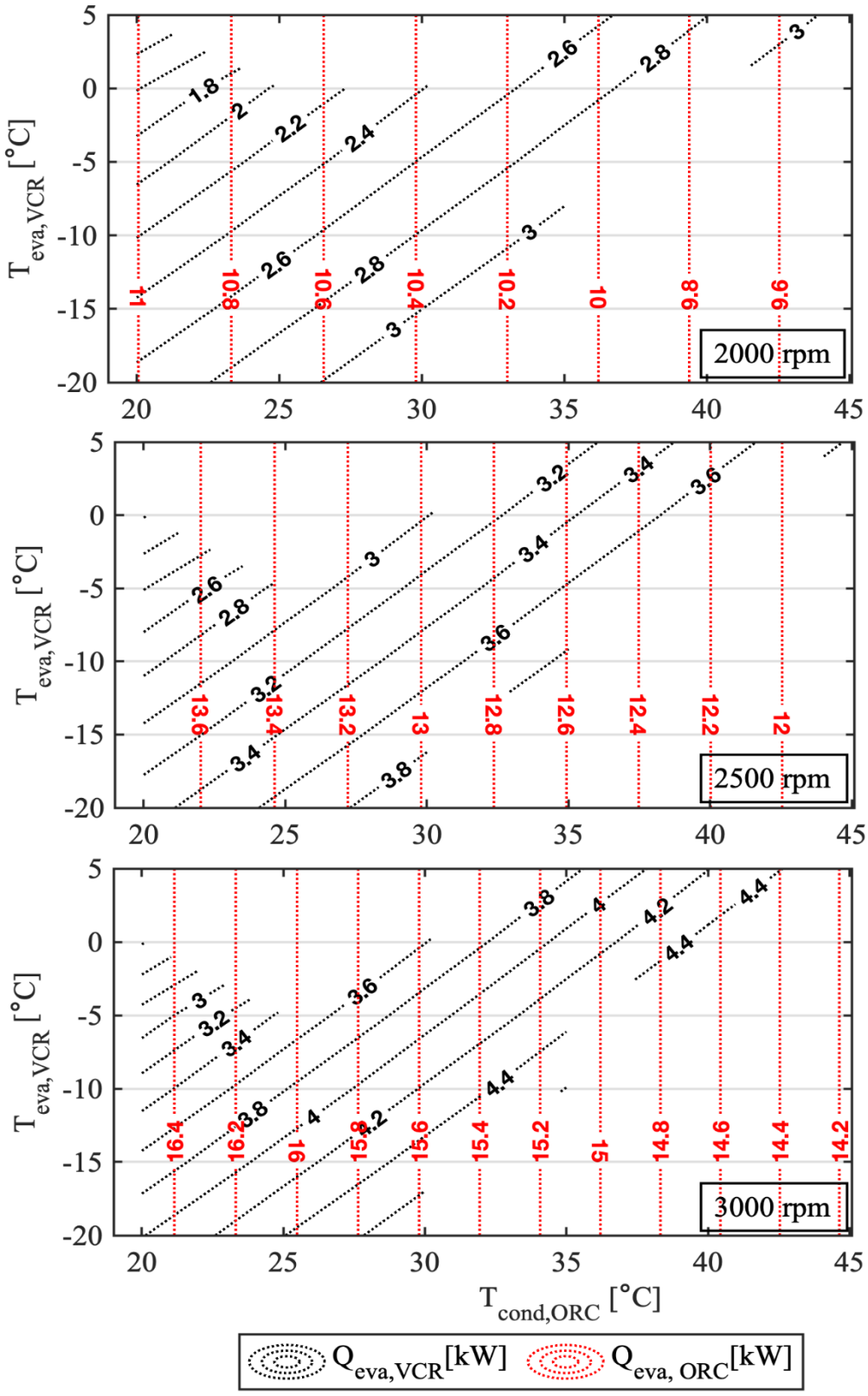

Figure 4-15: Variation of $Q_{eva,ORC}$ and $Q_{eva,VCR}$ under the influence of condensation temperatures of ORC and VCR for different speeds and evaporation temperature of ORC is 80.53 °C. (2000 rpm, 2500 rpm, and 3000 rpm).

Likewise, at a rotational speed of 3000 rpm with the evaporating temperature of the VCR, $T_{eva,VCR}$, at -20 °C, $Q_{eva,VCR}$ peaks at 4.75 kW when the condensation temperature of the ORC, $T_{cond,ORC}$, is 30 °C, and it dips to its lowest value of 3.98 kW at a $T_{cond,ORC}$ of 20 °C. Maintaining the same 3000 rpm, but with a $T_{eva,VCR}$ = 5 °C, $Q_{eva,VCR}$ reaches its highest at 4.58 kW when $T_{cond,ORC}$ is 45 °C, and it falls to its lowest at 3.74 kW when $T_{cond,ORC}$ is 35 °C. Nevertheless, the highest recorded $Q_{eva,VCR}$ across the assessed operational conditions is 4.75 kW, observed at 3000 rpm with a $T_{con,ORC}$ of 30 °C and $T_{eva,VCR}$ of -20 °C.

4.9.2 Effects of $T_{cond,ORC}$ on heat to cooling efficiency η_{H-C}

Figure 4-16 and Figure 4-17 provide a visual representation of how the heat to cooling efficiency varies with changes in $T_{cond,ORC}$ and $T_{eva,VCR}$ across different shaft speeds. It's evident that the heat-to-cooling efficiency increases as the ORC condensation temperature rises, and this relationship becomes more pronounced at higher condensation temperatures. Conversely, the heat-to-cooling efficiency exhibits a declining pattern as the VCR evaporation temperature increases. This can be explained by the fact that, with fixed condensation temperature and constant shaft speed, the cooling capacity, $Q_{eva,VCR}$, decreases as the VCR evaporation temperature rises. Since the heat absorbed by the ORC evaporator remains relatively constant at different condensing temperatures, any increase in cooling capacity results in an improvement in the heat to cooling efficiency.

As observed at 500 rpm, η_{H-C} ranges from 24 % to 30% when $T_{eva,VCR}$ is held at -20 °C, and this variation occurs as $T_{cond,ORC}$ increases from 20 °C to 45 °C. Conversely, at $T_{eva,VCR}$ = 5 °C, η_{H-C} corresponds to $T_{cond,ORC}$ = 40 °C at 28 % and it reaches 32% at $T_{cond,ORC}$ = 45 °C. The highest overall η_{H-C} of 32% is achieved when $T_{cond,ORC}$ is set to 45 °C, and $T_{eva,VCR}$ is maintained at 5 °C. It's worth noting that the rotor speed has no

impact on the heat-to-cooling efficiency, with the magnitude remaining consistent across all speeds considered.

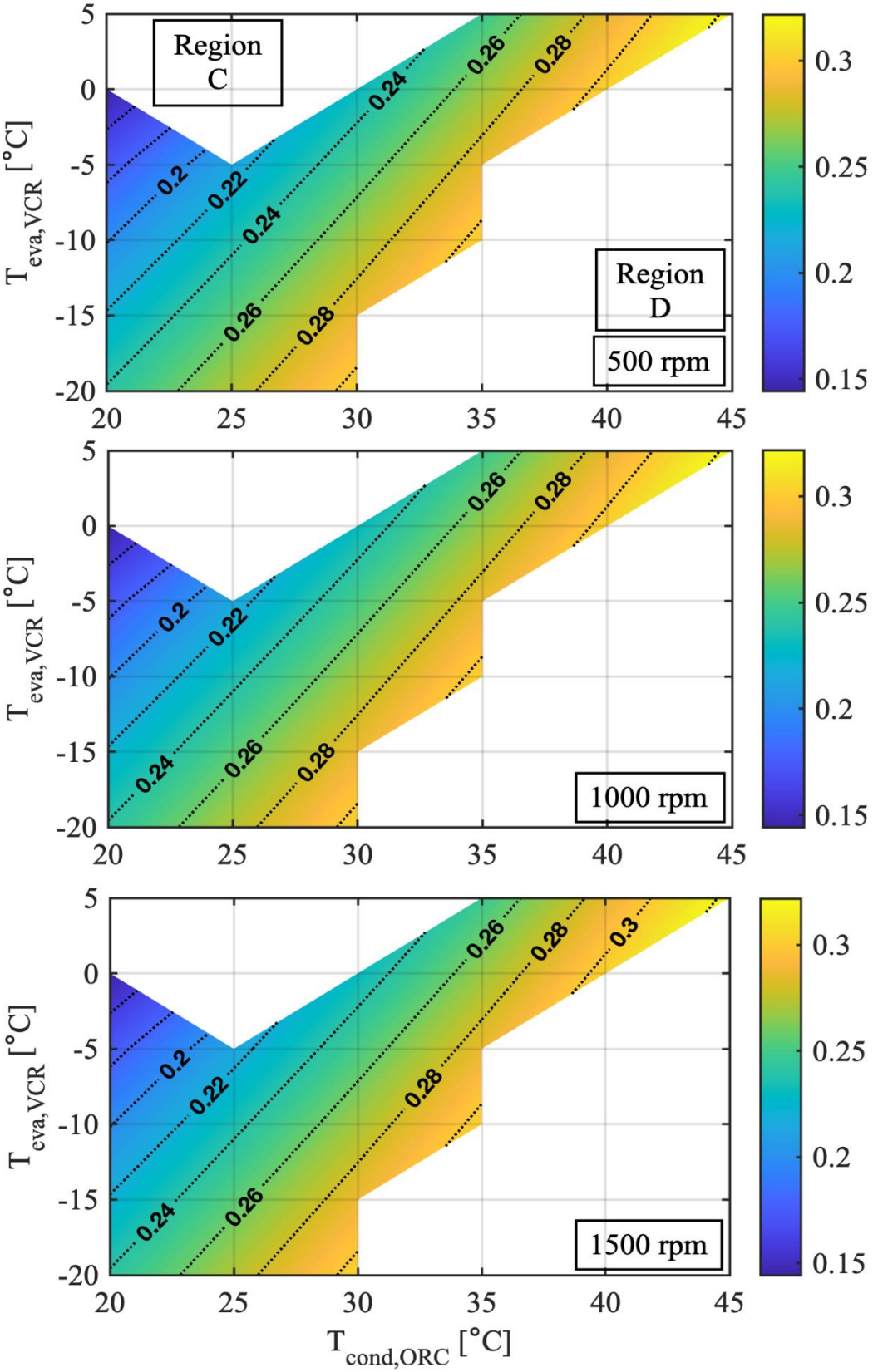

Figure 4-16: Variation of η_{H-C} under the influence of condensation temperatures of ORC and VCR for different speeds and evaporation temperature of ORC is 80.53 °C. (500rpm, 1000 rpm, and 1500 rpm).

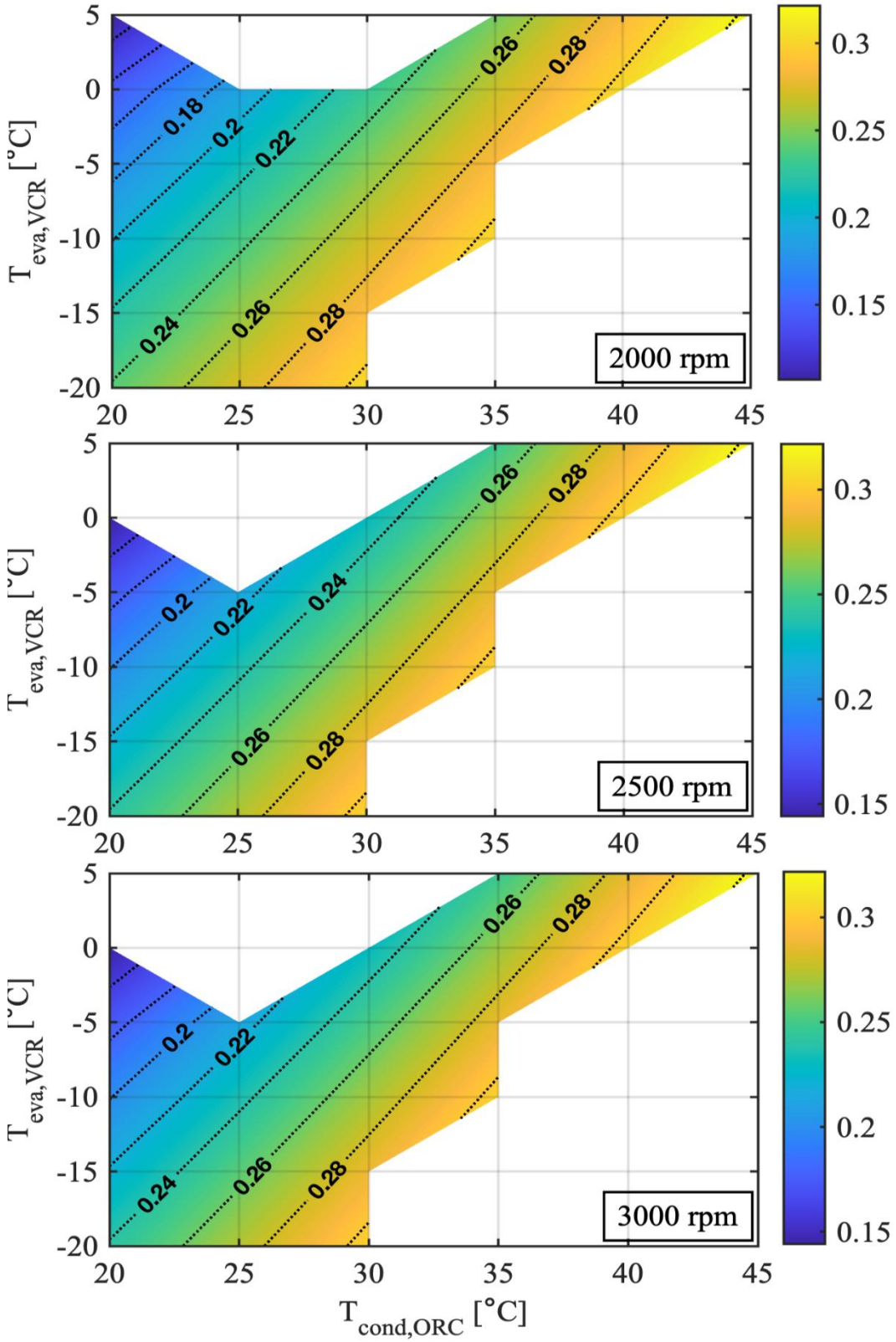

Figure 4-17: Variation of η_{H-C} under the influence of condensation temperatures of ORC and VCR for different speeds and evaporation temperature of ORC is 80.53 °C. (2000 rpm, 2500 rpm, and 3000 rpm).

From Figure 4-14 to Figure 4-17, there are two distinct areas identified as (Region C) and (Region D) where specific conditions impact the system's behaviour. In Region C, lower $T_{cond,ORC}$ and higher $T_{eva,VCR}$ result in the highest output power from the expander. This increase in power output leads to higher compressor discharge pressure and temperature. However, if these parameters reach critical pressure or temperature, the refrigerant fails to fully condense. As a consequence, the system model terminates without generating cooling effects, especially at high $T_{eva,VCR}$. In Region D, as $T_{cond,ORC}$ begins to rise, the output power of the expander decreases, causing a drop in the compressor discharge pressure. Since both the ORC and VCR subsystems operate under the same ambient conditions, the condensation temperature should not be lower than $T_{cond,ORC}$. Consequently, the system is unable to produce cooling effects under these conditions.

4.10 Effect of ORC degree of superheating and subcooling

4.10.1 Effects on $Q_{eva,ORC}$ and $Q_{eva,VCR}$

Figure 4-18 and Figure 4-19 depict the impact of ΔT_{sup} (temperature difference in superheating) and ΔT_{sub} (temperature difference in subcooling) within the ORC subsystem on $Q_{eva,ORC}$ and $Q_{eva,VCR}$, respectively. These analyses are conducted at $T_{eva,VCR}$ = 0 °C, and a speed shaft of 1000 rpm. ΔT_{sup} and ΔT_{sub} are varied across a range from 0 °C to 10 °C, resulting in nine different sets of conditions. In the case of the [0,0] set, where both ΔT_{sup} and ΔT_{sub}, $T_{eva,ORC}$ is adjusted from 66.19 °C to 89.74 °C while maintaining a constant $T_{cond,ORC}$ of 35 °C. The findings reveal that increasing ΔT_{sup} does not lead to an increase in either $Q_{eva,ORC}$ or $Q_{eva,VCR}$.

On the other hand, an increase in ΔT_{sub} resulted in an increase in $Q_{eva,ORC}$ w , as evident when comparing the three sets: [0,0], [0,5], and [0,10]. Specifically, when ΔT_{sub} increased from 0 °C to 10 °C while keeping ΔT_{sup} constant at 0 °C, $Q_{eva,ORC}$ increased by 6.4%.

However, it's worth noting that ΔT_{sub} has no effect on $Q_{eva,VCR}$, as demonstrated by the overlap of the results for [5,5] and [5,10] sets. Similarly, Figure 4-19 presents the variation in heat to cooling efficiency under the same assumptions applied in Figure 4-18.

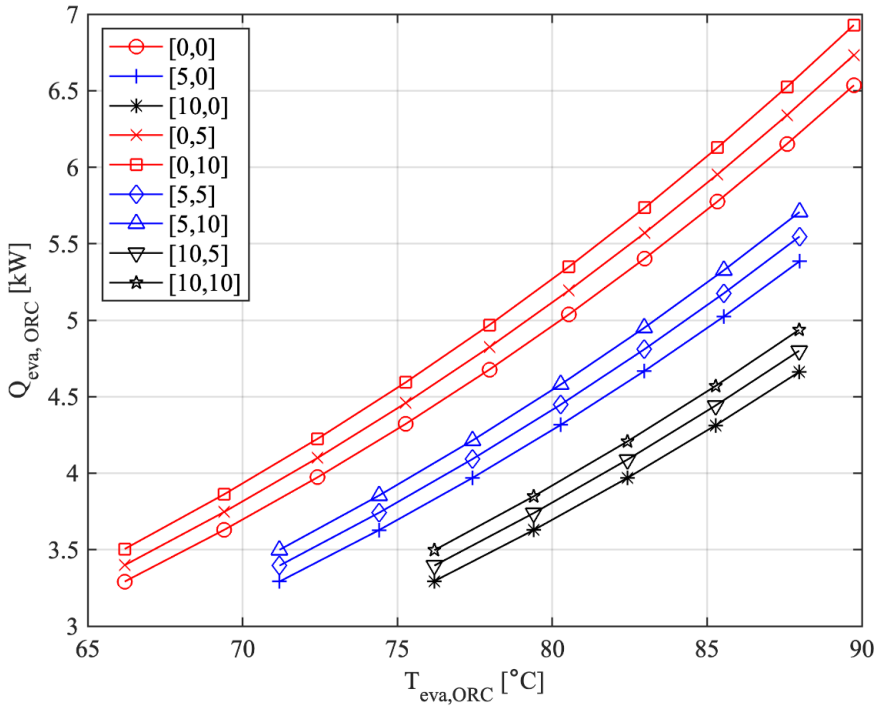

Figure 4-18: Influence of the degree of superheating (ΔTsup) and degree of subcooling (ΔTsub) on $Q_{eva,ORC}$. In legends, square parenthesis indicates [ΔTsup, ΔTsub].

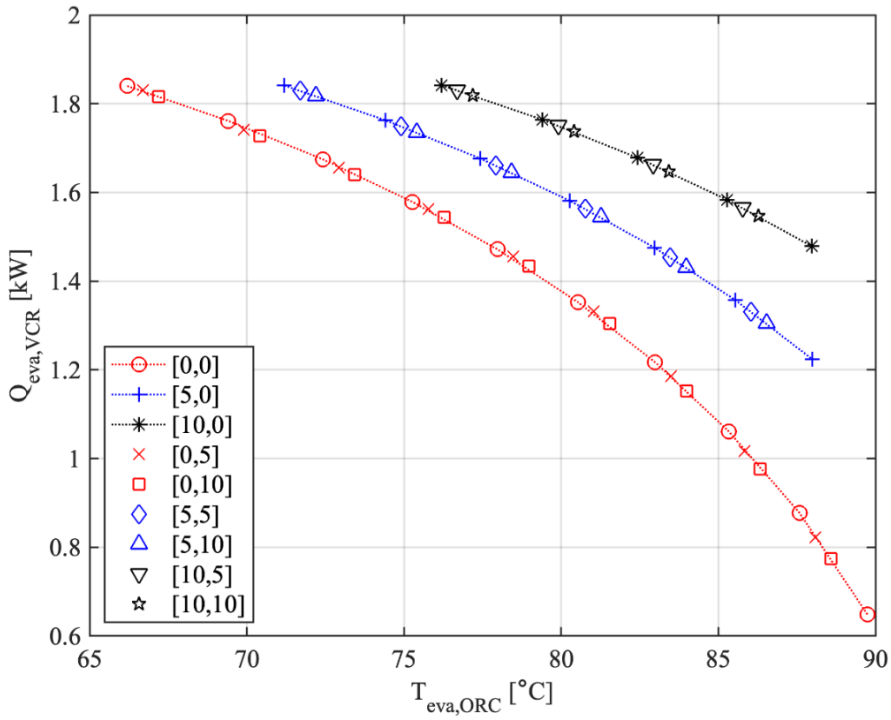

Figure 4-19: Influence of the degree of superheating (ΔTsup) and degree of subcooling (ΔTsub) on $Q_{eva,VCR}$. In legends, square parenthesis indicates [ΔTsup, ΔTsub].

4.10.2 Effects on η_{H-C}

Figure 4-20 shows that increasing ΔT_{sup} does not increase heat-to-cooling efficiency.

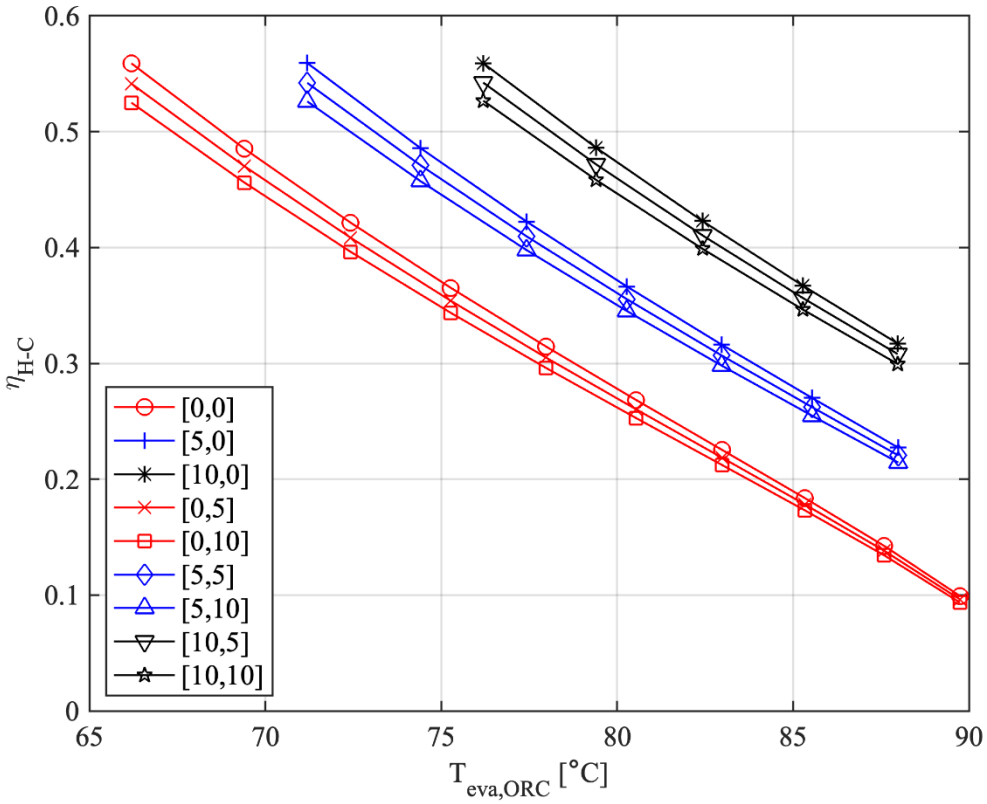

Figure 4-20: Influence of the degree of superheating (ΔTsup) and degree of subcooling (ΔTsub) on η_{H-C}. In legends, square parenthesis indicates [ΔTsup, ΔTsub].

Nevertheless, an increase in ΔT_{sub} led to a reduction in the heat-to-cooling efficiency. Specifically, as ΔT_{sub} increases from 0 °C to 10 °C while maintaining ΔT_{sup} at constant 0 °C, there was a 6.4% decrease in heat-to-cooling efficiency. This decline is linked to the increase in $Q_{eva,ORC}$ while $Q_{eva,VCR}$ remained unchanged.

4.11 Summary

This chapter explores the feasibility of utilizing a novel single rotor expander-compressor unit in cooling systems by integrating a vapor compression refrigeration (VCR) cycle with an organic Rankine cycle (ORC). The thermal performance assessment focuses on examining the effects of the ORC evaporation temperature range between 62.75 °C and

89.7 °C, the VCR evaporation temperature from -20 °C to 5 °C, the ORC condensation temperature spanning 20 °C to 45 °C, and rotational speeds from 500 rpm to 3000 rpm, all while maintaining a constant hot water source temperature at 95 °C. The increase in the compressor's discharge pressure is notably affected by the displaced volume on each side of the unit and becomes more pronounced with a higher inlet pressure of the expander. This effect is especially significant when the expansion process takes place on the larger side, which has a greater displacement volume compared to the smaller side. Additionally, a higher condensation temperature within the ORC leads to a reduction in the compressor's discharge pressure. As the ORC evaporator temperature rises from 62.5 °C to 89.7 °C, the cooling output, $Q_{eva,ORC}$ escalates from 1.6 kW to 3.56 kW and from 9.6 kW to 21.2 kW, which is an increase of approximately 120%, at shaft speeds of 500 rpm and 3000 rpm, respectively. Also, at a speed of 500 rpm and an evaporation temperature of the VCR at -20 °C, the heat-to-cooling efficiency ranges from 40% to 9% as the ORC evaporation temperature is increased from 72.4 °C to 89.7 °C. Conversely, when $T_{eva,VCR}$ = 5 °C, the heat-to-cooling efficiency is 51% at $T_{eva,ORC}$ = 62.7 °C and drops to 6% at $T_{eva,ORC}$ = 80.5 °C. Similarly, as the condensation temperature of the ORC increases from 20 °C to 30 °C, the refrigerating effect, $Q_{eva,ORC}$ also rises. Specifically, at speeds of 500 rpm and 3000 rpm, $Q_{eva,ORC}$ increases from 0.66 kW to 0.79 kW and from 3.98 kW to 4.75 kW, respectively.

Furthermore, at 500 rpm and $T_{eva,VCR}$ maintained at -20 °C, the heat to cooling efficiency exhibited a range from 24 % to 30 % as $T_{cond,ORC}$ increased from 20 °C to 45 °C. Conversely, when $T_{eva,VCR}$ was set at 5 °C, the heat to cooling efficiency reached 28% at $T_{cond,ORC}$ = 40 °C and peaked at 32% when $T_{cond,ORC}$ = 45 °C. In summary, the highest levels of cooling effect and heat-to-cooling efficiency attained were 5.38 kW and 56%, respectively. These values were achieved when the evaporation temperature of the ORC

and VCR were set to 62.75°C and -5°C, respectively, while the condensation temperature of the ORC was set at 20.5°C. Notably, the cooling effect displayed a linear increase with rotor speed, whereas the heat-to-cooling efficiency remained unaffected by variations in rotor speed.

Chapter 5: Detailed Exergy analysis of ORC-VCR combined by single rotor expander-compressor.

5.1 Introduction

The major concern of the first law of thermodynamics is the maintenance of a constant amount of energy. As a consequence of this, it is unable to pinpoint the precise position or mechanism of any irreversibilities that may exist within the system's component parts. The application of exergy analysis is dependent on the principles of the conservation of energy and mass, as well as the second law of thermodynamics. These laws must be satisfied for the analysis to be successful. The equilibrium between the exergy that is lost and the net exergy that is transported across the control volume boundary in the form of work, heat, or mass flow is what defines the exergy balance for an open system that is operating in a state of steady equilibrium. This chapter presents a comprehensive investigation into the destruction of exergy that occurs in an ORC-VCR that is coupled by a single rotor expander-compressor (compander).

The layout of the ORC-VCR system, which will be analysed from the perspective of exergy, can be seen in Figure 3-1. The operational conditions of the system and the variations in how it operates are comparable to those parameters, which were introduced and addressed earlier in Chapter 3. This system will be evaluated based on its overall exergy efficiency as well as the effects of the operational conditions on the amount of exergy that is destroyed by each individual component of the system.

5.2 Exergy destruction during expansion and compression processes

5.2.1 Effects of EPR and VCR evaporation temperature variation

The amount of exergy lost during expansion and compression processes in a single rotor expander-compressor at various EPR ratios and for a range of VCR evaporation temperatures is depicted in Figure 5-1.

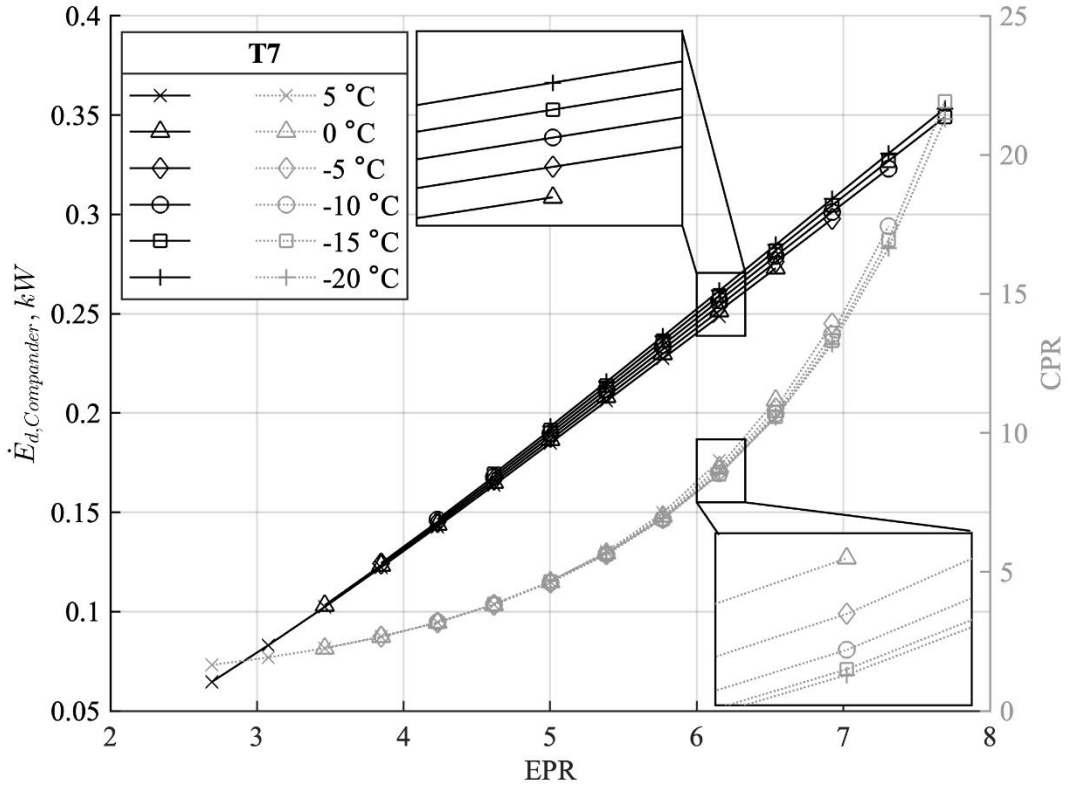

Figure 5-1: Exergy destruction during expansion and compression with variation of EPR CPR ratios.

During the expansion process, the working fluid is subjected to high temperatures and pressures on the side of the expander. This working fluid then expands to the point where it reaches the condensation pressure. The mechanical power that was delivered to the compressor side as a result of this expansion. During this process, in which the condition of the working fluid is changed from high pressure and temperature to low pressure and temperature, certain amounts of exergy are destroyed.

This exergy destruction is connected with the variation in temperature that exists between the conditions at the input and the output of the expansion process. In addition, raising the EPR ratio results in an increase in the mass flow rate entering the expander side, which in turn results in an increase in the quantity of exergy that is being destroyed. During the compression process, increasing the EPR ratio results in an increase in the input power to the compressor side, which, in turn, results in an increase in the discharge pressure of the compressor. Because the VCR evaporation temperature stays the same under specific conditions, the inlet pressure to the compression process also remains the same. However, because the volume flow rate is set to the maximum flow at 1000 rpm, the pressure difference between the inlet and outlet of the compressor side will be significantly increased. Because of this rise in the pressure difference, there is a corresponding increase in the amount of exergy that is destructed on the compression side.

Figure 5-2 illustrates the exergy destruction by the compander due to the combination of the expansion and compression processes measured against the overall COP for a variety of VCR evaporation temperatures and shaft speeds. The figure depicted in this section maintains a constant input pressure of 8 bar and a constant output pressure of 1.3 bar on the expansion side, while allowing for varying pressure on the compression side. As can be seen in the figure, lowering the temperature at which VCR evaporation occurs leads to an increase in the overall COP, whereas the amount of exergy that is destroyed remains practically the same regardless of the VCR evaporation temperature. However, the majority of the increase in total COP was due to an improvement in the ORC's thermal efficiency, and this may be the reason why the majority of the exergy destruction in the compander occurred on the expansion side rather than the compression side. In addition, a proportional increase in the input power on the compression side occurred as a result of the increased amount of shaft speed that occurred. Along with this increase in power,

there is also a proportionate increase in the amount of exergy that is destructed on both the expansion and the compression sides.

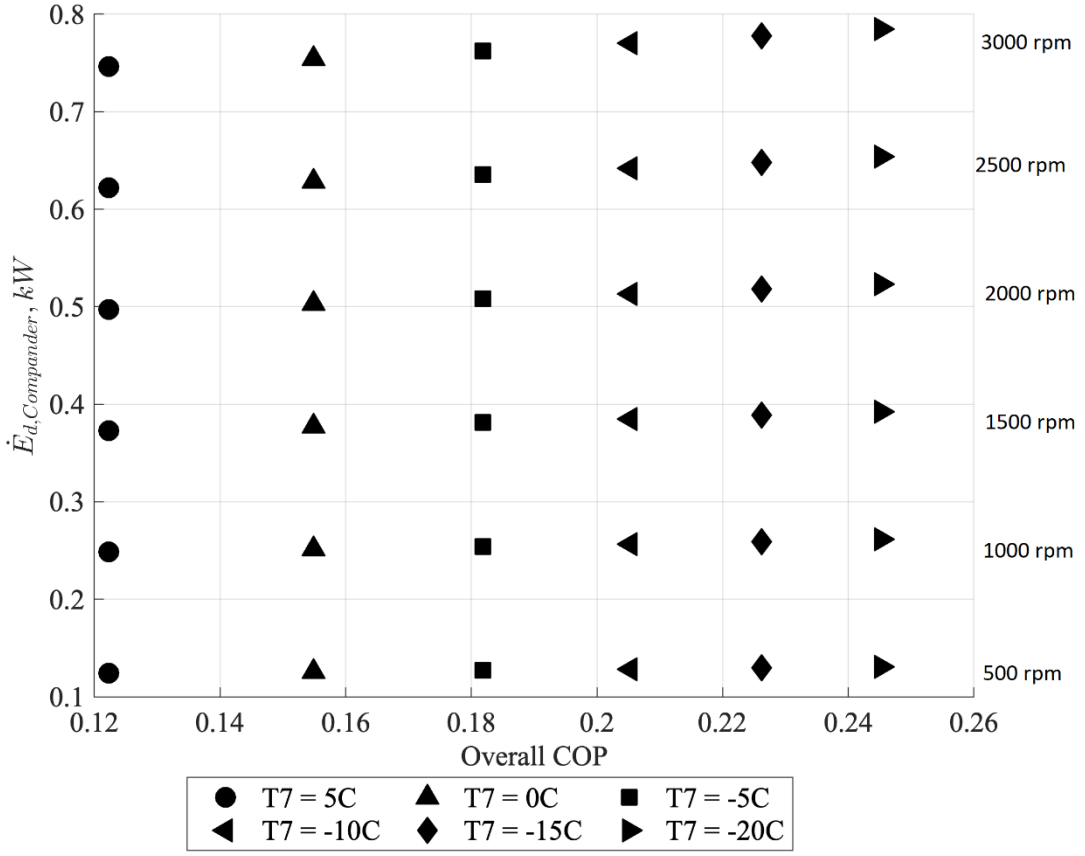

Figure 5-2: exergy destruction during expansion and compression for different VCR evaporation temperatures, shaft speed, and overall COP.

5.2.2 Effect of shaft speed variation

Figure 5-3 illustrates the exergy destruction within the compander as influenced by the fluctuation of shaft speed across various EPRs. As depicted in the diagram, it can be observed that an increase in shaft speed results in a corresponding rise in the level of exergy destruction. This can be attributed to the fact that the mass flow rate of the working fluid in both the expansion and compression chambers increases due to the increase of the volume flow rate associated with the shaft speed. In addition, for a given shaft speed and a range of EPRs, lowering the EPR results in a lower quantity of exergy destruction.

This is because the pressure and temperature differential between the inlet and outflow of the expansion chamber is relatively small.

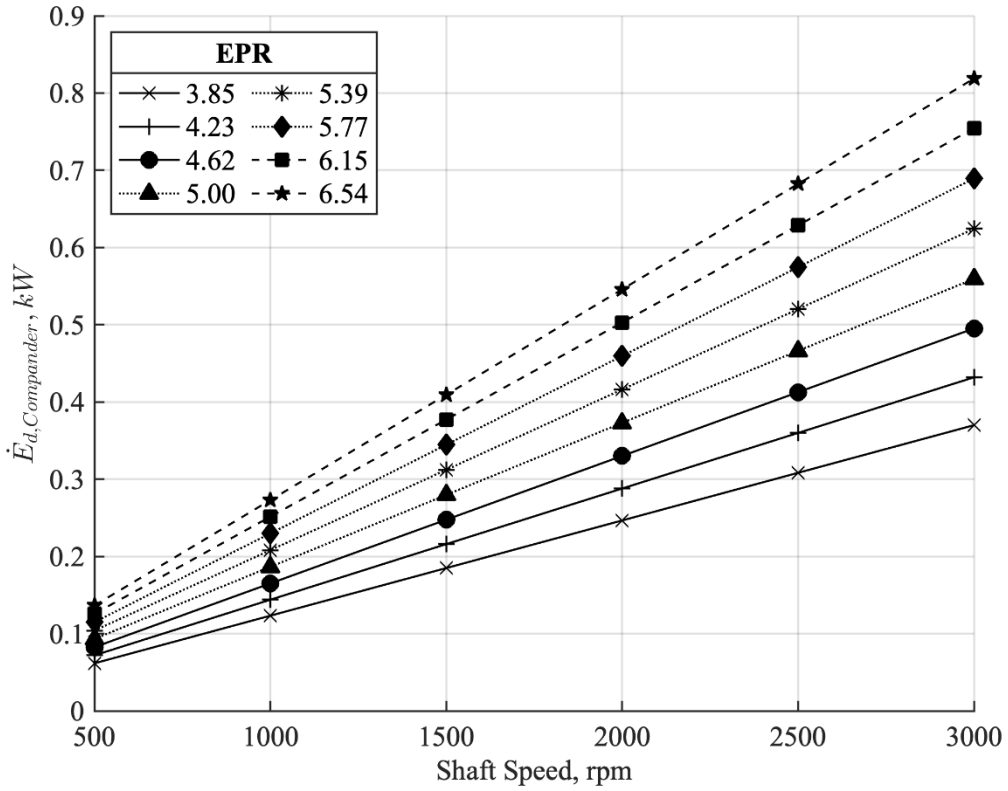

Figure 5-3: Exergy destruction during expansion and compression processes against the shaft speed for different EPR ratio.

5.3 Effect of ORC and VCR evaporation temperatures and shaft speed

5.3.1 Overall Exergy efficiency

The variation in the overall exergy efficiency of the system is shown in Figure 5-4 and Figure 5-5 under various evaporation temperatures of ORC and VCR when the shaft speeds were as follows: 500 rpm, 1000 rpm, 1500 rpm, 2000 rpm, 2500 rpm, and 3000 rpm. The overall exergy efficiency exhibits a consistent decreasing pattern for all the considered rotor speeds.

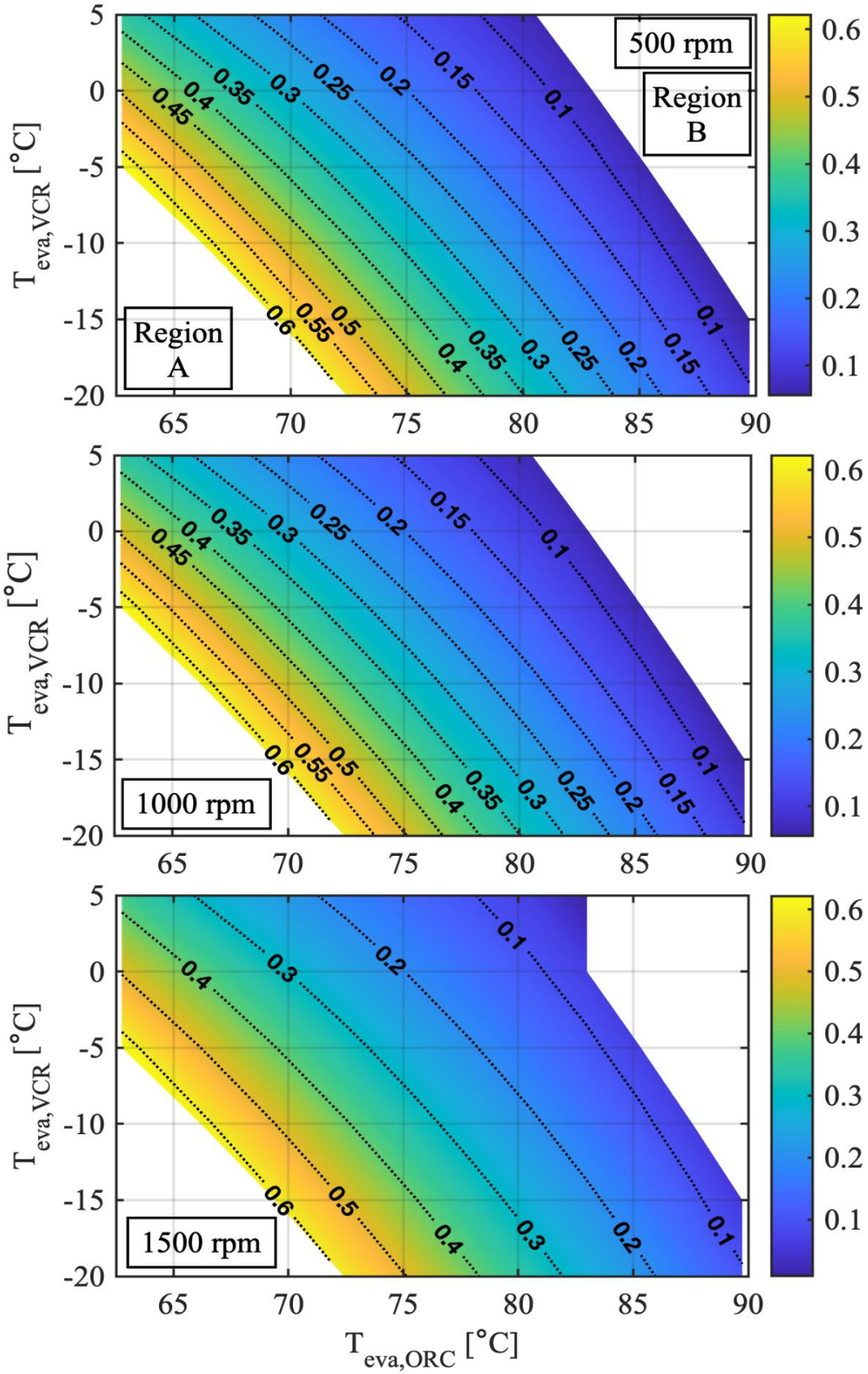

Figure 5-4: Overall Exergy efficincy for different ORC amd VCR evaporation temperatures and shaft speed 500 rpm, 1000 rpm, and 1500 rpm.

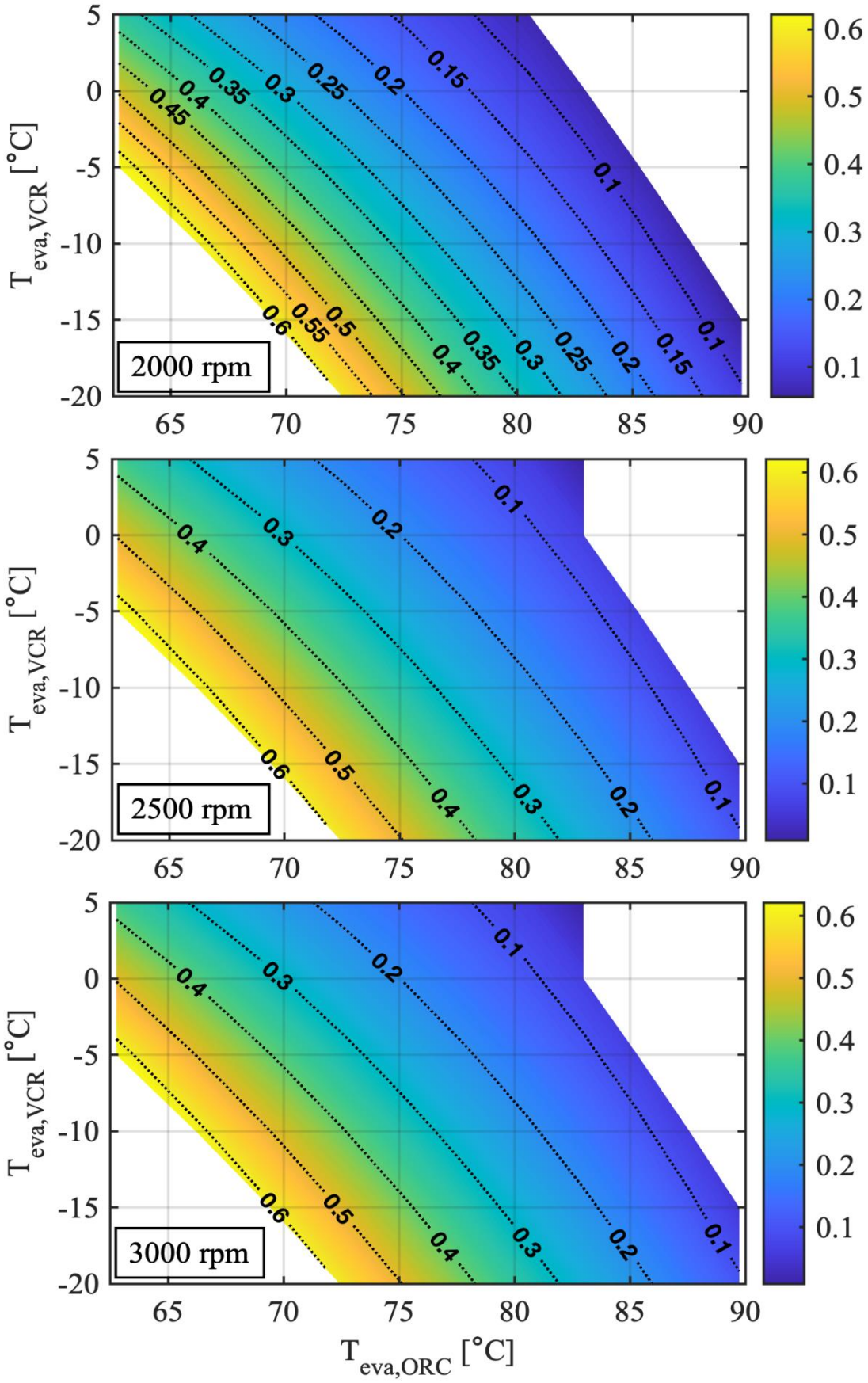

Figure 5-5: Overall Exergy efficincy for different ORC amd VCR evaporation temperatures and shaft speed 2000 rpm, 2500 rpm, and 3000 rpm.

This decline is due to the heightened exergy destruction in the cooling process $\dot{E}_{cooling}$ within the VCR evaporator, as well as the exergy destruction $\dot{E}_{in}$ in the pump and evaporator of ORC. The increase in $\dot{E}_{in}$ is driven by a substantial rise in exergy flow in stream 2, compared to the comparatively smaller increase in exergy flow in stream 1 resulting from the higher ORC evaporation temperature.

Furthermore, the exergy flow in stream 7, which comes after the expansion valve, decreases, leading to an enhancement in the cooling exergy, $\dot{E}_{cooling}$, as the ORC evaporation temperature is raised. However, the exergy destruction in the ORC sub-cycle is more significant than that in the VCR sub-cycle. Therefore, a higher ORC evaporation temperature contributes to an increase in the overall exergy efficiency across all operating speeds. At a shaft speed of 500 rpm, it has been noted that the overall exergy efficiency ranges from 11% to 60% as the ORC evaporation temperature is elevated from 72.4°C to 89.7°C, with the VCR evaporation temperature maintained at -20°C. On the other hand, when the VCR evaporation temperature at 5 °C, the overall exergy efficiency when the ORC evaporation temperature at 62.7 °C is 37 % and when ORC evaporation temperature at 80.5 °C is 7 %. It is observed that the highest overall exergy efficiency of 63 % is obtained when the ORC evaporation temperature at 62.75 °C and VCR evaporation temperature at -5 °C. Furthermore, as seen in Figure 5-4 and Figure 5-5, the overall exergy efficiency is independent of the change of shaft speed.

5.3.2 Exergy destruction for all component

Exergy destruction of the ORC-VCR components is depicted in Figure 5-6 under various ORC evaporation temperatures as well as VCR evaporation temperatures. As can be seen in the figure, the amount of exergy lost throughout the ORC evaporation process increases in direct proportion to the temperature at which the process takes place. Exergy was destroyed at a lower rate at lower evaporation temperatures, while it was destroyed at the

highest rate at higher evaporation temperatures. The rise in the temperature of the ORC evaporation process causes an increase in the amount of exergy that is lost within the compander. This is because the temperature difference that exists between the expansion and compression processes also increases. The exergy destruction in the VCR condensers was also increasing due to the increase of the heat rejection during the condensation process associated with the increase of the compressor discharge pressure. The exergy destruction in the VCR expansion valve was increasing significantly due to the higher temperature difference between the higher-pressure side and the lower-pressure side of the VCR subsystem. This is because the temperature difference that exists between the expansion and compression processes also increases. The exergy destruction in the VCR condensers was also increasing due to the increase of the heat rejection during the condensation process associated with the increase of the compressor discharge pressure. The exergy destruction in the VCR expansion valve was increasing significantly due to the higher temperature difference between the higher-pressure side and the lower-pressure side of the VCR subsystem.

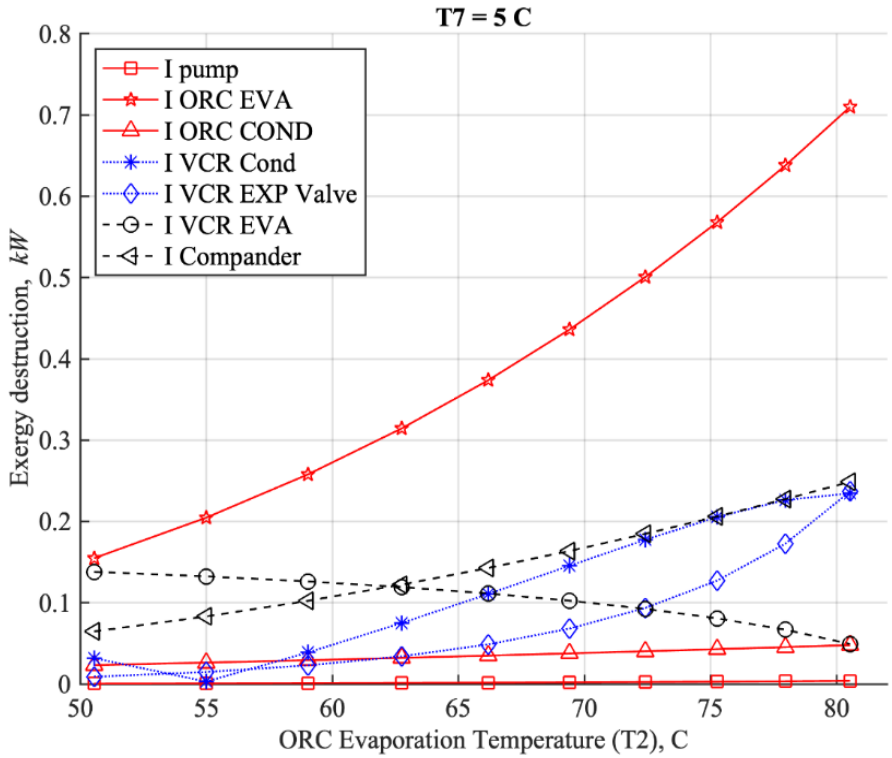

Figure 5-6: Exergy destruction with variation of ORC evaporation temperature and VCR evaporation temperature at 5℃

The exergy destruction contribution of the ORC-VCR components is depicted in Figure 5-7 at a variety of ORC evaporation temperatures. As can be seen in the picture, the ORC evaporator is responsible for the largest and most important portion of the total exergy destruction that occurs under the conditions that are being addressed. Heat transfer across the ORC evaporator contributes significantly to the irreversibility, mostly because of the significant temperature differential across the device. When the ORC evaporation temperature is lower, the VCR evaporator in the VCR subsystem has a greater contribution to the total exergy destruction.

However, when the ORC evaporation temperature is higher, the compander has a greater contribution due to the combination of exergy destruction in the processes of expansion and compression. There is a significant relationship between the isentropic efficiency of the expansion and compression sides of the device and the irreversibilities that occur within

these processes. During the design phase of the device, more attention needed to be paid to the device in order to reduce the amount of exergy that was lost within the compander.

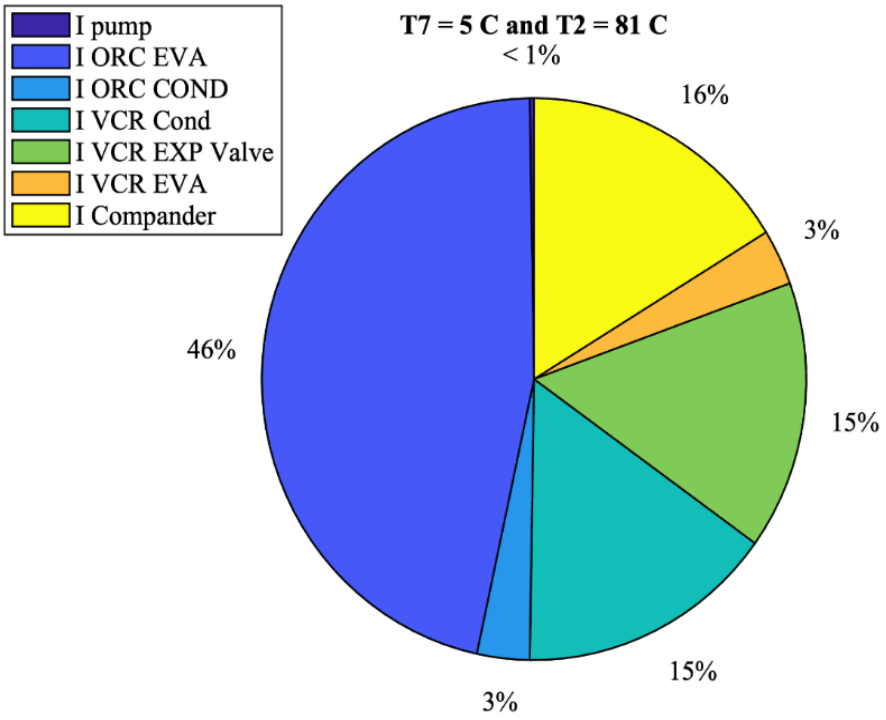

Figure 5-7: Exergy destruction distribution when ORC evaporation temperature at 81℃ and VCR evaporation temperature at 5℃.

Figure 5-8 shows the exergy destruction when the VCR evaporation temperature reduced to 0℃. The exergy destruction in the ORC side stays constant similar to what presented in Figure 5-6.

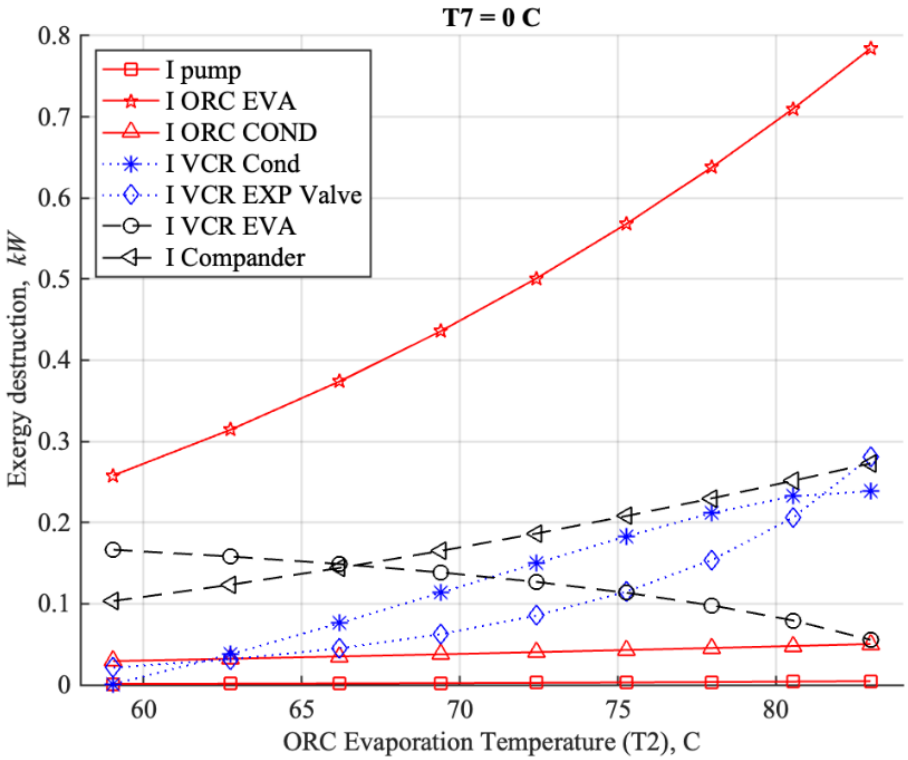

Figure 5-8: Exergy destruction with variation of ORC evaporation temperature and VCR evaporation temperature at 0℃

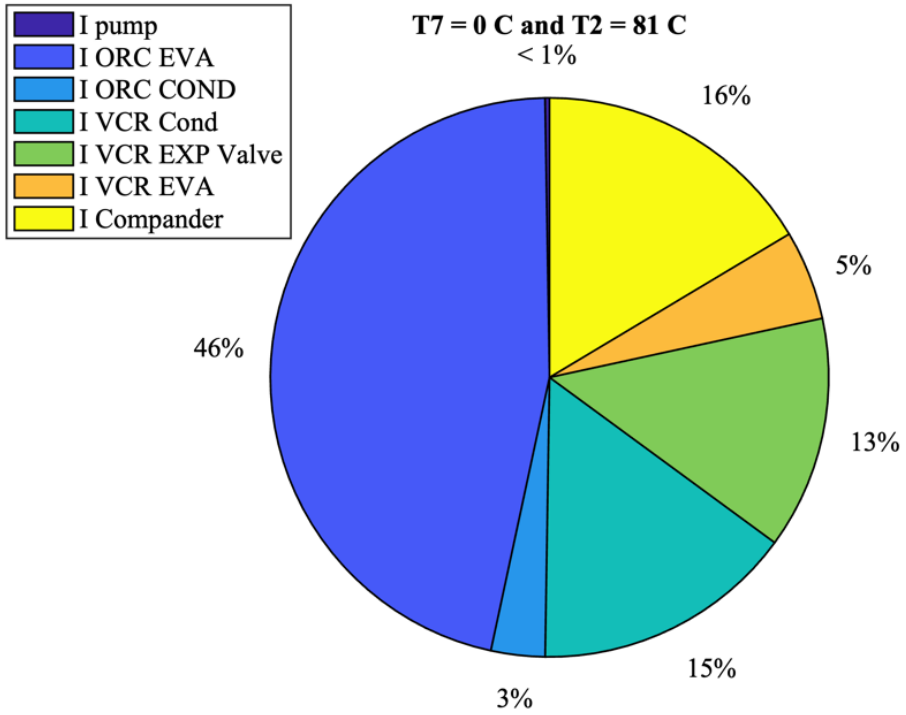

Figure 5-9: Exergy destruction distribution with variation of ORC evaporation temperature and VCR evaporation temperature at 0℃

However, the exergy destruction in VCR side increases slightly and this increment mostly happened in the VCR evaporator and the expansion valve. As shown in Figure 5-9, decreasing the VCR evaporation temperature from 5℃ to 0℃ leads to increasing the exergy destruction in the VCR evaporator by 2% and expansion valve by 2%.

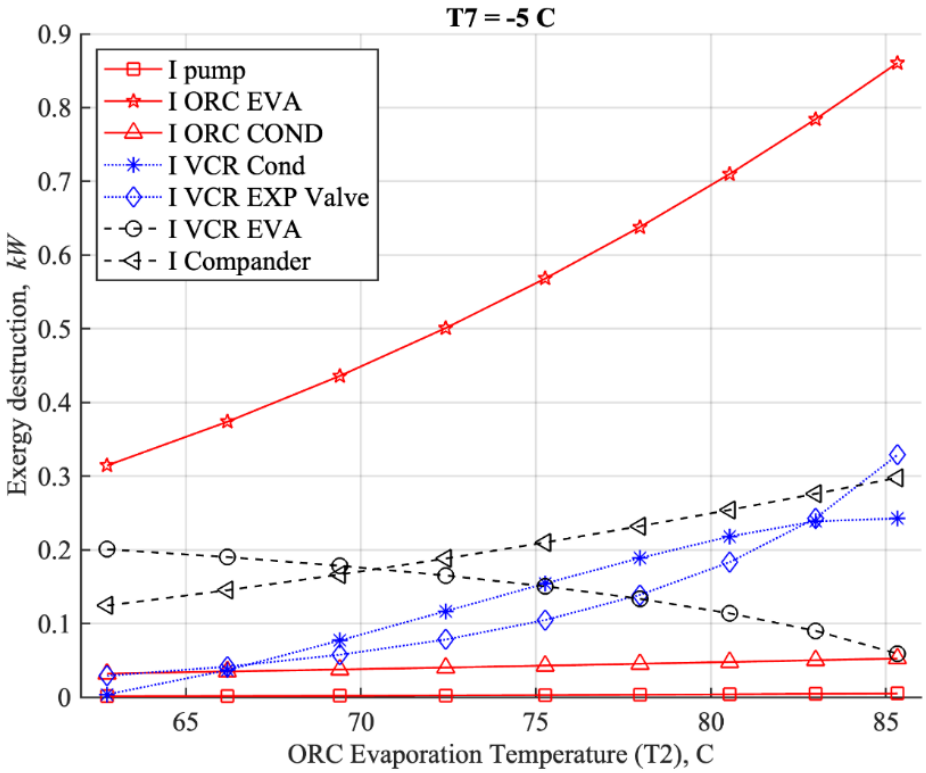

Figure 5-10: Exergy destruction with variation of ORC evaporation temperature and VCR evaporation temperature at -5℃

Figure 5-10 shows the exergy destruction when the VCR evaporation temperature reduced to -5℃, and similar to Figure 5-6 the exergy destruction increases in the VCR side with decreasing the VCR evaporation temperature. Decreasing the VCR evaporation temperature from 5℃ to -5℃ can lead to increase the exergy destruction in the compander, and VCR evaporator by 1%, and 4%, respectively. However, Decreasing the VCR evaporation temperature from 5℃ to -5℃ can lead to decrease the exergy destruction in the VCR condenser and VCR expansion valve by 1%, and 3%, respectively. The decrease in exergy destruction that was seen in the VCR condenser and expansion valve can be

related to the temperature drop that occurred during the evaporation process of the VCR. This temperature drop, in turn, caused a pressure drop at the inlet of the compressor, which led to the reduction in exergy destruction. In addition to this, assuming that the power that is fed into the compressor remains constant, the pressure that is output by the compressor will fall in direct proportion to this.

Figure 5-12 presented the exergy destruction with variation of ORC evaporation temperature when the VCR evaporation temperature reduced to -10℃. similarly, the major effects of reducing the VCR evaporation temperature increase the exergy destruction in the VCR side. As shown in Figure 5-12 and Figure 5-13, reducing the VCR evaporation temperature from 5℃ to -10℃ led to increase the exergy destruction in the compander and the VCR evaporation temperature by 1%, and 7%, respectively. However, the exergy destruction in the VCR condenser and expansion valve reduced by 2%, and 4% respectively.

Figure 5-14 shows the effect of ORC evaporation temperature variation on the exergy destruction when the VCR evaporation temperature reduced to -15℃. the behaviour of the exergy destruction growth and reduction at -15℃ evaporation temperature similar to the behaviour of 5℃. However, the amount of the exergy destruction contribution increases in some equipment and reduced in others. As shown in Figure 5-14 and Figure 5-15, reducing the VCR evaporation temperature from 5℃ to -15℃ led to increase the exergy destruction in the compander and the VCR evaporator by 1%, and 10%, respectively. reducing the VCR evaporation temperature from 5℃ to -15℃ led to decrease the exergy destruction in the VCR condenser and expansion valve by 4%, and 5%, respectively.

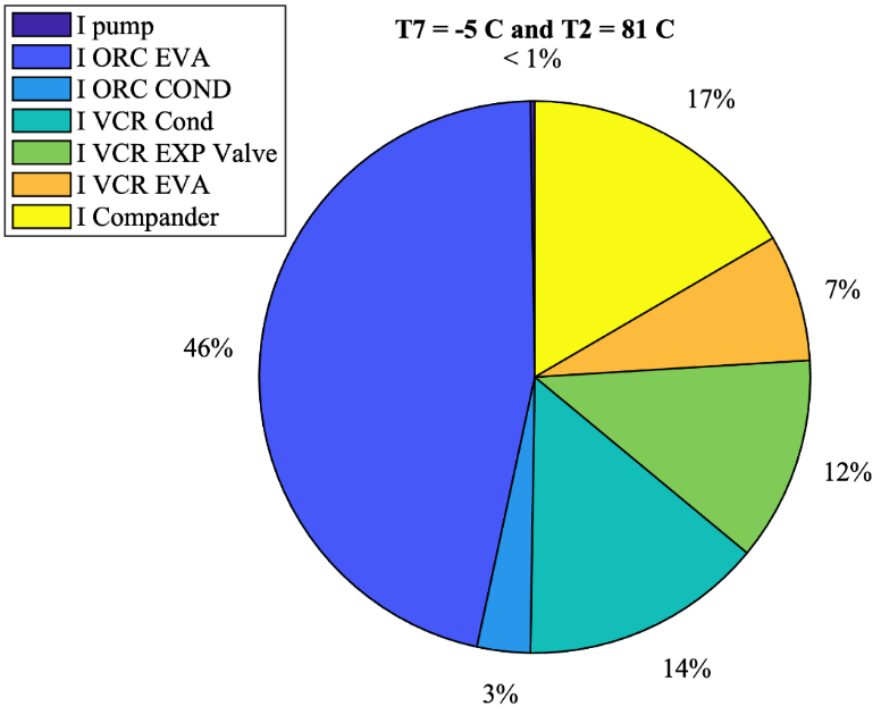

Figure 5-11: Exergy destruction distribution with variation of ORC evaporation temperature and VCR evaporation temperature at -5℃

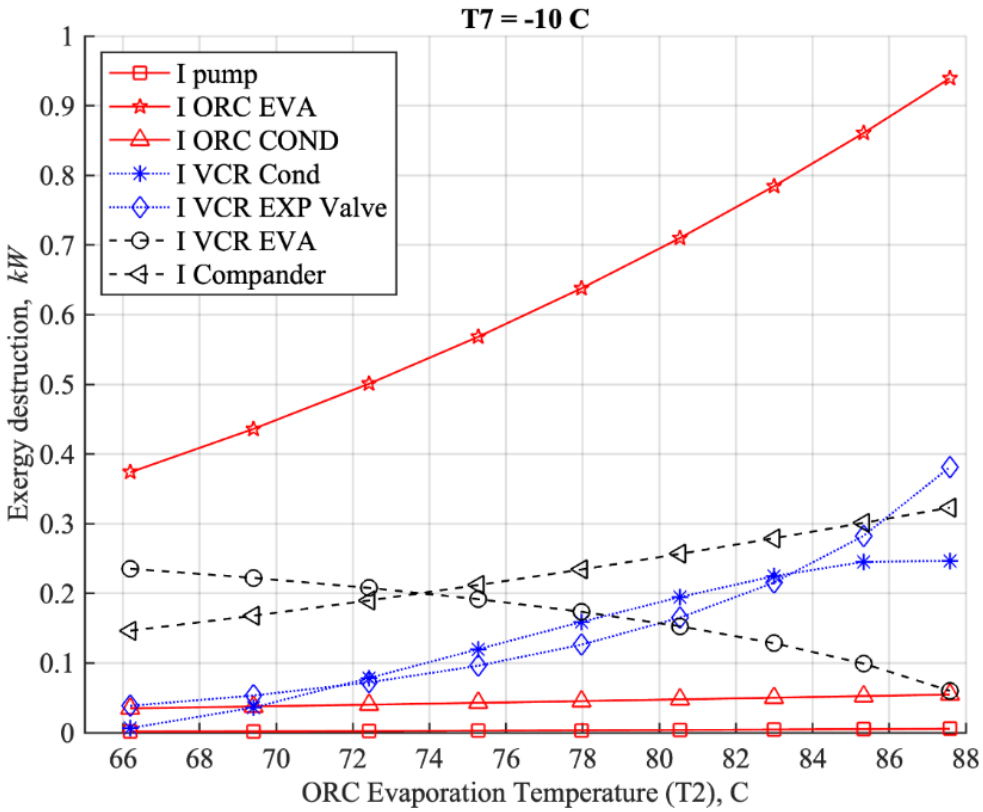

Figure 5-12: Exergy destruction with variation of ORC evaporation temperature and VCR evaporation temperature at -10℃.

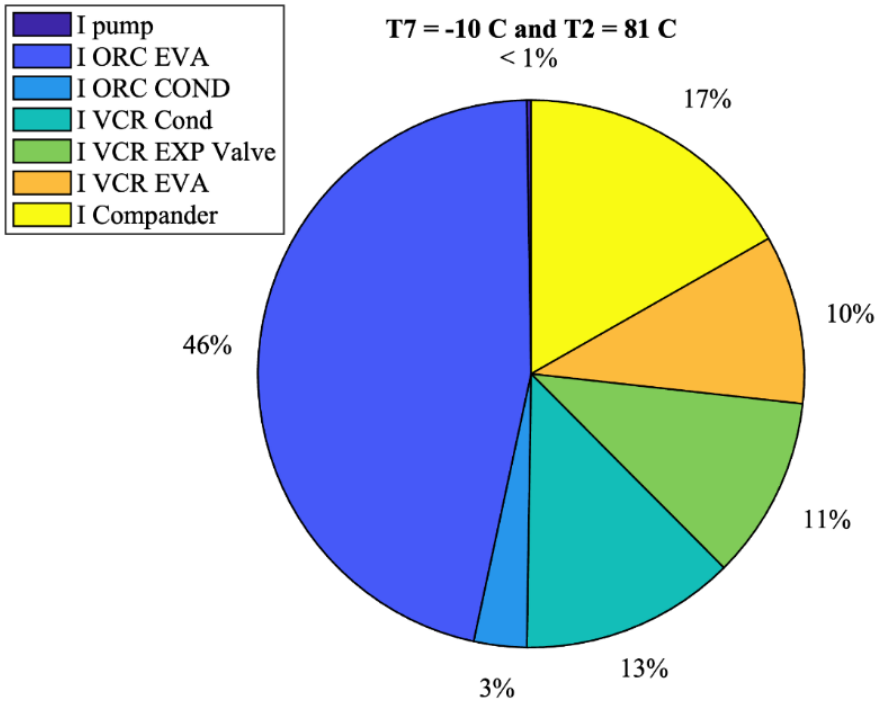

Figure 5-13: Exergy destruction distribution with variation of ORC evaporation temperature and VCR evaporation temperature at -10℃.

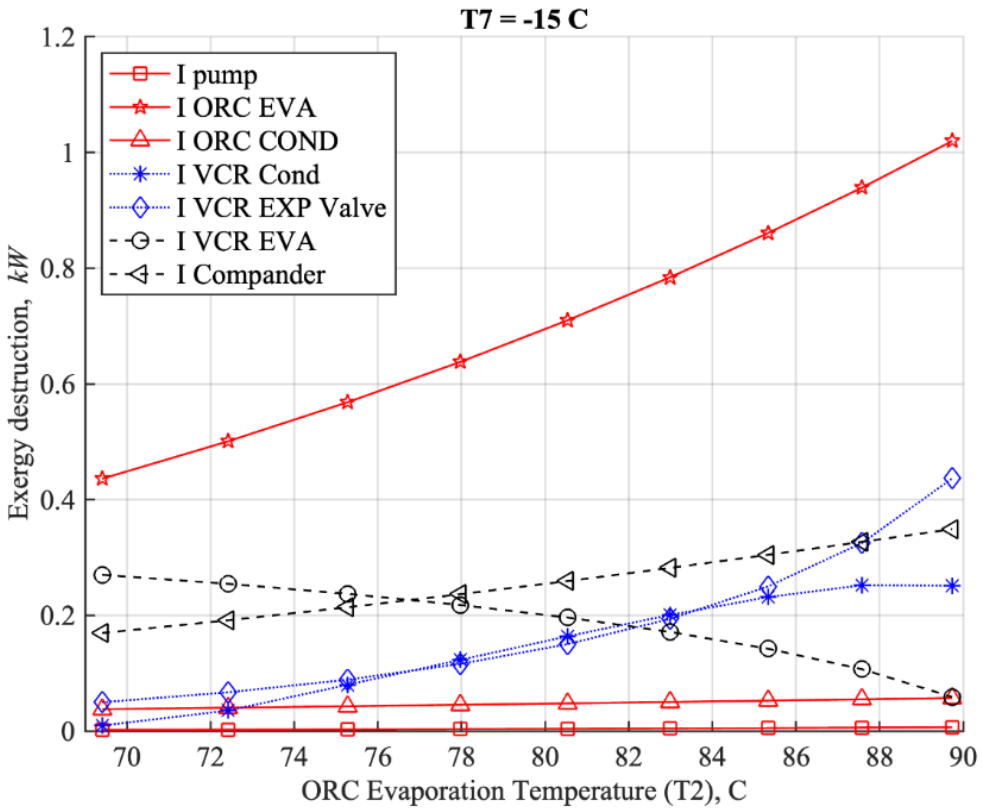

Figure 5-14: Exergy destruction with variation of ORC evaporation temperature and VCR evaporation temperature at -15℃.

Figure 5-16 presented the exergy destruction in the ORC-VCR system components of different ORC evaporation temperature when the VCR evaporation temperature reduced to -20℃. As seen in Figure 5-16, the exergy destruction in the VCR side is affected by reducing the VCR evaporation temperature to -20℃. These effects can be seen clearly in the exergy destruction contribution of each equipment that presented in Figure 5-17. reducing the VCR evaporation temperature from 5℃ to -20℃ led to increase the exergy destruction in the compander and the VCR evaporator by 1%, and 13%, respectively. reducing the VCR evaporation temperature from 5℃ to -20℃ led to decrease the exergy destruction in the VCR condenser and expansion valve by 7%, and 6%, respectively.

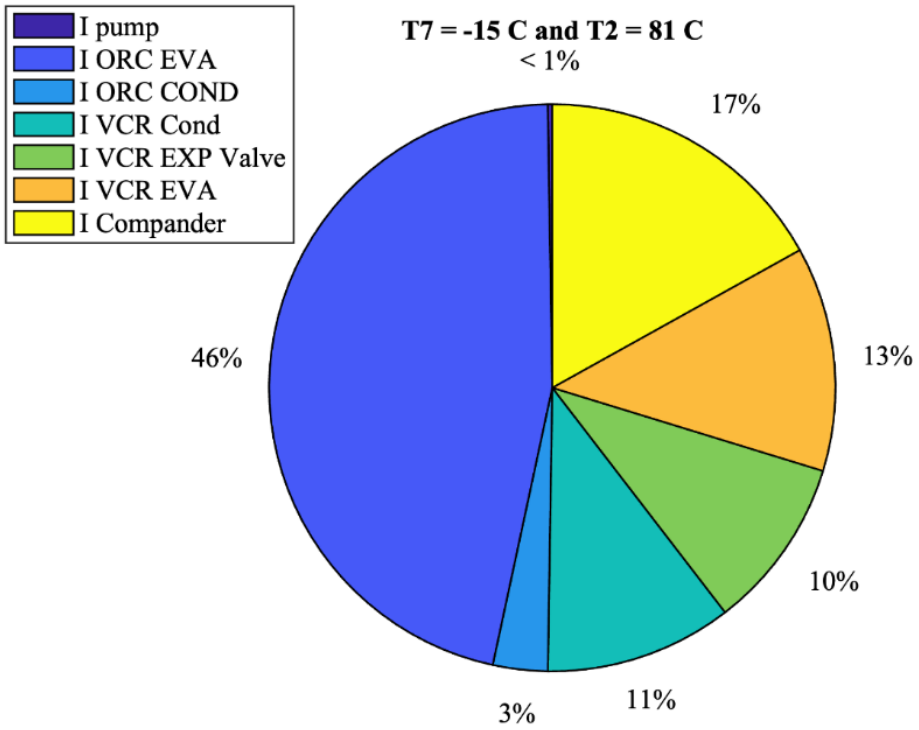

Figure 5-15: Exergy destruction distribution with variation of ORC evaporation temperature and VCR evaporation temperature at -15℃.

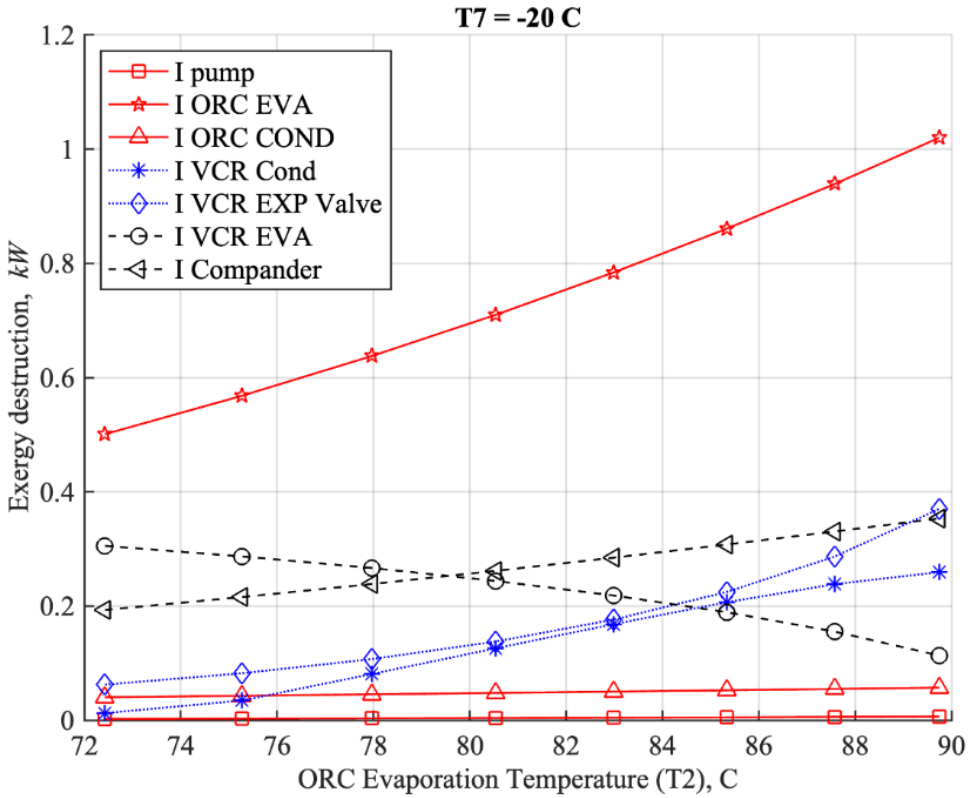

Figure 5-16: Exergy destruction with variation of ORC evaporation temperature and VCR evaporation temperature at -20℃.

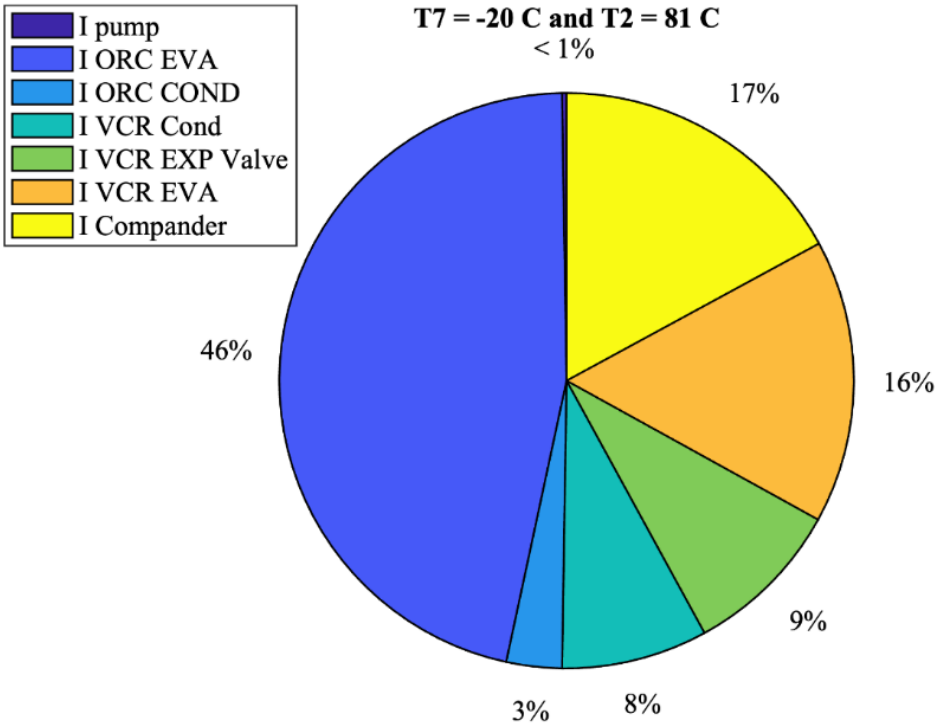

Figure 5-17: Exergy destruction distribution with variation of ORC evaporation temperature and VCR evaporation temperature at -20℃.

5.4 Effect of ORC condensation temperature and VCR evaporation temperature and shaft speed

5.4.1 Overall Exergy efficiency

Figure 5-18 and Figure 5-19 show the Overall exergy efficiency of ORC-VCR coupled by the single rotor expander-compressor (compander) with variation of ORC condensation temperature and VCR evaporation temperature. Also, with the variation of the shaft speeds; 500rpm, 1000rpm, 1500rpm, 2000rpm, 2500rpm, and 3000rpm. The overall exergy efficiency rises as the ORC condensation temperature increases. This is because the power required by the compressor decreases, leading to a reduction in the compressor discharge pressure. Consequently, there is less exergy destruction in the expansion valve, resulting in an increase in the cooling effect of the VCR and, consequently, an improvement in overall exergy efficiency. It is worth noting that, at a rotor speed of 500 rpm and with a VCR evaporation temperature of -20°C, the overall exergy efficiency varies from 33% to 39% as the ORC condensation temperature increases from 20°C to 45°C.

On the other hand, when VCR evaporation temperature at 5 °C, the overall exergy efficiency corresponding to ORC condensation temperature at 40 °C is 14 % and that of ORC condensation temperature at 45 °C is 16 %. It is found that the highest overall exergy efficiency of 39% is obtained when ORC condensation temperature at 30 °C and VCR evaporation temperature at -20 °C.

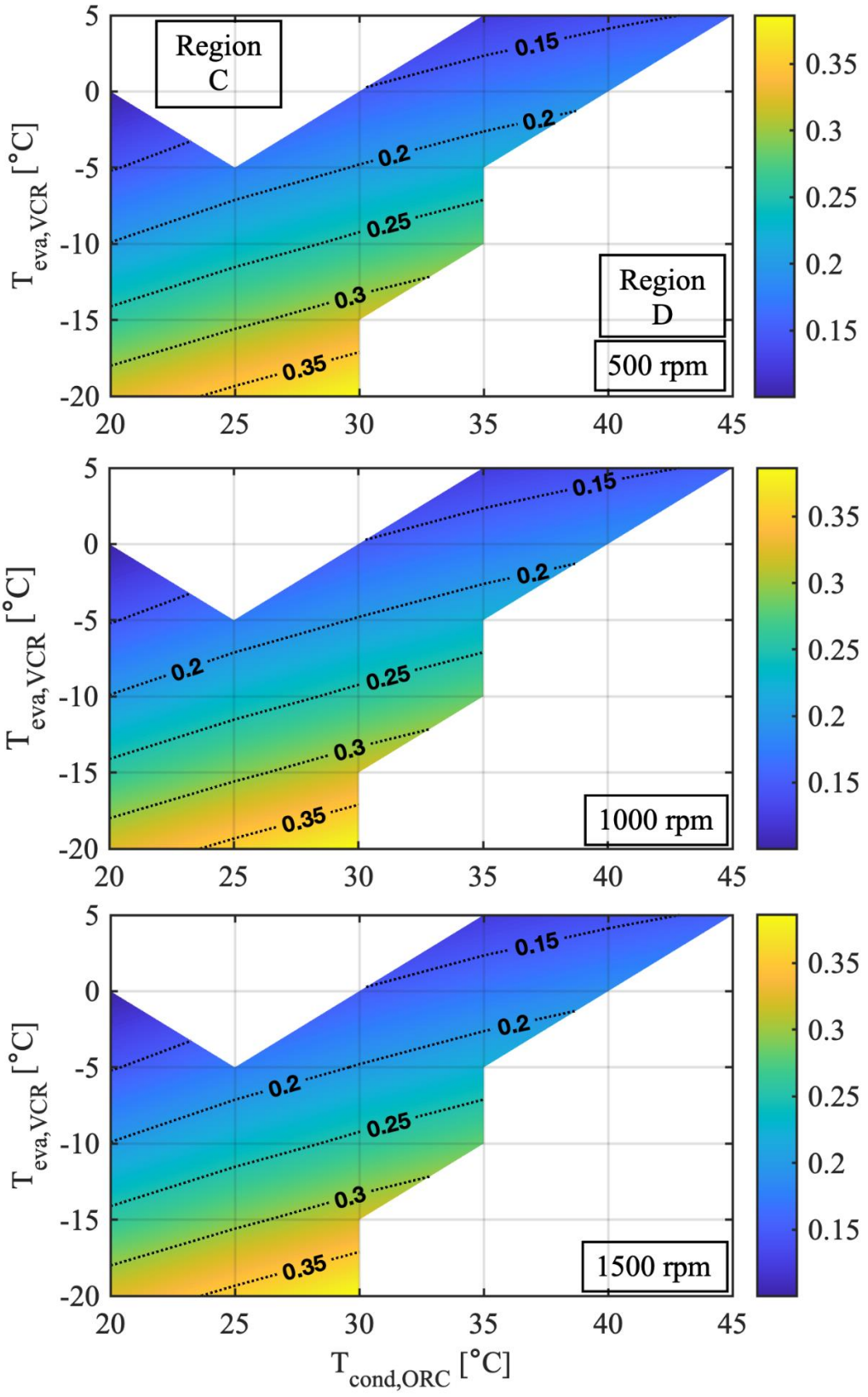

Figure 5-18: Overall exergy efficiency with variation of ORC condensation temperature and VCR evaporation temperature when shaft speeds 500rpm, 1000rpm, and 1500rpm.

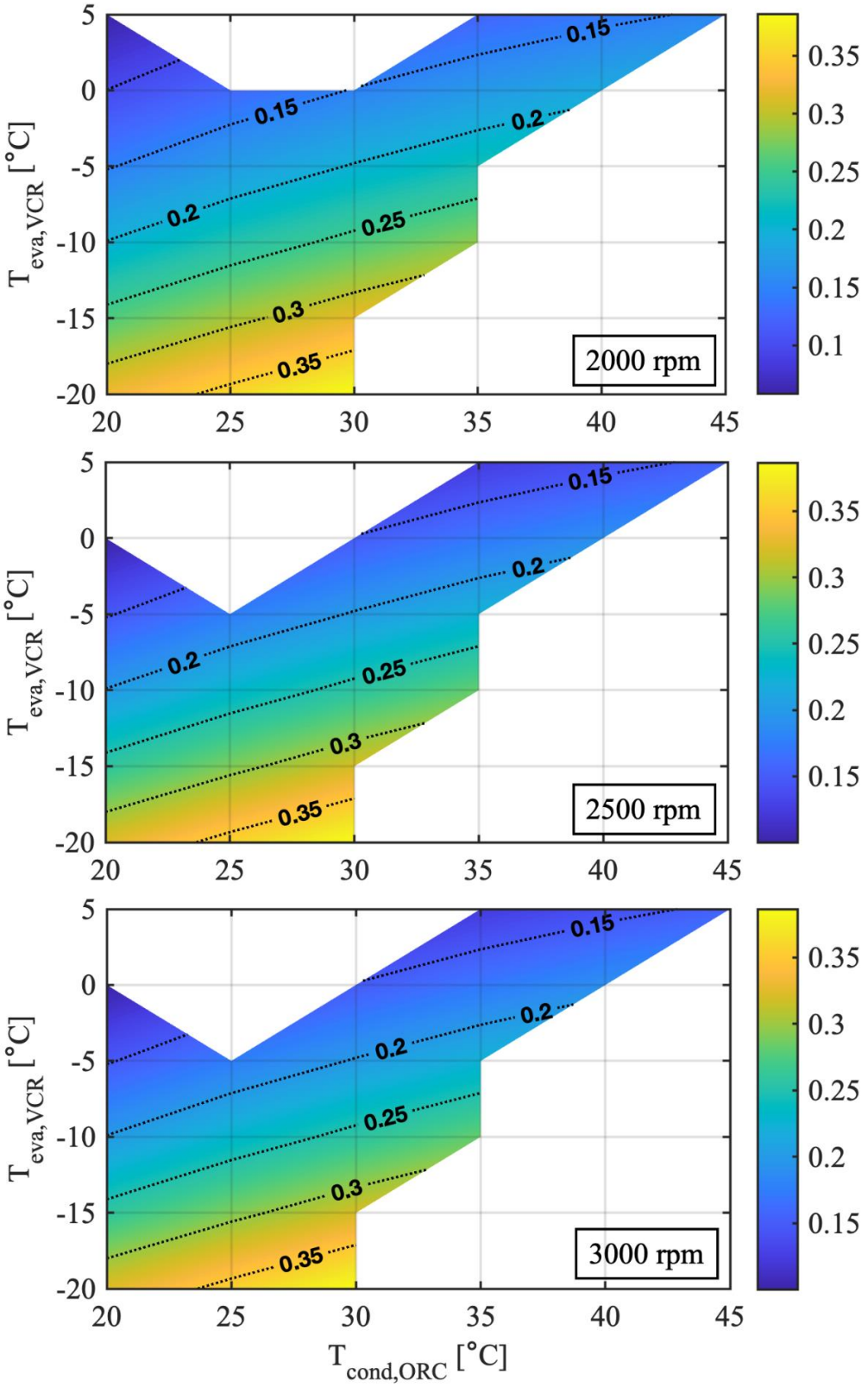

Figure 5-19: Overall exergy efficiency with variation of ORC condensation temperature and VCR evaporation temperature when shaft speeds 2000rpm, 2500rpm, and 3000rpm.

5.4.2 Exergy destruction for all component

Figure 5-20 shows the exergy destruction of ORC-VCR system under the variation of the ORC condensation temperature when the VCR evaporation temperature at 5°C. Increasing the ORC condensation temperature increases the exergy destruction within the ORC condenser due to the increase of the rejected heat. However, the exergy destruction in the VCR condenser was decreasing because increasing the condensation temperature of the ORC leads to reduce the power supplied from the expansion side of the compander to the compression side.

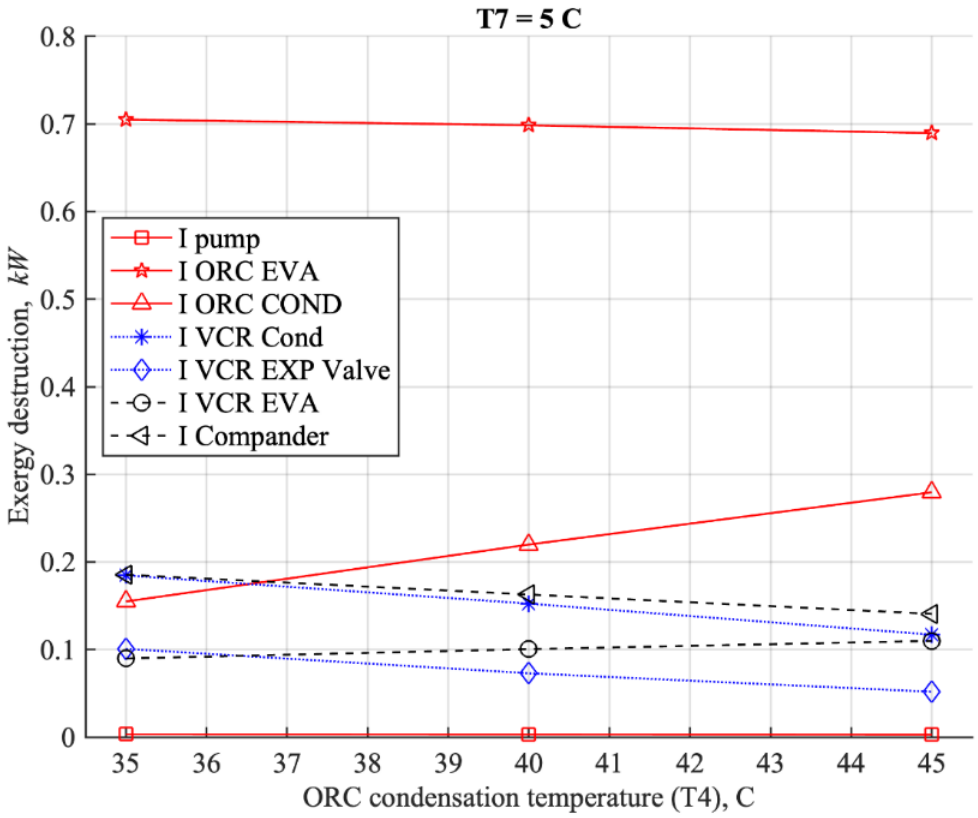

Figure 5-20: Exergy destruction with variation of ORC condensation temperature and VCR evaporation temperature at 5℃.

Thus, the heat rejected in the VCR condenser decreased. Moreover, the decrease in the exergy destruction within the VCR expansion valve due to the reduce in the temperature difference between the high-pressure side and lower-pressure side of the VCR subsystem.

In the VCR evaporator, almost stays constant even there is a slightly increasing because the VCR evaporation temperature is constant at 5°C.

Figure 5-21 shows the contribution of each component in the total of the exergy destruction when the ORC condensation temperature at 35°C and the VCR evaporation temperature at 5°C. It is clear that most of the exergy destruction contribution occur in the ORC evaporator followed by the compander and the VCR condenser where they contribute significantly. After that, the ORC condenser contribution followed by the VCR expansion valve then the VCR evaporator and lastly the ORC pump which has a very small contribution.

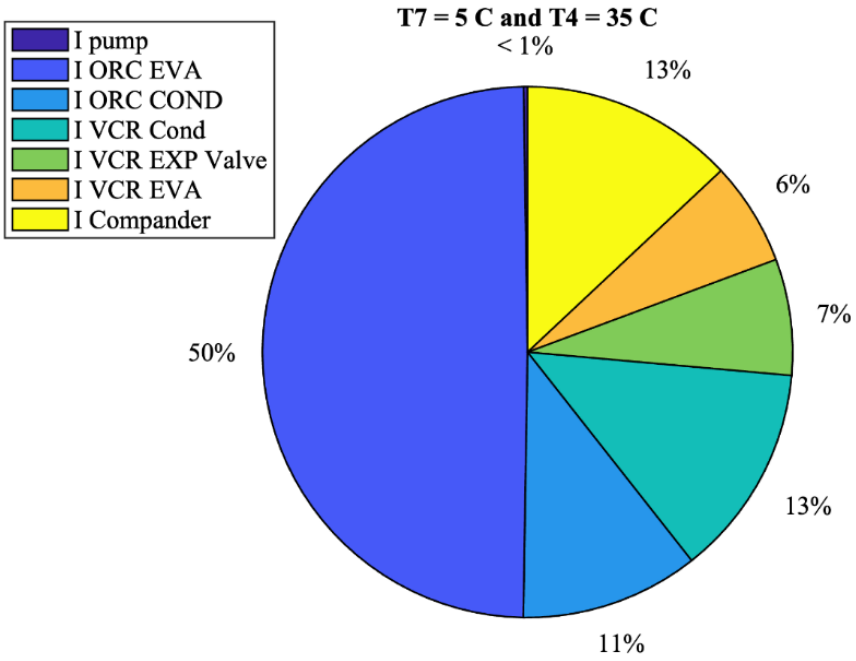

Figure 5-21: Exergy destruction distribution when ORC condensation temperature at 35℃ and VCR evaporation temperature at 5℃.

Figure 5-22 shows the effects of ORC condensation variation on the exergy destruction of each component of the system when the VCR evaporation temperature at 0°C. When the VCR evaporation temperature at 5℃ with the increasing of the ORC condensation temperature from 20℃ to 45℃ led to decrease the exergy destruction in the VCR

condenser from 0.24 kW to 0.09 kW while the exergy destruction in the VCR expansion valve was reduced from 0.23 to 0.079 kW. Moreover, the exergy destruction in the compander decreases from 0.26 kW to 0.15 kW. However, the VCR evaporator has different behaviour since the exergy destruction increases from 0.09 kW to 0.15 kW.

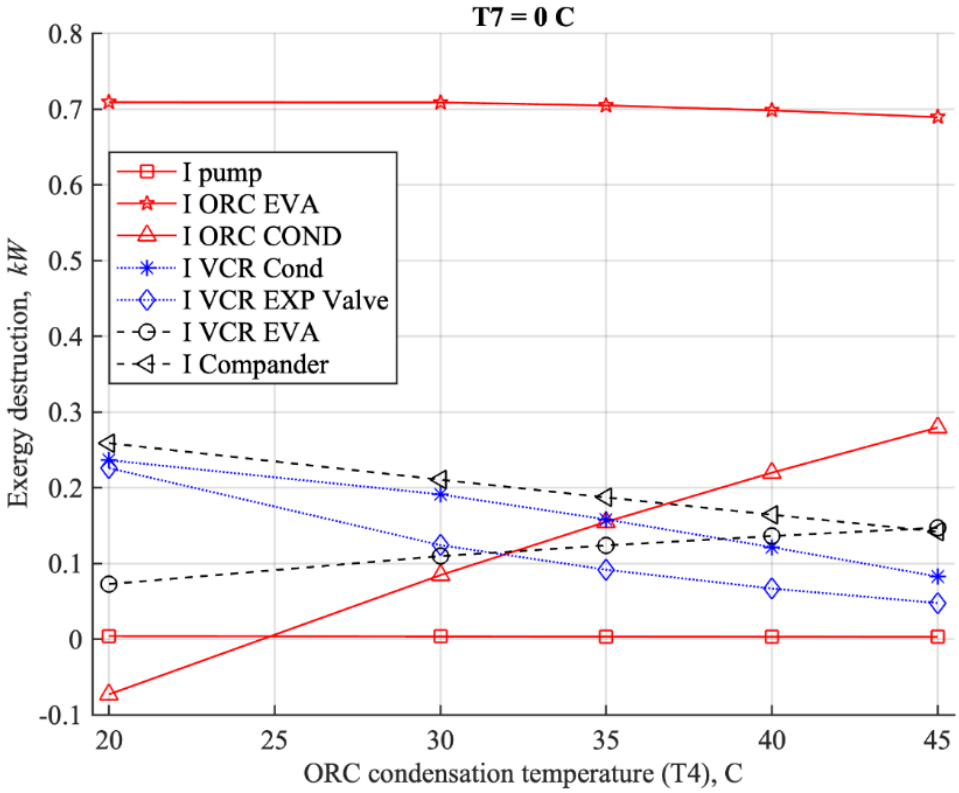

Figure 5-22: Exergy destruction with variation of ORC condensation temperature and VCR evaporation temperature at 0℃.

In Figure 5-22 it can be seen that ORC condenser exergy destruction line was starting below zero when the ORC condensation temperature below 25℃. It is important to clear that the exergy cannot be in negative and in this section the condenser line always shows negative exergy when the condensation below 25℃ that is because during the design of the ORC-VCR system the dead state temperature was selected as 25℃ as described in the chapter 3.

Figure 5-23 presented the exergy destruction contribution of each component when the ORC condensation temperature at 35℃ and the VCR evaporator temperature at 0℃.

Reducing the VCR evaporation temperature from 5℃ to 0℃, lead to increase the VCR evaporator exergy destruction contribution by 3%. On other hand, the contribution of the expansion valve and the VCR condenser were reduced by 1%, and 2%, respectively.

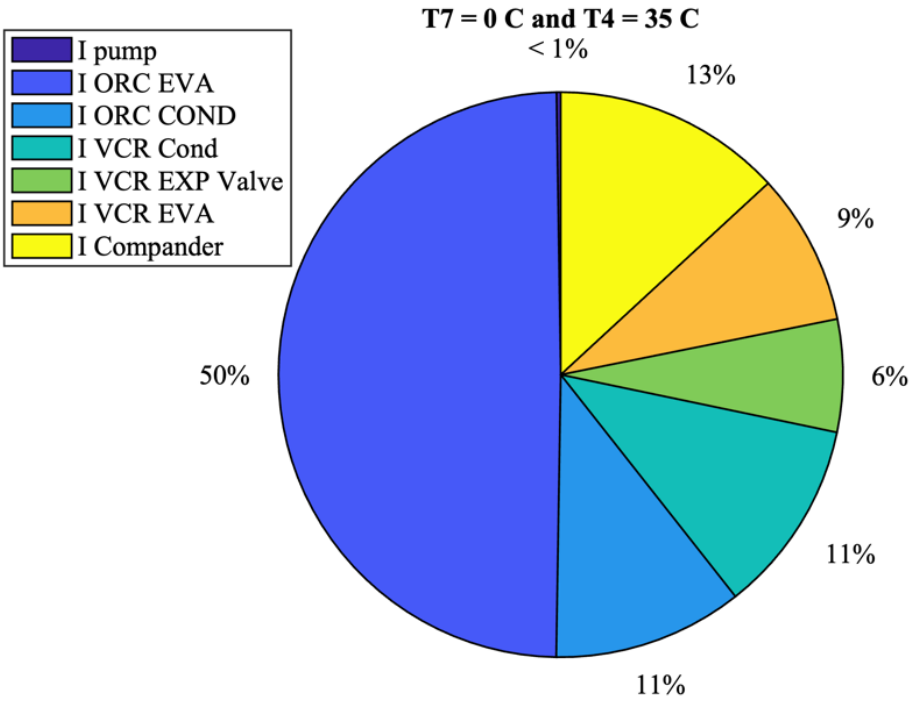

Figure 5-23: Exergy destruction distribution when ORC condensation temperature at 35℃ and VCR evaporation temperature at 0℃.

Figure 5-24 shows the exergy destruction for the ORC-VCR component with the variation of ORC condensation temperature when the VCR evaporation temperature at -5℃. when the condensation temperature of the ORC varies from 20℃ to 45℃, the exergy destruction of the VCR shows the same trend when the VCR evaporation temperature was at 5℃. and the exergy destruction contribution at -5℃ is presented in Figure 5-25. Reducing the VCR evaporation temperature from 5℃ to -5℃ while ORC condensation temperature at 35℃ led to increase the exergy destruction contribution of the VCR evaporator by 5% while the contribution of the compander says constant. However, the contribution of the VCR condenser and expansion valve were reduced by 4%, and 1%, respectively.

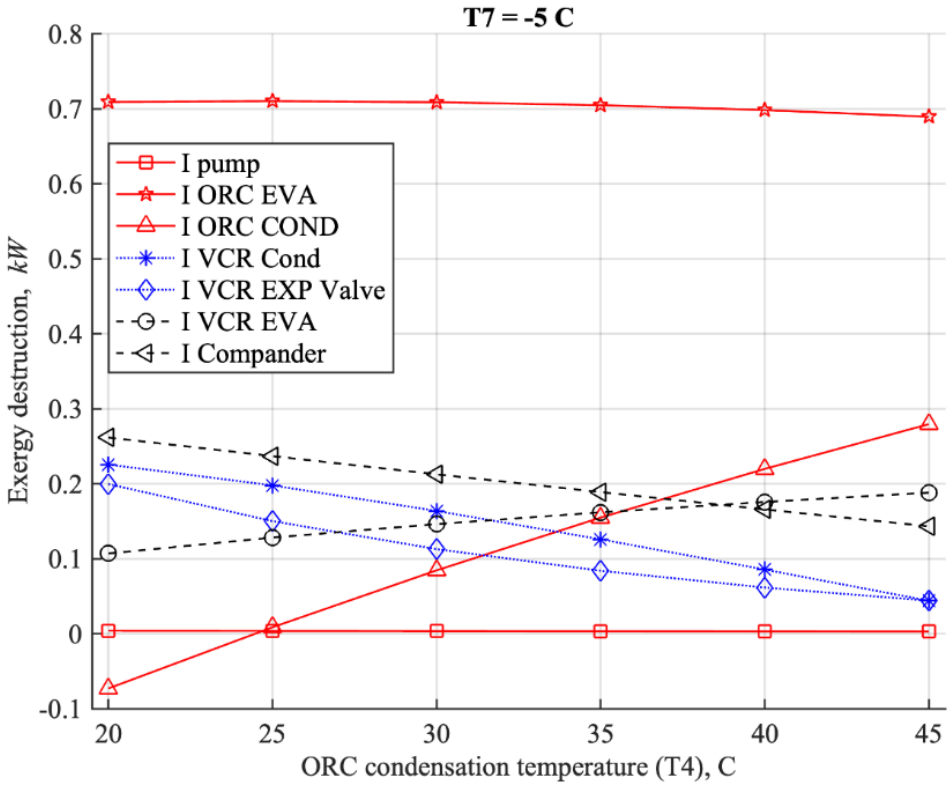

Figure 5-24: Exergy destruction distribution when ORC condensation temperature at 35℃ and VCR evaporation temperature at -5℃.

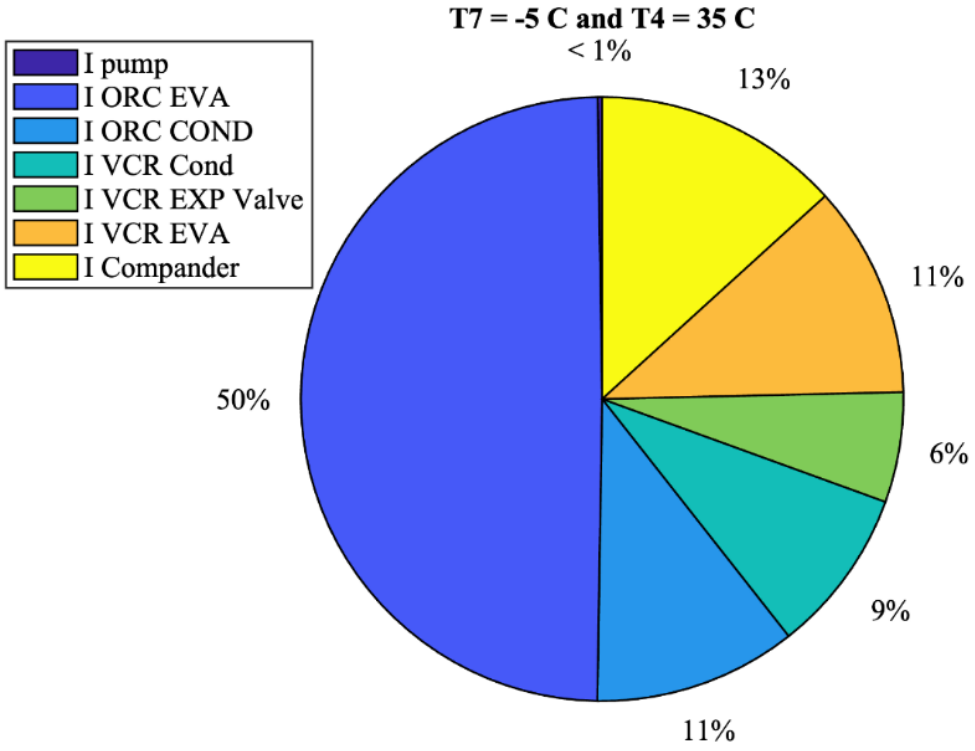

Figure 5-25: Exergy destruction distribution with variation of ORC condensation temperature and VCR evaporation temperature at -5℃.

Figure 5-26 shows the exergy destruction of the ORC-VCR component with variation of ORC condensation temperature when the VCR evaporation temperature was constant at -10℃. At higher ORC condensation temperature, the power supplied to the VCR side is reduced, and with the effect of the lower VCR evaporation temperature, the exergy destruction in both the VCR condenser and the expansion valve will be reduced significantly.

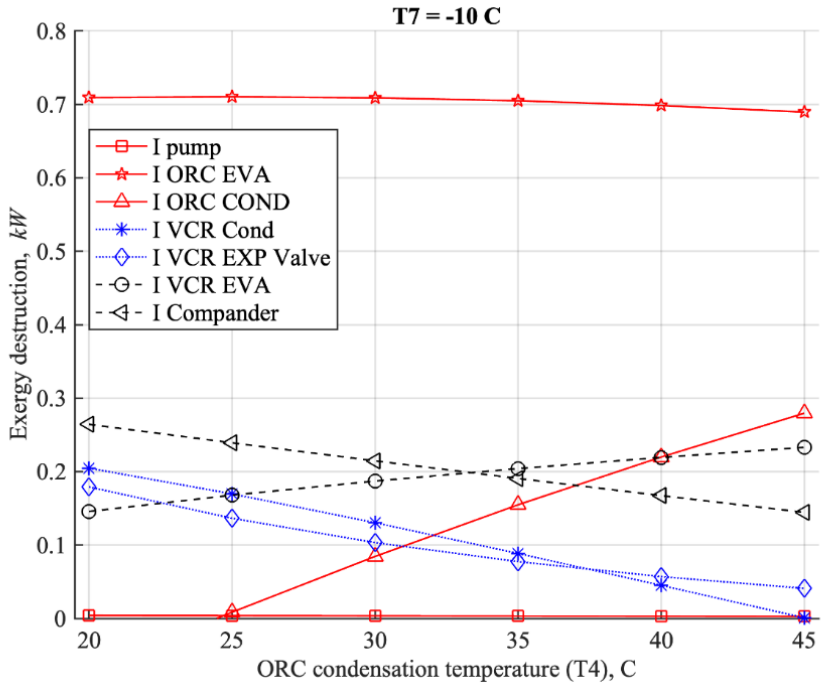

Figure 5-26: Exergy destruction distribution when ORC condensation temperature at 35℃ and VCR evaporation temperature at -10℃.

Figure 5-27 shows the exergy destruction contribution of the ORC-VCR component when the ORC condensation temperature and VCR evaporation temperature were 35℃ and -10℃, respectively. Reducing the VCR evaporation temperature from 5℃ to -10℃ led to increase the VCR evaporator contribution in the total exergy destruction by 8%. The VCR condenser and expansion valve contributions were reduced by 7% and 2%, respectively. However, the compander contribution in the total exergy destruction stays constant. Figure 5-28 shows the exergy destruction of the ORC-VCR component with variation of ORC condensation temperature when the VCR evaporation temperature at -15℃.

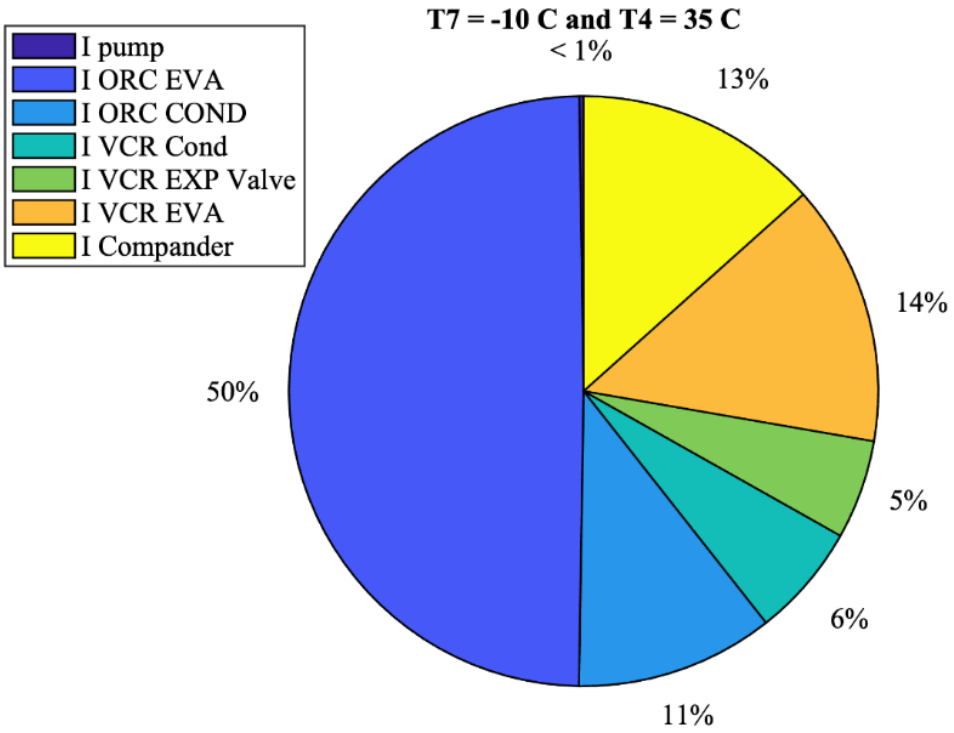

Figure 5-27: Exergy destruction distribution with variation of ORC condensation temperature and VCR evaporation temperature at -10℃.

It can be seen in the figure that at higher ORC condensation temperature and lower VCR evaporation temperature such as -10℃ and -15℃ the VCR side behave different than at higher VCR evaporation temperature and that can be explained by the empty areas in Figure 5-18 and Figure 5-19 where the system cannot produce cooling effects.

Figure 5-29 presented the contribution of the ORC-VCR component in the total exergy destruction when the ORC condensation temperature and VCR evaporation temperature were 35℃ and -15℃, respectively. Reducing the VCR evaporation temperature from 5℃ to -15℃ led to increase the contribution of the VCR evaporator and the compander by 12% and 1%, respectively. VCR condenser and expansion valve were reduced by 10% and 2%, respectively.

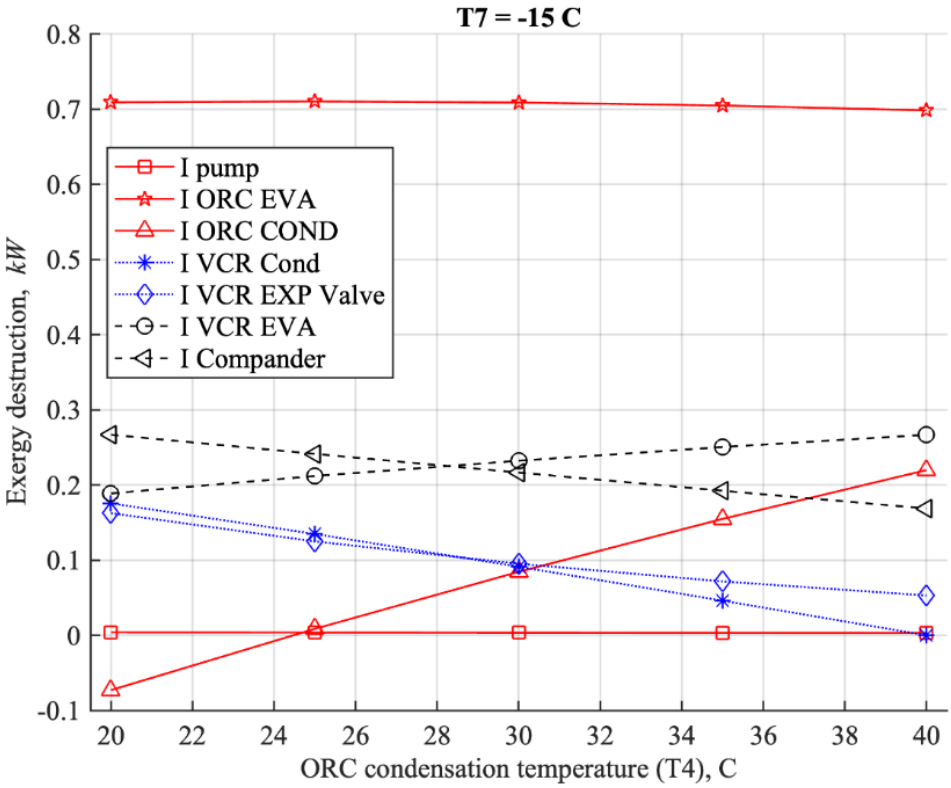

Figure 5-28: Exergy destruction distribution when ORC condensation temperature at 35℃ and VCR evaporation temperature at -15℃.

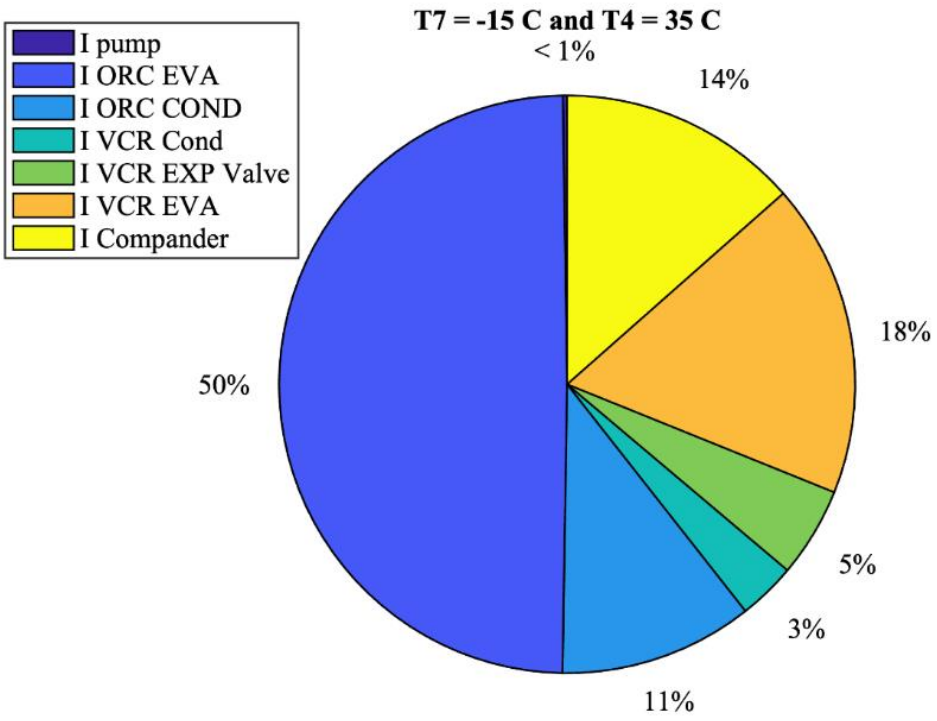

Figure 5-29: Exergy destruction distribution with variation of ORC condensation temperature and VCR evaporation temperature at -15℃.

Figure 5-30 shows the exergy destruction of ORC-VCR with the variation of ORC condensation temperature when the VCR evaporation temperature at -20℃. The exergy destruction at this temperature for all of the components follows the same pattern that is observed when the VCR evaporation temperature is set to -15℃. On the other hand, the exergy destruction that took place in the VCR evaporator showed a very little increase.

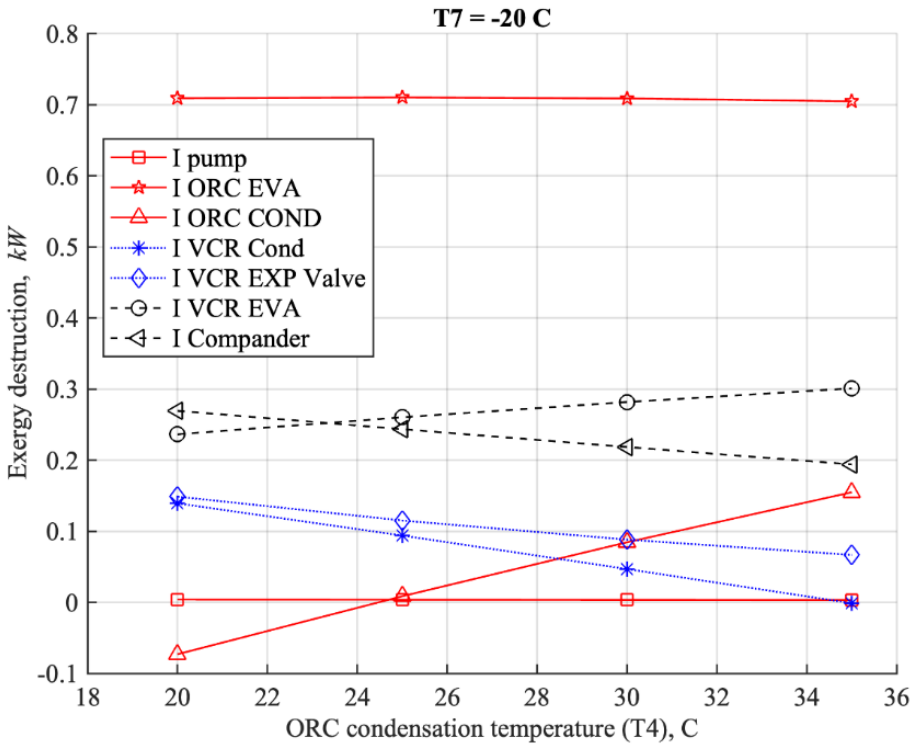

Figure 5-30: Exergy destruction distribution when ORC condensation temperature at 35℃ and VCR evaporation temperature at -20℃.

Figure 5-31 presented the contribution of the components in the total exergy destruction of ORC-VCR when the ORC condensation temperature and VCR evaporation temperature were 35℃ and -20℃, respectively. Reducing the VCR evaporation temperature from 5℃ to -20℃ can significantly increase the contribution of the VCR evaporator. However, at this time the system was not producing any cooling effects, as can be deduced from the extremely minimal contribution made by the VCR condenser to the overall destruction of exergy.

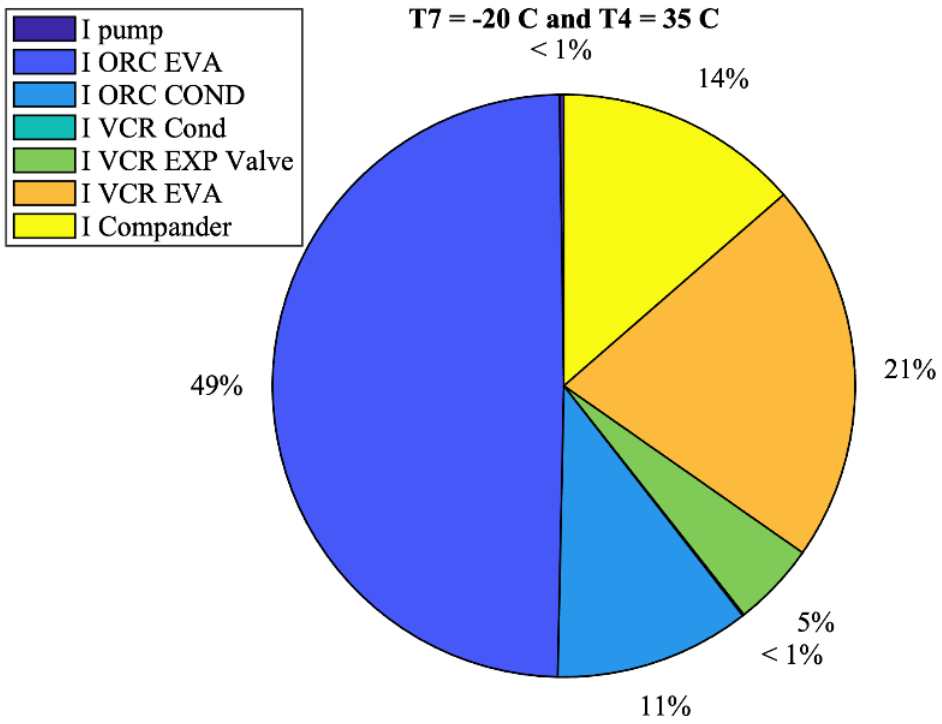

Figure 5-31: Exergy destruction distribution with variation of ORC condensation temperature and VCR evaporation temperature at -20℃.

5.5 Effect of degree of superheating and subcooling on the overall exergy efficiency

Figure 5-32 illustrates how changes in ΔT_{sup} and ΔT_{sub} in the ORC subsystem impact the overall exergy efficiency when the VCR evaporation temperature is held at 0°C, and the shaft speed is set to 1000 rpm. The values of ΔT_{sup} and ΔT_{sub} range from 0°C to 10°C, resulting in nine different conditions. In the case of the [0,0] set, the ORC evaporation temperature varies from 66.19°C to 89.74°C, while the ORC condensation temperature remains constant at 35°C. The findings indicate that increasing ΔT_{sup} does not lead to an improvement in overall exergy efficiency. Additionally, it is observed that increasing ΔT_{sub} has no impact on the overall exergy efficiency, as demonstrated by the overlap between the [5,5] and [5,10] conditions.

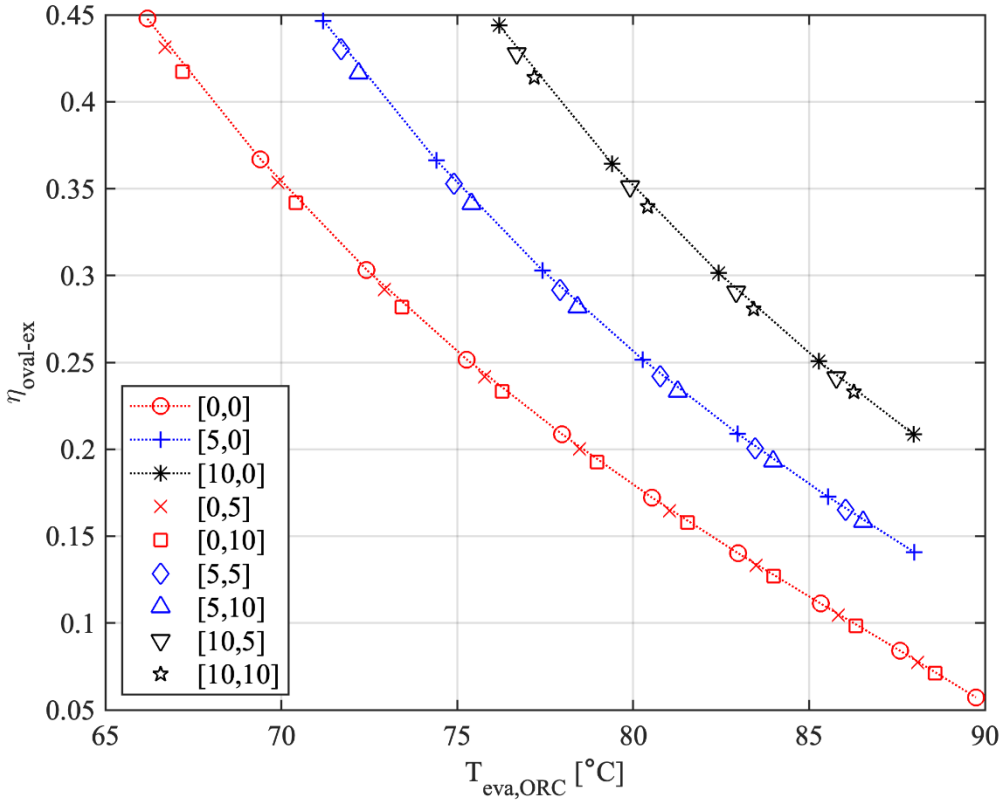

Figure 5-32: Influence of the degree of superheating (ΔTsup) and degree of subcooling (ΔTsub) on the overall exergy efficiency in legends, square parenthesis indicates [ΔTsup, ΔTsub].

5.6 Summary

Exergy analysis was performed on an ORC-VCR system that was connected by a single-rotor expander-compressor (compander) in this chapter. In this study, a detailed exergy destruction analysis of the ORC-VCR component as well as an analysis of the total exergy efficiency with varying system parameters were given. The ORC evaporation and condensation temperatures, the VCR evaporation temperature, the EPR and CPR ratios, and the single rotor expander-compressor shaft speed were the primary parameters that were analysed in this study. According to the findings, a rise in the EPR ratio results in an increase in the CPR ratio, and when both ratios are combined, the amount of exergy that is destroyed in the compander increases significantly. In addition, when considering the amount of exergy destruction contributed by each component of the ORC-VCR, the ORC evaporator has the most significant impact on the overall amount of exergy destruction.

There is potential for a sizeable increase in the contribution made by the VCR evaporator if the temperature at which evaporation occurs in the VCR is lowered.

At 500 rpm and VCR evaporation temperature at -20 °C, the overall exergy efficiency varies between 37% to 7% when ORC evaporation temperature increases from 72.4 °C to 89.7 °C. On the other hand, when the VCR evaporation temperature at 5°C, the exergy efficiency when the ORC evaporation temperature at 62.7 °C is 37% and when ORC evaporation temperature at 80.5 °C is 7%.

Furthermore, at 500 rpm and VCR evaporation temperature at -20 °C, the overall exergy efficiency varies between 30% to 39% when ORC condensation temperature increases from 20 °C to 45 °C. On the other hand, when VCR evaporation temperature at 5 °C, and the ORC condensation temperature at 40 °C the overall exergy efficiency was 14% and when the ORC condensation temperature at 45 °C it was 16%.

In general, the highest levels of overall exergy efficiency achieved was 63%. This result was achieved by setting the ORC evaporation temperature to 62.75°C and the VCR temperature to -5°C, while the ORC condensation temperature was maintained at 20.5°C. It was observed that variations in rotor speed did not alter the overall exergy efficiency.

Chapter 6: Study on different working fluids for ORC-VCR combined by single rotor expander-compressor.

6.1 Introduction

In this chapter, the MATLAB model begin by making the assumption that the vapor compression cycle is operating under a constant duty condition, indicating a steady cooling or refrigeration load. Moreover, it was assumed that the evaporator temperature of the VCR remains constant at 0°C throughout the investigation. By making these assumptions, a certain baseline was established for the performance and requirements of the VCR. The generated MATLAB model was compared to the ASPEN model for validation purposes as shown in Table 6-1:

Table 6-1: Comparison of MATLAB to ASPEN model.

	Inputs					Outputs			
Models	Working fluid	Heat source °C	ORC Evaporation Pressure, bar	ORC condensation pressure, bar	$T_{eva,VCR}$, °C	$\dot{m}_{ORC}$, kg/s	$\dot{m}_{VCR}$, kg/s	$\dot{W}_{ORC-Expander}$, kW	$\dot{Q}_{VCR-EVA}$, kW
ASPEN model	ORC: R245fa VCR: R134a	95	8	1.3	0	0.0233	0.011	0.6192	0.867
MATLAB model		95	8	1.3	0	0.0234	0.011	0.6192	0.866

After establishing the VCR's duty and evaporator temperature as fixed values, it was proceeded to examine the power requirements for the refrigeration cycle by having the condenser temperature. The present investigation enables the quantification of the power requirement of the organic Rankine cycle within the overall system. Consequently, this

factor displays an influence on the amount of heat that the organic Rankine cycle must recover in order to satisfy the precise cooling demands of the vapor compression refrigeration system, as it determines the mass flow rate of the ORC.

In this chapter, six working fluids have been chosen as potential candidates for an ORC-VCR integrated system, and they have been compared to one another. After then, the technical characteristics of the working fluids are discussed. The comparison was based on an analysis of the working fluids' energy and exergy properties as well as the environmental impact. In this research, the same working fluid was used throughout both cycles of the ORC-VCR.

6.2 Perspective organic working fluids

Six different working fluids were under consideration for research in the ORC-VCR system. The candidates under consideration are R245fa, R123, R134a, R1234ze(E), R1234yf, and Butane. R245fa and R123 were considered in this study due to the fact that they are frequently used in ORC power plants [72]. R134a is one of the most extensively studied and utilized working fluids in VCRs. R1234ze(E) and R1234yf are being considered as possible replacements to R134a in the industry. Butane is hydrocarbons working fluids and they showed an attractive performance in single fluid ORC-VCR systems [143, 144].

Based on their chemical specifications and environmental characteristics, the refrigerants mentioned above can be divided into several separate groups. Butane is a member of the family of hydrocarbons (HCs) that are generally considered to be benign to the environment. Because of their negligible impact on the global climate, hydrofluoroolefins (HFOs) like R1234ze(E) and R1234yf are widely considered to be environmentally superior alternatives. R245fa and R134a, on the other hand, are hydrofluorocarbons (HFCs) and are well-known for their efficiency in a variety of cooling applications;

nevertheless, their global warming potential (GWP) is larger than that of HFOs. However, R123 is a hydrochlorofluorocarbon (HCFC), which is different from HFCs and HFOs and has properties that are intermediate between them, and its usage is restricted because of its impact to ozone depletion.

The specifications of the selected working fluids are presented in Table 6-2. The typical values of parameters used for modelling ORC-VCR are presented in Table 6-3. The influences of some operating parameters on the ORC-VCR system performance have been studied and presented in the following subsections. The parameters included: condensation temperature, ORC evaporation temperature, VCR evaporation temperature, expander isentropic efficiency, and compressor isentropic efficiency. In each case the parameter has been varied according to the range showed in Table 6-3 Table 6-3: ORC-VCR modelling parameters values.. The other parameters stied constant while one parameter was varied.

Table 6-2. Specifications of working fluid candidates [140, 145, 146].

Working Fluid	Molar Mass (kg/kmol)	Critical Temperature (°C)	Critical Pressure (Mpa)	ODP	GWP
R245fa	134.05	154.01	3.651	0	820
R123	152.93	183.68	3.66	0.012	76
R134a	102.03	101.06	4.06	0	1430
R1234ze(E)	114.04	109.36	3.64	0	6
R1234yf	114.04	94.70	3.38	0	4
Butane	58.13	151.98	3.80	0	20

Table 6-3: ORC-VCR modelling parameters values.

Parameter	Value	Range
ORC, Evaporation Temperature (°C)	90	65 – 90
Condensation Temperature (°C)	30	25 – 45
VCR, Evaporation Temperature (°C)	5	-20 – 5
Expander Isentropic Efficiency (%)	80	50 – 90
Compressor Isentropic Efficiency (%)	80	Fixed
ORC, Pump Isentropic efficiency (%)	75	Fixed

6.3 Influences of variation in condensation temperature

6.3.1 Influences of variation of condensation temperature on COPs

The impacts of condensation temperature on the overall performance of ORC-VCR are illustrated in Figure 6-1. R1234yf had the COPs that was measured to be the greatest, followed by R134a, R1234ze, R245fa, butane, and R123.

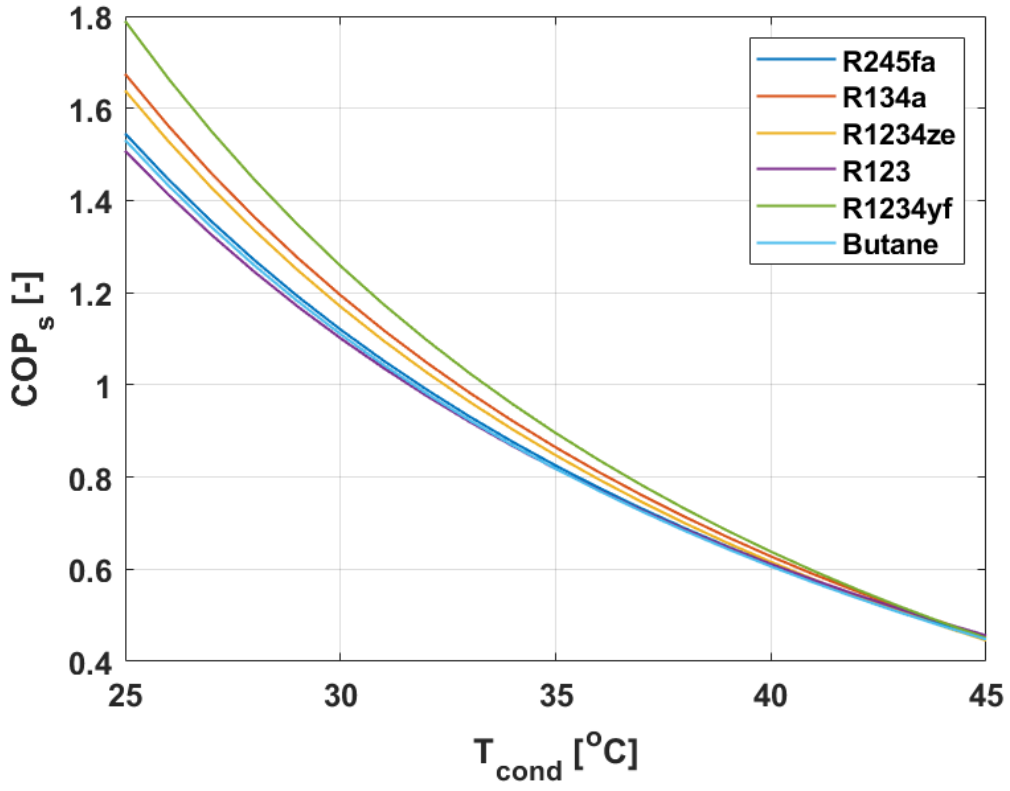

Figure 6-1: Influences of variation of condensation temperature on COPs

It has been found that the temperature of the condensation has a significant impact on the COPs. This is due to the fact that it has an impact on both cycles, whose condensers have the same temperature. It is recommended that the condensation temperature be raised in ORC systems in order to reduce the amount of heat that is rejected, which will result in improved thermal efficiency. Increasing the condensation temperature will, however, necessitate an increase in the amount of power supplied by the compressor in the VCR system. As shown in Figure 6-1, When the condensation temperature increased, the COP_s decreases. As the condenser temperature rises, the pressure and enthalpy at the compressor's outlet rise as well. This is because the temperature and pressure at the compressor's inlet remain constant. This proves that the stance is correct.

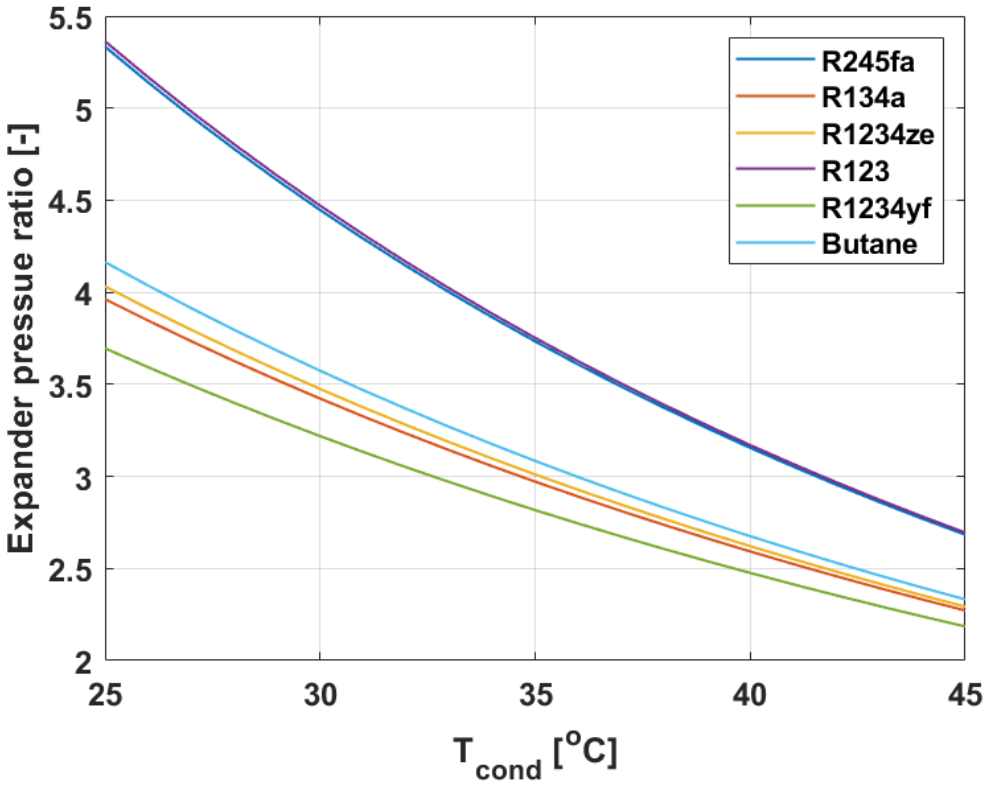

Figure 6-2: Influence of condensation temperature on the expander pressure ratio

6.3.2 Influence of condensation temperature on the expander pressure ratio

The influence that condensation temperature has on the expander pressure ratio EPR is illustrated in Figure 6-2 for different working fluids in ORC-VCR. The EPR will decrease as the condensation temperature rises, which will be associated with an increase in the condensation pressure of the ORC. When the condenser temperature is high, the suggested working fluids exhibit smaller variances in EPR values compared to when the temperature is low in the condenser.

6.3.3 Influence of condensation temperature on the compressor pressure ratio

The compressor pressure ratio CPR is shown here along with how it varies with the condensation temperature in Figure 6-3. The change in EPR is inversely proportional to the variation in CPR. The increase in CPR that occurs as the condensation temperature rises is the result of an increase in the pressure that is released by the compressor because

of the temperature rise. Both R123 and R245fa exhibit approximately identical compressor pressure ratio values regardless of the condenser temperatures they are subjected to.

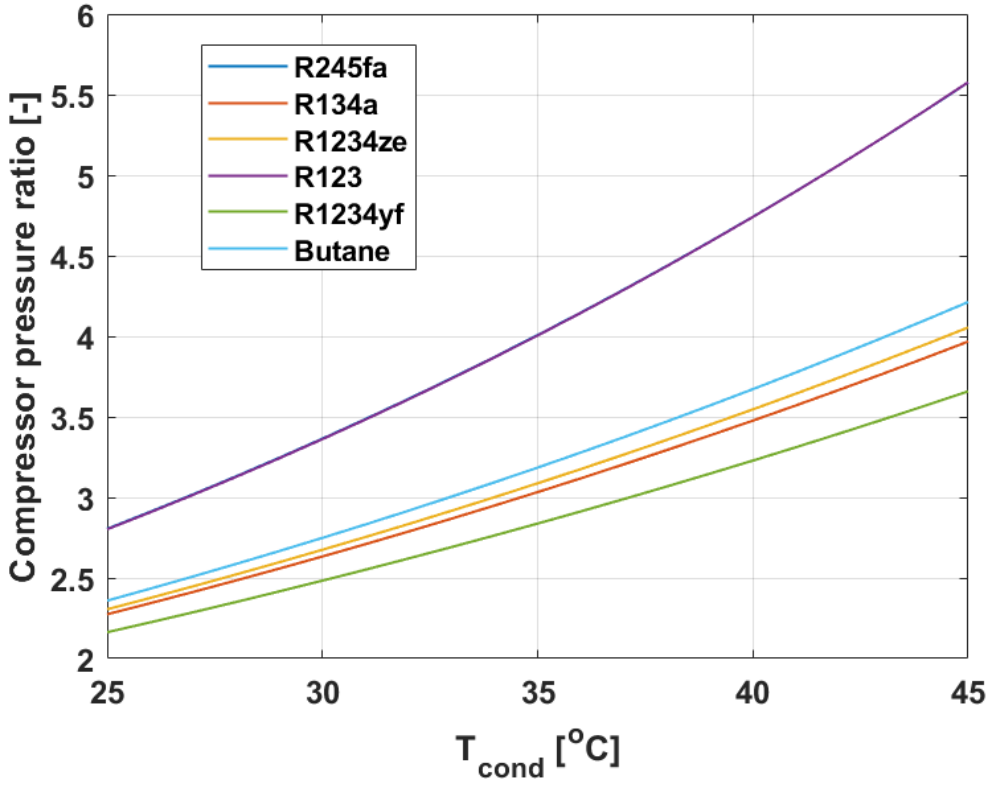

Figure 6-3: Influence of condensation temperature on the compressor pressure ratio

6.3.4 Influence of condensation temperature on overall exergy efficiency

Figure 6-4 depicts the variation of the ORC-VCR system overall exergy efficiency denoted as η_{exe} in relation to the condenser temperature for all considered refrigerants .

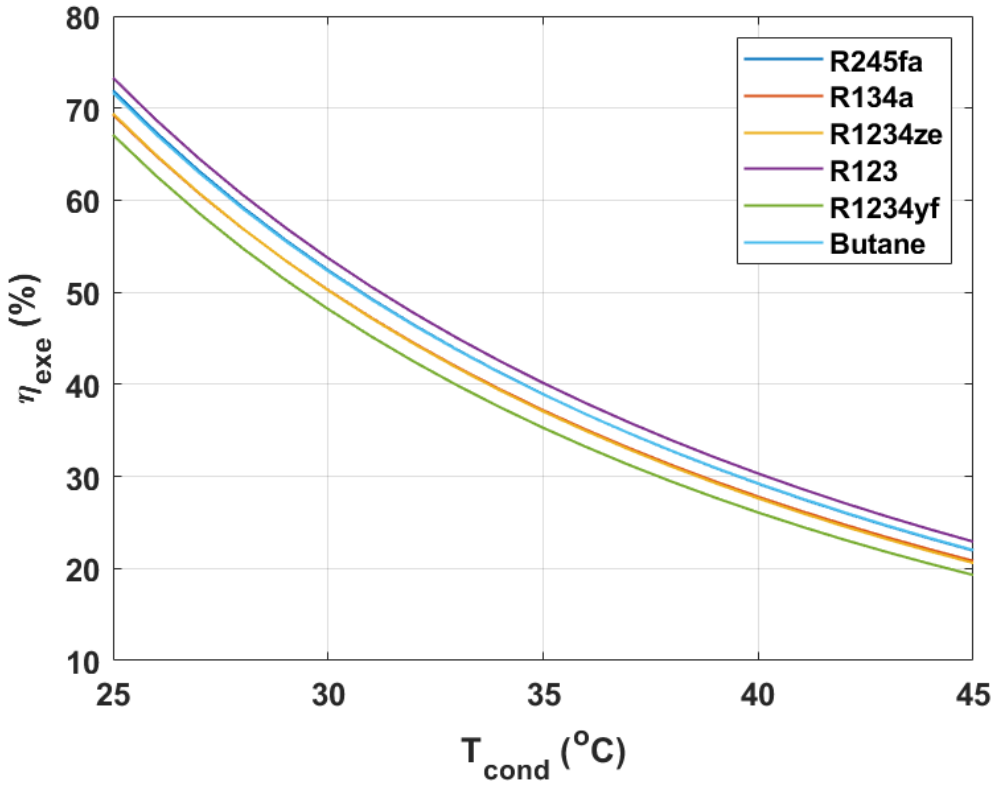

Figure 6-4: Influence of condensation temperature on η_{exe}.

The figure clearly demonstrates that the condenser temperature has a significant impact on the η_{exe}. The influence discussed here arises from the effect of the condenser temperature on both the Organic Rankine Cycle and Vapor Compression Refrigeration cycle. It demonstrates that there is a decrease in the overall exergy efficiency for all refrigerants when the condenser temperature is increased. The observed pattern can be assigned to the thermophysical properties of the working fluids. Nevertheless, it should be noted that a rise in the condenser temperature leads to a decline in the $E_{cooling}$ while increasing the E_{in}, in accordance with the thermophysical characteristics of the employed refrigerants. Among the various refrigerants that have been studied, it has been observed that R123 and R245fa exhibit the highest levels of exergy efficiency. However, R1234yf demonstrates the lowest exergy efficiency across all investigated condenser temperatures.

6.3.5 Influence of condensation temperature on η_{H-C}

Figure 6-5 shows that if the condenser temperature is kept too high, the system's heating to cooling efficiency decreases. Among the six available refrigerants, R123 is the most efficient refrigerant in terms of the heating to cooling efficiency at both low and high condenser temperatures. Utilizing R1234yf results in the lowest possible value of efficiency.

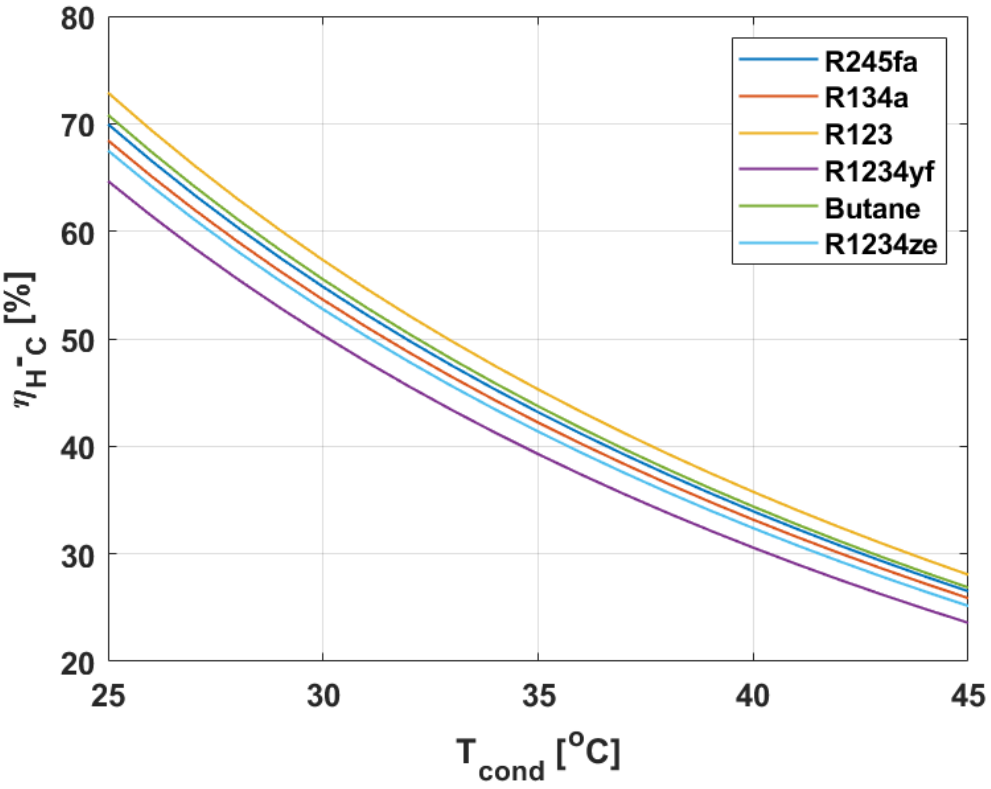

Figure 6-5: Influence of condensation temperature on heat to cooling efficiency.

6.3.6 Influence of condensation temperature on $\dot{m}_{ORC}$

The correlation between an increase in condenser temperature and a rise in mass flow rate of ORC system is illustrated in Figure 6-6. Because of an increase in the condenser's temperature, an increase in the compressor power is resulted in VCR. Because of the condition, there is also an increase on the power generated by the expander in ORC. As a direct consequence of this, ORC mass flow rate goes up as well. As a consequence of

these factors, the overall mass flow rate of the combined system rises. R123 achieved the lowest $\dot{m}_{ORC}$ (or $\dot{m}_{total}$), whereas R1234yf achieved the greatest value for all condenser temperatures. R123 also achieved the lowest $\dot{m}_{ORC}$. When compared to the various other refrigerants, R123 is the better one.

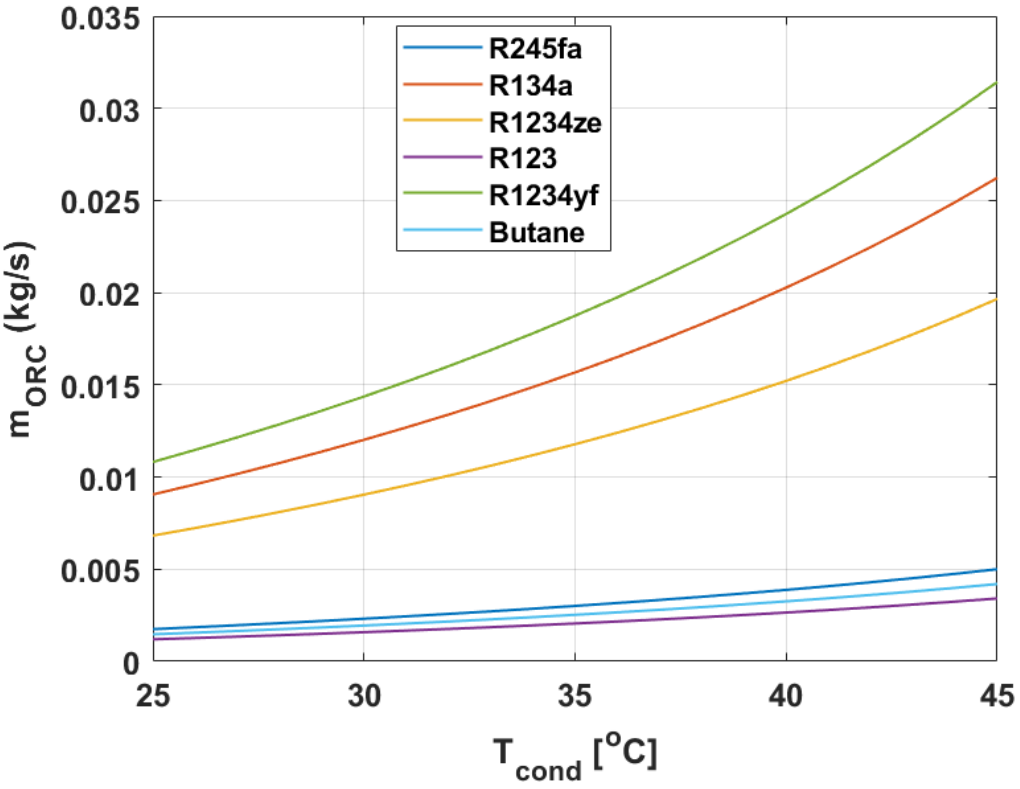

Figure 6-6: Influence of condensation temperature on $\dot{m}_{ORC}$.

6.4 Influences of variation in ORC evaporation temperature

6.4.1 Variation of ORC evaporation temperature on COP_s

As shown in Figure 6-7. ORC evaporation temperature has a positive effect on the COP_s of the system. This may be understood by the fact that when the evaporator's temperature rises, it also increases its saturation pressure, which lowers the CMR. As a result, under the specific working circumstances, the compressor requires less power. It is also important to note that the ORC evaporation temperature must be lower than 72 °C for

R123 to exhibit the maximum COP_s.R1234yf displays the highest COP_s, but only after the ORC evaporation temperature has been raised over 72 °C.

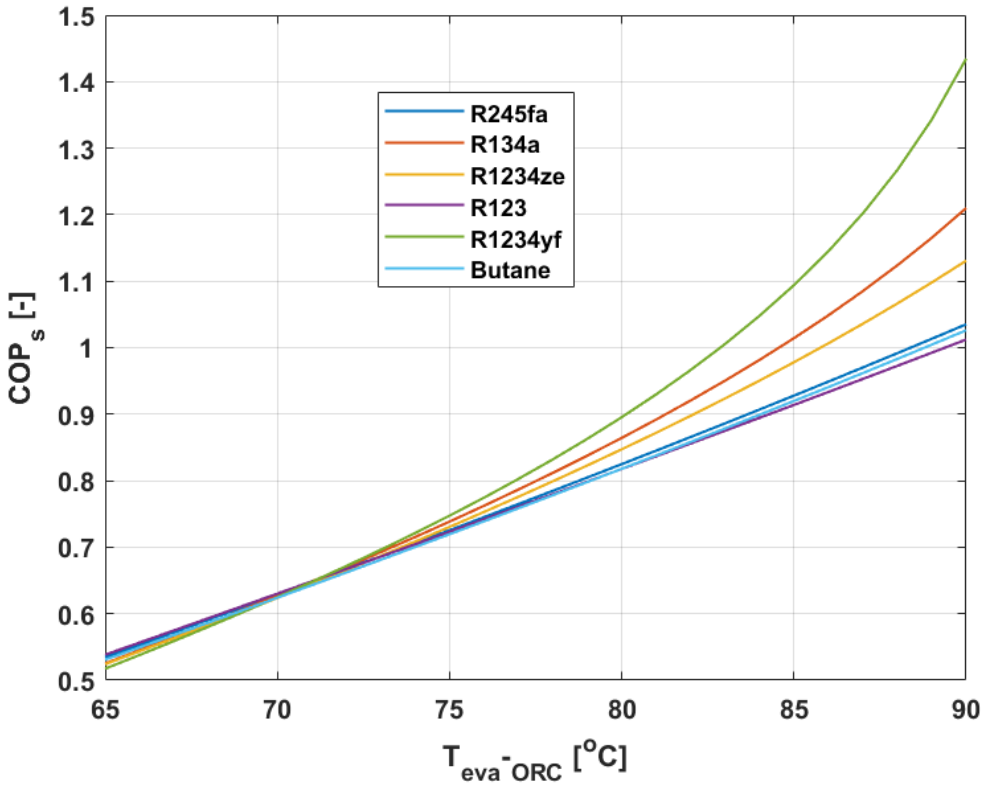

Figure 6-7: COPs against ORC evaporation temperature.

6.4.2 Variation of ORC evaporation temperature on EPR

The variation in the EPR that occurs when the ORC operates at different evaporation temperatures is depicted in Figure 6-8. The figure demonstrates that an increase in the amount of ORC evaporation results in an increase in the EPR, that is because of an increase in the pressure at the expander inlet. The EPR that is highest is shown by R123, followed by R245fa, and the EPR that is lowest is shown by R1234fy.

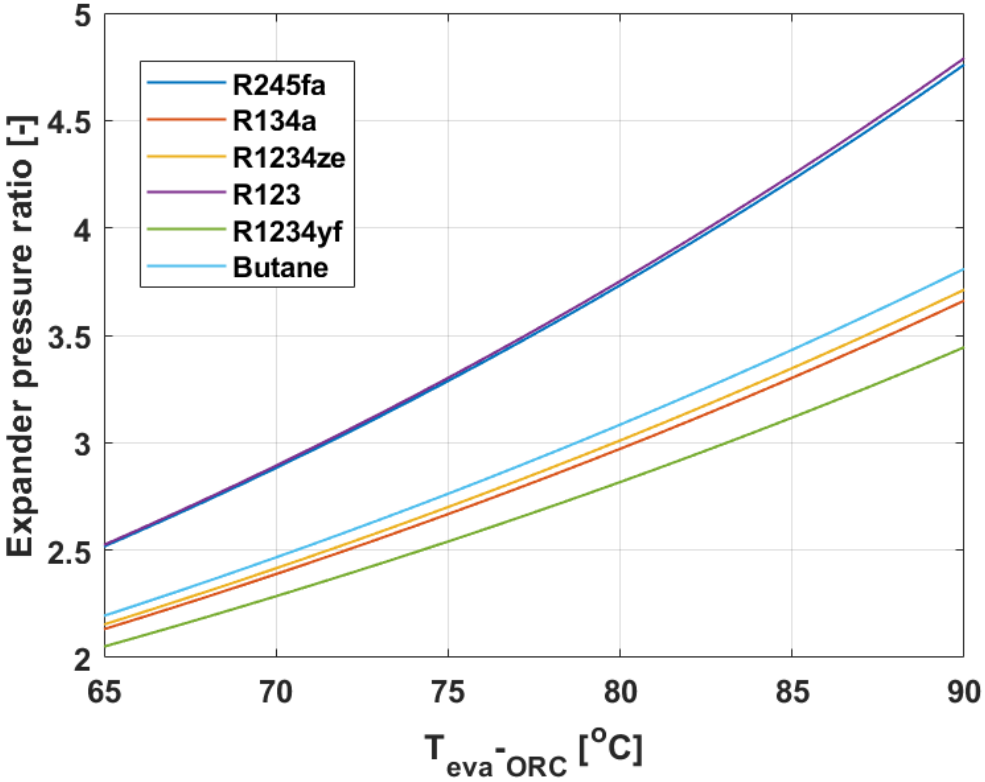

Figure 6-8: Variation of ORC evaporation temperature on EPR.

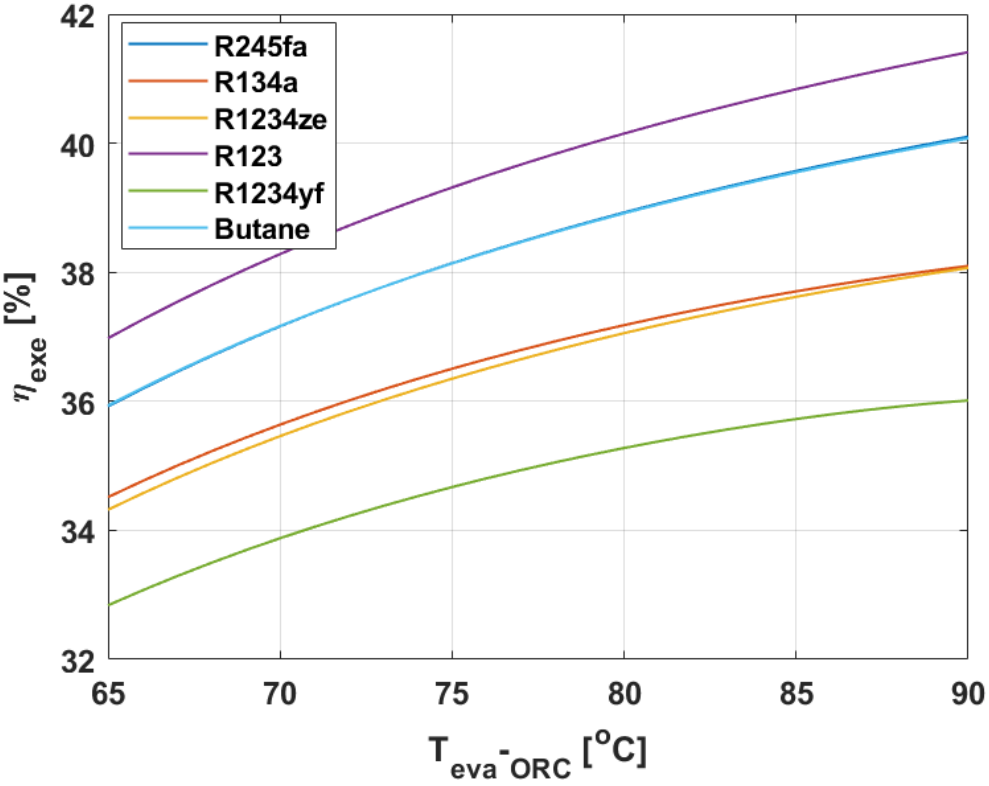

Figure 6-9: Variation of ORC evaporation temperature on η_{exe}

6.4.3 Variation of ORC evaporation temperature on ηexe

Figure 6-9 shows the variation in overall exergy efficiency for all considered refrigerants in the typical arrangement with respect to evaporator temperature of ORC. As shown in the Figure 6-9, the overall exergy efficiency gets better as evaporator temperature gets higher. Interestingly, while this change in evaporator temperature has no effect on $E_{cooling}$, it does raise the input specific exergy. As evaporator temperature rises, however, m_{ORC} falls. As a result of all of these modifications, E_{in} drops while evaporator temperature rises.

6.4.4 Variation of ORC evaporation temperature on η_{H-C}

Increasing the ORC evaporator temperature improves the ORC-VCR heat-to-cooling efficiency, as shown in Figure 6-10.

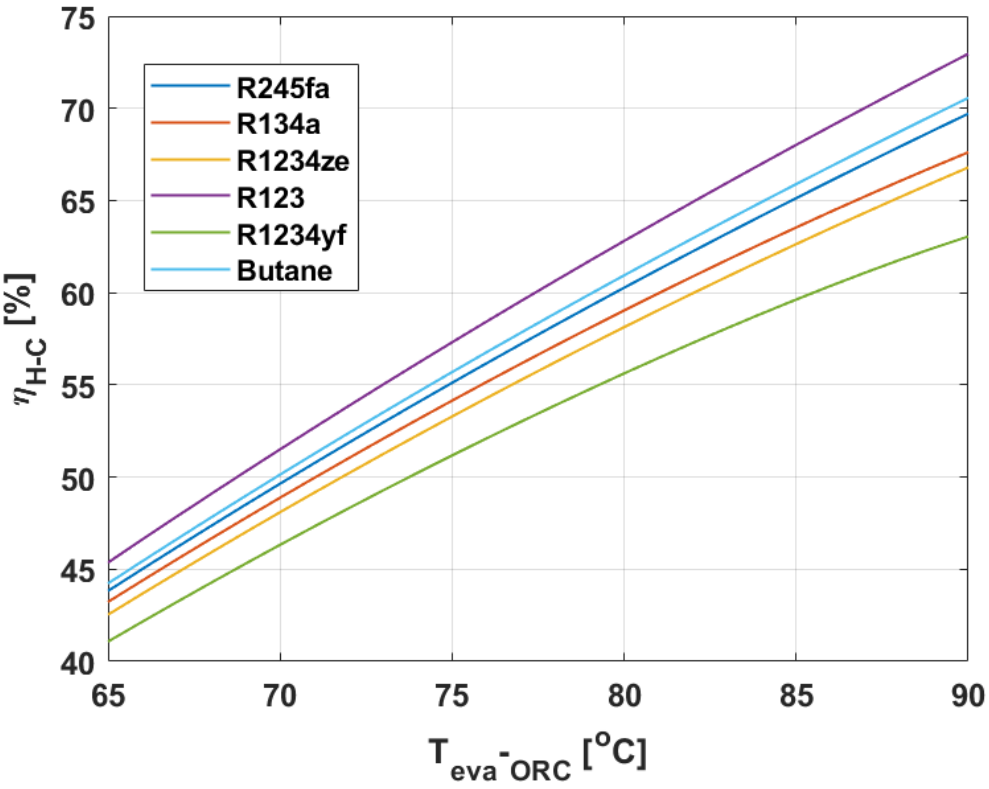

Figure 6-10: Variation of ORC evaporation temperature on heating to cooling efficiency.

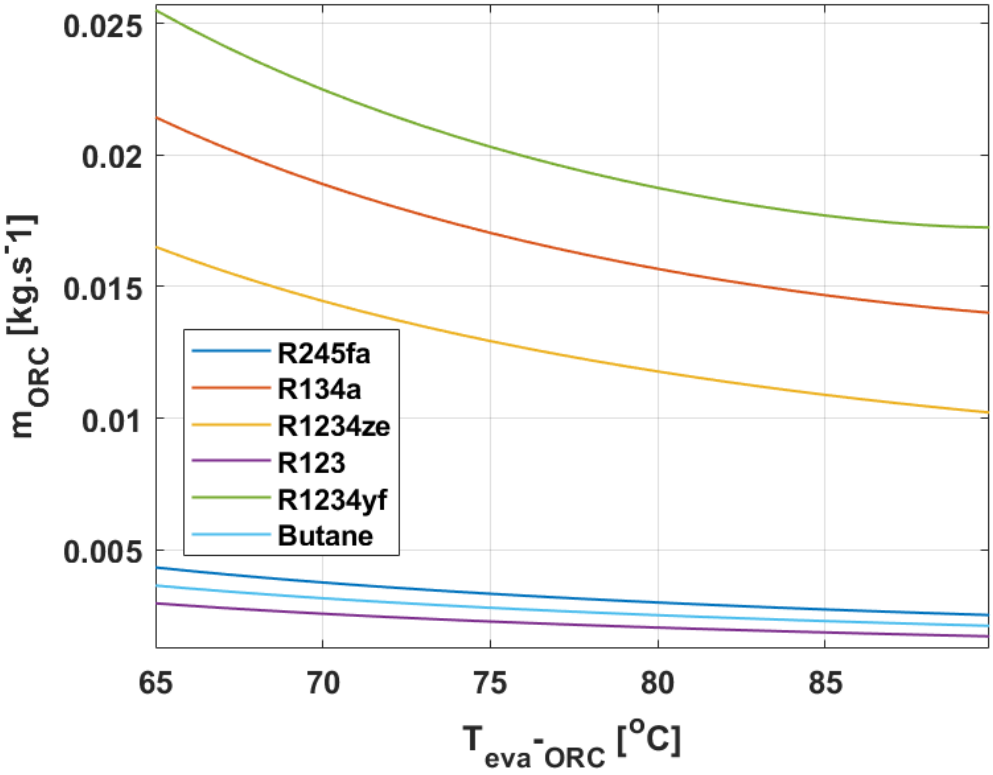

Figure 6-11: Variation of ORC evaporation temperature on m˙_ORC.

This increasing take place despite an unchanged requirement for cooling. At the same time, the mass flow rate of the ORC working fluid falls as shown in Figure 6-11, resulting in a lower rate of input heat. As a result, heat-to-cooling efficiency is improved by increasing ORC's evaporator temperature. Raising the temperature of the ORC evaporator from 65 to 90 °C yields a notable enhancement of around 50% in the heat-to-cooling efficiency for all employed working fluids. Among the refrigerants under consideration, R123 demonstrates the highest heat-to-cooling efficiency, followed by Butane, R245fa, R134a, and R1234ze. Conversely, R1234yf has the lowest performance in terms of heat-to-cooling efficiency.

6.4.5 Variation of ORC evaporation temperature on $\dot{m}_{ORC}$

Figure 6-11 shows the effect of evaporator temperature of ORC on the ORC mass flow rate for all considered refrigerants in the typical system. By the increase of evaporator

temperature ORC mass flow rate increases. The rise of the evaporator temperature inside an ORC, results in an elevated ORC mass flow rate, predominantly attributable to the intensified vaporization process. This is a consequence of the increased availability of heat, which facilitates the transformation of the working fluid from a liquid state to a gaseous state. Furthermore, in order to provide a consistent rate of heat transfer within the evaporator, the ORC system requires an increased circulation of working fluid as the temperature in the evaporator increases. This results in a higher mass flow rate. Among all refrigerant R123 achieves the minimal ORC mass flow rate for all examined evaporator temperature in ORC, whilst R1234yf attains the maximal ORC mass flow rate. R123 exhibits a greater heat vaporization capacity in comparison to R1234yf, resulting in its ability to absorb a higher amount of heat energy per unit of mass at equivalent temperatures. Consequently, R123 proves to be more efficient when employed in ORC systems.

6.5 Influences of variation in expander isentropic efficiency

6.5.1 Variation of expander efficiency on COP_s

Figure 6-12 shows the variation of expander isentropic efficiency with COP_s. The figure presents a positive impact of expander isentropic efficiency on COP_s that due to the increase in the output power which will improve the thermal efficiency of the ORC.

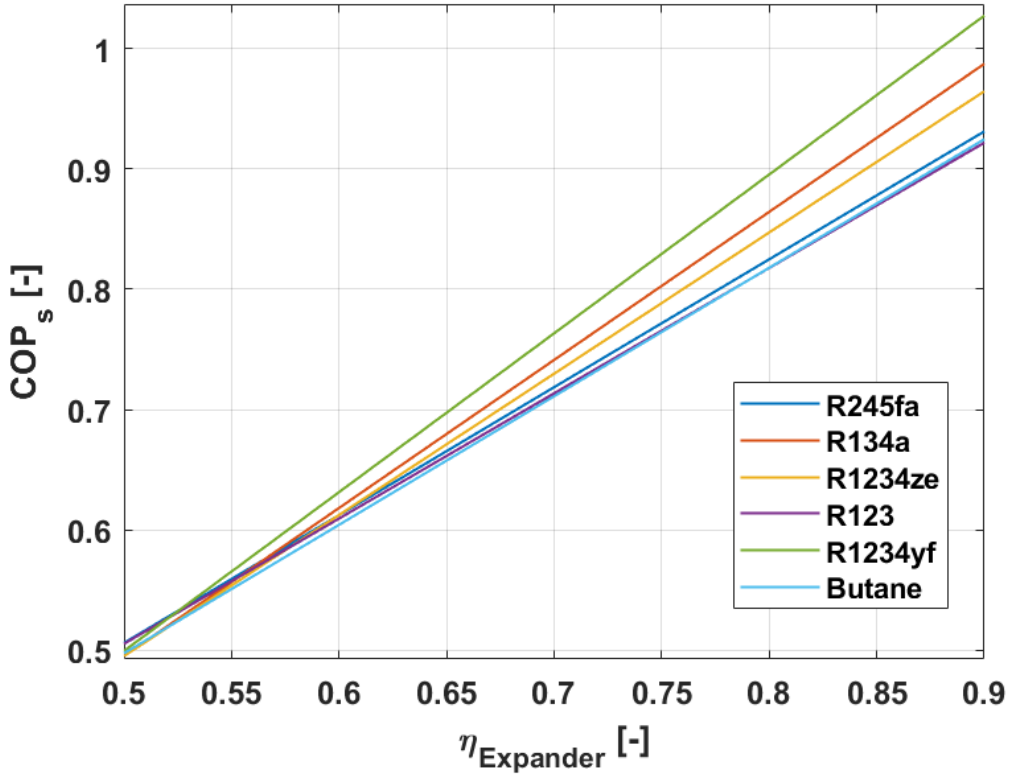

Figure 6-12: COPs against expander isentropic efficiency.

6.5.2 Variation of expander efficiency on $\dot{m}_{ORC}$

Figure 6-13 presents the exergy efficiency of the ORC-VCR system $\eta_{ex,sys}$ variation with the expander isentropic efficiency. The figure showed there is a great impact on the exergy efficiency, and it is related to reduction of the exergy destruction in the expander. Figure 6-13 shows the VCR evaporation temperature variation effects on the exergy efficiency. All the working fluids shows the same behaviour in both low and high evaporation temperatures. From the figure, increasing the evaporation temperature leads to a dramatic decrease in the exergy efficiency.

The specific work produced by the expander increases when η_{exp} is increased, while maintaining a constant boiler specific heat. Significantly, the variation in η_{turb} does not have any effect on the VCR cycle, implying that it does not influence factors like the VCR evaporator heat rate or the power of the compressor. As a result, while the efficiency of

the expander is increased, the power output of the expander remains same. In light of the fact that the power output of the expander is determined by the multiplication of the mass flow rate and the specific work of the expander, it is imperative to decrease the mass flow rate of ORC in order to maintain a consistent expander power, as depicted in Figure 6-13.

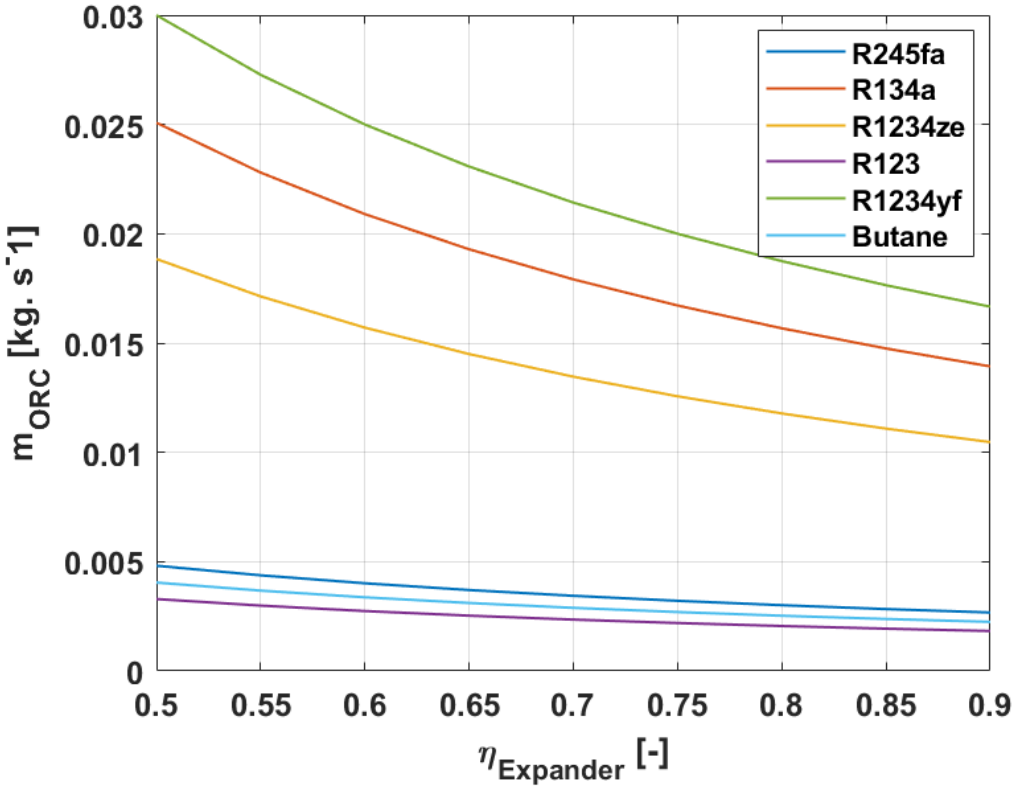

Figure 6-13: Variation of expander efficiency on ORC mass flow rate

6.5.3 Variation of expander efficiency on η_{exe}

The mass flow rate of the ORC drops as η_{exp} increases, leading to a corresponding decrease in Ein. While $E_{cooling}$, remains constant, E_{in}, drops due to an improvement in the η_{exp}. Consequently, this decreases in E_{in} leads to an increase in η_{exe} as shown in Figure 6-14.

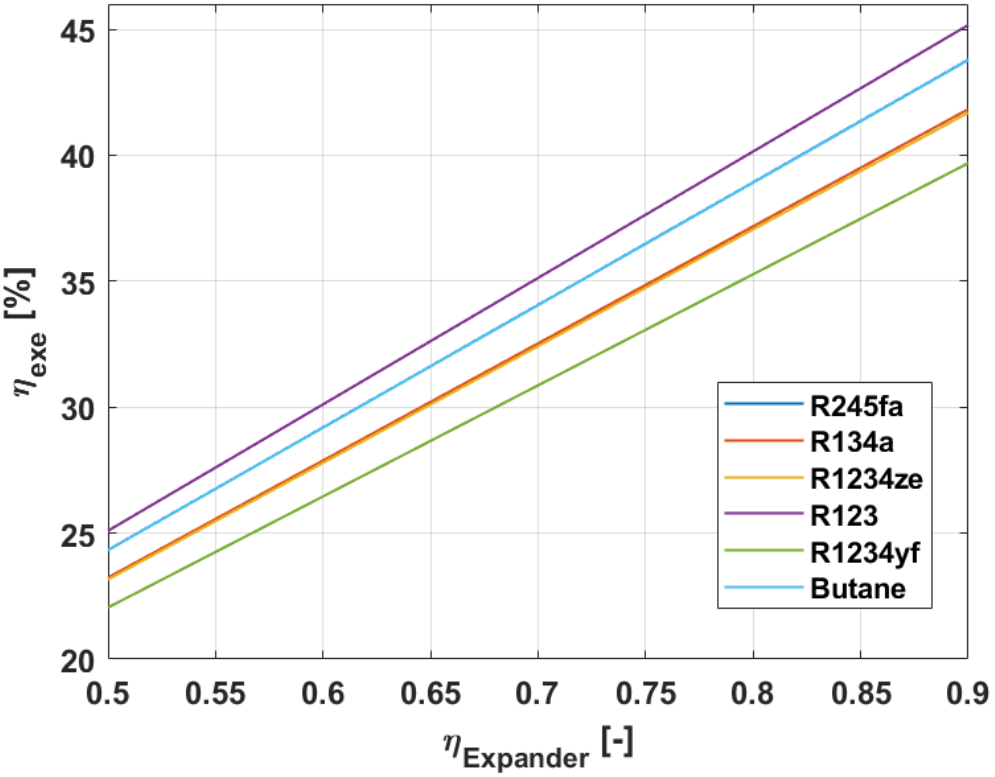

Figure 6-14: Variation of expander efficiency on η_exe

6.6 Influences of variation in VCR evaporator temperature

6.6.1 Variation of VCR evaporator temperature on η_{exe}

The impact of the evaporator temperature on η_{exe} is shown in Figure 6-15. As can be seen in figure, the exergy efficiency of the system drops when the temperature of the evaporator is increased. The quantity of exergy that is transferred along with the heat in the evaporator is reduced to a lesser extent as the temperature of the evaporator rises. This circumstance has a negative impact on the $\eta_{exe\text{-}VCR}$, which in turn has a detrimental effect on the η_{exe}.

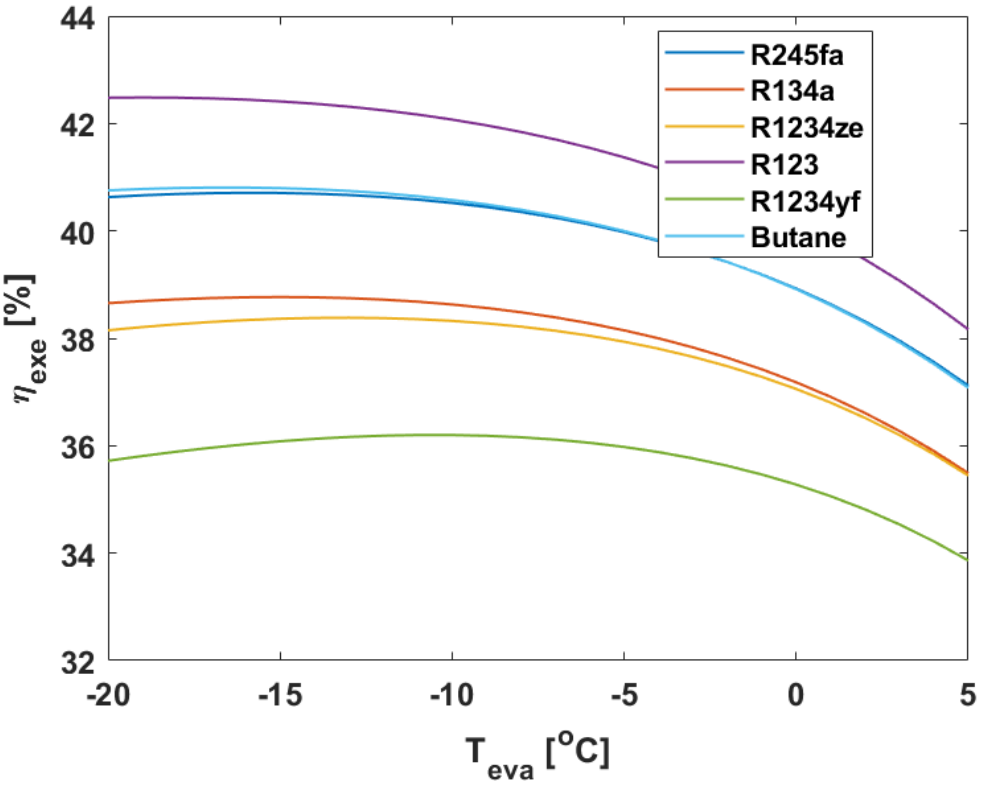

Figure 6-15: Variation of VCR evaporator temperature on η_{exe}

6.6.2 Variation of VCR evaporator temperature on CPR

Figure 6-16 displays the relationship between CPR and T_{eva} for all refrigerants within the presented system. The figure illustrates a negative correlation between CPR and T_{eva}, indicating a declining tendency in CPR as Teva increases. The reason for this phenomenon is that when the temperature of the evaporator increases, the evaporator pressure also increases, resulting in a drop in the CPR at a constant condenser temperature.

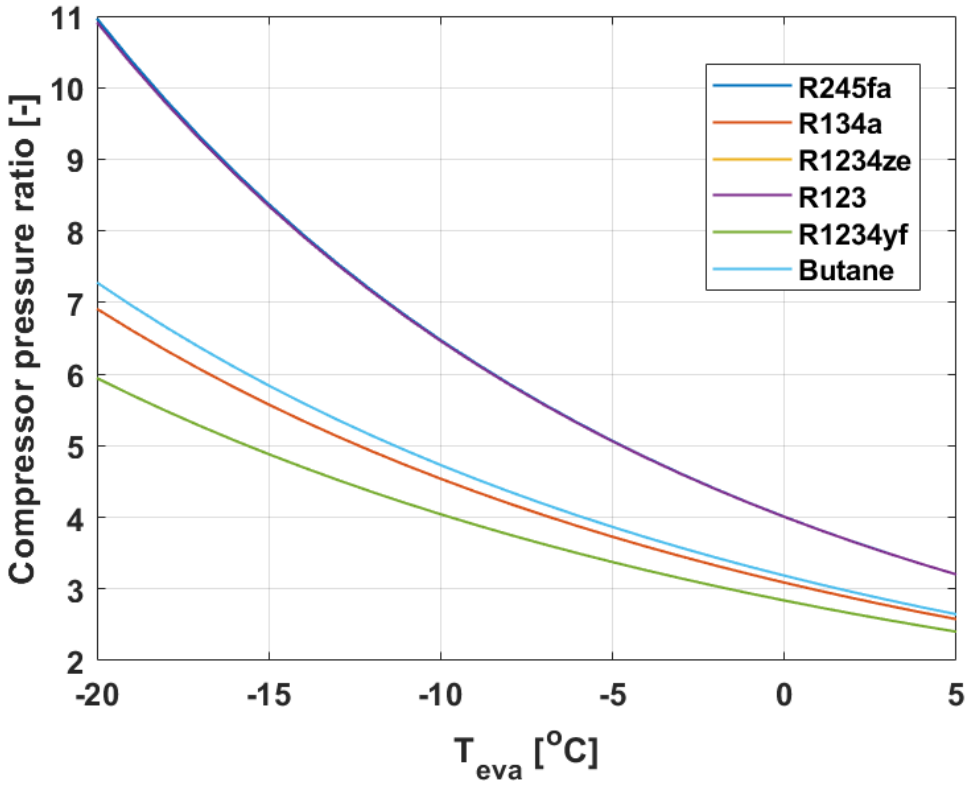

Figure 6-16: Variation of VCR evaporator temperature on CPR

6.6.3 Variation of VCR evaporator temperature on COP_s

According to Figure 6-17 the coefficient of performance of the system improves whenever the temperature of the evaporator in the VCR is raised to a higher level. As it was mentioned, an increase in the evaporator temperature results in a decrease in the CPR. The reduction in CPR results in a corresponding drop in the required compressor power which causes COP_{VCR} to increase, and this results in an increase in the COPs.

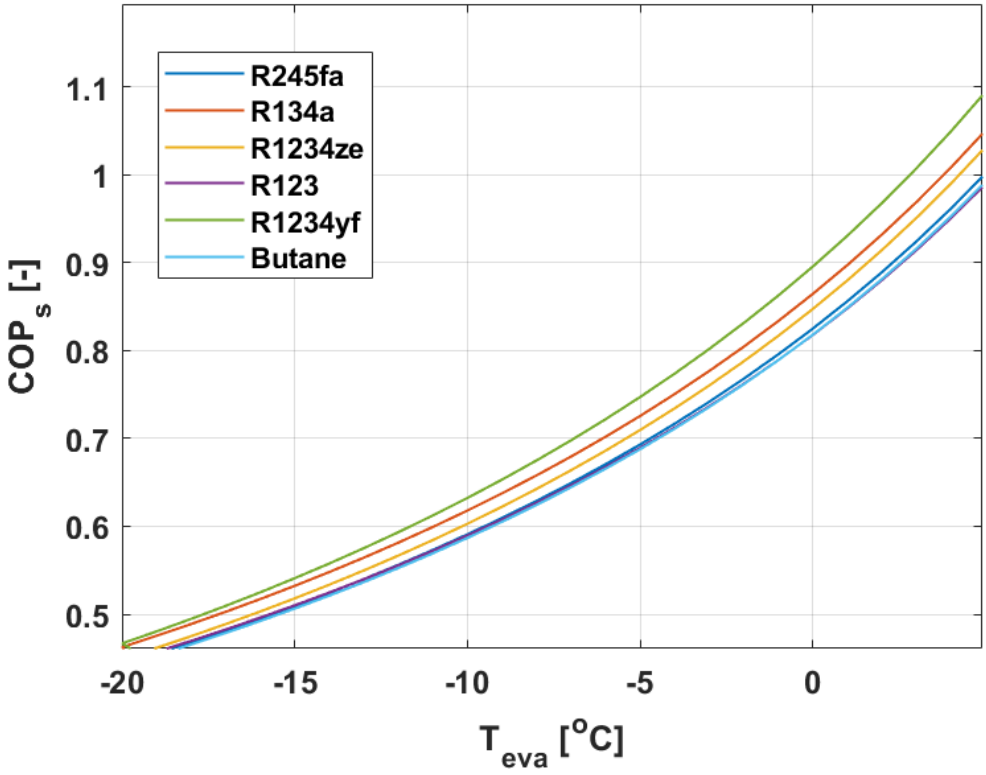

Figure 6-17: Variation of VCR evaporator temperature on COP_s

6.6.4 Variation of VCR evaporator temperature on η_{H-C}

The Figure 6-18 demonstrates that the heat-to-cold efficiency of the ORC-VCR system for selected refrigerants can be enhanced by manipulating the VCR evaporator temperature variability. But it's important to remember that this change in evaporator temperature mostly affects the VCR section and has little effect on the ORC unit, except for its mass flow rate. An increase in the VCR evaporator temperature leads to a corresponding increase in the specific enthalpy difference in the evaporator, hence enhancing the cooling effectiveness. Nevertheless, the elevated evaporator temperature leads to a corresponding rise in the working pressure within the VCR unit. Consequently, this leads to a decrease in the pressure differential within the VCR compressor, resulting in a reduced demand for driving power. As a result, the ORC expander produces a reduced

amount of power, so directly affecting the mass flow rate of the ORC system. The heat transfer within the ORC heat exchanger is also influenced by the reduced mass flow rate. Consequently, the enhancement in heat-to-cold efficiency can be observed by increasing the temperature of the VCR evaporator, as depicted in the provided Figure 6-18.

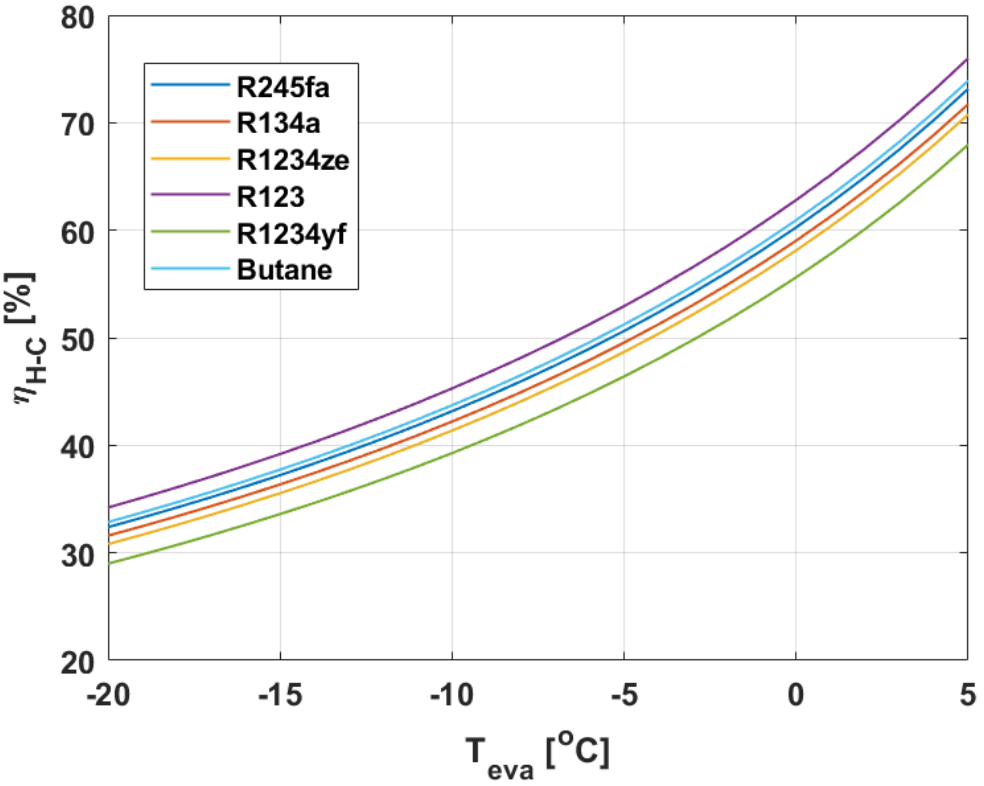

Figure 6-18: Variation of VCR evaporator temperature on heating to cooling efficiency.

6.7 Exergy analysis

6.7.1 Variation of ORC evaporator temperature on ORC evaporator exergy destruction

Increasing the evaporator temperature in an ORC typically results in a reduction in exergy degradation within the evaporator as shown in Figure . This enhancement is a result of an increased temperature difference between the high-temperature heat source and the working fluid in the evaporator of the Organic Rankine Cycle. This bigger temperature

differential allows for more effective heat transfer and energy conversion, while simultaneously minimizing the occurrence of irreversibilities. The efficiency of the Organic Rankine Cycle generally increases, enabling it to extract a greater amount of useful work from a given heat input. This improvement is particularly evident when there is a higher temperature differential, as the ORC approaches the upper limit of efficiency known as the Carnot efficiency. As a result, increasing the temperature of the evaporator serves to reduce exergy losses and so leads to a decrease in the overall exergy destruction within the evaporator.

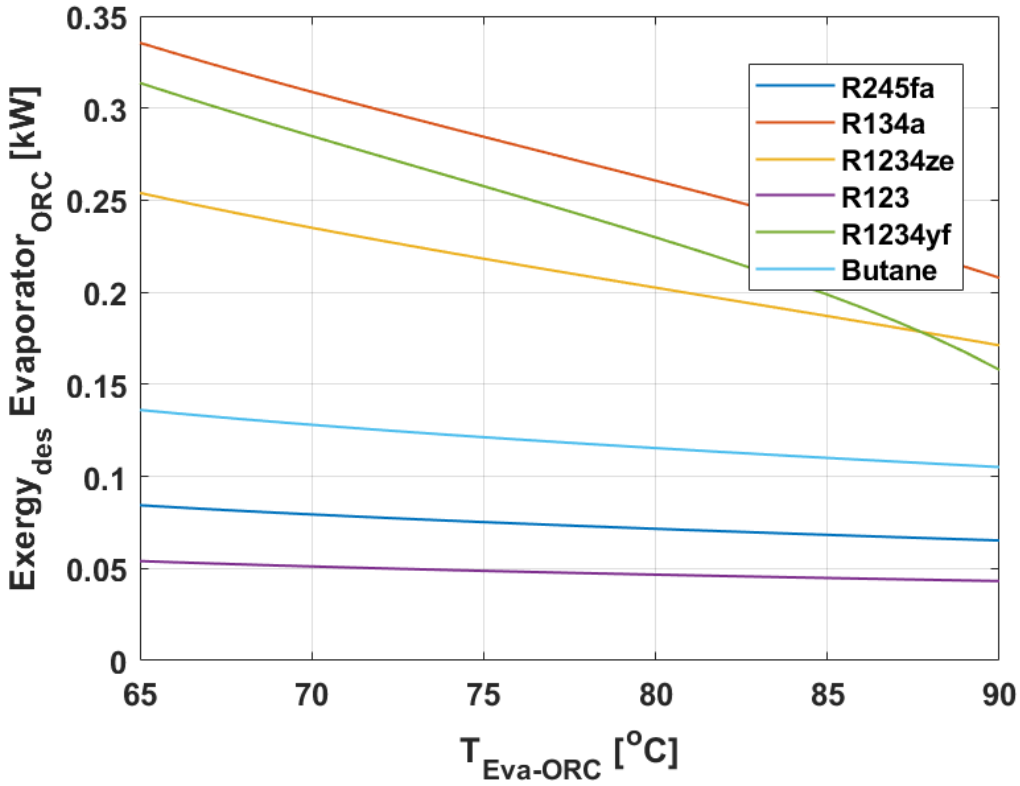

Figure 6-19: Variation of ORC evaporator temperature on ORC's evaporator exergy destruction

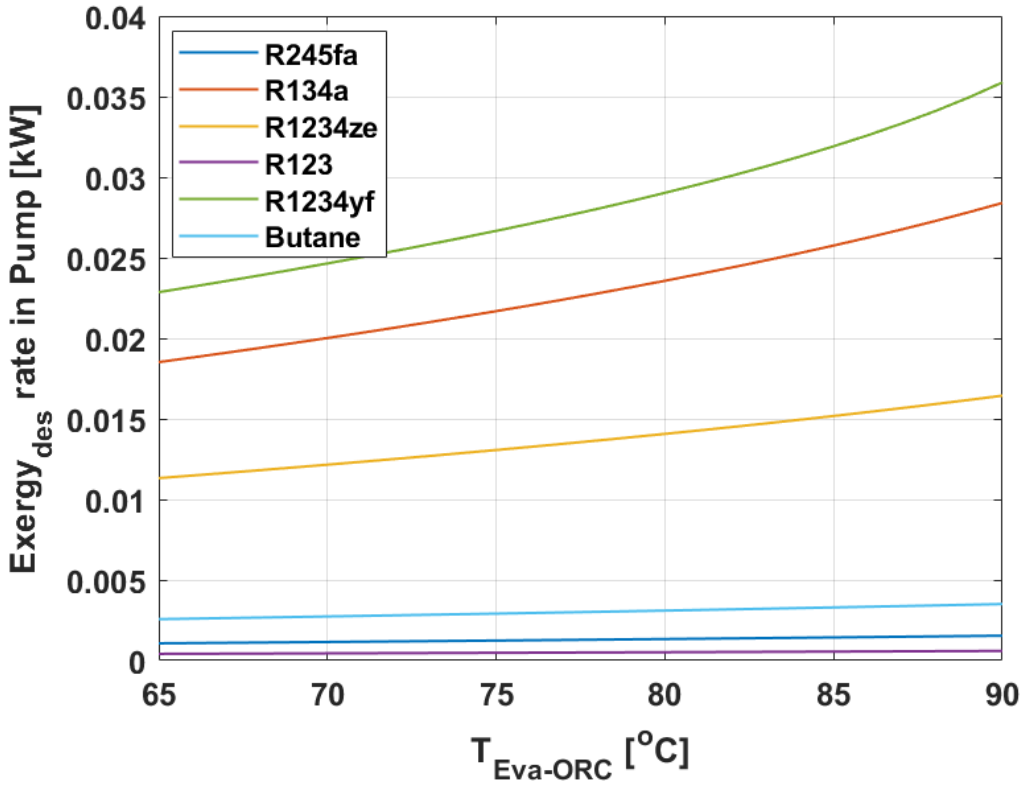

Figure 6-20: Variation of ORC evaporator temperature on pump exergy destruction

6.7.2 Variation of ORC evaporator temperature on pump exergy destruction

Figure 6-20 shows the distribution of exergy destruction in ORC-VCR with different working fluids. The figure shows exergy destruction associated with the change of ORC evaporation temperature. It can be noticed that exergy destruction increases with the increasing of ORC evaporation temperature. Mostly the increment in exergy destruction due to the lower utilisation of the input thermal energy.

When the temperature of the ORC's evaporator is increased, the amount of exergy that is lost in the pump is also increased. This is because the working fluid encounters a higher specific volume as a result of the rising evaporator temperature. This means that a greater volume of fluid needs to be pressed by the pump in order to maintain the same mass flow rate. Because the amount of work that must be done by the pump is mostly connected to

the change in specific volume, the higher evaporator temperatures result in a higher amount of work that must be done because the specific volume increases. Due to the increased amount of work that needs to be done, the pump's exergy destruction has increased as a result.

6.7.3 Variation of condenser temperature on expansion valve exergy destruction

Increasing the temperature of the condenser in the presented system will often result in

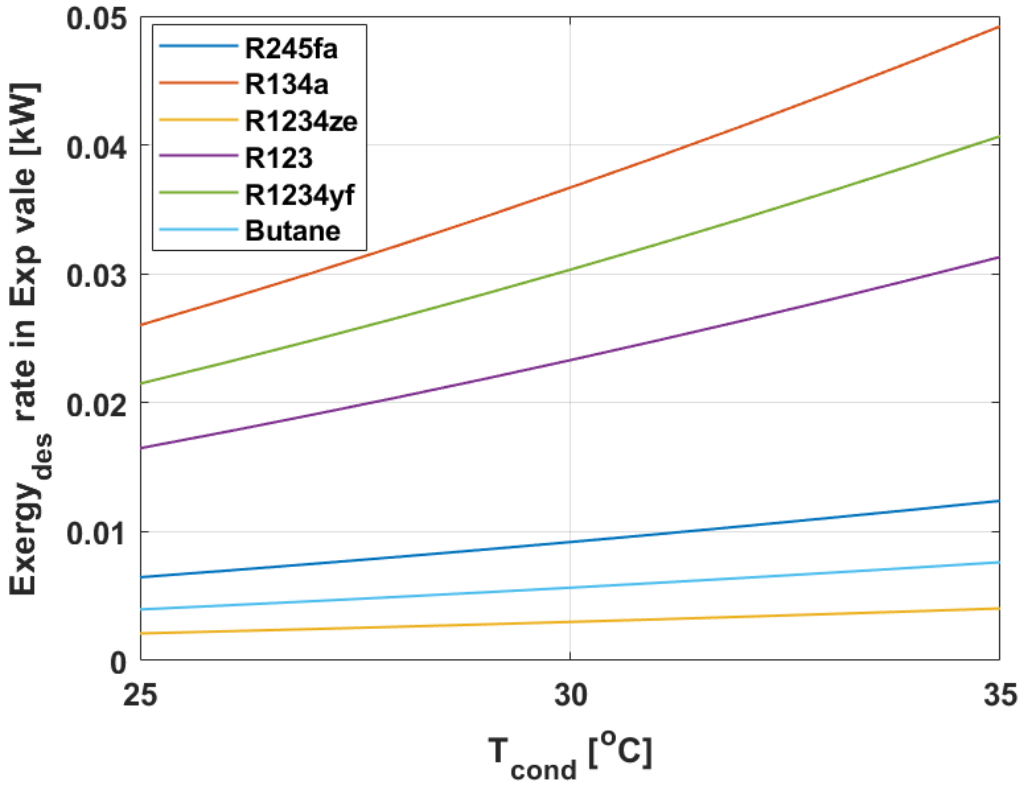

Figure 6-21: Variation of condenser temperature on expansion valve exergy destruction

an increase in the amount of exergy destruction that occurs in the VCR's expansion valve as depicted in Figure 6-21. This takes place as a consequence of the changing temperature differential that exists across the expansion valve. When the temperature of the condenser is raised, the temperature gap between the side of the VCR system with the high temperature (the condenser) and the side with the low temperature (the evaporator) gets

greater. As a consequence of this, the expansion valve must be able to manage a more considerable drop in temperature, which results in a greater loss of exergy during the process of expansion. Consequently, raising the temperature of the condenser in the VCR system has a tendency to cause a greater exergy destruction within the expansion valve.

6.7.4 Exergy destruction in different components

In this section, the rate of exergy destruction within the condenser for six different refrigerants: R245fa, R134a, R1234ze, R123, R1234yf, and Butane was investigated. The exergy destruction in the expander is the highest in the presented system for all selected refrigerants. There is a significant temperature decrease observed between the high-temperature heat source and the condenser in an ORC system for all studied refrigerants. This significant temperature reduction experienced throughout the cycle, leads to irreversibilities during the expansion process in the expander where the working fluid converts thermal energy into mechanical work. In contrast, the pump exhibits lowest exergy degradation due to its principal function of elevating the pressure of the working fluid, which entails low variation in temperature for all refrigerants.

In the condenser out of all refrigerants that were analysed, it was shown that R134a demonstrates the most significant level of exergy destruction, with a value of 0.06 kW as shown in Figure 6-22. This observation indicates that, within the specific system being studied, R134a exhibits the highest exergy destruction in the condenser. In contrast, R123 exhibits an interesting characteristic of having the lowest exergy destruction rate, at just 0.009 kW. This suggests that R123 exhibits favourable performance in terms of reducing exergy destruction within the VCR condenser. The exergy destruction rates of R1234ze, Butane, and R1234yf are 0.045 kW, 0.023 kW, and 0.057 kW, respectively.

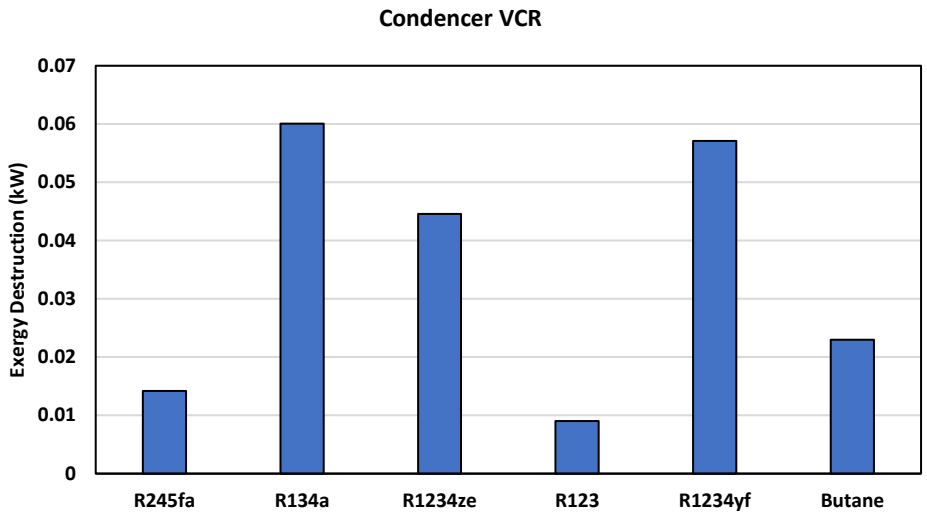

Figure 6-22: Exergy destruction in VCR condenser

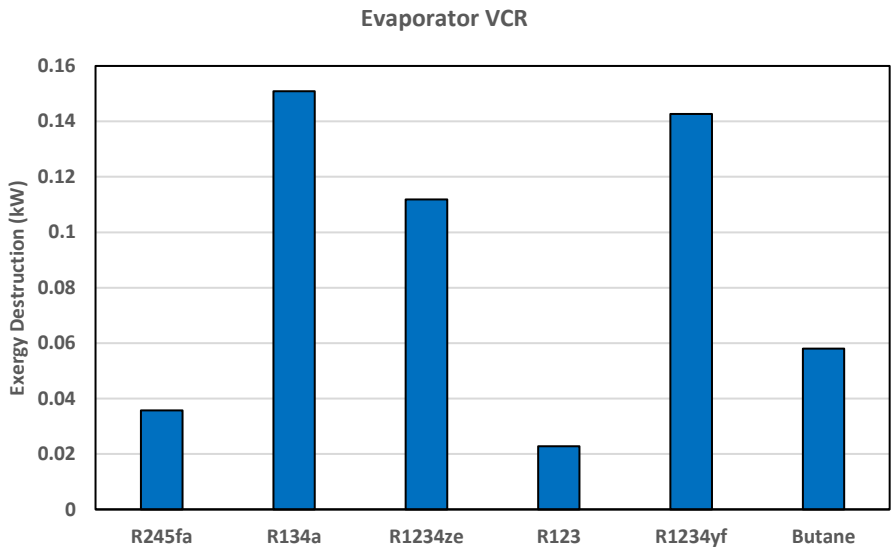

Figure 6-23: Exergy destruction in VCR evaporator

Figure 6-23 showed that the evaporator in a VCR used six distinct refrigerants, with exergy destruction rates of 0.036 kW, 0.151 kW, 0.112 kW, 0.023 kW, 0.143 kW, and 0.058 kW for R245fa, R134a, R1234ze, R123, R1234yf, and Butane, respectively. R123 had the lowest exergy destruction among these refrigerants, measuring in at 0.023 kW, demonstrating its greater energy efficiency within the VCR evaporator. When compared

to the other refrigerants, R134a's exergy destruction rate of 0.151 kW is the greatest, indicating more energy losses in this part of the system.

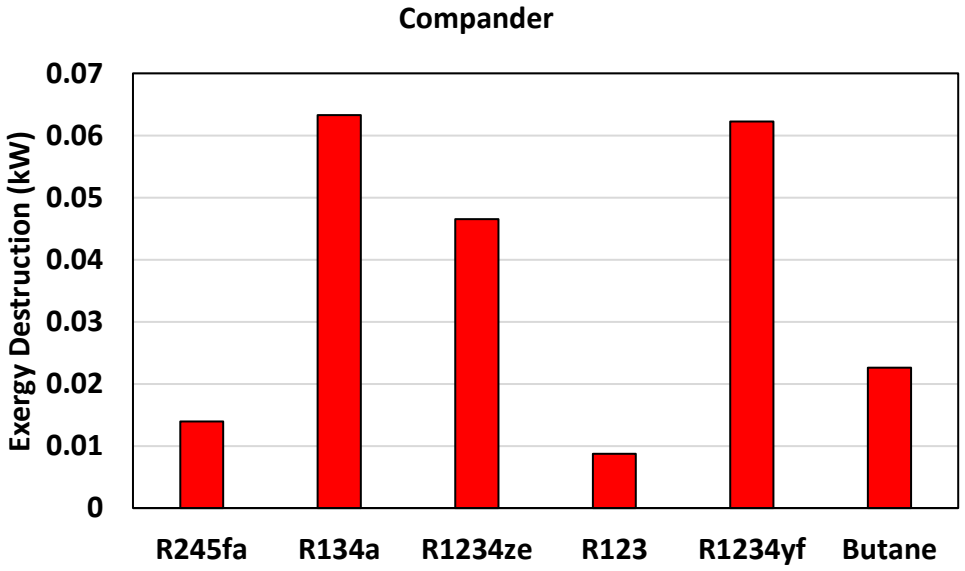

Figure 6-24: Exergy destruction in compander

According to Figure 6-24, R134a and R1234yf have the highest exergy destruction rate at 0.063 and 0.062 kW, respectively. R134a causes the greatest exergy loss in the compander. R123 has the lowest exergy destruction rate at 0.0087 kW. R123 reduces compander exergy losses, making it a more energy-efficient choice for this component. R1234ze and Butane had intermediate exergy destruction rates of 0.047 kW, 0.023 kW. R245fa had a mid-range exergy destruction rate of 0.014 kW.

When it comes to the expansion valve section, the exergy destruction is as follows: 0.008 kW for R245fa, 0.041 kW for R1234ze, 0.031 kW for R123, 0.004 kW for R1234yf, 0.049 kW for Butane, and 0.012 kW for R245fa, R134a, and R1234ze, and 0.012 kW for Butane as shown in Figure 6-25. Notably, R123 had the lowest rate of exergy loss, which was measured at 0.004 kW. This indicates that the expansion valve in R123 makes better use of the energy that is available. On the other side, the rate of exergy destruction in R1234yf was the greatest, coming in at 0.049 kW. Because of this, when R1234yf is utilized as the refrigerant, this component suffers from a greater loss of energy.

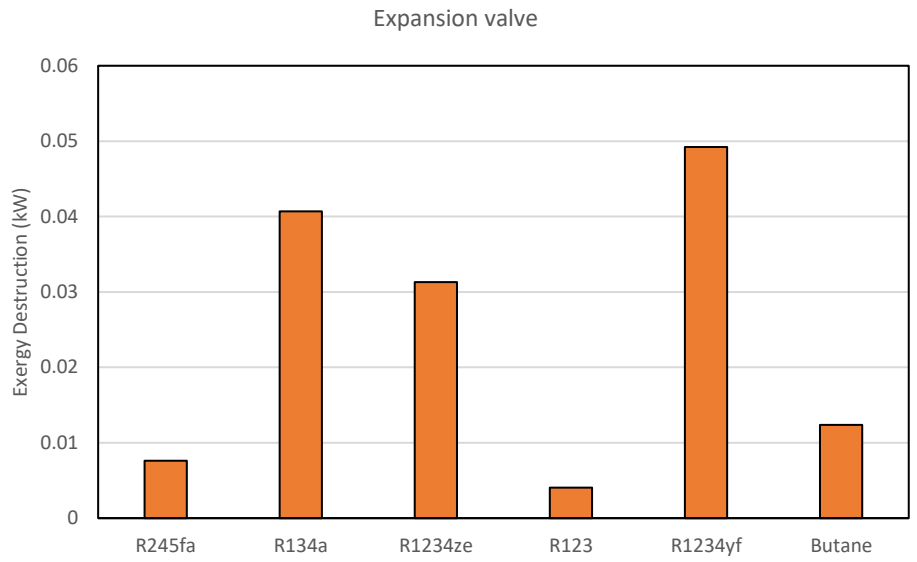

Figure 6-25: Exergy destruction in expansion valve

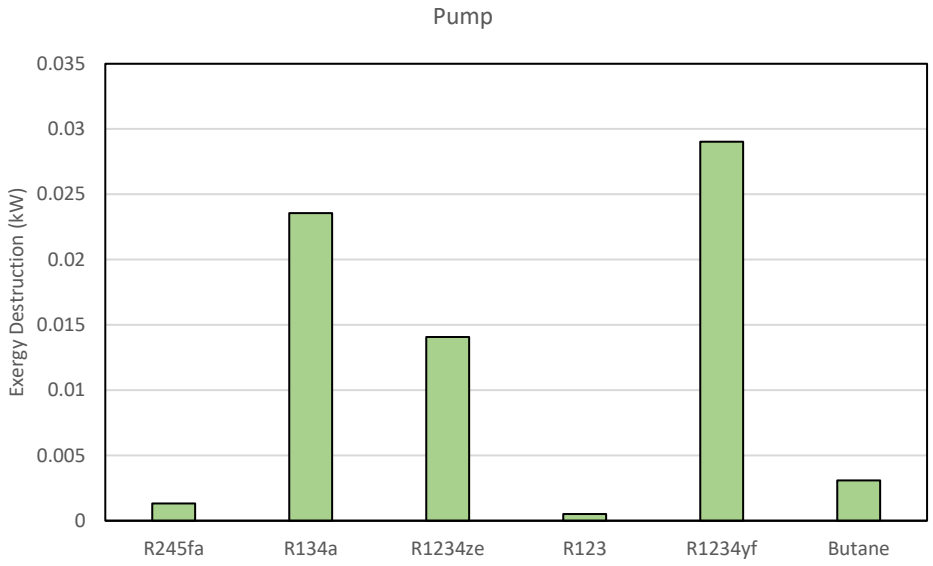

Figure 6-26: Exergy destruction in pump

The rates of exergy destruction for R245fa, R134a, R1234ze, R123, R1234yf, and Butane were found to be 0.001 kW, 0.024 kW, 0.014 kW, 0.001 kW, 0.029 kW, and 0.003 kW, respectively, as shown in Figure 6-26. It is worth mentioning that R134a and R1234yf demonstrated the most substantial rates of exergy destruction, measuring 0.024 kW and 0.029 kW, respectively. These findings suggest considerable exergy losses occurring

within the pump component when employing these specific refrigerants. The exergy destruction of R1234ze was observed to be 0.014 kW, which falls within the average range. In comparison, R245fa, R123, and Butane exhibited comparatively lowest levels of exergy degradation, measuring at 0.001 kW, 0.001 kW, and 0.003 kW, correspondingly.

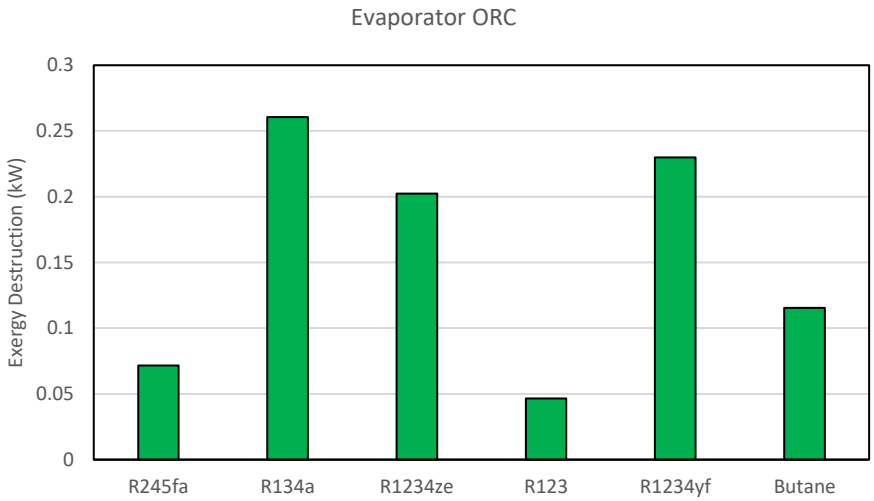

Figure 6-27: Exergy destruction in ORC evaporator.

According to the Figure 6-27, the rates of exergy destruction for R245fa, R134a, R123, and R1234yf, as well as Butane, are, respectively, 0.072 kW, 0.261 kW, 0.202 kW, 0.047 kW, 0.23 kW, and 0.115 kW. It is important to note that R134a and R1234yf exhibited the highest rates of exergy degradation, with respective values of 0.261 kW and 0.23 kW. This indicates that a significant amount of exergy is lost by the ORC evaporator component whenever these refrigerants are utilized. Additionally, R1234ze had a rate of 0.202 kW, which placed it in the category of large exergy destruction. The quantity of exergy destruction by butane is considered to be in the average range when it is measured at 0.115 kW. On the other hand, R245fa and R123 reveal an average exergy loss of 0.072 kW and 0.047 kW, respectively.

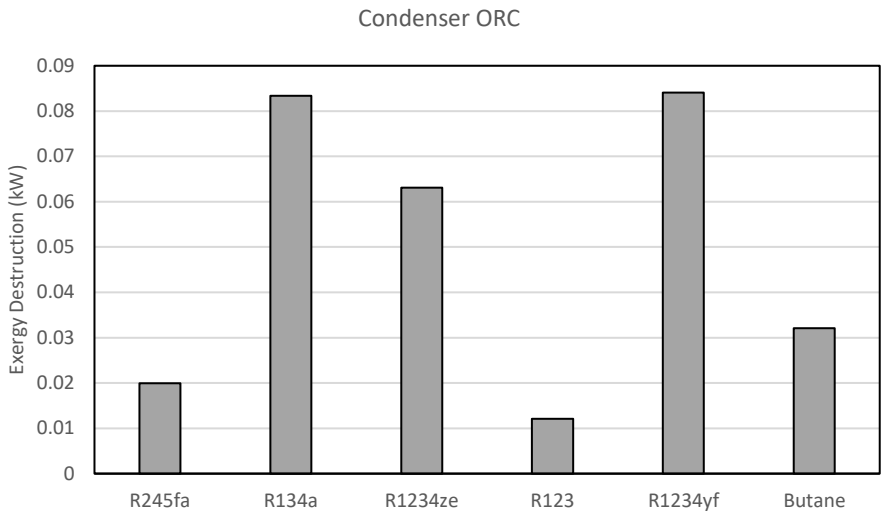

Figure 6-28: Exergy destruction in the ORC condenser

The exergy destruction values for six refrigerants of R245fa, R134a, R1234ze, R123, R1234yf, and Butane in the ORC condenser, as depicted in Figure 6-28, are 0.02 kW, 0.083 kW, 0.063 kW, 0.012 kW, 0.084 kW, and 0.032 kW, respectively. The exergy destruction of R134a was found to be the highest, whereas R123 had the lowest exergy destruction, suggesting lowest irreversibility. Similar to other components, R1234yf also exhibits a rather high rate of exergy degradation.

These results mentioned above highlight the significance of choosing the best refrigerant for the system's VCR evaporator to achieve highest efficiency and performance.

6.8 CO_2 emissions analysis

Figure 6-29 shows the examination of CO_2 emissions related to the system, including different refrigerants and specific operational circumstances, provides significant findings on environmental consequences. The selected combination of evaporator and condenser temperatures, consisting of an organic Rankine cycle evaporator temperature of 80°C, a vapor compression cycle evaporator temperature of 0°C, and a condenser temperature of 35°C, is used as a reference point for comparison.

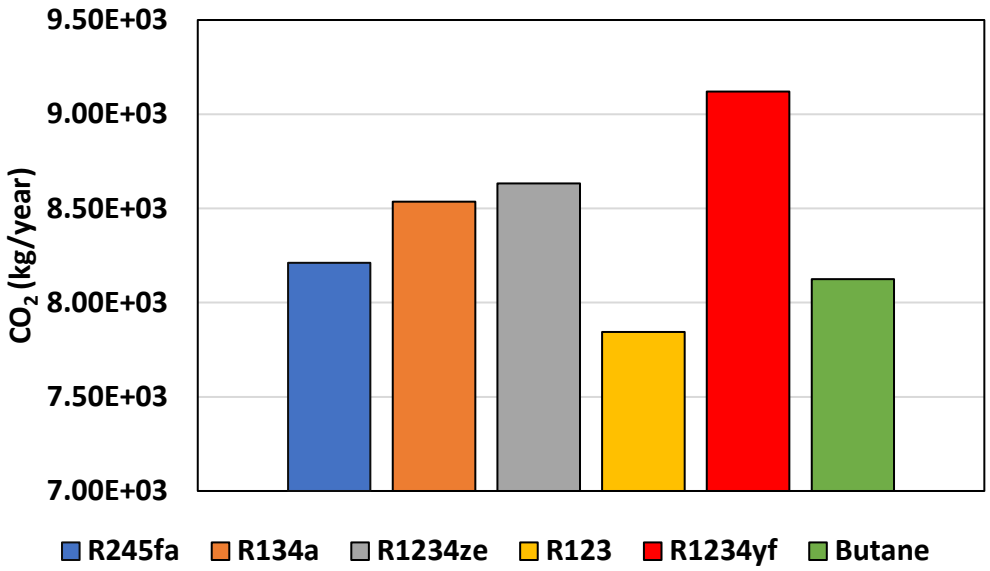

Figure 6-29: CO_2 emissions due to power supply to ORC-VCR for different working fluids.

With a value of 9.12e3 kg/year, R1234yf has the highest quantity of CO_2 emissions of all of the refrigerants that were considered. This discovery emphasizes the necessity of selecting an appropriate refrigerant in order to optimize the system's impact on the environment and get the best possible results. R1234ze has an emission value of 8.63e3 kg/year, and then R134a comes along with an emission value that is slightly lower at 8.54e3 kg/year. The next refrigerant on the list is R245fa, which emits 8.21e3 kg/year of carbon dioxide into the atmosphere, illustrating the range of CO2 emissions observed among several refrigerants. The list is completed by the inclusion of butane and R123, which have emission levels of 8.12e3 kg/year and 7.84e3 kg/year, respectively.

The specific heat capacity of the refrigerants is one of the most important aspects to consider. R1234yf and R123 have different specific heat capacities, which implies that in order to achieve the same level of temperature increase, they need significantly different quantities of heat energy. When compared to R123, the specific heat capacity of R1234yf is significantly larger.

This indicates that the quantity of heat required to raise the temperature of the refrigerant by the same amount is greater. Because of this, it is expected that a greater amount of heat will be recovered from the waste, which will result in a higher mass flow rate of fuel and, as a consequence of this, a rise in the amount of CO_2 emissions.

The aforementioned findings highlight the significance of taking into account both the thermodynamic properties and the environmental consequences of refrigerants throughout the process of designing and optimizing systems. The selection of a refrigerant has the potential to make a substantial impact on the carbon footprint of a system. Opting for a refrigerant with lower carbon dioxide (CO2) emissions can play a pivotal role in promoting sustainability and mitigating environmental harm.

6.9 Summary

In this chapter, a complete analysis of the performance and environmental impacts of integrating an ORC with a VCR system are presented. One of the most important topics that has been discussed in this chapter is an analysis of six distinct working fluids, as well as an evaluation of the system's influence on the environment, which is primarily driven by the recovery of waste heat from a refrigerated truck through the use of an ORC. It has been examined how different parameters affect the system's COP and heating-to-cooling efficiency. The parameters included the condenser and evaporator temperatures for the ORC and VCR systems, the efficiency of the compressor and expander, and the pressure ratios of the expander and compressor. In addition, the impact of the ORC's mass flow rate and analysis the exergy efficiency for each of the six chosen refrigerants were considered. In order to obtain more deeper understanding, the exergy analysis was performed to determine the exergy destruction occurring in each individual component. Moreover, the CO_2 emissions were conducted by considering the system's fuel usage, emphasizing the environmental consequences of this integrated system.

Based on the results, R123 consistently showcases the highest exergy efficiency under varying evaporation temperatures, both in the ORC and VCR. Additionally, R123 also stands out with the highest heat-to-cooling efficiency across most of the conditions. R123 and R1234yf consistently displays the highest overall COP in terms of condensation temperatures and a range of evaporation temperatures in the VCR. It is also evident that R123 has the most efficient performance with the lowest exergy destruction rates across all scenarios. Conversely, R134a consistently underperforms with the highest exergy destruction rates among the compared substances. In addition, utilizing R123 as the working fluid in both ORC and VCR systems requires a lower amount of heat for the ORC evaporator. This reduced heat requirement subsequently leads to decreased fuel consumption by the prime mover, which in turn results in lower CO_2 emissions

In overall the chapter represents a useful step in evaluating the feasibility and sustainability of the ORC-VCR integration, offering valuable insights into its efficiency and environmental impact.

Chapter 7: Conclusions.

The main objective of the present study is to numerically investigate the potential of a new single rotor expander-compressor device in cooling application through combined vapor compression refrigeration (VCR) cycle and an organic Rankine cycle (ORC) is investigated. A numerical model of the ORC-VCR cycle has been developed using ASPEN Plus and further validated both the new single rotor expander-compressor device and the ORC-VCR system with previously published experimental data and shows deviation of less than 1% and of about 5.6%, respectively. An influence of the several operating parameters such as evaporation temperature of ORC (62.75 °C – 89.7 °C) and VCR (-20 °C – 5 °C), condensation temperature of ORC (20 °C – 45 °C) and speed (500 – 3000 rpm) at constant hot source (water) temperature of 95 °C on performance of VCR system have been investigated from energy, exergy and environment point of view. The performance indicator used to represent energy, exergy and environment are overall COP and heating to cooling ratio, exergy destruction and exergy efficiency, and CO2 emissions, respectively. Moreover, the thermal performance behaviour of different prospective refrigerants such as R245fa, R123, R134a, R1234ze(E), R1234yf, and Butane used in ORC and VCR is analysed in terms of energy, exergy, and environmental perspectives.

Following are the main conclusions of the present research work:

- The increase in the compressor's discharge pressure is closely linked to the volume displacement on each side and is especially noticeable when the expander's inlet pressure rises, particularly during the expansion process in chamber B, which displaces a greater volume than chamber A. Additionally, a higher condensation

temperature in the ORC results in a reduced discharge pressure from the compressor.

- Thermal performance of the VCR is sensitive to the evaporator temperature and condensation temperature of ORC, and speed of the single rotor expander-compressor device. Refrigerating effect generated by VCR increases, heating to cooling efficiency decreases with increase in the evaporator temperature and condensation temperature of ORC. The most significant cooling performance and heat to cooling efficiency reached were 5.38 kW and 56%, respectively. These figures were reached when the ORC's evaporation temperature was adjusted to 62.75°C and the VCR's temperature was set to -5°C. Additionally, the ORC's condensation temperature was set to 20.5°C. Notably, the cooling effect exhibited a consistent increase with changes in rotor speed, while alterations in rotor speed had no impact on the heat-to-cooling efficiency.
- When considering the amount of exergy destruction contributed by each component of the ORC-VCR, the ORC evaporator has the most significant impact on the overall amount of exergy destruction. There is potential for a sizeable increase in the contribution made by the VCR evaporator if the temperature at which evaporation occurs in the VCR is lowered. the highest levels of overall exergy efficiency achieved was 63% when the evaporation temperatures for the ORC and VCR were set at 62.75°C and -5°C, respectively, with the ORC condensation temperature fixed at 20.5°C, the overall exergy efficiency did not vary with changes in the rotor speed. In the analysis of different working fluids, both the thermal performance and the system's influence on the environment were evaluated. R123 demonstrates the highest exergy efficiency in both ORC and VCR under various evaporation temperatures and excels in heat to cooling

efficiency. Both R123 and R1234yf display the top COP for a range of conditions in the VCR, with R123 exhibiting the lowest exergy destruction rates. In contrast, R134a often has the highest exergy destruction rates. Using R123 in ORC and VCR reduces the heat needed for the ORC evaporator, leading to less fuel consumption and CO_2emissions. Overall, this chapter provides crucial insights into the efficiency and environmental impact of ORC-VCR integration.

Bibliography

[1] EPA, "Inventory of U.S. Greenhouse Gas Emissions and Sinks: 1990-2020," *U.S. Environmental Protection Agency,* vol. EPA 430-R-22-003, 2022.

[2] E. Institute, "Oil consumption worldwide from 1998 to 2022. ," 2023, Available: https://www.statista.com/statistics/265239/global-oil-consumption-in-barrels-per-day/.

[3] T. Covert, M. Greenstone, and C. R. Knittel, "Will we ever stop using fossil fuels?," *Journal of Economic Perspectives,* vol. 30, no. 1, pp. 117-138, 2016.

[4] M. A. Huijbregts *et al.*, "Is cumulative fossil energy demand a useful indicator for the environmental performance of products?," ed: ACS Publications, 2006.

[5] (2020). *Is the climate warming?* Available: https://royalsociety.org/topics-policy/projects/climate-change-evidence-causes/question-1/

[6] I. E. Agency, *The Future of Cooling: Opportunities for energy-efficient air conditioning*. OECD Publishing, 2018.

[7] T. Peters, "A Cool World Defining the Energy Conundrum of Cooling for All, University of Birmingham, UK," ed, 2018.

[8] P. Agreement, "Paris agreement," in *Report of the Conference of the Parties to the United Nations Framework Convention on Climate Change (21st Session, 2015: Paris). Retrived December*, 2015, vol. 4, p. 2017: HeinOnline.

[9] A. K. Sleiti, W. A. Al-Ammari, and M. Al-Khawaja, "Review of innovative approaches of thermo-mechanical refrigeration systems using low grade heat," *International Journal of Energy Research,* vol. 44, no. 13, pp. 9808-9838, 2020.

[10] M. Benedetti, D. Dadi, L. Giordano, V. Introna, P. E. Lapenna, and A. Santolamazza, "Design of a database of case studies and technologies to increase the diffusion of low-temperature waste heat recovery in the industrial sector," *Sustainability,* vol. 13, no. 9, p. 5223, 2021.

[11] D. o. E. (DOE), "Waste Heat Recovery Systems. Chapter 6: Innovating Clean Energy Technologies in Advanced Manufacturing-Technology Assessments.," in "In Quadrennial Technology Review 2015-An Assessment of Energy Technologies and Research Opportunities," 2015.

[12] G. Yu, G. Shu, H. Tian, H. Wei, and L. Liu, "Simulation and thermodynamic analysis of a bottoming Organic Rankine Cycle (ORC) of diesel engine (DE)," *Energy,* vol. 51, pp. 281-290, 2013.

[13] J. Ling-Chin, H. Bao, Z. Ma, W. Taylor, and A. P. Roskilly, "State-of-the-art technologies on low-grade heat recovery and utilization in industry," *Energy Conversion-Current Technologies and Future Trends,* vol. 21, 2018.

[14] I. Johnson, W. T. Choate, and A. Davidson, "Waste heat recovery. Technology and opportunities in US industry," BCS, Inc., Laurel, MD (United States)2008.

[15] X. She, Y. Yin, M. Xu, and X. Zhang, "A novel low-grade heat-driven absorption refrigeration system with LiCl–H2O and LiBr–H2O working pairs," *International Journal of Refrigeration,* vol. 58, pp. 219-234, 2015.

[16] B. F. Tchanche, G. Lambrinos, A. Frangoudakis, and G. Papadakis, "Low-grade heat conversion into power using organic Rankine cycles - A review of various applications," (in English), *Renewable & Sustainable Energy Reviews,* Review vol. 15, no. 8, pp. 3963-3979, Oct 2011.

[17] X. Ping, F. Yang, H. Zhang, C. Xing, M. Yu, and Y. Wang, "Investigation and multi-objective optimization of vehicle engine-organic Rankine cycle (ORC) combined system in different driving conditions," *Energy,* vol. 263, 2023.

[18] A. Saedi, A. Jahangiri, M. Ameri, and F. Asadi, "Feasibility study and 3E analysis of blowdown heat recovery in a combined cycle power plant for utilization in Organic Rankine Cycle and greenhouse heating," *Energy,* vol. 260, 2022.
[19] C. Chen, F. Witte, I. Tuschy, O. Kolditz, and H. Shao, "Parametric optimization and comparative study of an organic Rankine cycle power plant for two-phase geothermal sources," *Energy,* vol. 252, 2022.
[20] Z. Xu, R. Wang, and C. Yang, "Perspectives for low-temperature waste heat recovery," *Energy,* vol. 176, pp. 1037-1043, 2019.
[21] H. Jouhara, N. Khordehgah, S. Almahmoud, B. Delpech, A. Chauhan, and S. A. Tassou, "Waste heat recovery technologies and applications," *Thermal Science and Engineering Progress,* vol. 6, pp. 268-289, 2018.
[22] S. Brückner, S. Liu, L. Miró, M. Radspieler, L. F. Cabeza, and E. Lävemann, "Industrial waste heat recovery technologies: An economic analysis of heat transformation technologies," *Applied Energy,* vol. 151, pp. 157-167, 2015.
[23] K. Rahbar, S. Mahmoud, R. K. Al-Dadah, N. Moazami, and S. A. Mirhadizadeh, "Review of organic Rankine cycle for small-scale applications," *Energy conversion and management,* vol. 134, pp. 135-155, 2017.
[24] W. Goetzler, R. Zogg, J. Young, and C. Johnson, "Alternatives to vapor-compression HVAC technology," *Ashrae Journal,* vol. 56, no. 10, p. 12, 2014.
[25] İ. Dinçer, *Refrigeration systems and applications*, Third ed. (no. Book, Whole). Chichester, West Sussex, UK: Wiley, 2017.
[26] B. H. Gebreslassie, M. Medrano, and D. Boer, "Exergy analysis of multi-effect water–LiBr absorption systems: From half to triple effect," *Renewable energy,* vol. 35, no. 8, pp. 1773-1782, 2010.
[27] R. Maryami and A. Dehghan, "An exergy based comparative study between LiBr/water absorption refrigeration systems from half effect to triple effect," *Applied Thermal Engineering,* vol. 124, pp. 103-123, 2017.
[28] A. Razmi, M. Soltani, F. M. Kashkooli, and L. G. Farshi, "Energy and exergy analysis of an environmentally-friendly hybrid absorption/recompression refrigeration system," *Energy conversion and management,* vol. 164, pp. 59-69, 2018.
[29] W. Wu, B. Wang, W. Shi, and X. Li, "An overview of ammonia-based absorption chillers and heat pumps," *Renewable and Sustainable Energy Reviews,* vol. 31, pp. 681-707, 2014.
[30] P. Srikhirin, S. Aphornratana, and S. Chungpaibulpatana, "A review of absorption refrigeration technologies," *Renewable and sustainable energy reviews,* vol. 5, no. 4, pp. 343-372, 2001.
[31] B.-J. R. Mungyeko Bisulandu, R. Mansouri, and A. Ilinca, "Diffusion absorption refrigeration systems: An overview of thermal mechanisms and models," *Energies,* vol. 16, no. 9, p. 3610, 2023.
[32] L. Ji, S. K. Shukla, Z. Zuo, X. Lu, X. Ji, and C. Wang, "An overview of the progress of new working pairs in absorption heat pumps," *Energy Reports,* vol. 9, pp. 703-729, 2023.
[33] L. G. Farshi, C. I. Ferreira, S. S. Mahmoudi, and M. Rosen, "First and second law analysis of ammonia/salt absorption refrigeration systems," *International journal of refrigeration,* vol. 40, pp. 111-121, 2014.
[34] C. Jawahar and R. Saravanan, "Experimental studies on air-cooled NH3–H2O based modified gax absorption cooling system," *International journal of refrigeration,* vol. 34, no. 3, pp. 658-666, 2011.
[35] P. Satzger, T. Berlitz, F. Ziegler, D. Stitou, and B. Spinner, "Improvements of energy efficiency of cascading sorption machines," 1996.
[36] L. Garousi Farshi, S. Seyed Mahmoudi, M. Rosen, and M. Yari, "A comparative study of the performance characteristics of double-effect absorption refrigeration systems," *International journal of energy research,* vol. 36, no. 2, pp. 182-192, 2012.

[37] D.-W. Sun, "Comparison of the performances of NH3-H2O, NH3-LiNO3 and NH3-NaSCN absorption refrigeration systems," *Energy Conversion and Management,* vol. 39, no. 5-6, pp. 357-368, 1998.
[38] W. Jiang, S. Li, L. Yang, and K. Du, "Experimental investigation on performance of ammonia absorption refrigeration system with TiO2 nanofluid," *International Journal of Refrigeration,* vol. 98, pp. 80-88, 2019.
[39] X. Zhang, L. Cai, T. Chen, J. Qiao, and X. Zhang, "Vapor-liquid equilibrium measurements and assessments of Low-GWP absorption working pairs (R32+ DMETEG, R152a+ DMETEG, and R161+ DMETEG) for absorption refrigeration systems," *Energy,* vol. 224, p. 120082, 2021.
[40] A. I. Papadopoulos, A.-S. Kyriakides, P. Seferlis, and I. Hassan, "Absorption refrigeration processes with organic working fluid mixtures-a review," *Renewable and Sustainable Energy Reviews,* vol. 109, pp. 239-270, 2019.
[41] M. K. Ojha, A. K. Shukla, P. Verma, and R. Kannojiya, "Recent progress and outlook of solar adsorption refrigeration systems," *Materials Today: Proceedings,* vol. 46, pp. 5639-5646, 2021.
[42] D. Wang, Y. Li, D. Li, Y. Xia, and J. Zhang, "A review on adsorption refrigeration technology and adsorption deterioration in physical adsorption systems," *Renewable and Sustainable Energy Reviews,* vol. 14, no. 1, pp. 344-353, 2010.
[43] P. Boruta, T. Bujok, Ł. Mika, and K. Sztekler, "Adsorbents, working pairs and coated beds for natural refrigerants in adsorption chillers—state of the art," *Energies,* vol. 14, no. 15, p. 4707, 2021.
[44] K. Ullah, R. Saidur, H. Ping, R. Akikur, and N. Shuvo, "A review of solar thermal refrigeration and cooling methods," *Renewable and Sustainable Energy Reviews,* vol. 24, pp. 499-513, 2013.
[45] D. Wang, J. Zhang, X. Tian, D. Liu, and K. Sumathy, "Progress in silica gel–water adsorption refrigeration technology," *Renewable and Sustainable Energy Reviews,* vol. 30, pp. 85-104, 2014.
[46] E. Anyanwu, "Review of solid adsorption solar refrigeration II:: An overview of the principles and theory," *Energy Conversion and Management,* vol. 45, no. 7-8, pp. 1279-1295, 2004.
[47] M. Fernandes, G. Brites, J. Costa, A. Gaspar, and V. Costa, "Review and future trends of solar adsorption refrigeration systems," *Renewable and Sustainable Energy Reviews,* vol. 39, pp. 102-123, 2014.
[48] A. Mahesh and S. Kaushik, "Solar adsorption cooling system: An overview," *Journal of Renewable and Sustainable Energy,* vol. 4, no. 2, p. 022701, 2012.
[49] S. Xu, L. Wang, and R. Wang, "Thermodynamic analysis of single-stage and multi-stage adsorption refrigeration cycles with activated carbon–ammonia working pair," *Energy conversion and management,* vol. 117, pp. 31-42, 2016.
[50] S. Mitra, P. Kumar, K. Srinivasan, and P. Dutta, "Development and performance studies of an air cooled two-stage multi-bed silica-gel+ water adsorption system," *international journal of refrigeration,* vol. 67, pp. 174-189, 2016.
[51] J. Xu, W. Zhang, Z. Liu, Q. Pan, R. Wang, and T. Ge, "Energy and exergy analyses of a hybrid adsorption refrigeration system for simultaneous production of cold water and dry air," *Energy Conversion and Management,* vol. 286, p. 117088, 2023.
[52] M. Verde, L. Cortés, J. Corberán, A. Sapienza, S. Vasta, and G. Restuccia, "Modelling of an adsorption system driven by engine waste heat for truck cabin A/C. Performance estimation for a standard driving cycle," *Applied Thermal Engineering,* vol. 30, no. 13, pp. 1511-1522, 2010.
[53] S. Vasta, "Adsorption Air Conditioning for Automotive Applications: A Critical Review," 2023.

[54] K. Daou, R. Wang, and Z. Xia, "Desiccant cooling air conditioning: a review," *Renewable and sustainable energy reviews,* vol. 10, no. 2, pp. 55-77, 2006.
[55] L. Si, F. Cheng, W. Zhang, and X. Li, "Research on solar-driven interfacial evaporation regeneration performance of different solutions for liquid desiccant cooling system," *International Journal of Heat and Mass Transfer,* vol. 213, p. 124354, 2023.
[56] M. Sahlot and S. B. Riffat, "Desiccant cooling systems: a review," *International Journal of Low-Carbon Technologies,* vol. 11, no. 4, pp. 489-505, 2016.
[57] J. Luo and H. Yang, "A state-of-the-art review on the liquid properties regarding energy and environmental performance in liquid desiccant air-conditioning systems," *Applied Energy,* vol. 325, p. 119853, 2022.
[58] H. Li, Y. Dai, Y. Li, D. La, and R. Wang, "Case study of a two-stage rotary desiccant cooling/heating system driven by evacuated glass tube solar air collectors," *Energy and Buildings,* vol. 47, pp. 107-112, 2012.
[59] M. Dezfouli, K. Sopian, and K. Kadir, "Energy and performance analysis of solar solid desiccant cooling systems for energy efficient buildings in tropical regions," *Energy Conversion and Management: X,* vol. 14, p. 100186, 2022.
[60] K. Sudhakar, M. S. Jenkins, S. Mangal, and S. S. Priya, "Modelling of a solar desiccant cooling system using a TRNSYS-MATLAB co-simulator: A review," *Journal of Building Engineering,* vol. 24, p. 100749, 2019.
[61] X. Chen, S. Omer, M. Worall, and S. Riffat, "Recent developments in ejector refrigeration technologies," *Renewable and Sustainable Energy Reviews,* vol. 19, pp. 629-651, 2013.
[62] J. Chen, H. Havtun, and B. Palm, "Conventional and advanced exergy analysis of an ejector refrigeration system," *Applied Energy,* vol. 144, pp. 139-151, 2015.
[63] K. Chunnanond and S. Aphornratana, "Ejectors: applications in refrigeration technology," *Renewable and sustainable energy reviews,* vol. 8, no. 2, pp. 129-155, 2004.
[64] F. Aligolzadeh and A. Hakkaki-Fard, "A novel methodology for designing a multi-ejector refrigeration system," *Applied Thermal Engineering,* vol. 151, pp. 26-37, 2019.
[65] G. Alexis, "Exergy analysis of ejector-refrigeration cycle using water as working fluid," *International Journal of energy research,* vol. 29, no. 2, pp. 95-105, 2005.
[66] J. R. Barbosa Jr, G. B. Ribeiro, and P. A. de Oliveira, "A state-of-the-art review of compact vapor compression refrigeration systems and their applications," *Heat Transfer Engineering,* vol. 33, no. 4-5, pp. 356-374, 2012.
[67] J. Wu, G. Liu, A. Marson, A. Fedele, A. Scipioni, and A. Manzardo, "Mitigating environmental burden of the refrigerated transportation sector: Carbon footprint comparisons of commonly used refrigeration systems and alternative cold storage systems," *Journal of Cleaner Production,* vol. 372, p. 133514, 2022.
[68] R. Yumrutaş, M. Kunduz, and M. Kanoğlu, "Exergy analysis of vapor compression refrigeration systems," *Exergy, An international journal,* vol. 2, no. 4, pp. 266-272, 2002.
[69] C. C. Copeland, "Improving the Performance of Steam Turbine Chiller Plants," *ASHRAE J,* vol. 61, no. 8, 2019.
[70] J. Controls, "Model YST Steam-Turbine Drive Centrifugal Liquid Chillers Design Level F," 2008, Available: https://www.johnsoncontrols.com/en_ca/-/media/jci/be/united-states/hvac-equipment/chillers/files/be_yst_spec_engineeringguide.pdf.
[71] R. Dixit, "Insights into Advanced Steam Turbine Centrifugal Chiller Technology," 2018.
[72] J. Bao and L. Zhao, "A review of working fluid and expander selections for organic Rankine cycle," *Renewable and sustainable energy reviews,* vol. 24, pp. 325-342, 2013.
[73] S. Quoilin, M. Van Den Broek, S. Declaye, P. Dewallef, and V. Lemort, "Techno-economic survey of Organic Rankine Cycle (ORC) systems," *Renewable and Sustainable Energy Reviews,* vol. 22, pp. 168-186, 2013.

[74] P. Artuso, A. Rossetti, S. Minetto, S. Marinetti, L. Moro, and D. Del Col, "Dynamic modeling and thermal performance analysis of a refrigerated truck body during operation," *International Journal of Refrigeration,* vol. 99, pp. 288-299, 2019.
[75] P. Gao, L. Wang, and F. Zhu, "Vapor-compression refrigeration system coupled with a thermochemical resorption energy storage unit for a refrigerated truck," *Applied Energy,* vol. 290, p. 116756, 2021.
[76] S. W. Spence, W. J. Doran, D. W. Artt, and G. McCullough, "Performance analysis of a feasible air-cycle refrigeration system for road transport," *International Journal of Refrigeration,* vol. 28, no. 3, pp. 381-388, 2005.
[77] S. Tassou, G. De-Lille, and Y. Ge, "Food transport refrigeration–Approaches to reduce energy consumption and environmental impacts of road transport," *Applied Thermal Engineering,* vol. 29, no. 8-9, pp. 1467-1477, 2009.
[78] H. Chen, D. Y. Goswami, and E. K. Stefanakos, "A review of thermodynamic cycles and working fluids for the conversion of low-grade heat," *Renewable and Sustainable Energy Reviews,* vol. 14, no. 9, pp. 3059-3067, 2010.
[79] J. Larjola, "<Electricity from industrial waste heat using high-speed organic Rankine cycle (ORC).pdf>," *International Journal of Production Economics 41,* vol. 227-235, 1995.
[80] Y. Dai, J. Wang, and L. Gao, "Parametric optimization and comparative study of organic Rankine cycle (ORC) for low grade waste heat recovery," *Energy Conversion and Management,* vol. 50, no. 3, pp. 576-582, 2009.
[81] L. Liu, T. Zhu, and J. Ma, "Working fluid charge oriented off-design modeling of a small scale Organic Rankine Cycle system," *Energy Conversion and Management,* vol. 148, pp. 944-953, 2017.
[82] L. Shao, J. Zhu, X. Meng, X. Wei, and X. Ma, "Experimental study of an organic Rankine cycle system with radial inflow turbine and R123," *Applied Thermal Engineering,* vol. 124, pp. 940-947, 2017.
[83] Z. Miao, J. Xu, and K. Zhang, "Experimental and modeling investigation of an organic Rankine cycle system based on the scroll expander," *Energy,* vol. 134, pp. 35-49, 2017.
[84] B.-S. Park, M. Usman, M. Imran, and A. Pesyridis, "Review of Organic Rankine Cycle experimental data trends," *Energy Conversion and Management,* vol. 173, pp. 679-691, 2018.
[85] J. P. Roy, M. K. Mishra, and A. Misra, "Performance analysis of an Organic Rankine Cycle with superheating under different heat source temperature conditions," *Applied Energy,* vol. 88, no. 9, pp. 2995-3004, 2011.
[86] M. J. Lee, D. L. Tien, and C. T. Shao, "Thermophysical capability of ozone-safe working fluids for an organic rankine cycle system," *Heat recovery systems & CHP,* vol. 13, no. 5, pp. 409-418, 1993.
[87] T. C. Hung, T. Y. shai, and S. K. Wang, "A review of organic rankine cycles (ORCs) for the recovery of low-grade waste heat.pdf," *Energy,* vol. 22, no. 7, pp. 661-667, 1997.
[88] R. Saidur, M. Rezaei, W. K. Muzammil, M. H. Hassan, S. Paria, and M. Hasanuzzaman, "Technologies to recover exhaust heat from internal combustion engines," *Renewable and Sustainable Energy Reviews,* vol. 16, no. 8, pp. 5649-5659, 2012.
[89] X. Wang *et al.*, "Working fluid selection for organic Rankine cycle power generation using hot produced supercritical CO2 from a geothermal reservoir," *Applied Thermal Engineering,* vol. 149, pp. 1287-1304, 2019.
[90] B. Dong, G. Xu, T. Li, X. Luo, and Y. Quan, "Parametric analysis of organic Rankine cycle based on a radial turbine for low-grade waste heat recovery," *Applied Thermal Engineering,* vol. 126, pp. 470-479, 2017.
[91] J. Nouman, "Comparative studies and analyses of working fluids for Organic Rankine Cycles," Master Thesis, KTH Royal Institute of Technology, 2012.

[92] L.-x. Zhang *et al.*, "Nominal condensing capacity and performance evaluation of evaporative condenser," *Applied Thermal Engineering,* vol. 107, pp. 79-85, 2016.
[93] B.-T. Liu, K.-H. Chien, and C.-C. Wang, "Effect of working fluids on organic Rankine cycle for waste heat recovery," *Energy,* vol. 29, no. 8, pp. 1207-1217, 2004.
[94] T.-C. Hung, "Waste heat recovery of organic Rankine cycle using dry fluids," *Energy Conversion andManagement,* vol. 42, pp. 539-553, 2001.
[95] V. Maizza and A. maizza, "Working fluids in non-steady flows for waste energy recovery systems," *Applied Thermal Engineering,* vol. 16, no. 7, pp. 579-590, 1999.
[96] T. yamamoto, T. Furuhata, N. Arai, and K. Mori, "Design and testing of the Organic Rankine Cycle," *Energy,* vol. 26, pp. 239-251, 2001.
[97] S. J. Zhang, H. X. Wang, and T. Guo, "Performance comparison and parametric optimization of subcritical Organic Rankine Cycle (ORC) and transcritical power cycle system for low-temperature geothermal power generation," (in English), *Applied Energy,* Article vol. 88, no. 8, pp. 2740-2754, Aug 2011.
[98] G. Qiu, H. Liu, and S. Riffat, "Expanders for micro-CHP systems with organic Rankine cycle," *Applied Thermal Engineering,* vol. 31, no. 16, pp. 3301-3307, 2011.
[99] T. Wang, Y. Zhang, Z. Peng, and G. Shu, "A review of researches on thermal exhaust heat recovery with Rankine cycle," *Renewable and sustainable energy reviews,* vol. 15, no. 6, pp. 2862-2871, 2011.
[100] O. Badr, P. O'Callaghan, M. Hussein, and S. Probert, "Multi-vane expanders as prime movers for low-grade energy organic Rankine-cycle engines," *Applied Energy,* vol. 16, no. 2, pp. 129-146, 1984.
[101] R. Reed, "Optimization of a Scroll Expander Applied to an Ammonia/Water Combined Cycle System for Hydrogen Production."
[102] V. Lemort, S. Quoilin, C. Cuevas, and J. Lebrun, "Testing and modeling a scroll expander integrated into an Organic Rankine Cycle," *Applied Thermal Engineering,* vol. 29, no. 14-15, pp. 3094-3102, 2009.
[103] Y. Liang, Z. Yu, and W. Li, "A waste heat-driven cooling system based on combined organic Rankine and vapour compression refrigeration cycles," *Applied Sciences,* vol. 9, no. 20, p. 4242, 2019.
[104] D. Prigmore and R. Barber, "Cooling with the sun's heat Design considerations and test data for a Rankine Cycle prototype," *Solar Energy,* vol. 17, no. 3, pp. 185-192, 1975.
[105] N. Lior, "Solar energy and the steam Rankine cycle for driving and assisting heat pumps in heating and cooling modes," *Energy Conversion,* vol. 16, no. 3, pp. 111-123, 1977.
[106] H. Wang, R. Peterson, and T. Herron, "Design study of configurations on system COP for a combined ORC (organic Rankine cycle) and VCC (vapor compression cycle)," *Energy,* vol. 36, no. 8, pp. 4809-4820, 2011.
[107] M. Chahartaghi, M. Einanlou, and S. M. Hashemian, "Energy and exergy analyses of a combined cooling, heating and power system with prime mover of phosphoric acid fuel cell with organic Rankine cycle," *Applied Thermal Engineering,* vol. 193, p. 116989, 2021.
[108] S. Aphornratana and T. Sriveerakul, "Analysis of a combined Rankine–vapour–compression refrigeration cycle," *Energy Conversion and management,* vol. 51, no. 12, pp. 2557-2564, 2010.
[109] A. Mahmoudan, P. Samadof, M. Sadeghzadeh, M. Jalili, M. Sharifpur, and R. Kumar, "Thermodynamic and exergoeconomic analyses and performance assessment of a new configuration of a combined cooling and power generation system based on ORC–VCR," *Journal of Thermal Analysis and Calorimetry,* vol. 145, pp. 1163-1189, 2021.
[110] Y. Liang, A. Mckeown, Z. Yu, and S. F. K. Alshammari, "Experimental study on a heat driven refrigeration system based on combined organic Rankine and vapour compression cycles," *Energy Conversion and Management,* vol. 234, p. 113953, 2021.

[111] H. Wang *et al.*, "Performance of a combined organic Rankine cycle and vapor compression cycle for heat activated cooling," *Energy,* vol. 36, no. 1, pp. 447-458, 2011.
[112] S. D. Garland, J. Noall, and T. M. Bandhauer, "Experimentally validated modeling of a turbo-compression cooling system for power plant waste heat recovery," *Energy,* vol. 156, pp. 32-44, 2018.
[113] A. Grauberger, D. Young, and T. Bandhauer, "Experimental validation of an organic rankine-vapor compression cooling cycle using low GWP refrigerant R1234ze (E)," *Applied Energy,* vol. 307, p. 118242, 2022.
[114] J. Fenton, J. SUBERT, K. HINCHLIFFE, G. BIANCHI, and S. TASSOU, "Air Cycle Feasibility Using a Novel, Single Rotor Compander for Refrigeration and Heating," in *IIR International Rankine 2020 Conference-Heating, Cooling and Power Generation*, Glasgow, UK.
[115] Y. Zhang *et al.*, "The roticulating concept air compressor: experimental and numerical investigation," in *IOP Conference Series: Materials Science and Engineering*, 2019, vol. 604, no. 1, p. 012070: IOP Publishing.
[116] J. Subert, J. P. Fenton, K. Hinchliffe, and I. M. Arbon, "Design optimization and test of the novel FeTu 'compander', utilising organic fluids within a closed cycle for HVACR applications," *IOP Conference Series: Materials Science and Engineering,* vol. 1180, no. 1, 2021.
[117] G. Bianchi and S. Tassou, "Air Cycle Feasibility Using a Novel, Single Rotor Compander for Refrigeration and Heating," 2020.
[118] O. N. Igobo and P. A. Davies, "Review of low-temperature vapour power cycle engines with quasi-isothermal expansion," *Energy,* vol. 70, pp. 22-34, 2014.
[119] Y. M. Kim, D. K. S. , and J. H. L. , "A Scroll Expander with Heating Structure and Their Systems," presented at the International Compressor Engineering Conference, Purdue, July 12-15, 2004, 2004. Available: https://docs.lib.purdue.edu/icec/1635
[120] H. Jiang *et al.*, "Performance assessment of an organic Rankine–Vapor compression cycle (ORC-VCR) for Low-Grade compression heat recovery," *Energy Conversion and Management,* vol. 275, p. 116492, 2023.
[121] L. Sun, W. Han, and H. Jin, "Energy and exergy investigation of a hybrid refrigeration system activated by mid/low-temperature heat source," *Applied Thermal Engineering,* vol. 91, pp. 913-923, 2015.
[122] R. Long, Y. Bao, X. Huang, and W. Liu, "Exergy analysis and working fluid selection of organic Rankine cycle for low grade waste heat recovery," *Energy,* vol. 73, pp. 475-483, 2014.
[123] A. Vidal, R. Best, R. Rivero, and J. Cervantes, "Analysis of a combined power and refrigeration cycle by the exergy method," *Energy,* vol. 31, no. 15, pp. 3401-3414, 2006.
[124] B. Saleh, "Energy and exergy analysis of an integrated organic Rankine cycle-vapor compression refrigeration system," *Applied Thermal Engineering,* vol. 141, pp. 697-710, 2018.
[125] Z. Hajabdollahi, F. Hajabdollahi, M. Tehrani, and H. Hajabdollahi, "Thermo-economic environmental optimization of Organic Rankine Cycle for diesel waste heat recovery," *Energy,* vol. 63, pp. 142-151, 2013.
[126] S. Sanaye and H. Hajabdollahi, "4 E analysis and multi-objective optimization of CCHP using MOPSOA," *Proceedings of the Institution of Mechanical Engineers, Part E: Journal of Process Mechanical Engineering,* vol. 228, no. 1, pp. 43-60, 2014.
[127] AspenTech. (2022). *AspenPlus Software* Available: https://www.aspentech.com/
[128] K. I. Al-Malah, *Aspen plus: chemical engineering applications*. John Wiley & Sons, 2022.

[129] E. Querol, B. Gonzalez-Regueral, A. Ramos, and J. L. Perez-Benedito, "Novel application for exergy and thermoeconomic analysis of processes simulated with Aspen Plus®," *Energy,* vol. 36, no. 2, pp. 964-974, 2011.
[130] X. Pei, B. He, L. Yan, C. Wang, W. Song, and J. Song, "Process simulation of oxy-fuel combustion for a 300 MW pulverized coal-fired power plant using Aspen Plus," *Energy Conversion and Management,* vol. 76, pp. 581-587, 2013.
[131] P. Kaushal and R. Tyagi, "Advanced simulation of biomass gasification in a fluidized bed reactor using ASPEN PLUS," *Renewable energy,* vol. 101, pp. 629-636, 2017.
[132] D. Unlu and N. D. Hilmioglu, "Application of aspen plus to renewable hydrogen production from glycerol by steam reforming," *International journal of hydrogen energy,* vol. 45, no. 5, pp. 3509-3515, 2020.
[133] B. Bao, M. M. El-Halwagi, and N. O. Elbashir, "Simulation, integration, and economic analysis of gas-to-liquid processes," *Fuel Processing Technology,* vol. 91, no. 7, pp. 703-713, 2010.
[134] M. S. Khan *et al.*, "A new correlation for performance prediction of small and large capacity single-effect vapor absorption refrigeration systems," *Cleaner Energy Systems,* vol. 1, p. 100002, 2022.
[135] M. S. Khan *et al.*, "Comparative Energy and Exergy Analysis of Large Capacity Ammonia-Water and Water-Lithium Bromide Vapor Absorption Refrigeration (VAR) Cycles," in *ASME International Mechanical Engineering Congress and Exposition*, 2021, vol. 85673, p. V011T11A041: American Society of Mechanical Engineers.
[136] W. Chen and K. Chua, "Energy performance analysis and optimization of a coupled adsorption and absorption cascade refrigeration system," *Applied Energy,* vol. 301, p. 117518, 2021.
[137] H. Sihombing, H. Ambarita, W. Naibaho, and E. Setiawan, "Effect of multi–stages vapor compression refrigeration cycle using refrigerant R32 for Air-Conditioning unit," in *IOP Conference Series: Materials Science and Engineering*, 2020, vol. 725, no. 1, p. 012017: IOP Publishing.
[138] S. T. Kadam *et al.*, "Thermo-economic and environmental assessment of hybrid vapor compression-absorption refrigeration systems for district cooling," *Energy,* vol. 243, p. 122991, 2022.
[139] D. Meinel, C. Wieland, and H. Spliethoff, "Economic comparison of ORC (Organic Rankine cycle) processes at different scales," *Energy,* vol. 74, pp. 694-706, 2014.
[140] E. W. Lemmon, M. L. Huber, and M. O. McLinden, "NIST reference fluid thermodynamic and transport properties–REFPROP," *NIST standard reference database,* vol. 23, no. 2002, p. v7, 2002.
[141] B. Saleh, "Parametric and working fluid analysis of a combined organic Rankine-vapor compression refrigeration system activated by low-grade thermal energy," *Journal of advanced research,* vol. 7, no. 5, pp. 651-660, 2016.
[142] O. Nematollahi, Z. Hajabdollahi, H. Hoghooghi, and K. C. Kim, "An evaluation of wind turbine waste heat recovery using organic Rankine cycle," *Journal of cleaner production,* vol. 214, pp. 705-716, 2019.
[143] M. T. Nasir and K. C. Kim, "Working fluids selection and parametric optimization of an Organic Rankine Cycle coupled Vapor Compression Cycle (ORC-VCC) for air conditioning using low grade heat," *Energy and Buildings,* vol. 129, pp. 378-395, 2016.
[144] K. H. Kim and H. Perez-Blanco, "Performance analysis of a combined organic Rankine cycle and vapor compression cycle for power and refrigeration cogeneration," *Applied Thermal Engineering,* vol. 91, pp. 964-974, 2015.
[145] X. Bu, H. Li, and L. Wang, "Performance analysis and working fluids selection of solar powered organic Rankine-vapor compression ice maker," *Solar Energy,* vol. 95, pp. 271-278, 2013.

[146] A. Mota-Babiloni, J. Navarro-Esbrí, Á. Barragán, F. Molés, and B. Peris, "Drop-in energy performance evaluation of R1234yf and R1234ze (E) in a vapor compression system as R134a replacements," *Applied Thermal Engineering,* vol. 71, no. 1, pp. 259-265, 2014.